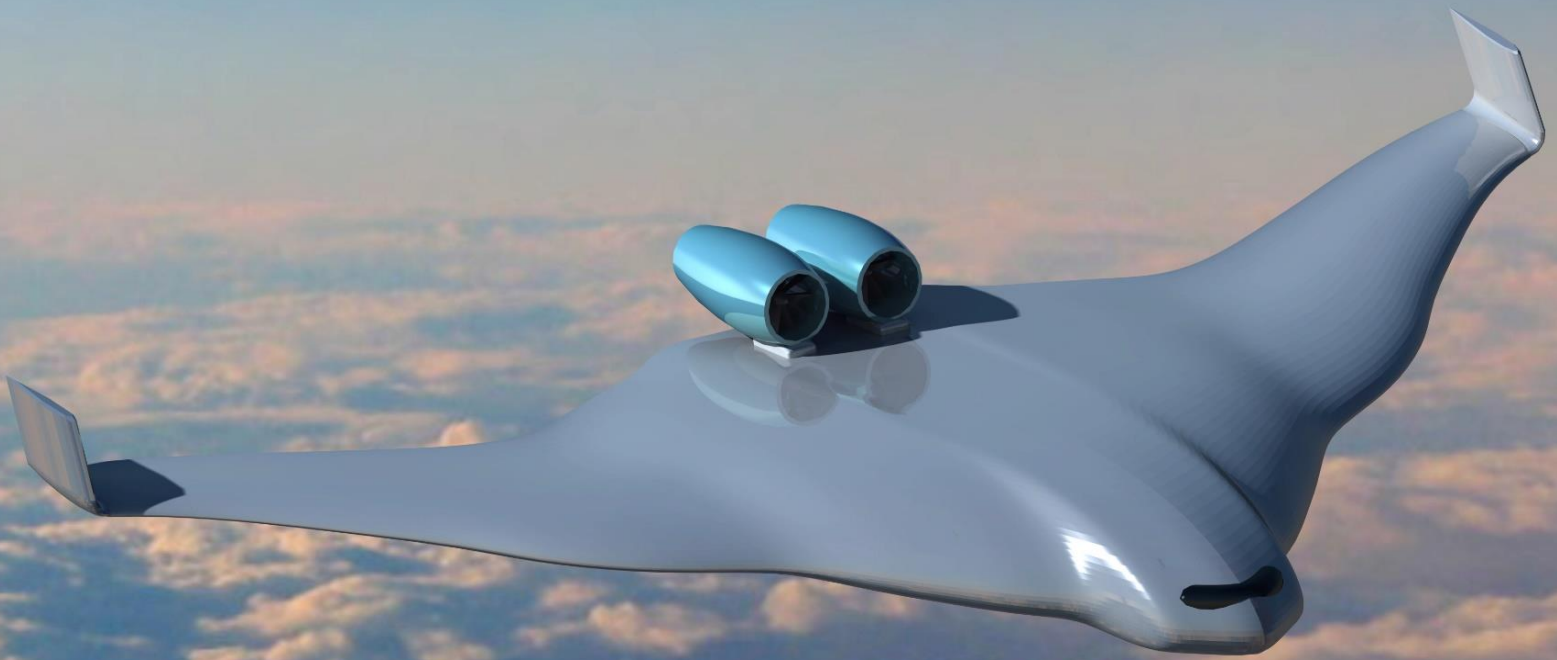# Hydrojet

Final Report
DSE Group 02

This page was intentionally left blank

Hydrojet

by

DSE Group 02

to obtain the degree of Bachelor of Science
at the Delft University of Technology.

Name	Student Number
Bram Amant	4672291
Simon Andreas	4649729
Prewesh Ardjoensing	4647084
Kevin Bislip	4536908
Elliott Desmit	4652282
Gilles Dijkman	4550099
Merlijn Hunik	4676475
Shivan Ramdin	4606248
Arnish Sitaram	4645200
Stijn Van Dam	4674901

Due date: 22 June, 2020
Course: AE 3200
Project Supervisor: Dr. R. M. Groves, Principal Tutor
Dr. E. Smeur, Coach
D. Van Baelen, Coach

TUDelft

Preface

This report is the fourth and final report of Group 02 in the Design Synthesis Exercise (DSE) organised by the Faculty of Aerospace Engineering at the Delft University of Technology. It contributes to obtaining the Bachelor of Science in Aerospace Engineering.

The aim of this report is to research the feasibility of a liquid hydrogen, turbofan-powered, blended wing body (BWB) passenger aircraft, featuring a capacity of 236 pax and a range of 4500 km, to give the aviation industry a push in the direction of long-term sustainable (civil) aviation. It is the result of the work performed by ten aerospace bachelor students, who have been facilitated by the TU Delft to work on this project for eleven weeks. Readers are expected to have a basic background in (aerospace) engineering, as this feasibility study is performed on a thorough technical level.

Details about the hydrogen turbofan design and accompanied emissions can be found in Section 7.3 and Subsection 7.3.6, respectively. Readers specifically interested in the integration of the required fuel volume with the BWB planform are referred to Section 7.5 and Figure 5.3 for visualisation. If readers wish to know about the hydrogen supply and corresponding ground station, Chapter 8 elaborates upon that. For airline policy makers, the operational and safety aspects can be found in Chapter 10, and sustainability aspects in Chapter 11.

Finally, DSE Group 02 would like to take this opportunity to thank their principal tutor, Dr. Roger M. Groves and their two coaches, Dr. Ewoud Smeur and Dirk Van Baelen, who have guided the project from start to end, and provided the accompanying assessment. Their support and feedback have been essential to the improvement of the performance of each individual and the group as a whole, and to the outcome of the project.

Contents

List of Acronyms

Acronym	Explanation
ADS-B	Automatic Dependent Surveillance-Broadcast
AoA	Angle of Attack
AP	Aircraft Planform
APU	Auxilary Power Unit
AR	Aspect Ratio
ATM	Air Traffic Management
AV	Avionics
AVL	Athena Vortex Lattice
bgge	baggage
BC	Boundary Condition
BEP	Break-Even-Point
BLI	Boundary Layer Ingestion
BPR	Bypass Ratio
BWB	Blended Wing Body
CASM	Cost per Available Seat Mile
CCE	Commercial Cabin Equipment
CFD	Computational Fluid Dynamics
CC	Combustion Chamber
CG	Center of Gravity
COMD	Combustion Chamber Design
COVID-19	Coronavirus
CPR	Compressor Pressure Ratio
DATCOM	Data Compendium
DOC	Direct Operational Cost
DSE	Design Synthesis Exercise
EAS	Equivalent Airspeed
EASA	European Union Aviation Safety Agency
ECS	Environmental Control System
FCOM	Flight Crew Operating Manual
F/A	Fuel to Air Ratio
$(F/A)^{stoic}$	Stoichiometric Fuel to Air Ratio
FBS	Functional Breakdown Structure
FE	Fuel Economy
FEM	Finite Element Method
FFD	Functional Flow Diagram
FMS	Flight Management System
FPR	Fan Pressure Ratio
G	Gas Turbine Parameter
GDU	Garmin Display Unit
GF	Growth Factor
GH2	Gaseous Hydrogen
GMU	Magnetometer
GPS	Global Positioning System
GRS	Ground Radio Service
HAM	High Aspect Ratio Method
HLD	High Lift Device
HPC	High Pressure Compressor
HPT	High Pressure Turbine
HPRA	Hydrogen Powered Regional Aircraft
ICAO	International Civil Aviation Organisation
IDE	Integrated Development Environment
IPS	Ice Protecting System
JIT	Just-in-Time
KLM	Royal Dutch Airlines
LCN	Load Classification Number
LDI	Lean Direct Injection
L/D	Lift over Drag Ratio
LH	Liquid Hydrogen
LPT	Low Pressure Turbine
LE	Leading Edge

Acronym	Explanation
LG	Landing Gear
LE	Leading Edge
LH2	Liquid Hydrogen
LPC	Low Pressure Compressor
M	Boil-off Rate
MAAMF	Mylar Aluminium Aluminium Mylar Fabric
MAC	Mean Aerodynamic Chord
ME	Engineering of the Manufacturing
MIT	Massachusetts Institute of Technology
MLG	Main Landing Gear
MLI	Multi-layered Insulation
MLW	Maximum Landing Weight
MTOM	Maximum Take-off Mass
MTOW	Maximum Take-off Weight
N	Number of Engines
NACA	National Advisory Committee for Aeronautics
NDT	Non-destructive Testing
NO_x	Nitrogen Oxides
OEI	One Engine Inoperative
OEM	Operational Empty Mass
OEW	Operational Empty Weight
pax	passengers
PCO	Powerplant Cooling
PEM	Proton Exchange Membrane
PEMFC	Proton Exchange & Membrane Fuel Cell
PET	Polyethylene Terephthalate
PFP	Powerplant Fire Protection
PFS	Powerplant Fuel System
PIN	Powerplant Integration
PPm	Parts Per Million
PRO	Propulsion
POW	Power
RAMS	Reliability, Availability, & Maintainability and Safety
REQ	Requirement
ROC	Rate of Climb
ROI	Return On Investment
RR	Recyclability Rate
SF	Shrink Factor
SFC	Specific Fuel Consumption
SHM	Structural Health Monitoring
SOFC	Solid Oxide Fuel Cell
STK	Stakeholder
SRIA	Strategic Research & and Innovation Agenda
SWOT	Strenghts, Weaknesses, Opportunities & Threats
TAS	True Airspeed
TBD	To be determined
TCAS	Traffic Alert and Collision Avoidance System
TE	Trailing Edge
TIT	Turbine Inlet Temperature
TOP	Take-off Parameter
TRL	Technology Readiness Level
TS	Thrust Setting
TSFC	Thrust Specific Fuel Consumption
TUR	Turbofan
UAV	Unmanned Aerial Vehicle
UHC	Unburned Hydrocarbons
ULD	Unit Loading Device
VLM	Vortex Lattice Method
XLEMAC	X-position of the leading edge MAC

List of Symbols

Symbol	Explanation
a	Acceleration
a_0	Speed of sound at sea level
a_x	Maximum deceleration
A	Aspect Ratio
A_{max}	maximum cross sectional area
A_{bypass}	Bypass area
A_{core}	Core Area
AR	Aspect Ratio
b	Span
c	Chord
c_e	Elevon chord length
c/V	Climb Gradient
C_d	Airfoil drag coefficient
C_D	Drag Coefficient
C_{D_0}	Zero-lift Drag Coefficient
$C_{D_{LG}}$	Landing Gear Drag Coefficient
$C_{D_{misc}}$	Miscellaneous Drag Coefficient
C_f	Skin friction coefficient
C_{f_c}	Skin friction coefficient per component
C_l	Airfoil Lift Coefficient
C_{l_b}	Basic airfoil lift coefficient
$C_{l_{des}}$	Design lift coefficient
$C_{l_{max}}$	Maximum Airfoil Lift Coefficient
C_{l_α}	Airfoil lift curve slope
$C_{l_{\delta a}}$	Roll moment derivative w.r.t. δa
C_{l_P}	Roll moment derivative w.r.t. roll rate
C_{n_β}	Yaw moment derivative w.r.t. sideslip
C_L	Wing Lift Coefficient
$C_{L_{des}}$	Design lift coefficient
$C_{L_{max}}$	Maximum Lift Coefficient
$C_{L_{TO}}$	Take-off Lift Coefficient
C_{L_α}	Wing Lift Curve Slope
C_m	Moment coefficient
c_{mac}	Airfoil moment coefficient around aerodynamic centre
C_{mac}	Moment coefficient around aerodynamic centre
C_{m_α}	Moment coefficient derivative
C_P	Specific Heat
$C_{P,a}$	Specific Heat Air
$C_{P,g}$	Specific Heat Gas
$C_{p,0}$	minimum pressure coefficient
c_r	Root chord
d	Landing gear height
D_{LH2}	Diameter of liquid hydrogen tank
D	Drag
D_i	Inlet diameter
D_h	Highlight diameter
D_{rotor}	Space between two wind turbines
D_{runway}	Landing Distance
e	Oswald Efficiency Factor
E	Endurance
E_{in}	Energy needed for the ground station
E_{loiter}	Loiter Endurance
f	Drag estimation correction factor
f_{land}	Ratio MLW/MTOW
F_{Tot}	Total propulsion force of motor
FF	Form Factor
FF_{end}	Fuel fraction at end of cruise
FF_{start}	Fuel fraction at start of cruise

Symbol	Explanation
GF	Growth Factor
g	Gravitational Acceleration
L/D_{cruise}	Lift over Drag Ratio during Cruise
L/D_{loiter}	Lift over Drag Ratio during Loiter
h	Air Convection Coefficient
h_{fg}	latent heat of vaporisation
$h_{winglet}$	Winglet Height
I	Second moment of area
IF_c	Interference factor
K	Thermal conductivity insulation
k_a	technology factor
K_g	Gust Alleviation Coefficient
K_G	Thermal Conductivity of Air
K_I	Stress intensity factor
K_Ic	Fracture toughness
l	Length
l_n	Nacelle length
L	Lift
LCN	Load Classification Number
m	Mass
$m_{payload}$	Payload Mass
$\dot{m}$	Mass Flow Turbofan
$\dot{m}_{core}$	Core mass flow
$\dot{m}_{bypass}$	Bypass flow
$\dot{m}_ref$	Aircraft refuelling mass flow
$\dot{M}_{boil}$	Boil-off Rate of Liquid Hydrogen
M	Moment
M_{MW}	Distance main wheel - aft CG
M_{GH2}	Minimum Gaseous Hydrogen Tank Mass
M_cr	critical Mach number
M_{cruise}	Cruise Mach Number
M_D	Dive Mach Number
M_{DD}	Drag Divergence Mach Number
M_f	Mass fraction
M_{ff}	Mass fuel fraction
$M_{takeoff}$	Take-off Mach Number
$M_{landing}$	Landing Mach Number
M_{perp}	perpendicular mach number
n	Load Factor
$ng\%$	Weight fraction on nose landing gear
$n_{containers}$	number of cargo containers
n_{max}	Maximum Load Factor
n_{min}	Minimum Load factor
n_g	Gust Load Factor
n_{MG}	Number of main landing gears
n_{pplant}	Number of wing mounted engines
n_{stack}	Nuber of cells in the stack
n_t	Amount of nose tyres
N	Distance nosewheel - aft CG
$N_{cabincrew}$	Number of cabin crew
N_{chord}	Number of vortices along the chord
N_{eng}	Number of Engines
N_{mw}	Number of main wheels
N_{pax}	Number of passengers
N_{UD}	Nusselt Number
N_span	Number of spanwise vortices
N_{pilots}	Number of pilots
P_{GH2}	Internal Gauge Pressure of Gaseous Hydrogen Tank
P_{LH2}	Pressure of Liquid Hydrogen during refuelling

Symbol	Explanation
p_w	Wheel pressure
P	Roll rate
P_1	Inlet Pressure
P_2	Pressure before Fan
P_{ECS}	Optimal Pressure for ECS System
P_{FC}	Optimal Pressure for Fuel Cell
P_i	Point mass i
P_{in}	Power needed for the for the ground station
P_m	Static load on MLG
P_M	Power needed for electrical motor
$P_{n_{dyn}}$	Dynamic load on nose landing gear
Q_i	Inner Wing Fuel Ratio
Q_i	Heat
Q_0	Outer Fuel Ratio
r	nose landing gear radius
R_{ad}	Rayleigh Number
R_{GH2}	Inner Radius of the Gaseous Hydrogen Sphere
R_{LH2}	Largest Radius of the Onboard Liquid Hydrogen tank
R	Range
R^2	Coefficient of Determination
Re	Reynolds number
s_t	Tyre deflection
S	Surface Area
S_c	Sutherland's constant
S_{ch}	Shock absorber stroke
S_A	landing gear frontal area
SF	Shrink Factor
S_i	Surface Area inner wing
S_o	Surface Area outer wing
S_{ref}	Reference wing surface area
S_{wet}	Wetted surface area
t	Time
t_{ins}	Thickness of Insulation
t_{GH2}	Thickness of Gaseous Hydrogen Tank
t_{LH2}	Thickness of Onboard Liquid Hydrogen Tank
t/c	Thickness over Chord Ratio
$(t/c)_{max}$	Maximum thickness over Chord Ratio
$t/c_{streamwise}$	t/c in streamwise direction
T	Thrust
T	Temperature
T_0	Sea level thrust
T_{bypass}	Bypass thrust
$T_{chocked}$	Chocked Thrust
T_{core}	Core Thrust
T_{LH2}	Hydrogen Storage Temperature
T_q	Torque
T_S	Insulation Outer Surface Temperature
T_{TO}	Take-Off thrust
T_∞	Cruise Temperature
U_{EAS}	Gust velocity
V	Velocity
V_{shear}	Shear force
V_1	Decision Speed
V_2	Take-off safety speed
V_{28}	Exhaust velocity bypass
V_8	Exhaust velocity core
V_A	Design manoeuvring speed
V_B	Maximum gust design speed
V_{cell}	Fuel cell voltage
V_{cruise}	Cruise speed
V_C	Cruise Speed
V_D	Dive Speed
V_{EF}	Engine failure speed
V_f	Flutter speed
V_{MCG}	Ground minimum control speed
V_{MCL}	Landing minimum control speed
V_{min}	Minimum speed
V_R	Rotation Speed
V_{Ref}	Landing reference speed
V_S	Stall speed
V_{S0}	Landing stall speed

Symbol	Explanation
V_{SR}	Reference stall speed
$V_{tyre_{max}}$	Maximum operational tyre speed
w_{LG}	Landing gear width
w	Width
W	Weight
W_{req}	Required Work
W_{prop}	Propulsion System Weight
y	Height from neutral axis
y_k	Ratio Wing Span/Reference Span
y_{MG}	Distance centre line - main landing gear
Y_i	Point mass i distance from center body
x_{ac}	Aerodynamic centre location
$(x/c)_m$	position of the maximum thickness
x_{cg}	Longitudinal centre of gravity
x_{np}	Neutral point location
xx	x-axis
z	Height of the main landing gear
$\overline{A}$	Material allowable compressive stress factor
α	Angle of Attack
α_0	Zero lift angle of attack
$\alpha_{C_{L_{max}}}$	Angle of Attack at maximum lift coefficient
$\alpha_{L=0}$	zero lift angle of attack
α_{stall}	Stall angle
α_{trim}	Trim angle of attack
β_t	Thermal Expansion Coefficient
β	Prandtl-Glauert compressibility Correction factor
δa	Aileron deflection
Δ	Change in / difference in
Δy	Sharpness Parameter
η	Fuel Economy
η_{gear}	Gear efficiency
η_s	Ole0-pneumatic shock absorber efficiency
η_t	Tyre efficiency
η_{tf}	Turbine Fan efficiency
η_{nozzle}	Nozzle efficiency
ϵ	Insulation Surface Emissivity
γ	Ratio of specific heat
λ	Taper Ratio
Λ	Sweep Angle
$\Lambda_{0.5c}$	mid-chord wing sweep
Λ_{LE}	Sweep Angle leading edge
Λ_m	sweep angle at maximum thickness
μ	Dynamic viscosity
μ_{CRR}	Coefficient of rolling resistance
μ_g	Gust mass parameter
$\mu_{Traction}$	Static friction coefficient of traction
∇	Gradient of
Φ	Flow potential
π	Pi
Π	Pressure Ratio
Π_{fan}	Pressure ratio fan
Π_{HPC}	Pressure ratio HPC
Π_{LPC}	Pressure ratio LPC
ρ	Density
ρ_0	Sea level air density
ρ_{cruise}	Cruise air density
σ	Altitude correction factor
σ_{axial}	Axial stress
σ_{long}	Longitudinal stress
σ_{sb}	Stefan-Boltzmann Constant
σ_n	Normal stress
σ_y	Yield stress of material
σ_θ	Hoop stress
τ	Residence Time
τ_a	Aileron effectiveness parameter
τ_{set}	Thrust setting
Φ	Equivalence ratio
ϕ	Tip clearance angle
ω	Angular speed
ψ	Overturn angle

Executive Overview

There is a growing concern for the impact of the aviation industry on the environment. This could become a risk for the industry when people decide to fly less because of this 'flight shame'. A possibility to solve this problem is a hydrogen powered regional aircraft: the Hydrojet. Hydrogen not only has the possibility for very low to no emissions, thus reducing flight shame but is also an inexhaustible source, as it can be generated from water and electrical power. However, a known problem for the integration of hydrogen as a fuel in current aviation is the large amount of volume needed for the same amount of internal energy. Also, the safety when using such a fuel can become a problem.

In this report, the feasibility of such a Hydrojet is examined. First, a recap is given of the design choices and analysis performed during the midterm phase. Then, a more detailed Class II analysis and weight estimation is performed, resulting in the final design. Finally, the operations will be discussed, as well as the possible methods and results for sustainability, the compliance with the requirements, a financial analysis checking the marketability of the aircraft, and lastly the post DSE activities will be discussed.

First and foremost, in order to achieve a goal, the parameters must be set which define when such a goal is achieved. These goals are defined numerically by the top level requirements, and will be checked for compliance once the design has progressed to the next phase.

Top Level Requirements

Sustainability:
HPRA-STK-SUS-1: The aircraft shall emit zero emissions, except for water during operation.
HPRA-STK-SUS-2: The aircraft shall be 90% (weight fraction) recyclable.

Performance:
HPRA-STK-PERF-1: The range of the aircraft shall be sufficient to fly between any two airports in the European Common Aviation Area.
HPRA-STK-PERF-2: Flight times of the aircraft shall be comparable with existing commercial aviation.

Engineering Budget:
HPRA-STK-ENBU-1: The aircraft shall be able to carry 236 passengers and their luggage.
HPRA-STK-ENBU-2: The aircraft shall have a minimum lifetime of 25 years.
HPRA-STK-ENBU-3: The ground hydrogen storage facility shall be suitable to service a fleet of 10 aircraft.

Safety and Reliability:
HPRA-STK-SR-1: The aircraft shall have a 50% availability including turnaround time and maintenance.
HPRA-STK-SR-2: The aircraft shall meet all European aviation standards.
HPRA-STK-SR-3: The aircraft shall have emergency procedures implemented for emergency hydrogen loss.

Cost:
HPRA-STK-COS-1: The aircraft shall have a maximum cost of €100 million.
HPRA-STK-COS-2: The operational costs shall not exceed those of existing comparable commercial aviation.

Design Choice

In order to fulfil these requirements, a feasible design choice must be made which has the most potential to fulfil this statement. Moreover, a firm sustainability strategy must be made to ensure that this will indeed be done. This strategy has been defined as: *Design the Hydrojet system in such a way that its production, operation and retirement can be carried out indefinitely on a big scale without causing harm to the environment, the society or the economy*.

There have been identified three main components to this definition of sustainability. Namely *production and assembly, operations and maintenance, and retirement*. To ensure a sustainable approach to all three components, a general overview was maintained keeping track of all relevant parameters, such that progression can be tracked to see improvements in sustainability

as defined above.

The concept chosen during the conceptual design phase is a blended wing body (BWB) with hydrogen powered turbofan engines, a fuel cell as auxiliary power unit, and an electric motor in the landing gear for taxiing. This concept was chosen as it has a very high theoretical lift over drag. Moreover, the turbofan engines have a high thrust over weight with very decent efficiency. This means that in total, this combination is estimated to use little fuel per mile. The only downside is the low technological readiness level of the BWB.

A preliminary analysis was performed during the midterm phase, of which the results are summarised in Table 1. Using these values, the subsystem can be designed in more detail. These subsystems have been identified as follows: The planform, which consists of the wings including the control surfaces, and the fuselage of the BWB with the cabin layout. The landing gear, such that a feasible integration can be shown. The power and propulsion which consists of the turbofan, the fuel cell, the fuelling system and the motor in the landing gear. Finally, there are the ground facilities, which consist of the hydrogen storage as well as production.

Table 1: Initial specifications of the Turbofan Blended Wing Body [1]

OEM [kg]	MTOM [kg]	W_F [kg]	T/W_{prop} [-]	η[%]	Clean L/D [-]	S [m^2]	T [kN]	Cost [€ million]
42,984	76,785	8,801	3.35	36	26.95	214.2	227.5	95

Class-II Design

Once this first estimation has been completed, and a design choice has been specified, a more detailed Class-II design can take place, taking into account various geometric parameters as well as more in-depth analyses of the subsystems. Using a Class-I weight estimation, these geometries and other parameters of the subsystems can be calculated, the method of which will be described below. This is then inputted into the Class-II weight estimation. This outputs the new operational empty mass (OEM) and maximum take-off mass (MTOM), which can then be inputted into the Class-I estimation again. By iterating this loop several times, the difference between the OEM obtained from Class-I and Class-II will become smaller. The iterations are completed when this difference is smaller than 1 %. This is then taken as the final design point.

Aircraft Flight Performance

In order to converge to a design, all of the subsystems must be defined in equations such that the right geometries can be outputted, with OEM and MTOM as input. However, first the aircraft flight performance must be specified, such that a relation can be found to the required thrust loading and wing loading. This is then used by the other subsystems.

This is done by first specifying all of the relevant performance requirements the aircraft must comply with. From here, a list of design speeds can be specified. Using these speeds, as well as the requirements and several known methods and equations, the wing loading-thrust loading diagram can be constructed. From this diagram, the required thrust loading, and wing loading can be obtained, which are 0.314, and 1772 N/m^2, respectively. Using the known weight this results in a thrust and wing area.

With the wing- and thrust loading defined, the flight envelopes can be constructed, such that the maximum load factor and the operational range of the Hydrojet can be calculated. The flight envelope is based on CS-25 requirements, as well as some basic formulas. A maximum load factor of 2.69 can be derived from the flight envelope.

To then further describe the performances of the aircraft, the climb performance and flight ceiling is calculated. This is done using several known performance equations, then constructing a climb performance over altitude graph from which these values are derived. A flight ceiling of 18.2 km and a rate of climb of over 28 m/s at sea level is found. This shows that the Hydrojet is capable of steep climb, and if necessary, can climb above the troposphere, which can be an interesting marketing opportunity.

To finalise the performance of the aircraft, the payload-range diagram must be constructed as well. This will define the harmonic and ferry range as well. The standard range equation for jet aircraft will be used, as well as some requirements. A harmonic range of 1125 km, a design range of 4500 km, and a ferry range of 10360 km is found, respectively. It is thus seen that the aircraft without payload has a substantially larger range.

Aircraft Planform Design

Having the performances of the aircraft defined, the planform can now be designed. First, requirements are set that act as boundaries to which the planform must abide. This allows for a preliminary estimation of what the planform should look like, as for the general shape and the layout defining where each subsystem is integrated. Using the required number of passengers, namely 236, and a standard amount of cargo per passenger as well as a cargo density of 160 kg/m^3, it is found that 28.2 m^3 is required to hold all the cargo. Moreover, the Class-I estimation resulted in a fuel weight as well. Using also the cryogenic density of liquid hydrogen and taking into account the boil-off effect, it is found that 137.18 m^3 is needed for fuel. Using these values, the planform layout has been defined and is depicted in Figures 1 and 2. Note that in Figure 2, the cargo is placed on top of the cabin, thus the cabin has the area of what is shown in the figure, as well as the area depicted as cargo. Additionally, behind the cabin there will also be room for toilets and facilities where 1.87 m height is not essential. However, these have not been indicated in Figure 1.
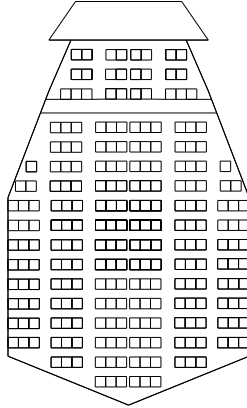

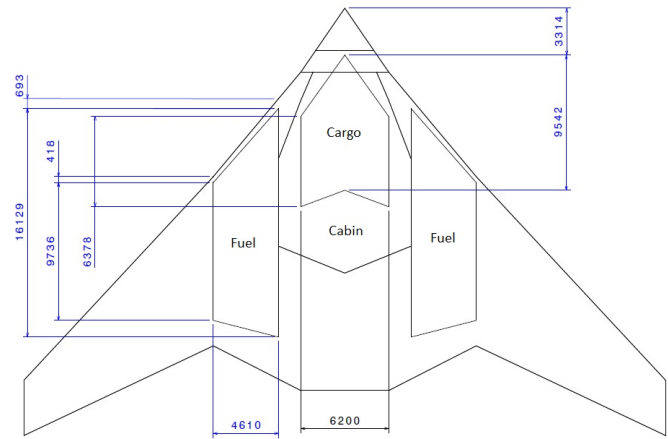Figure 1: Cabin layout of the Hydrojet

Figure 2: Planform layout with the cabin, cargo holds and fuel tanks. Dimensions are in mm.

With this first estimation of the wing geometry, an aerodynamic analysis can then be applied such that the right airfoil can be selected, and calculations can then be performed on the wing to find a more accurate representation of its performances. The airfoil selection is based on the following parameters. It must have a high lift over drag, as this will naturally result in a better fuel economy. It must also have a sufficiently high $C_{l_{max}}$, for good take-off and landing performance. Furthermore, the thickness of the airfoil was taken into account as well due to the integrated blended wing body. And finally, the airfoil must have a slightly negative $C_{m_{ac}}$, which is then made positive by sweep and a negative twist from the start of the outer wing towards the tip. Based on these criteria, the selected airfoil for the inner part where the fuel tanks and passengers are located is the **NACA 25112**, since this airfoil has good performance qualities, as well as the desired $C_{m_{ac}}$ and thickness. The **MH 45** airfoil is then chosen for the outer wing, since for the outer wing a lower thickness is desired, such that the drag divergence number does not become too low, which could limit the cruise speed. Furthermore, based on flight performance and aerodynamics, it was decided that no high lift devices had to be implemented. Using then some known relations, as well as some semi-empirical equations, an aerodynamic analysis can be performed. The following is then found, which is summarised in Table 2.

Table 2: Outputs of the aerodynamic analysis performed on the BWB

$C_{L_{des}}$	0.153	Takeoff C_{L_α}	3.7832 $1/rad$	Takeoff α_{stall}	24.44 °
Clean $C_{L_{max}}$	0.9536	Cruise C_{L_α}	4.6928 $1/rad$	Cruise α_{stall}	20.20 °
		Landing C_{L_α}	3.7781 $1/rad$	Landing α_{stall}	25.36 °

Apart from the layout and aerodynamics, the wing needs to be designed with stability and control in mind as well. After estimating the CG range (0.1201 - 0.1984 MAC), the optimal longitudinal Mean Aerodynamic Chord (XLEMAC) can be determined, which is 11.04 m from the nose. With this XLEMAC some parameters of the outer wing are decided like the taper ratio, span and sweep angle. Since the Hydrojet does not have a tail, it has to be trimmable with only the wing. For this purpose, a wing twist angle of -1.7 degrees is needed so that the wing tips could function as the horizontal stabiliser. The elevons, a combination of ailerons and elevators, are sized on a roll rate requirement of 20 deg/s and were found to have a

maximum needed deflection of 16 degrees, leaving enough available deflection for pitch control. Furthermore, winglets are added to function as vertical stabiliser such that the aircraft is directionally stable. The Hydrojet is also evaluated on dynamic stability using the Athena Vortex Lattice software and found to be stable in all eigenmotions.

Landing Gear

The landing gear is designed to provide ground stability, to allow ground manoeuvres and for shock absorption during landing. First of all, the widely used tricycle configuration is chosen for among other its stability characteristics. Next, the nose landing gear and main landing gear are positioned to allow for a big enough tip-back and overturn angle. The tyres are sized and selected according to the loads, pressures and maximum operating speed of the tyres. Finally, the shock absorbers are selected and sized. Oleo-pneumatic shock absorbers are selected because of their high efficiency and low weight. Lastly, the material for the struts was chosen to be Titanium 10V-2Fe-3Al because of its high strength-to-weight ratio.

Power and Propulsion

Only the power and propulsion system is now left to design for the aircraft. Once this is done, the entire aircraft will be defined and the iteration process as was mentioned earlier can be executed. First, the power system will be sized. The power system must be able to provide power to the avionics and actuators, cabin equipment, the landing gear taxiing system, ice protection system, cooling system, and the environmental control system of power. The total amount of power needed during each flight phase is presented in Table 3.

Table 3: Required electrical power

Flight phase	Taxi-out	Take-off	Cruise	Landing	Taxi-in
Total power [kW]	300.36	198.87	318.85	183.26	300.36

Having then defined the total required power, the power system can then be sized, which is a fuel cell. The type of fuel cell used is a proton-exchange membrane fuel cell (PEMFC), since this only emits water, has high reliability and also has a fast start up in case of emergency. Several combinations of current density and voltage are used to come with the lowest possible fuel flow to get the desired power output while still remaining a feasible design point. It is then found that minimising current density is desirable. Thus, choosing the lowest value that is still feasible in the design, a current density of 0.4 A/cm^2 is chosen, from which a voltage of 0.71 is obtained as well. Using then 650 W/kg of weight and 1100 W/L, a total fuel cell weight of 496.6 kg and fuel cell volume of 293.5 L is found as well.

Next, the turbofan will be designed. The goal for designing the turbofan is to keep the emissions and fuel usage to a minimum. In general, the parameters that are considered to affect either the fuel usage or the NO_x emissions are: the fan pressure ratio (FPR), the compressor pressure ratio (CPR), the residence time τ of the combustion, equivalence ratio Φ, the combustor chamber design (COMD), turbine inlet temperature (TIT) and the bypass ratio (BPR).

Thus, in order to optimise emissions and fuel usage, these six parameters must all be optimised simultaneously. To do this, first the TIT and Φ were determined based on which give the lowest amounts of NO_x emissions empirically. This is chosen as starting point such that the emission variable is eliminated as much as possible, right from the start. Then, as the BPR only determines the thrust specific fuel consumption, it was selected based on current limitations. Using these numbers, as well as the known thrust, an optimum can then be found for the FPR and CPR by calculating all of the different stages within the turbofan. During calculations the CPR has been subdivided in low pressure compressor (LPC) and high pressure compressor (HPC) compressors. Once these are determined, the τ can be found by analysing the combustor itself. After performing the necessary calculations, the results have been summarised in Table 4. Furthermore, some semi-empirical relations can be used to determine the dimensions of the turbofan.

Table 4: Results of calculations and optimisations done for the turbofan.

FPR	LPC ratio	HPC ratio	Φ	TIT	Fuel mass flow cruise	TSFC$_{cruise}$	Fuel mass flow take-off	TSFC$_{take-off}$
1.4	1.3	22.1382	0.3	1600 K	0.2795 kg/s	$6.329 \cdot 10^3$ kg/s/kN	0.4193 kg/s	$3.053 \cdot 10^3$ kg/s/kN

The liquid hydrogen tanks were designed such that they fit into the inner wing while keeping a shape that was as elliptical as possible in order to store all the required liquid hydrogen volume of 138.4 m^3. Baffles were implemented into the tank to prevent sloshing. External foam insulation was used to reduce the frost build-up and the boil-off of hydrogen. The tank wall material used is Al 2219-T87 due to its good fracture toughness. Polyurethane foam was used as insulation material since it does not degrade by mechanical or thermal stresses for at least 14 years. A protective structure was added to protect the foam

from hydrogen embrittlement and external damage. Each of the liquid hydrogen tanks have a total wall thickness of 0.104m, where 0.08m is insulation to meet the allowed boil-off mass rate for 7 hours.

Ground facilities

The last subsystem that is going to be elaborated is the ground facilities. The ground facilities will convert water into hydrogen gas using Proton Exchange Membrane (PEM) electroysis. The pure oxygen that is also produced by this process will be collected and sold to licensed oxygen distributors for medical and educational use. This is done to eliminate any waste. The ground facilities will be entirely powered by three onshore 3MW wind turbines and solar panels using an area of 2055 m by 801.1 m. The green energy sources will also be used to provide energy for the converter and cooler located at the airport. This will be done by connecting the green energy sources to the power grid providing it green electricity. This electricity is then taken up again from the main power grid connected to the airport. This will ensure that the ground facilities work entirely on green sustainable energy, which fit the sustainability goal of the Hydrojet. For storage of the gaseous hydrogen, three spherical, steel 300M, underground tanks will be used, each with a thickness of 0.753 m and a radius of 7.24 m. Using three tanks will ensure that there will always be hydrogen available for refuelling the aircraft. However, since the tanks will be located underground, an additional monitoring system will be installed to ensure safety at all time. The gaseous hydrogen will be transported using underground pipelines to the airport. The compressor and cooler will be available there, converting the gaseous hydrogen to liquid hydrogen.

Final Design

At this stage, all of the subsystems have been described, together with some design choices and also the relevant formulas describing their geometric and performance parameters as a function of their relative inputs. This enables the use of the iteration process, as had been discussed before. After the fourth, the difference in OEM, MTOM and lift over drag is for all of them less than 1 %, and the iteration process is deemed successful. From this iteration a MTOM of 92,315 kg, and an OEM of 52,920 kg is obtained. A fifth iteration showed that it is indeed converged. The final design, as it is in this phase of design, is showcased in Figure 3.
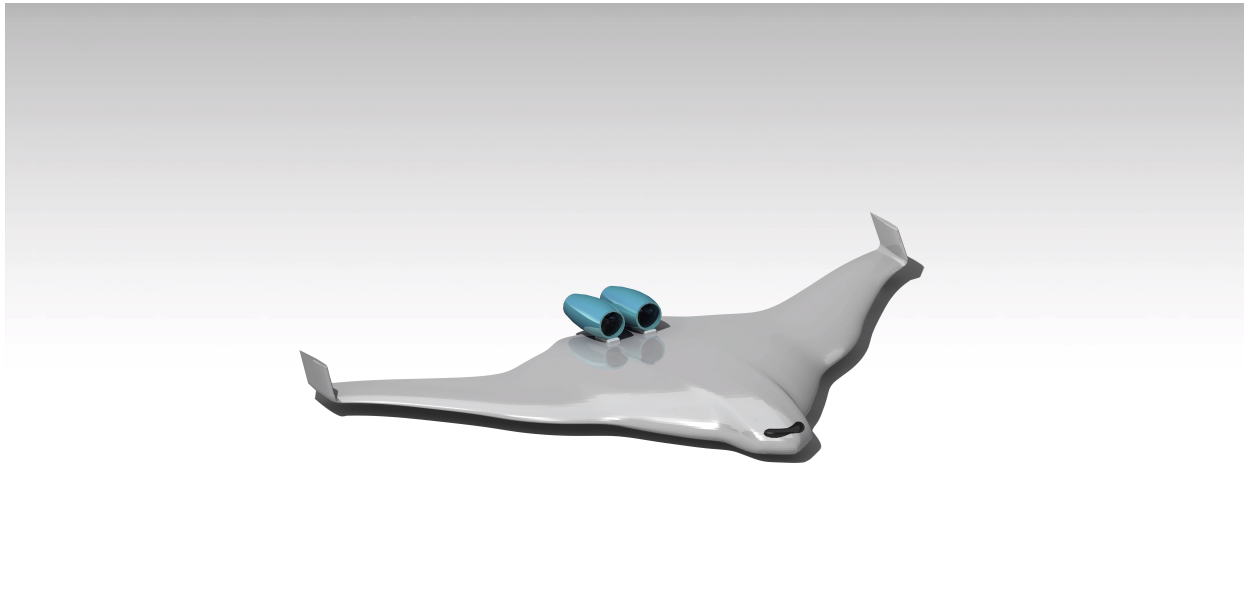

Figure 3: Final Design Portrait

Operations and Logistics

Now that the final design is known, the operations of the aircraft can be looked at. The operations of this design will consist of ground facility operations and aircraft operations. The ground operations will include production, transport and conversion of hydrogen, and refuelling of the aircraft. The production remains the same as was described previously. The transport of gaseous hydrogen will be done through pipelines starting at the polymer electrolyte membrane (PEM) electrolyser into the gaseous hydrogen tanks up until the compressor and cooler at the airport. After the hydrogen gas has been liquefied, it will be transported to the aircraft by trailers. When there is no pipeline infrastructure for gaseous hydrogen, a short term - or emergency - solution is to convert the gaseous hydrogen to liquid hydrogen when it is being produced by the PEM electrolyser.

The liquid hydrogen will then be transported using trailers to the airport. For the conversion & refuelling a compressor and cooler is used. Refuelling the aircraft will consist of liquefying the new hydrogen gas and pumping the liquid hydrogen into the fuel tank of the aircraft. Additionally, the boil-off hydrogen located in the tank of the aircraft after a flight will be recycled by liquefying it again using the compressor and cooler. The aircraft operations will consist of multiple flights a day. Every aircraft has a different destination and thus a different flight time. To give an overview of the aircraft operations, two different scenarios are discussed: a flight with the maximum range and a short haul flight (maximum 3 hours). Every flight cycle starts with a visual inspection while the aircraft is being refuelled and passengers board the aircraft. Then the pilots go through the common take-off procedures and the Hydrojet will take-off after getting permission from air traffic control. For a long range flight, these procedures take around 1.5 hours for the maximum range and around 1 hour for short-haul flights. Next is the cruise phase, which take 3 to 5 hours depending on the type of flight. Finally, the aircraft is unloaded which completes the flight cycle.

RAMS Requirements

Furthermore, the Reliability, Availability, Safety and Maintenance (RAMS) characteristics have been analysed for the Hydrojet. The reliability has only been analysed of the unconventional parts of the aircraft which are the engines, the hydrogen tank and the fuel cell. The engines decrease the reliability due to the novelty of the engine design. The hydrogen tank design is unconventional even for hydrogen tanks themselves. This will decrease the reliability of the design as well. The fuel cell is still a relatively new technology, however due to the low number of components already very reliable. Next, the availability of the entire plane has been calculated based on assumed operation times. The availability of this aircraft is 81.37 %. Maintenance cycles have also been established. Light maintenance will be done throughout the entire aircraft while there are also large scheduled maintenance checks. The safety has been taken into account in the entire design such that design will be feasible. Especially since the design is a hydrogen aircraft, special attention is paid to the fuel tanks. Procedures during emergency situations such as tank leakage or evacuation are established and result in a safer overall design.

Sustainability

A major part of the Hydrojet design revolves around sustainability. Therefore, a sustainability analysis is performed as well, which includes the sustainable production, operation and retirement of the Hydrojet. Throughout the production of the Hydrojet, sustainability will be implemented. This means that toxic and hazardous by-products will be minimised and the energy will originate from green energy sources. Measures will also be taken to mitigate the exhaust fumes by applying filters on ovens and autoclaves for example. Also, the production will follow the lean manufacturing philosophy. During operation of the Hydrojet, fuel will be produced based on green energy sources. This will continue throughout the lifetime of Hydrojet of 25 years. To measure the operational sustainability and costs, an estimation for the Fuel Economy has been made. This has been done by comparing the amount of Energy per 100 km per passenger. The Hydrojet has a fuel economy of 0.861 MJ/100km/kg and the current industry average is 0.894 MJ/100km/kg. Hence the Hydrojet is 3.6 % more fuel efficient. Furthermore, the emissions have been analysed as well. Since burning hydrogen only leads to NO_x emissions, a reduction in total harmful emissions of 99.986 % compared to current civil aviation is achieved. Sustainability on the retirement will be done by recycling most of the aircraft at End-of-Life. 91.3% of the aircraft will be recycled. Lastly a carbon neutral approach is given top obtain no carbon footprint for the total product. This is done by looking at the emissions of different phases of the aircraft and ground facilities. The only two phases that have carbon dioxide emission are the Hydrojet production and retirement phases. The total aircraft has an emission of 981,480 for the production and retirement thereof.

Financial Analysis

For the Hydrojet to be profitable, the costs associated with its development and production have to be estimated. These were estimated using specific costs and the mass for each subsystem from the Class-II mass estimation. The total development cost was estimated to be €4215 million and the production cost per unit €108.6 million. The operational costs of the aircraft affect how attractive it is to potential buyers. This was divided into several parts and semi-empirical methods were used to estimate the costs of these parts. The Direct Operational Cost per flight of the design range of 4500 km was estimated to be €57,995. Furthermore, to better understand the position of the Hydrojet within the current market a strengths, weaknesses, opportunities and threats (SWOT) analysis was done, highlighting the strengths, weaknesses, opportunities and threats. This can be found in Figure 4.

INTERNAL

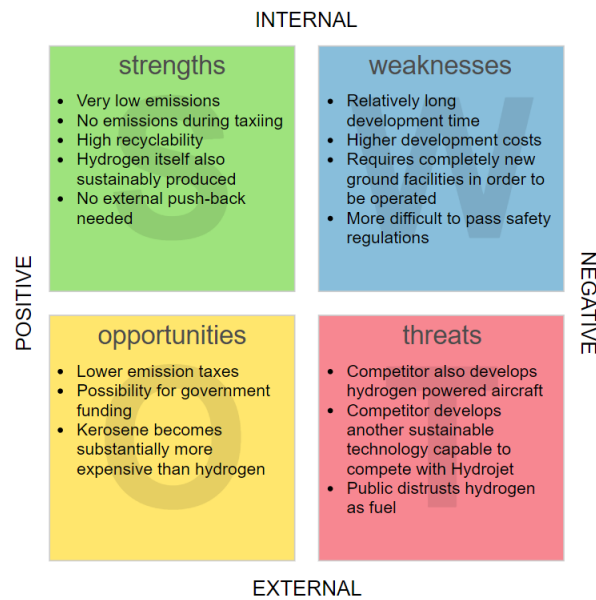| strengths	weaknesses
• Very low emissions • No emissions during taxiing • High recyclability • Hydrogen itself also sustainably produced • No external push-back needed	• Relatively long development time • Higher development costs • Requires completely new ground facilities in order to be operated • More difficult to pass safety regulations
opportunities	threats
• Lower emission taxes • Possibility for government funding • Kerosene becomes substantially more expensive than hydrogen	• Competitor also develops hydrogen powered aircraft • Competitor develops another sustainable technology capable to compete with Hydrojet • Public distrusts hydrogen as fuel

POSITIVE

NEGATIVE

EXTERNAL

Figure 4: SWOT analysis for the marketability of the Hydrojet

Even though the Hydrojet has a lot of strengths that competitors do not have, for the Hydrojet to be competitive its unit cost should not be too high. The unit cost of several competitors was collected and with a weighted average a competitive price of €119.6 million was calculated. This pricing did not take into account the fact that the Hydrojet can be sold for substantially more, because of its sustainability and efficiency. To estimate the potential market share of the Hydrojet the size of the medium range aircraft market was determined accounting for the growth until 2030. Assuming an emission reduction goal for the airliners of 50 % and estimating the market share of hydrogen aircraft in the alternative fuel market, the amount of potential Hydrojet sales was estimated. With this market share the return on investment was assessed. It was estimated that the breakeven point would be at 222 aircraft. Outside of the aviation market further market expansion in other hydrogen related industries can be gained by using the knowledge and experience of developing this system.

Post DSE Activities

After the DSE period is finished, there are still possibilities for future activities. The first of those activities is performing more research into those areas which are known to contain the possibility of inaccuracies. Among these are, first off, the aerodynamics. The wing was slightly over designed causing higher drag than needed. Perhaps a more in-depth analysis could optimise this. The simulation using AVL can also be iterated and improved for better results. Furthermore, since the fuel tanks have a complex shape, a detailed analysis was out of the scope for this project. A more detailed thermodynamic and mechanical analysis could perhaps improve the uncertainties of the design. For the propulsion systems, there has been no real analysis done on the positioning of the engines on the actual aircraft, as well as on the pylon facilitating this integration. More research should be done looking into this aspect of design. And finally, for the materials and structures no real analysis has been performed yet concerning the fatigue life. Such an analysis could perhaps confirm the feasibility of the current design, or otherwise warrant a slight redesign. And lastly, once this design phase is truly finished, and the go ahead is given, there is the possibility for the next phase, which is the detailed design phase.

Conclusion

The feasibility of the Hydrojet from an engineering standpoint has been confirmed, with a design featuring a span of 45 m, a length of 27 m and an MTOM of 92 metric tonnes that complies with all top-level requirements except for the €100 Million production cost (currently €108 Million). Considering the potential of the design, this requirement is not far out of reach. As a consequence, the sustainability of the Hydrojet is confirmed, provided that water can be recycled from sources not serving as potable water. Finally, from a financial standpoint, a Hydrojet unit price of €130 Million and a CASM of 7.8 euro cents was determined. With the added value of great sustainability and at least 3.6 % improved fuel efficiency, the Hydrojet guarantees competitiveness and progress in the current and future market of commercial aviation. Therefore, the overall design of the Hydrojet and its accompanying ground facilities provide a small step for passenger air travel, but a giant leap towards long-term sustainable aviation.

1
Introduction

As the consequences of climate change become more apparent, the protection of the environment is becoming a bigger concern for the general public. With the continual growth of the aviation industry comes a growing impact on the environment. This impact persuades many passengers to choose a more sustainable alternative over air travel, especially for regional flights[1]. These passengers feel a sense of shame for using air travel and contributing to the increase of harmful emissions. This 'flight shame' could push more people to fly less[2], which can have devastating effects on the future of commercial aviation. The aviation industry has the responsibility for its own survival and for the protection of our environment, to look at alternatives to conventional fossil fuel powered aircraft. One solution could be a hydrogen powered aircraft: the Hydrojet. The main reasons for using hydrogen as an energy source are the security of its supply in a sustainable way and the fact that it has the potential of greatly reducing engine emissions. While hydrogen is three times lighter than kerosene for the same amount of energy, the volume needed to store that amount of liquid hydrogen is four times as much as for kerosene. Multiple concepts for hydrogen passenger aircraft have been proposed but none have been realised and proven to be competitive with conventional aircraft. Designing such an aircraft is a challenging task, but since no sustainable alternatives to conventional regional aircraft are in operation, it is also an important one.

The aim of this report is to research the feasibility of the Hydrojet design from an engineering, sustainable and financial perspective such that the top level requirements, set by the project tutor, are met. This is done by designing each subsystem of the concept chosen in the conceptual design phase. After a detailed mass estimation, a performance analysis is done so the subsystems can be designed individually after that. The system is divided into the subsystems planform, landing gear, power and propulsion, and ground facilities. A sustainability and financial analysis are done for the final design to check if it complies with the top level requirements.

This reports begins in Chapter 2 with an overview of the conceptual design process and its results. After that both the Class-I and Class-II mass estimation methods are explained including the iterations between them in Chapter 3. Next, the analysis of the aircraft performance is done in Chapter 4, after which the design of the subsystems are shown. This starts with the planform design in Chapter 5, which consists of the layout, aerodynamics, stability and control and the structure. The next subsystem is the landing gear, which is described in Chapter 6 followed by the power and propulsion system in Chapter 7. The latter is subdivided into the power system, the propulsion, the fuel cell and the fuel tanks. The final subsystem, the ground facilities, is described in Chapter 8. The mass estimation, performance and subsystem chapters also each include verification, validation and risk sections. After that, the final design is presented in Chapter 9 including the interface diagrams and system risk analysis. In Chapter 10 the operations and logistics are discussed, including the reliability, availability, maintainability and safety (RAMS) characteristics. The sustainability in terms of production, operation and retirement of the aircraft is evaluated in Chapter 11 as not only the aircraft but also the aspects surrounding it need to be sustainable. In Chapter 12, a financial analysis is shown in which the market is studied to determine if the Hydrojet can be profitable. In Chapter 13 the compliance matrix is presented. Finally, in Chapter 14 the activities that will occur after the Design Synthesis Exercise (DSE) are discussed.

---

[1] `https://www.bbc.com/news/business-49890057` [accessed on 27 May 2020]

[2] `https://www.bbc.com/future/article/20190909-why-flight-shame-is-making-people-swap-planes-for-trains` [accessed on 29 June 2020]

Conceptual Design

In this chapter, first the main conclusions of the Midterm Report [1] will be presented, after which a functional analysis is performed. Hence, this chapter is the starting point for the subsystem design phase, since the subsystem requirements follow directly from this.

2.1. System Requirements

The requirements from the Baseline Report can be categorised into three categories: Top level requirement, stakeholder requirements and cost, schedule and use of resources requirements.[2] The requirements are listed below in that order.

Top Level Requirements

Sustainability:
HPRA-STK-SUS-1: The aircraft shall emit zero emissions, except for water during operation.
HPRA-STK-SUS-2: The aircraft shall be 90% (weight fraction) recyclable.

Performance:
HPRA-STK-PERF-1: The range of the aircraft shall be sufficient to fly between any two airports in the European Common Aviation Area.
HPRA-STK-PERF-2: Flight times of the aircraft shall be comparable with existing commercial aviation.

Engineering Budget:
HPRA-STK-ENBU-1: The aircraft shall be able to carry 236 passengers and their luggage.
HPRA-STK-ENBU-2: The aircraft shall have a minimum lifetime of 25 years.
HPRA-STK-ENBU-3: The ground hydrogen storage facility shall be suitable to service a fleet of 10 aircraft.

Safety and Reliability:
HPRA-STK-SR-1: The aircraft shall have a 50% availability including turnaround time and maintenance.
HPRA-STK-SR-2: The aircraft shall meet all European aviation standards.
HPRA-STK-SR-3: The aircraft shall have emergency procedures implemented for emergency hydrogen loss.

Cost:
HPRA-STK-COS-1: The aircraft shall have a maximum cost of €100 million.
HPRA-STK-COS-2: The operational costs shall not exceed those of existing comparable commercial aviation.

Stakeholder Requirements

Passenger Requirements:
PRA-STK-PAS-1 The aircraft shall be comfortable for the duration of the flight.
PRA-STK-PAS-2 The propulsion system shall not be substantially louder than conventional propulsion systems.

Residents Requirements:
HPRA-STK-RES-1 The noise produced by the aircraft shall not be of more harm than current aircraft to the residents in the vicinity of the airport.

Airport Requirements:
HPRA-STK-APOR-1 The ground system required shall be implementable in the existing airport infrastructure.
HPRA-STK-APOR-2 The aircraft size shall not exceed the limits of the airport.

Crew Requirements:
HPRA-STK-CREW-1 The work pressure during operation shall not be too straining on cabin personnel.
HPRA-STK-CREW-2 The aircraft shall be controllable by the pilots.
HPRA-STK-CREW-3 The cockpit shall have an engine information display.

Cost, Schedule, Use of Resources

Cost:
HPRA-REQ-COS-3 The maximum cost per available seat mile (CASM) shall not exceed €0.13.

Schedule:
HPRA-REQ-SCH-1 The total aircraft assembly time shall be no longer than 80 days.

Use of Resources:
HPRA-REQ-URE-1 Lean manufacturing shall be implemented as aircraft manufacturing philosophy.
HPRA-REQ-URE-3 The aircraft components shall be produced on multiple sites.
HPRA-REQ-URE-4 The aircraft production facilities shall work on sustainable power.
HPRA-REQ-URE-5 The production equipment shall have a lifetime to at least manufacture a fleet of 10 aircraft.

These requirements define what the product will look like and are therefore called the 'system requirements'. These are taken into consideration at every level of the design phase, and are broken down into further 'subsystem requirements' to design these subsystems relevantly on a deeper level. In the end, if all subsystems comply with their corresponding subsystem requirements and are consequently integrated correctly, the system itself should comply with the system requirements, confirming that the final product is indeed the desired outcome outlined at the start.

2.2. Sustainability Strategy

To guarantee performance of the Hydrojet system (the product) in the long term, it needs to be sustainable. To ensure that any final product contributes to its set sustainability objectives, its design has to incorporate a proper sustainability strategy. The sustainability objective for the Hydrojet project is given here:

Design the Hydrojet system in such a way that its production, operation and retirement can be carried out indefinitely on a big scale without causing harm to the environment, the society or the economy.

This objective is approached by, first of all, incorporating an organisational position in the team structure responsible of implementing the strategy: The Sustainability Officer. This person is responsible for keeping the sustainability goals up to date and known within the team, as well as making sure each engineering department chief implements the corresponding sustainability.

To organise this specifically, there will be a focus on the three main aspects mentioned in the objective:

- Production & Assembly
- Operation & Maintenance
- Retirement

For production and assembly, mainly a qualitative implementation of sustainability is intended, such as selecting energy efficient and waste-minimising manufacturing processes. For operation and maintenance and the retirement, a more thorough quantitative analysis will be made. To organise this specifically, a global overview is made containing all the product's variables that are either direct inputs, derived from direct inputs and/or outputs of external design calculations, sorted per department.

This method allows us to easily track the progress of the design in specific areas, such as the current Recyclability Rate (RR) of the aircraft. This RR is set up using two main inputs: the mass breakdown of the aircraft, which becomes increasingly detailed throughout the project, and the RR of the materials that make up these parts. In this way, a so-called recyclability tree is constructed which is updated along the way. When the total RR dips under the required 90 % (see Req. HPRA-STK-SUS-2), the Sustainability Officer has to discuss with the Materials Department on how to correct this. The same goes for the emissions requirement, where the overview shows the current emissions in grams per kilogram of burned fuel depending on the propulsive

design.

In a more general way, this approach contributes to a fluent systems engineering organisation, facilitates design iterations and assures reproducibility of the work done. This makes the design phase itself sustainable. Finally, after the design of the complete Hydrojet system is made, an analysis will be done estimating the carbon emissions produced throughout the system, and establish policies to cancel these out. This way it is attempted to make the entire Hydrojet system carbon-neutral.

2.3. Concept Selection Description

In order to derive a feasible concept that best fulfils the requirements stated above, a trade-off must be performed by taking into account various criteria deemed critical to the success of the design. Therefore, these criteria must first be defined. After a short analysis, the following criteria were found: thrust over weight of the propulsion system, fuel efficiency of the propulsion system, the lift over drag in clean configuration, the operational empty weight, and the technological readiness level. These criteria were chosen as they most completely encompass the given requirements, while not becoming too many and thereby being convoluted. It should be noted that during this design phase, the cost was estimated as a direct function of operational empty weight, so this means also cost is encompassed in these criteria.

Following these criteria, the chosen design became a blended wing body (BWB), with hydrogen powered turbofan engines, a fuel cell as auxiliary power unit, and an electric motor in the landing gear for taxiing. This is because the blended wing body has a very high theoretical lift over drag in clean configuration, making it very efficient in cruise. The estimated operational empty weight of the blended wing body was very promising too. Moreover, the turbofan engines are also relatively efficient, but were deemed the better option as they have a very high thrust over weight. The only down-side of this design choice is the low technological readiness level of a blended wing design. But since this criterion has been given a relatively low weight, the trade-off indeed put forth the design as is described above.

2.4. Concept Design Characteristics

Now that the final concept has been selected and described, this section will go over the initial design characteristics of the Hydrojet, which will serve as the starting point for the subsystem requirements. Tables 2.1 and 2.2 show the initial aerodynamic parameters and BWB specifications. First of all, a Class-I mass estimation is carried out in order to find the Operational Empty Mass (OEM) and Maximum Take-Off Mass (MTOM) of the aircraft based on reference aircraft. Next, the aerodynamic parameters of the BWB are estimated, also based on reference BWB aircraft for as far as this is possible. Namely, the maximum lift coefficient, $C_{L_{max}}$, and the Oswald efficiency factor, e, both are estimated based on conventional aircraft instead, due to the lack of information on BWBs. Therefore, the accuracy of these parameters is lower. From these parameters, the drag polar is derived and the maximum clean lift-to-drag ratio, L/D, is found.

Table 2.1: Summary of the preliminary aerodynamic analysis [1]

Configuration	$C_{L_{max}}$ [-]	C_{D_0} [-]	e [-]	A [-]
Take-off	2.0	0.0204	0.87	
Clean	1.0	0.00671	0.82	7.57
Landing	2.22	0.0307	0.92	

With all the aerodynamic parameters known, the wing loading - thrust loading diagram is constructed in order to analyse the flight performance characteristics of the aircraft. From this analysis, the required wing surface area, S, and thrust, T, are computed. Consequently, the propulsion system can be sized and the T/W_{prop} of the propulsion system and the fuel economy, η, is found. Lastly, a cost estimation method is performed, which is based on the OEM, and the aircraft cost is found. All the results are included in Table 2.2.

Table 2.2: Initial specifications of the Turbofan Blended Wing Body [1]

OEM [kg]	MTOM [kg]	W_F [kg]	T/W_{prop} [-]	η [%]	Clean L/D [-]	S [m^2]	T [kN]	Cost [€ million]
42,984	76,785	8,801	3.35	36	26.95	214.2	227.5	95

Before the subsystem design can begin using these preliminary concept characteristics, the various subsystems have to be identified. These are the following:

- Planform
- Landing Gear

- Power and Propulsion
- Ground Facilities

In short, the planform consists of the wings and fuselage of the BWB, together with the control surfaces and the internal layout of the cabin and fuel tanks. Next, the landing gear is sized such that feasible integration into the planform can be shown. The power and propulsion systems consist of the two turbofan engines, the fuel cell, the motor in the nosewheel and the corresponding systems needed to operate the aforementioned subsystems. Lastly, the ground facilities includes the airport integration, and the hydrogen production and storage. Besides these subsystems, the aircraft also consists of many other smaller subsystems that will not be designed in this project. This is since they do not influence the feasibility of the final design of the Hydrojet and thus do not contribute to the goal of this project. Rather, they consist of the "Additional subsystems", such as navigation systems, and the "Payload attributes" which support the payload, like the seats.

With the subsystems known, the initial cost and OEM breakdown is presented in Table 2.3 based on the Midterm report.[1] If all the subsystems are added together minus the ground facilities, the result is the complete empty aircraft at OEM. Also, the costs for the final assembly are added. The total cost adds up to €100 million, since this is the available budget according to requirement HPRA-STK-COS-1. The initial budget breakdown sets the cost and weight requirements for the different subsystems, which will ensure that the top level requirements can be met and a feasible design is achieved.

Table 2.3: Initial cost and OEM breakdown from the Midterm report [1]

	Cost breakdown [€ million]	OEM breakdown [kg]
Planform	63.1	20,750.0
Landing Gear	2.4	3,387.8
Power and Propulsion	9.3	7,622.5
Additional subsystems	12.4	8,469.4
Payload attributes	3.9	2,117.4
Final assembly	8.9	0.0
Total	100	42,347

These subsystems have to be designed by the different departments, who have to make sure that the subsystem requirements are met. This is accomplished by applying contingency management during the design of the subsystems, as described in the Baseline report.[2] Contingencies are included because experience has shown that parameters like cost and MTOM always exceed the target values by a certain percentage. By including margins, the targets are more easily met.

2.5. Subsystem Design Approach

At this point, the conceptual Hydrojet design has been discussed, and only some preliminary estimations have been made. In order to check whether the Hydrojet aircraft will be able to meet with the top level requirements, a more detailed design is needed. This means that the subsystems have to be sized and integrated together into the Hydrojet. Many dependencies are present between the different subsystems and even between the departments: the Hydrojet is a complex system. Consequently, an iterative design process is needed. In this section it will be explained briefly in which order the subsystems will be designed to cope with the design freedom, such that in the end a design is accomplished into which all the subsystems can be integrated.

First the planform shape has to be designed. The BWB essentially is composed of two parts: the outer wing part and the fuselage part. The planform design starts with the cabin layout, initial fuel tank shaping and airfoil selection. Then, the shape of the fuselage part of the BWB is formed, such that the cabin and fuel tank can be physically integrated. Next, the outer wing planform is determined mainly by stability and control analysis, for which a certain sweep angle is required. From this the total wing surface area is known, after which a performance analysis outputs the required thrust from the wing loading. This makes it possible to size the propulsion system. In addition, the landing gear can be sized when the planform and Centre of Gravity (CG) excursion are set. Finally, Class-I and II estimations are performed and the MTOM, fuel weight and subsystem weights are updated. At this point, the planform shape is set and the iteration process is started to find the converged design.

Figure 2.1 visualises this iteration process. The different departments and some of their outputs are interrelated with each other, as can be seen. As not all values can be visualised while keeping an overview, only the most important ones are present in the figure. Round boxes indicate the main departments. Class-I and II are not departments within the design but have their own process and are therefore also indicated as main departments. Rectangular boxes contain outputs from the departments and are inputs to others; the dependencies. They continuously change and affect other parameters. Diamond boxes indicate

outcomes from a department and are not inputs to other parameters. However, they still need to be checked after each iteration. For example, the centre of gravity range needs to be checked to make sure the design is still feasible. In case it is not feasible, the required changes will be made (visualised by the dotted lines).
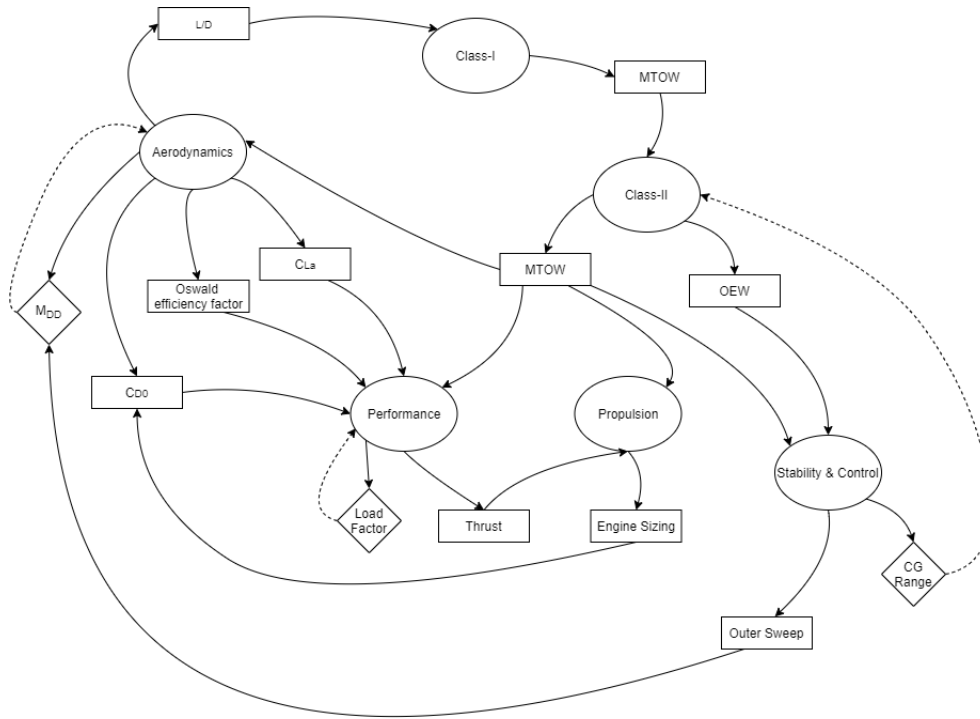

Figure 2.1: Iteration Process

An iteration always starts by updating the Class-I and II weights based on the latest design parameters. Then the flight performance, aerodynamics, stability and control, and propulsion parameters are updated in that order, after which a new mass estimation is performed. In the following chapters, the design process used for each iteration will be explained per subsystem.

2.6. Functional Analysis

In order to design the subsystems, more subsystem requirements are needed besides cost and weight and therefore a functional analysis is necessary. A functional analysis is used to establish what the aircraft must be able to do, and contains a Functional Flow Diagram (FFD), which can be found in Figures 2.2 and 2.3, and a Functional Breakdown Structure (FBS) in Figures 2.4 and 2.5

In the FFD the functions of the aircraft during operation are shown in chronological order with arrows indicating the next function in the order. Some functions can or have to be performed in parallel, these are preceded by an 'AND' junction. Functions that come after an 'OR' junction are optional. This junction indicates that only one of the functions have to be performed. The rhombus represents a conditional path, the function after the rhombus must only be performed if the condition inside of it is met. The top level functions (in red) are subdivided in several second level functions (in blue), which are also shown in chronological order in the same way as the top level.

In the FBS, the second level functions are once again subdivided into third level functions and shown in separate 'AND' trees. These third level functions are not necessarily in chronological order.

As mentioned before, the Functional Flow Diagram and Functional Breakdown Structure are used to find requirements for each subsystem, which will then be used for the detailed design process.
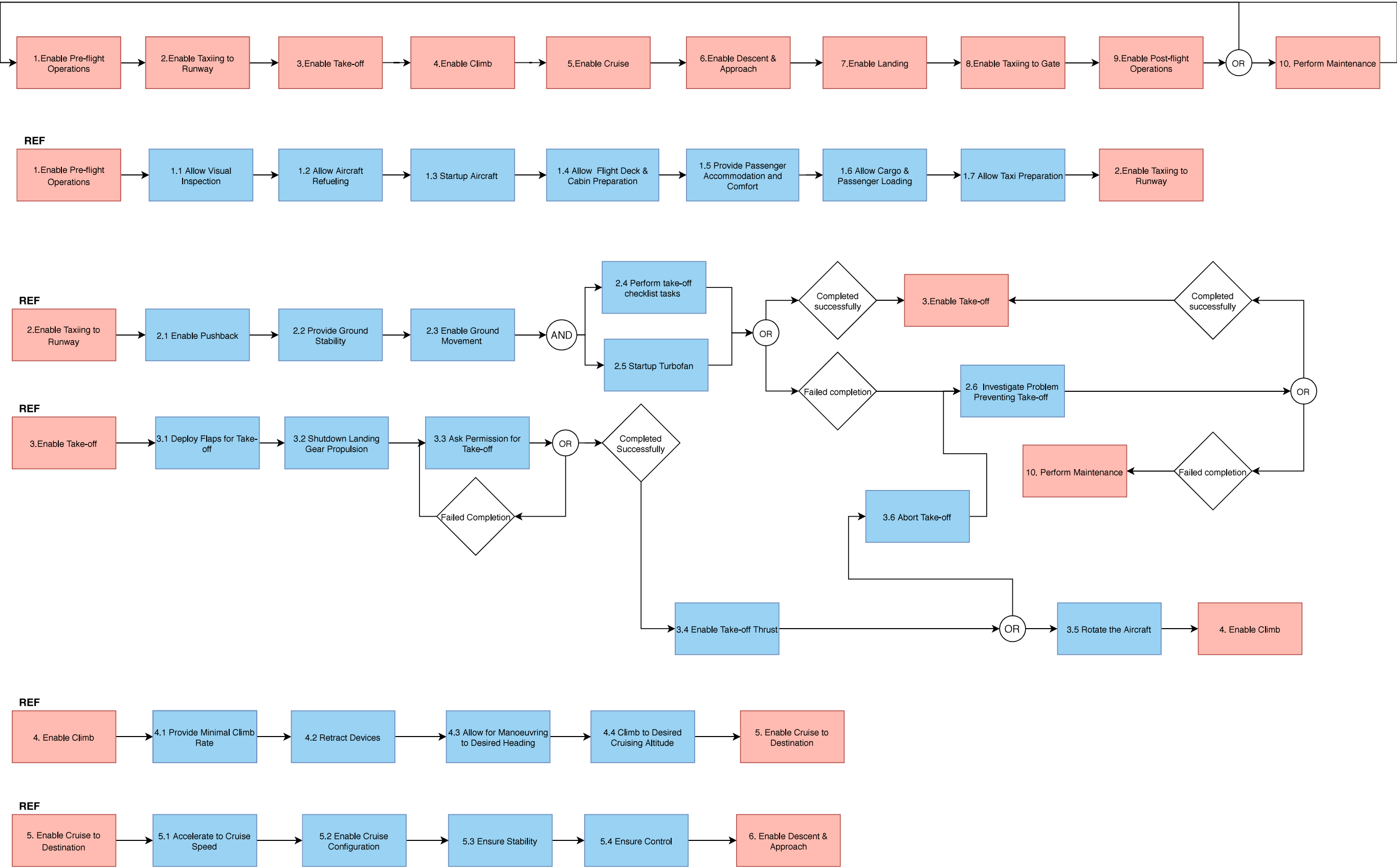
Turnaround
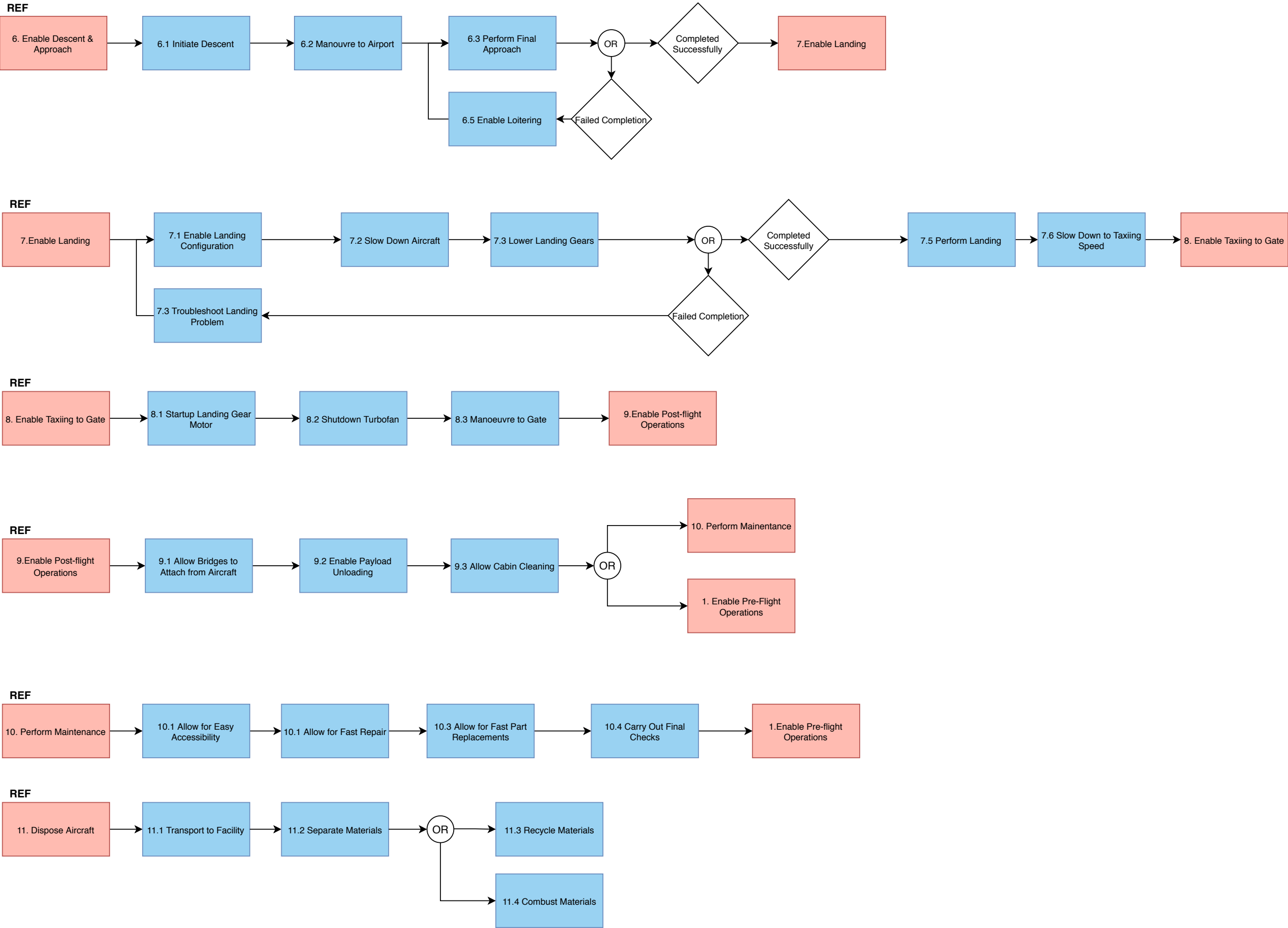

Figure 2.2: Functional Flow Diagram part 1

REF

6. Enable Descent & Approach → 6.1 Initiate Descent → 6.2 Manouvre to Airport → 6.3 Perform Final Approach → OR → Completed Successfully → 7.Enable Landing

6.5 Enable Loitering ← Failed Completion

REF

7.Enable Landing → 7.1 Enable Landing Configuration → 7.2 Slow Down Aircraft → 7.3 Lower Landing Gears → OR → Completed Successfully → 7.5 Perform Landing → 7.6 Slow Down to Taxiing Speed → 8. Enable Taxiing to Gate

7.3 Troubleshoot Landing Problem ← Failed Completion

REF

8. Enable Taxiing to Gate → 8.1 Startup Landing Gear Motor → 8.2 Shutdown Turbofan → 8.3 Manoeuvre to Gate → 9.Enable Post-flight Operations

REF

9.Enable Post-flight Operations → 9.1 Allow Bridges to Attach from Aircraft → 9.2 Enable Payload Unloading → 9.3 Allow Cabin Cleaning → OR → 10. Perform Mainentance

1. Enable Pre-Flight Operations

REF

10. Perform Maintenance → 10.1 Allow for Easy Accessibility → 10.1 Allow for Fast Repair → 10.3 Allow for Fast Part Replacements → 10.4 Carry Out Final Checks → 1.Enable Pre-flight Operations

REF

11. Dispose Aircraft → 11.1 Transport to Facility → 11.2 Separate Materials → OR → 11.3 Recycle Materials

11.4 Combust Materials

Figure 2.3: Functional Flow Diagram part 2
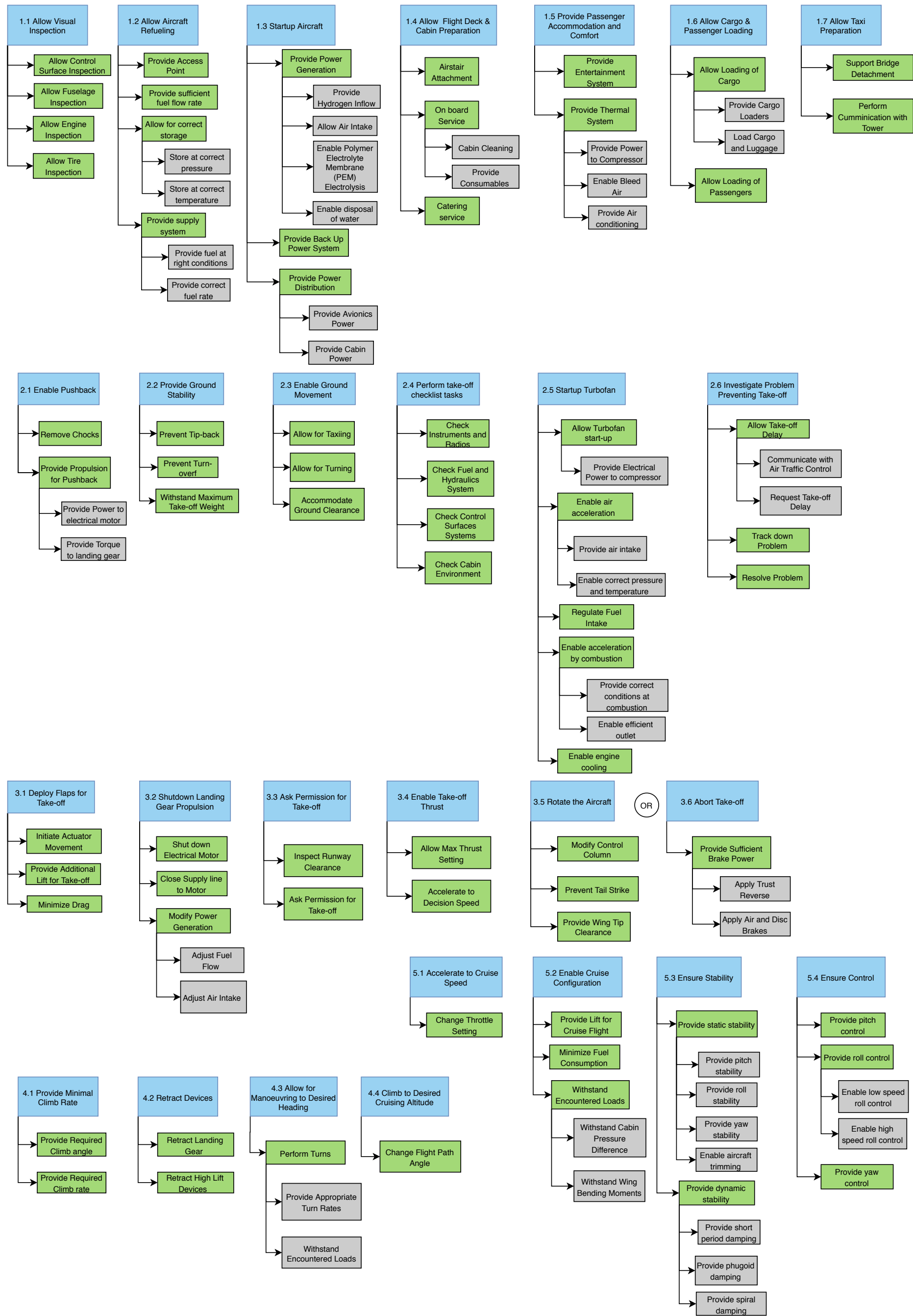
Figure 2.4: Functional Breakdown Structure part 1
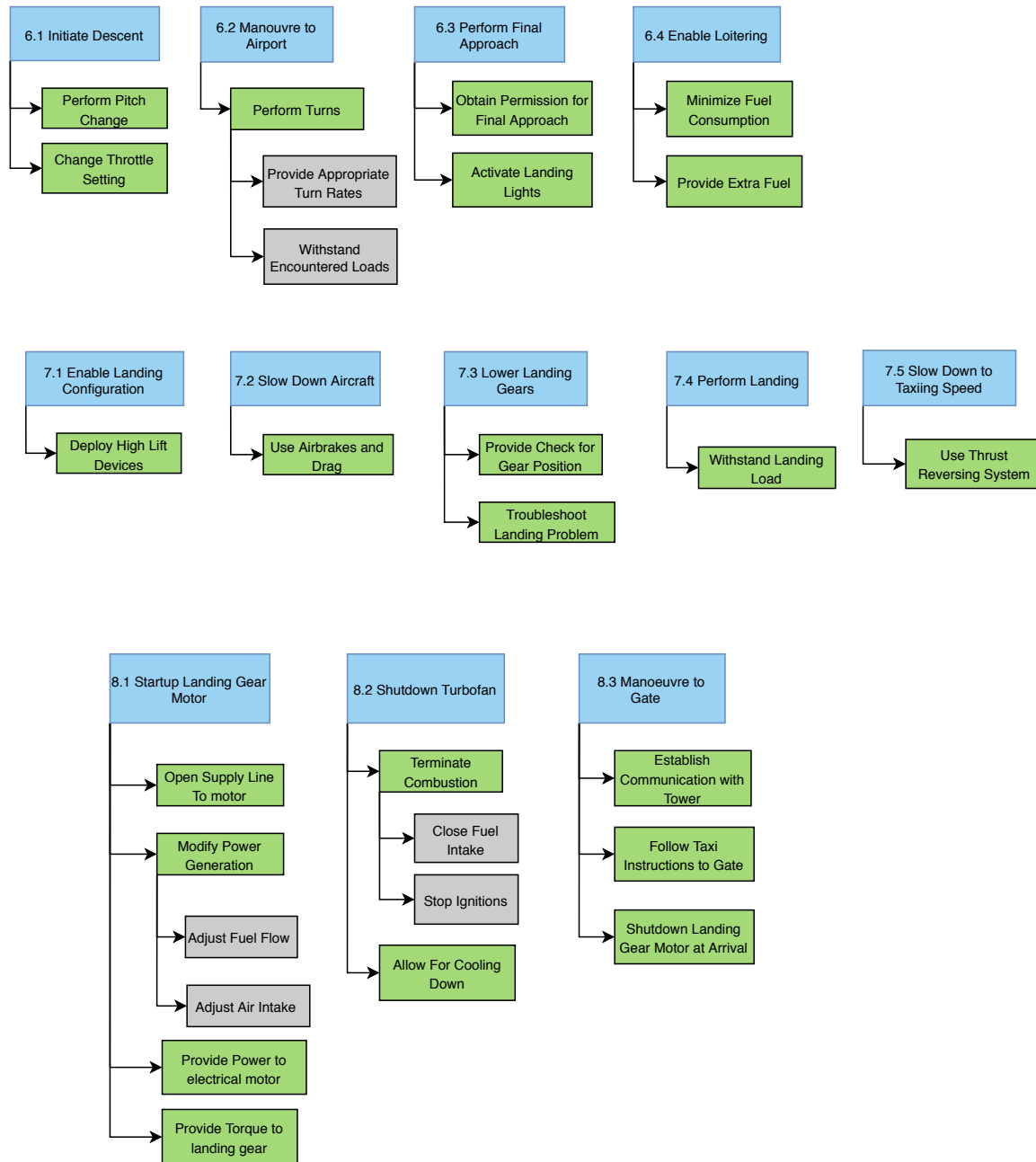
Figure 2.5: Functional Breakdown Structure part 2

<div align="right">

3

Mass Estimation

</div>

For the Hydrojet concept, a more accurate estimation is needed for further analysis and the iteration process. Since this concept consists of a BWB which is also completely propelled using hydrogen, there will be deviations from the traditional weight estimations used for conventional aircraft. The mass estimation can be split into two parts, namely the Class-I and Class-II estimation method. These methods are explained in Section 3.1 and 3.2, respectively. The Class-I was already presented in the Midterm Report [1] and is described briefly in this chapter. Finally, the influence of the results of the Class-I and Class-II method on the iteration process will be discussed in Section 3.3. The verification and validation of the Class-I and Class-II is discussed in Section 3.4.

3.1. Class-I Mass Estimation

The Class-I mass estimation method uses reference aircraft to obtain a regression to estimate the OEM and the MTOM based on statistical fuel fraction. This regression can be found in the Midterm Report.[1] This will give an initial value which serves as an input for the Class-II mass estimation. The Class-I method will result in an MTOM, OEM and fuel mass. The payload will be an input for this method as well but this is already known from the requirements. For the fuel mass, the statistical fuel fractions will be adapted for the mission design profile and the hydrogen propulsion. The main input that is affected by the hydrogen propulsion is the specific fuel consumption (SFC), since using a different fuel will result in a different consumption of the aircraft. The full explanation about the Class-I estimation can be found in the Midterm Report.[1] The inputs used for this design can be found in Table 3.1. The outputs are shown in Table 3.2.

Table 3.1: Inputs for Class-I mass estimation (before iterations)

Inputs			
$m_{payload}$ [kg]	30,000	L/D_{cruise} [-]	21
v_{cruise} [m/s]	260	L/D_{loiter} [-]	22.6
Cruise range [m]	4,500,000	E_{loiter} [s]	3,600
Loiter range [m]	250,000	Gravimetric ratio H_2 [-]	3
SFC [kg/Ns]	5.89E-6	Climb mass fraction [-]	0.98667

Table 3.2: Outputs of Class-I mass estimation (before iterations)

Outputs	
MTOM [kg]	89,293.0
OEM [kg]	49,058.6
m_{fuel} [kg]	10,234.4
Fuel Fraction [-]	0.8854

3.2. Class-II Mass Estimation

The Class-II mass estimation method combines relevant geometry and load parameters, and corrective coefficients to calculate the weight of different components of the aircraft. The geometry and load parameters are estimated using typical values from reference aircraft and calculations.[1] [3] Since the Hydrojet is a BWB, the conventional Class-II weight estimation presented by Roskam, Raymer and/or Torenbeek, are not specific for this type of aircraft. For this reason the method of Howe, which is a Class-II mass estimation method specialised for blended wing bodies, will be used.[4] Additionally, the method of Howe has been selected due to "its ability to model and take geometrical differences into account, its relative accuracy for being a semi-analytical method and its short execution time."[5] The equations used for the Class-II estimation can be found in [4] and [6]. The inputs and outputs for the Class-II mass estimation are shown in Table 3.3 and 3.4, respectively. Most parameters are standard such as the taper ratio λ, the load factor n and the mean aerodynamic chored (MAC). Some less well-known parameters are the outer fuel ratio Q_o, which is the amount of fuel stored in the outer wing as a ratio of the total fuel and the point masses P1, P2, P3 with their respective distance from the center of the BWB Y1, Y2, Y3. A_{bar} is a constant that is suggested to be 1.5 in absence of more specific information. These parameters need to be taken into account due to the BWB configuration. The Howe method specifically gives an estimate for the BWB and uses other Class-II weight estimation methods to give an estimate for the different parts of the aircraft design. The different methods used for the different aircraft components can be seen in Table 3.5. This table shows that the wing and fuselage (thus the BWB) is estimated using two methods. The Bradley method uses a composite wing and the Howe method uses an all metal wing. Since the design of the wing will most likely be a combination of both materials, half of both masses is taken into account for the entire outer wing mass.

Table 3.3: Inputs Class-II mass estimation (before iteration)

Inputs							
MTOM (from Class-I) [kg]	89,293.0	t/c	0.15	T_{TO} [kN]	228	λ_{inner}	0.3835
V_{cruise} [m/s]	260	t/c outer kink	0.15	Mff [-]	0.885	λ_{outer}	0.4
$Range_{cruise}$ [km]	4500	$t/c_{inner\ wing}$	0.15	N_{pax} [-]	236	b_{outer} [m]	13.399
n [-]	3.67	t/c outer wing	0.15	N_{eng} [-]	2	$c_{kink_{outer}}$ [m]	9.77
AR [-]	4.10	t/c_{root}	0.15	N_{pilots} [-]	2	$c_{kink_{inner}}$ [m]	19.978
S [m^2]	493.68	Q_i [-]	1	p_{cabin} [psi]	11.3	S'_{outer} [m^2]	185.11
$S_{inner\ wing}$ [m^2]	310.41	n_{pplant} [-]	0	m_{pax} [kg]	85	S_{cabin} [ft^2]	1,266.93
$S_{outer\ wing}$ [m^2]	183.27	n_{MG} [-]	2	$MAC_{inner\ wing}$ [m]	18.79	S_{aft} [ft^2]	595.013
c_{root} [m]	25.478	P1 [kg]	6,362.57	$MAC_{outer\ wing}$ [m]	7.26	λ aft [-]	0.236
c_{tip} [m]	3.908	P2 [kg]	1,155.305	MAC [m]	14.51	$N_{cabin\ crew}$ [-]	8
location front spar/chord [-]	0.2	P3 [kg]	2,310.609	$w_{inner\ wing}$ [m]	18.41	l_{cabin} [m]	17.478
location rear spar/chord [-]	0.75	Y1 [m]	0	$AR_{inner\ wing}$ [m]	1.067	$n_{containers}$	7
ρ [kg/m^3]	1,900	Y2 [m]	0	$AR_{outer\ wing}$ [m]	3.92	m_{ULD}	80
S_{fin} [m^2]	0	Y3 [m]	3	$\Lambda_{LE_{inner}}$ [deg]	50	m_{bgge}	18.559
Q_o [-]	0	A_{bar} [-]	1.5	$\Lambda_{LE_{outer}}$ [deg]	47	BPR [-]	9.5

Table 3.4: Outputs Class-II mass estimation (before iteration)

Outputs							
m_{covers} [kg]	5,965.36	$m_{fuselage}$ [kg]	12,481.37	$m_{landing\ gear}$ [kg]	4,038.09	$m_{operational\ items}$ [kg]	1,468.40
m_{ribs} [kg]	2,294.37	m_{wing}[kg]	13,857.99	m_{engine} [kg]	9,361.03	OEM [kg]	5,1255.9
$m_{secondary}$ [kg]	3,946.32	$m_{vertical\ tail}$ [kg]	0	$m_{fixed\ equipment}$ [kg]	9,911.68	MTOM [kg]	91,774.8

Table 3.5: Mass estimation method per component [6]

Components	Mass Estimation Method
Wing	Howe/Bradley
Fuselage	Howe/Bradley
Landing Gears	Jenkinson
Engine	Raymer
Nacelle Group	Torenbeek
APU	Kundu
Instruments	GD
Hydraulics	Cranfield Lecture Notes
Furnishing	GD
API	Roskam
Electrical	Cranfield Lecture Notes
Flight Control	Cranfield Lecture Notes
Operational Items	Howe

3.3. Iteration Process & Results

Now that both the inputs and outputs have been given, it can be seen that the OEM and MTOM are being calculated twice. First for the Class-I mass estimation and after that again for the Class-II mass estimation. If the Class-II OEM is put back in the Class-I, an iteration loop is created. This is done in order to converge the OEM after an arbitrary number of iterations. In essence, if the difference of OEM of Class-I and OEM of Class-II is less than 1%, the mass estimation has converged and that mass will be the final mass of the design.[7] In between the iteration loops, the input values will be re-evaluated for each iterated mass estimation, meaning that for every mass estimation the inputs will change. Additionally, a check has been introduced in order to ensure that the value actually converges. This check is done by iterating again even though the difference is less than 1%. This is done in order to see whether the value truly converges and was not a coincidence the first time. The final values for the input and output for the Class-II mass estimation can be seen in Table 3.6 and Table 3.7, respectively.

Table 3.6: Inputs Class-II mass estimation (last iteration)

Inputs									
MTOM (from Class-I) [kg]	86,596.97	τ	0.12	T_{TO} [kN]	284.27	λ_{inner}	0.442		
V_{cruise} [m/s]	239.55	$\tau_{outer\ kink}$	0.098	Mff [-]	0.898	λ_{outer}	0.327		
$Range_{cruise}$ [km]	4,500	$\tau_{inner\ wing}$	0.12	N_{pax} [-]	236	b_{outer} [m]	13.397		
n [-]	2.69	$\tau_{outer\ wing}$	0.098	N_{eng} [-]	2	$c_{kink_{outer}}$ [m]	11.95		
AR [-]	4.23	τ_{root}	0.12	N_{pilots} [-]	2	$c_{kink_{inner}}$ [m]	22.5		
S [m^2]	510.84	Q_i [-]	1	p_{cabin} [psi]	11.3	S'_{outer} [m^2]	188.73		
$S_{inner\ wing}$ [m^2]	323.98	n_{pplant} [-]	0	m_{pax} [kg]	85	S_{cabin} [ft^2]	1,246.78		
$S_{outer\ wing}$ [m^2]	186.86	n_{MG} [-]	2	$MAC_{inner\ wing}$ [m]	20.44	S_{aft} [ft^2]	1,150.21		
c_{root} [m]	27	P1 [kg]	6,362.57	$MAC_{outer\ wing}$ [m]	8.61	λ_{aft} [-]	0.535		
c_{tip} [m]	3.906	P2 [kg]	1,155.305	MAC [m]	16.11	$N_{cabin\ crew}$ [-]	8		
location front spar/chord [-]	0.2	P3 [kg]	2,310.609	$w_{inner\ wing}$ [m]	18.61	l_{cabin} [m]	17.204		
location rear spar/chord [-]	0.75	Y1 [m]	0	$AR_{inner\ wing}$ [m]	1.069	$n_{containers}$	7		
ρ [kg/m^3]	1,900	Y2 [m]	0	$AR_{outer\ wing}$ [m]	3.842	m_{ULD}	80		
S_{fin} [m^2]	2.309	Y3 [m]	3	$\Lambda_{LE_{inner}}$ [deg]	50	m_{bgge}	17		
Q_o [-]	0	A_{bar} [-]	1.5	$\Lambda_{LE_{outer}}$ [deg]	45	BPR [-]	12		

Table 3.7: Outputs Class-II mass estimation (last iteration)

Outputs							
m_{covers} [kg]	5,077.337	$m_{fuselage}$ [kg]	13,385.71	$m_{landing\ gear}$ [kg]	4,061.87	$m_{operational\ items}$ [kg]	1,477.043
m_{ribs} [kg]	1,846.304	m_{wing}[kg]	12,739.50	m_{engine} [kg]	11,354.77	OEM [kg]	52,919.6
$m_{secondary}$ [kg]	3,784.924	$m_{vertical\ tail}$ [kg]	92.315	$m_{fixed\ equipment}$ [kg]	9,970.043	MTOM [kg]	92,315.2

3.4. Verification and Validation

For verification of the Class-I and Class-II mass estimation methods, unit testing has been done on the code. This ensured that both estimation methods presented the correct mass estimations.

3.4.1. Class-I

For the Class-I mass estimation, the statistical regression obtained from the reference aircraft has been calculated with two different methods, indicated by the points shown in Figure 3.1. The first method was a using linear regression between the OEM and the MTOM (the function $OEM(MTOM)$) and the second method was using a linear regression between OEM/MTOM and MTOM (the function $\frac{OEM}{MTOM}(MTOM)$. If the second function then is multiplied by MTOM, it becomes another version of the function $OEM(MTOM)$, which ought to be more accurate since it takes into account the ratio of OEM and MTOM, and becomes a quadratic equation. As expected, the second method showed a better R^2 value than the linear regression (a 7.5 % difference). Using both these regressions the OEM has been calculated which are, respectively, 50,488.1 kg and 58,598.0 kg. This is a difference of 16%. Comparing these values to the OEM from Table 3.7, it can be seen that these values are close the converged value and are thus therefore verified.
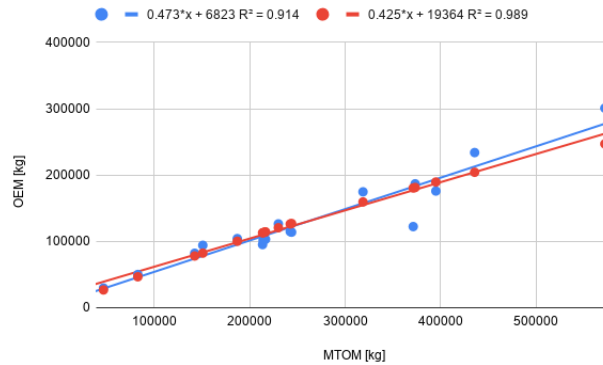

Figure 3.1: Linear regression compared to quadratic fraction regression.

3.4.2. Class-II

The Class-II method uses two types of methods to calculate the BWB mass. The other components are calculated using existing methods such as Raymer and Torenbeek, which have been considered as a benchmark in nowadays conceptual aviation design.[8] Therefore, these methods are considered to be validated. Consequently, the focus for unit testing has been on the BWB mass. The difference in BWB mass can be seen in Table 3.8 for both methods. These methods show quite a significant difference. This can be explained by the difference in components that both estimation methods take into account. Bradley uses the outer wing mass, the cabin mass and the mass aft body of the blended wing. Howe only takes the ribs, covers and a mass penalty of the inner and outer wings. For this reason the Bradley method was expected to be higher which is the case. Howe states that the simplifications made in the derivation of the wing covers leads to an accuracy of the estimations within 5% for $0.4 < y_k < 0.7$ and no more than 10% for $0.25 < y_k < 0.9$ where y_k is the ratio of the wing span to reference span. The Hydrojet has a y_k of 0.44 and 0.56 for the outer wing and inner wing, respectively. Therefore, the error should not be more than 5%.

Table 3.8: Howe and Bradley BWB estimation

Bradley Wing mass [kg]	Howe Wing mass [kg]	Difference [%]
15,364.46	10,715.71	43.38

For the Class-II weight estimation, a verification method is to input the values of an existing BWB into the program. If the program yields around the same magnitude for the MTOM and OEM, the program will be verified. A problem that was encountered using this method is that there was no data available about the geometry of existing blended wing designs. This task will thus be more explicitly done when there is more research available about BWB designs.

Moving on to validation, the weight fractions of different blended wing bodies can be used to validate the Class-II mass estimation. This has been shown in Table 3.9. Since the most comparable BWB design was the BWB250 due to its similar mission and number of passengers, this BWB design has been chosen to validate the Hydrojet.[9] From the table, it can be seen that the weight fractions do not differ significantly from the BWB250 design. Therefore, the Hydrojet is validated. Additionally, since there are no current full scale BWB designs built, a way to validate the Class-I and Class-II weight estimation is by actually building the Hydrojet and putting it on a scale, or waiting for another BWB design to be produced and validating with its weight. This will show whether the method is actually representing real BWB aircraft values. Furthermore, for the Class-II mass estimation, during the production of the various components of the BWB, each component can be put on a scale in order to compare its weight with the calculated weight from the Class-II weight estimation. Since both of these methods are in need of the aircraft actually being built, the validation will be postponed to the manufacturing phase of the Hydrojet due to the absence of other existing BWB aircraft.

Table 3.9: Difference in mass fractions between different BWB designs [9]

	OREIO	N2A-EXTE	SAX-40	BWB150	BWB250	BWB400	Hydrojet
Structure	0.254	0.241	0.315	0.241	0.225	0.264	0.283
Fuselage	0.12	0.144		0.183	0.149	0.185	0.145
Wing	0.129	0.078		0.053	0.068	0.071	0.138
Vertical tail	0.005	0.019		0.006	0.007	0.008	0.001
Landing gear	0.041	0.046	0.044	0.034	0.027	0.029	0.044
Engine & Nacelle	0.105	0.069	0.111	0.084	0.072	0.07	0.123
Fixed equipment	0.133		0.154	0.125	0.11	0.101	0.108
Engine systems	0.001			0.009	0.008	0.008	
Fuel systems	0.019			0.002	0.001	0.001	
APU	0.002			0.008	0.008	0.008	0.001
Flight cont. & Hydraulics	0.025	0.029		0.012	0.009	0.008	0.022
Electrical	0.008			0.006	0.003	0.003	0.017
Pneumatics & air-con	0.017	0.001		0.002	0.001	0.001	0.004
Furnishing & eqpt.	0.012	0.064		0.067	0.064	0.059	0.062
Instruments	0.009			0.019	0.015	0.012	0.0124
Load & Handling	0.025						
Empty Mass	0.518	0.469		0.484	0.434	0.464	0.540
Operational Items	0.005	0.007		0.045	0.036	0.037	0.016
OEM	0.523	0.476	0.624	0.529	0.469	0.501	0.573
Mission fuel	0.267	0.306	0.22	0.185	0.274	0.255	0.102
Payload	0.21	0.218	0.155	0.285	0.257	0.245	0.325
MTOM [t]	216	214	151	72	170	261	92.3

4

Aircraft Flight Performance

Once the Class-II weight estimation is done, the results can be used in calculations for the various subsystems. Prior to the detailed analyses of the different subsystems, the performance characteristics of the Hydrojet need to be assessed first in more detail. In this chapter, the flight performance of the Hydrojet will be analysed such that it will meet with the requirements that have been set with respect to performance. Firstly, the performance requirements are listed in Section 4.1. Then, the Hydrojet will be designed according to these requirements in Section 4.2, for which some of the aerodynamic and planform parameters from later sections are needed. Lastly, the flight performance models/codes will be verified and validated in Sections 4.3 and 4.4 respectively.

4.1. Performance Requirements

Before starting with the computation, an overview is needed of what the performance expectations are. Therefore, the requirements are given below.[2]

Performance

General:

HPRA-REQ-WEI-1 The maximum weights corresponding to the aircraft operating conditions, environmental conditions and loading conditions shall not exceed the highest weight at which compliance with each applicable structural loading and flight requirement is shown.

HPRA-REQ-WEI-2 The minimum weights at which compliance with each applicable requirement of this CS-25 is shown, shall not be lower than the design minimum weight.

HPRA-REQ-C&M-6 During take-off with a speed of V_2 the aircraft shall have a minimal manoeuvring bank angle of 30 degrees.

HPRA-REQ-C&M-7 During en-route with a speed of V_{FTO} the aircraft shall have a minimum bank angle of 40 degrees.

HPRA-REQ-C&M-8 During landing with a speed of V_{REF} the aircraft shall have a minimum bank angle of 40 degrees.

HPRA-REQ-C&M-9 The positive limiting load factor must be higher than 2.5 g with high lift devices retracted and 2.0 g with the high lift devices extended.

HPRA-REQ-C&M-10 The negative limiting load factor must be more negative than -1.0 g with high lift devices retracted up to V_C and 0 g with the high lift devices extended.

HPRA-REQ-STR-3 The negative limit manoeuvring load factor shall vary linearly from the value at V_C to zero at V_D.

Take-off:

HPRA-REQ-TO-1 The reference stall speed V_{SR} shall not be less than a 1.0 g stall speed.

HPRA-REQ-TO-2 The V_{EF} (calibrated airspeed at which the critical engine is assumed to fail) shall be higher than V_{MCG} (minimum ground control speed).

HPRA-REQ-TO-3 The V_1 (speed beyond which takeoff should no longer be aborted) shall be higher than V_{EF} plus the speed gained with the critical engine inoperative during the time interval between the instant at which the critical engine is failed and the instant at which the pilot recognises and reacts to the engine failure.

HPRA-REQ-TO-4 The $V_{2_{min}}$ shall not be less than $1.13 \cdot V_{SR}$ and $1.10 \cdot V_{MC}$.

HPRA-REQ-TO-5 The V_2 (take-off safety speed) shall be selected in such a way that it provides sufficient gradient of climb (TBD CS 25.121b).

HPRA-REQ-TO-6 The V_2 shall be larger than $V_{2_{min}}$.

HPRA-REQ-TO-7 The V_2 shall be larger than V_R plus the speed increment attained before reaching a height of 11 m above the take-off surface.

HPRA-REQ-TO-8 V_2 shall be higher than V_{MC}.

HPRA-REQ-TO-10 The accelerate-stop distance on a dry runway shall meet the CS25.109 requirement.

HPRA-REQ-TO-11 The accelerate-stop distance on a wet runway shall meet the CS25.109 requirement.
HPRA-REQ-TO-15 The control surface shall enable attitude control at the $V_{2_{min}}$ for take-off.

Cruise:
HPRA-REQ-PER-2 The aircraft shall have a range of at least 4500 km.
HPRA-REQ-PER-3 The aircraft shall have a cruise speed of at least 0.8 Mach.
HPRA-REQ-PER-4 V_D shall not exceed $V_C/0.8$.

Go-around:
HPRA-REQ-LCL-1 In the landing configuration the steady gradient of climb may not be less than 3.2 % with the engines at the thrust that is available 8 seconds after initiation of the go-around thrust setting and at a speed of V_{Ref} (CS 25.125).

Climb one-engine-inoperative (OEI):
HPRA-REQ-COE-1 The climb gradient with one-engine-inoperative shall be positive for two-engined aeroplanes, 0.3 % for three-engined and 0.5 % for four-engined.

Landing:
HPRA-REQ-LAN-1 The landing distance shall not exceed 2000 meters.
HPRA-REQ-LAN-3 A stabilised approach with a calibrated airspeed of not less than V_{Ref} shall be maintained down to a 15 m height.
HPRA-REQ-LAN-4 V_{Ref} shall be larger than $1.23 \cdot V_{SR0}$.
HPRA-REQ-LAN-5 V_{Ref} shall be larger than V_{MCL}.
HPRA-REQ-LAN-7 The aircraft shall have a minimum control speed (V_{MC}) lower than $1.13 \cdot V_{SR}$.

4.2. Aircraft Design Performance

In this section, the Hydrojet will be designed for the performance requirements. Firstly, the the so-called V-speeds will be presented, followed by the wing-loading thrust-loading diagram from which the required thrust will follow. Then, the flight envelope is constructed to define the manoeuvring space of the aircraft and the load factors it will encounter. After that, the climb performance diagram is created, which is mainly used to verify the wing-/thrust-loading diagram. Finally, the payload-range diagram is obtained with which the operational capabilities of the Hydrojet will be investigated.

4.2.1. V-Speeds

The so-called V-speeds follow almost directly from the performance requirements. They can be used by the stability and control department to size the control surfaces. In addition, they give the pilot the ability to safely operate the aircraft. For instance, the pilot should be able to safely abort or continue take-off in case an engine become inoperative before or after the decision speed V_1. In such a situation, the Hydrojet should still be controllable without any exceptional pilot skills. The V-speeds are presented in Table 4.1, divided between the take-off phase and landing phase. In Figure 4.1, a schematic is present with the V-speeds for take-off in increasing order for a successful take-off.

Table 4.1: The Hydrojet V-speeds for take-off and landing

Take-Off		Landing	
V_{MCG} [m/s]	63.86	V_S [m/s]	55.13
V_{EF} [m/s]	65.16	V_{SR} [m/s]	57.89
V_{MC} [m/s]	65.41	V_{MCL} [m/s]	65.41
V_1 [m/s]	68.59	V_{Ref} [m/s]	67.81
V_R [m/s]	69.99		
V_{2min} [m/s]	71.95		
V_2 [m/s]	73.49		

The V-speeds were found by first computing the stall speed of the aircraft and then to compute the other V-speeds according to the requirements in the following order: V_{SR} is a defined reference stall speed, V_{Ref} is the reference approach speed at 15 m above the runway and $V_{MC}=V_{MCL}$ is the minimum control speed with one-engine-inoperative (OEI) in clean and landing

configuration. V_{2min} is the minimum speed at which take-off with OEI can be performed, V_R is the speed at which the nosewheel separates from the ground, V_1 is the take-off decision speed, V_{EF} is the speed at which engine failure is assumed to occur, V_{MCG} is the minimum ground control speed and finally V_2 is the safety speed for take-off with OEI. The requirements which state that a minimum bank angle must be sustained at a certain speed, such as requirements HPRA-REQ-C&M-6 and HPRA-REQ-C&M-8, were converted to a load factor, which then was used to compute the stall speed for that load factor. For the first example with V_2, the bank angle of 30 deg is the same as a load factor of $1/\cos(30 \text{ deg}) = 1.15$.
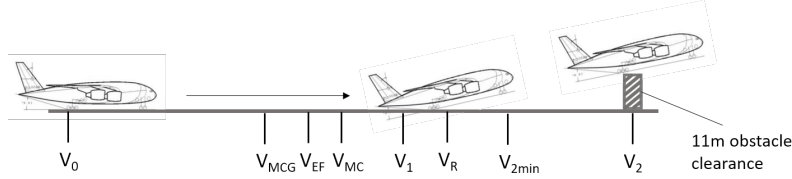
Figure 4.1: Take-off V-speeds. Edited from [10]

Now it is possible to, for instance, size the control surfaces such that they can provide rotation around the main landing gear at V_R. However, this is out of the scope of this project.

4.2.2. Wing Loading - Thrust Loading Diagram

Now that the V-speeds are known, the aircraft design can be further characterised. The wind loading - thrust loading diagram will result in the required wing surface area and the required maximum thrust as fractions of the MTOW. In this way, all flight performance requirements can be achieved and the propulsion system and wing will not be over designed. This diagram was also present in the Midterm report, but it is constantly updated with the latest aerodynamic parameters.[1] In this subsection, it will be explained how the wing loading (W/S) - thrust loading (T/W) diagram was constructed by stating the equations that correspond to each line in this diagram. The equations are based on the method presented in [3]. However, some equations have been modified. Namely, the landing requirement has been adapted for the runway altitude, multiple equations have been adjusted for aircraft weight and thrust setting if this was not the case already, the climb requirement has been revised substantially and finally, the OEI requirement was corrected for the number of engines.

First of all, the aircraft should be able to land on a runway such that the landing distance, D_{runway} does not exceed 2000 meters according to requirement HPRA-REQ-LAN-1. From this, the maximum allowable stall speed in landing configuration, V_{S0}, was found [3]:

$$V_{S0} = \sqrt{\frac{D_{runway}}{0.5847}} \tag{4.1}$$

It should be mentioned that the Hydrojet has no high lift devices, as will be explained in Subsection 5.3.4. Thus, the clean stall speed is the same as the landing stall speed. From this stall speed and a given $C_{L_{max}}$, the maximum wing loading that satisfies this stall speed can be obtained:

$$\frac{W}{S} = \frac{1}{f_{land}} \frac{1}{2} \rho_0 \cdot V_{S0}^2 \cdot C_{L_{max}} \cdot \sigma \tag{4.2}$$

Since this stall speed only needs to be achieved at maximum landing weight, the wing loading is corrected with a factor f_{land}, which is defined as the ratio between maximum landing weight and MTOW. This fraction is determined in the Class-I estimation in Chapter 3. Also, the altitude of the runway influences the air density, which is why the correction factor σ was added. It is defined as the ratio between runway air density and sea level air density. In the end, Equation 4.1 shows that V_{S0} has a maximum of 58.5 m/s and Table 4.1 showed that the stall speed of the Hydrojet equals 57.89 m/s. Thus, the Hydrojet meets with the landing distance requirement. Next, the take-off requirement line was established with equation [3]:

$$\frac{T}{W} = \frac{1}{TOP \cdot C_{L_{TO}} \cdot \sigma} \frac{W}{S} \tag{4.3}$$

The take-off parameter, TOP, is determined with the Raymer method, which relates the take-off distance and number of jet engines to the required TOP.[11] For the take-off distance, again 2000 meters is taken such that the aircraft can land and take-off from the same runway. The lift coefficient for take-off, $C_{L_{TO}}$, is related to $C_{L_{max}}$ as follows [3]:

$$C_{L_{TO}} = \frac{C_{L_{max}}}{1.1^2} \tag{4.4}$$

It was assumed that the runway is situated at sea level altitude, since the airports at which the Hydrojet is designed to operate, are located close to sea level altitude. Namely, the target market is Europe. This means that $\sigma = 1$ and that the Hydrojet will still be able to take-off from airports at higher altitudes, but at a take-off weight below MTOW. As an example, if the Hydrojet were to land on the airport of Madrid, which is located at 610 m altitude[1], a 17 % reduction of the design payload is needed for take-off. Landing is not affected and a 2000 m runway length is assumed. However, the runway length of this airport is at least 3500 m. Consequently, the Hydrojet can easily operate at MTOW at Madrid airport and the assumption $\sigma = 1$ is valid.

Besides take-off and landing, the propulsion system and wings also have to be sized for the cruise phase. This is to make sure that the Hydrojet can maintain horizontal flight at cruise velocity and altitude, where engine performance is affected by the low air density. The following equation incorporates all of these factors [3]:

$$\frac{T}{W} = \frac{f_{cruise}}{\tau_{set}} \left(\frac{\rho_0}{\rho} \right)^{3/4} \left[\frac{C_{D_0} \frac{1}{2} \rho V_{C_{TAS}}^2}{f_{cruise} \frac{W}{S}} + f_{cruise} \frac{W}{S} \frac{1}{\pi A e \frac{1}{2} \rho V_{C_{TAS}}^2} \right] \tag{4.5}$$

The correction factor f_{cruise} is defined as the maximum cruise weight over the MTOW and is incorporated because the aircraft will never fly at cruise altitude with MTOW. This fraction is also determined by the Class-I estimation. τ_{set} represents the thrust setting which is selected by the pilot in cruise. It was assumed that $\tau_{set}=80$ % since it is undesired to fly with 100 % thrust setting during cruise. The latter would mean that the flight ceiling is equal to the cruise altitude if the T/W for cruise is sizing for the design, and this would limit the operational use of the aircraft. Besides that, the thrust loading is also dependent on the air density at cruise altitude, since it is assumed that the thrust decreases with the air density according to the following relation [3]:

$$\frac{T}{T_0} = \left(\frac{\rho}{\rho_0} \right)^{3/4} \tag{4.6}$$

A cruise altitude of 10 km was selected, which lies in the lower range of typical cruise altitudes for passenger aircraft. This was done for two reasons: from Equation 4.5 it became clear that a cruise altitude of 11 or 12 km required less thrust than at 10 km, so 10 km was more critical. Even more important is the fact that NO_x emissions cause less harm to the ozone layer at 10 km compared to higher altitudes. This is because the ozone layer starts at 10 km[2] and relatively little ozone is present at that altitude. Lastly, the cruise requirement is also dependent on the aerodynamic parameters C_{D_0}, A, and e, and on the cruise velocity, $V_{C_{TAS}}$, in true airspeed (TAS). $V_{C_{TAS}}$ was found to be equal to 239.6 m/s at cruise altitude and cruise Mach 0.8, according to HPRA-REQ-PER-3, with which flight times of the aircraft will be comparable to existing commercial aviation. In the Midterm report, it was decided, based on reference aircraft, that the Hydrojet should be able to achieve a steady rate of climb, ROC, of 14 m/s at sea level altitude, MTOW and 100 % thrust setting.[1] From this, the T/W for the ROC requirement is computed as follows:

$$\frac{T}{W} = \frac{ROC}{\sqrt{\frac{W}{S} \frac{2}{\rho C_L}} + \frac{C_D}{C_L}} \tag{4.7}$$

This equation is the result of a small angle approximation, due to which it is assumed that the lift equals the weight. However, from this equation it is unknown at which C_L and corresponding airspeed, the minimum T/W can be achieved for a certain ROC. For this, two additional equations are required:

$$C_L = \frac{W}{S} \frac{2}{\rho V^2} \tag{4.8}$$

$$C_D = C_{D_0} + \frac{C_L^2}{\pi A e} \tag{4.9}$$

By combining Equations 4.7, 4.8 and 4.9, it becomes possible to compute the required T/W for a given W/S for a range of different airspeeds and thus to find the minimum T/W for that wing loading. This process in shown in Figure 4.2 and it is repeated for all W/S in the wing loading - thrust loading diagram.

Lastly, requirements HPRA-REQ-LCL-1 and HPRA-REQ-COE-1 state that a certain climb gradient, c/V, should be achieved in a go-around and OEI situation respectively. To compute the T/W required for a go-around, the following relation is used:

---

[1]https://skyvector.com/airport/LEMD/Madrid-Adolfo-Suarez-Madrid-Ba-Airport [accessed on 29 June 2020]

[2]https://ozonewatch.gsfc.nasa.gov/facts/SH.html#:~:text=The%20peak%20concentration%20of%20ozone,per%20million%20(0.0015%20percent). [accessed on 19 June 2020]

$$\frac{T}{W} = \frac{1}{\tau_{set}} \left[\frac{c}{V} + 2\sqrt{\frac{C_{D_0}}{\pi Ae}} \right] \tag{4.10}$$

c/V should equal 3.2 % and it is assumed that a thrust setting, τ_{set}, of 60 % can be achieved 8 seconds after initiation of the go-around thrust setting.

The equation for OEI is very similar to the go-around. However, the thrust setting is 100 % in this case and the thrust needs to be corrected for the fact that one engine is inoperative. In this case, $c/V = 0$ % is taken as an absolute minimum and the number of engines, $N_{eng} = 2$. In the end, it must be checked that $c/V > 0$ %.

$$\frac{T}{W} = \frac{N_{eng}}{N_{eng} - 1} \left[\frac{c}{V} + 2\sqrt{\frac{C_{D_0}}{\pi Ae}} \right] \tag{4.11}$$

Taking all the requirements explained above into account, the wing loading - thrust loading diagram in Figure 4.3 is constructed and a design point of $W/S = 1772$ N/m^2 and $T/W = 0.314$ is found, indicated by the red dot. The value of W/S is not chosen but depends on the MTOW and wing surface area, S. This is due to the fact that the MTOW follows from the class-II estimation performed in Chapter 3 and S from the aircraft planform, which will be defined in Chapter 5. Consequently, the aircraft has a relatively low wing loading and the required thrust, T, follows directly from the thrust loading diagram, by multiplying the T/W by the MTOW. The final inputs and outputs for this diagram can be found in Tables 4.2 and 4.3 respectively.
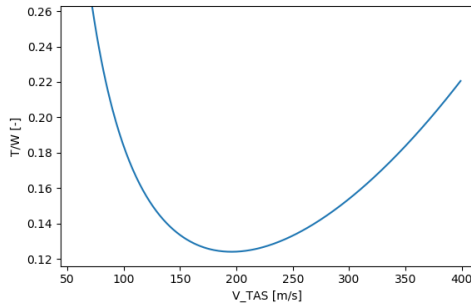
Figure 4.2: Thrust loading - V_{TAS} diagram (W/S=1800)
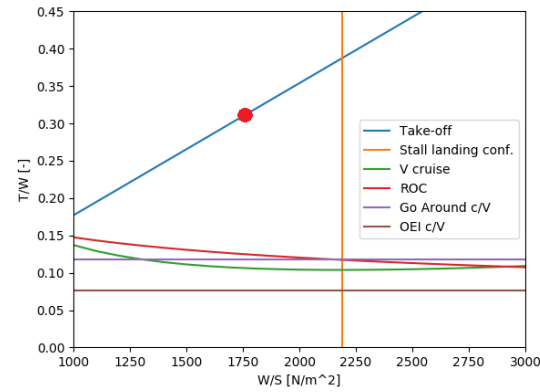
Figure 4.3: Wing loading - thrust loading diagram (W/S=1772, T/W=0.314)

Table 4.2: Inputs of the wing loading - thrust loading diagram

Inputs			
MTOW [kg]	92,315	$C_{L_{max}}$ [-]	0.952
S [m^2]	510.8	C_{D_0} [-]	0.003386
M_{cruise} [-]	0.8	A [-]	4.23
Cruise altitude [km]	10	e [-]	0.689
D_{runway} [m]	2,000	f_{land} [-]	0.910
Runway altitude [km]	0	f_{cruise} [-]	0.956
c/V Go-around [-]	0.032	ROC [m/s]	14
c/V OEI [-]	0.00		

Table 4.3: Outputs of the wing loading - thrust loading diagram

Outputs	
V_{S0} [m/s]	58.5
$V_{C_{TAS}}$ [m/s]	239.6
T [kN]	284.3

4.2.3. The Flight Envelope

The flight envelope is constructed to define the operational range within which the Hydrojet will be able to operate. Additionally, the maximum load factor that the aircraft may experience during flight is computed, for which the structure of the aircraft needs to be designed. The method used to construct the flight envelopes, is based on the CS-25 requirements and is presented in [12]. First the manoeuvrability envelope was constructed. From requirements HPRA-REQ-C&M-9 and HPRA-REQ-C&M-10 follows that the maximum limiting load factor must be at least 2.5 g and the minimum limiting load factor must be more negative than -1.0 g, so these values limit the top and bottom of the manoeuvrability envelope. The left limit is determined by the stall speed of the aircraft in equivalent airspeed (EAS), V_{Sn}, at different load factors n, ranging from -1 to 2.5. The line is computed with Equation 4.12 and the design manoeuvring speed, V_A, is the speed at which the aircraft stalls for the maximum load factor of 2.5.[12] This means that the aircraft is not able to sustain horizontal flight with a bank angle of $acos(\frac{1}{2.5}) = 66.4$ deg below this speed, but above the design manoeuvring speed that bank angle can be achieved.

$$V_{Sn} = \sqrt{\frac{|n|\frac{W}{S}}{\frac{1}{2}\rho_0 C_{L_{max}}}} \tag{4.12}$$

The right limit of the manoeuvrability envelope is set by the dive speed, V_D. Requirement HPRA-REQ-PER-4 states that V_D shall not exceed $V_C/0.8$, where V_C is the cruise velocity. However, at high altitudes, the dive speed will be limited by transonic conditions on the wing which could lead to buffeting. The A320[3] has a dive Mach number, M_D of 0.89 which was also selected for the Hydrojet. V_C and V_D were both converted into EAS based on the cruise altitude and V_D then defines the upper right corner of the envelope and V_C the right corner at $n = -1.0$. This means that requirement HPRA-REQ-STR-3 is complied with.

From the manoeuvrability envelope in Figure 4.4, it becomes clear that there is sufficient room for manoeuvres between V_A and V_C and that V_D is significantly higher than V_C. This is important since the dive speed should not accidentally be exceeded when flying at cruise velocity, since this could cause dangerous aerodynamic loads on the aircraft.

Table 4.4: Gust velocities U at different airspeeds [12]

Altitude [m]	Gust at V_B [m/s]	Gust at V_C [m/s]	Gust at V_D [m/s]
0 - 6,100	20.12	15.24	7.62
6,100 - 15,250	20.12 - 11.5	15.24 - 7.62	7.62 - 3.81

Next, the gust envelope is governed by the gust velocities presented in Table 4.4, which depend on the altitude and airspeed of the aircraft. Above 6100 m altitude, the gust velocities can be interpolated linearly according to that table. The load factor for gusts can be found with the following equation [12]:

$$n_g = 1 + \frac{1}{2}\frac{\rho_0 C_{L_\alpha}}{\frac{W}{S}} U_{EAS} V_{EAS} K_g \tag{4.13}$$

For this equation, C_{L_α} of the aircraft is required since it relates the change in lift to the change in angle of attack due to a vertical gust. U_{EAS} represents the gust velocity for a given altitude and airspeed. K_g is the gust alleviation coefficient, which can be computed with Equation 4.14. The gust velocities are thus straight lines in the gust envelope as can be seen in Figure 4.5, since n_g varies linearly with the EAS.
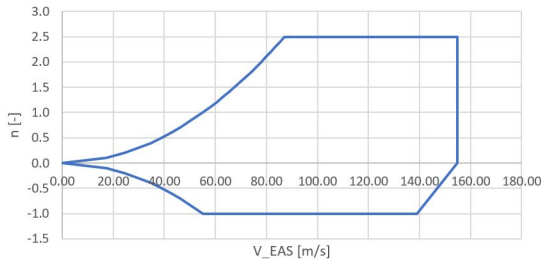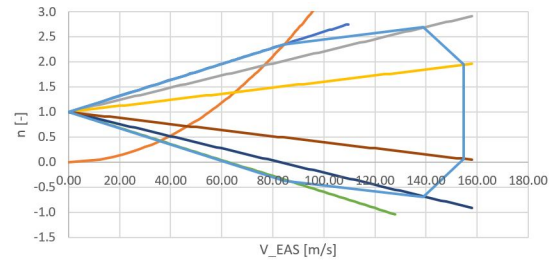

Figure 4.4: Manoeuvrability envelope

Figure 4.5: Gust envelope at 6100 m altitude

The bad weather design speed, V_B, corresponds to the intersection point between the gust speed at V_B and the stall curve. If the pilot is to fly below this speed during bad weather, there is a risk that the aircraft stalls due to a gust. The next corner of the gust envelope, is the intersection of the gust speed at V_C and V_C itself. The corners which lie the furthest to the right, are the intersections of the gust speed at V_D with V_D. Additionally, K_g had to be calculated [12]:

$$K_g = \frac{0.88\mu_g}{5.3 + \mu_g} \tag{4.14}$$

Where K_g is a function of μ_g and μ_g is computed as follows [12]:

$$\mu_g = \frac{2\frac{W}{S}}{9.80665 MAC \rho C_{L_\alpha}} \tag{4.15}$$

μ_g is thus dependent on the gust altitude via ρ. Therefore, it becomes apparent that the maximum and minimum load factor for gusts is dependent on the gust altitude via K_g and U_{EAS}, which decreases above 6100 m. This means that the most critical gust

---

[3]http://theflyingengineer.com/2012/03/18/diving-into-the-a320-dive-speeds/ [accessed on 16 June 2020]

altitude can be found, because K_g increases with altitude. Consequently, the maximum load factor increases with increasing altitude up till 6100 m, beyond which the increasing effect of K_g is mitigated by the decrease in gust velocity U_{EAS} and the maximum load factor decreases with altitude instead. Thus, 6100 m is the critical gust altitude, resulting in a maximum load factor of 2.69. The minimum load factor is limited by the manoeuvrability envelope and thus equals -1.0.

Table 4.5: Inputs of the flight envelopes

Inputs			
W/S [N/m2]	1772	$C_{L_{max}}$ [-]	0.952
M_D [-]	0.89	C_{L_α} [1/rad]	4.36
n_{max} [-]	2.5	MAC [m]	16.11
n_{min} [-]	-1.0	$V_{C_{TAS}}$ [m/s]	239.55
Gust altitude [km]	6.1		

Table 4.6: Outputs of the flight envelopes

Outputs			
V_A [m/s]	87.17	V_D [m/s]	154.7
V_B [m/s]	84.51	$n_{g_{max}}$	2.69
V_C [m/s]	139.0		

4.2.4. Climb Performance

Not only the flight envelope defines the operational use of the Hydrojet, but the climb performance too: it determines how fast the aircraft can climb at a certain altitude for a certain airspeed and it also determines the flight ceiling. Additionally, the climb performance diagram can be used to verify the wing loading - thrust loading diagram, since they are governed by the same fundamental equations of flight performance. Lastly, it becomes possible to create a flight profile and to update the corresponding fuel fractions for climb and descent, but this was not done in this project.

The steady ROC performance is computed with Equation 4.16. This equation also makes use of the small angle approximation and therefore assumes that the lift equals the weight. The goal is to construct a plot where the airspeed is plotted against the altitude for a range of different ROCs. This means that the ROC in Equation 4.16 is known, but the thrust and drag are dependent on the altitude via the air density, ρ, and the airspeed is also a variable. This means that this problem can only be solved numerically.

$$ROC_{st} = \frac{T \cdot V - D \cdot V}{W} \tag{4.16}$$

First, the thrust is written as a function of the air density. T_0 is the maximum thrust available at sea level altitude. Next, the drag is expressed as a function of the airspeed and drag coefficient C_D, which again can be split up as was already shown before in Equation 4.9. Lastly, the lift coefficient is simply by equation lift to the weight.

$$T = T_0 \left(\frac{\rho}{\rho_0} \right)^{\frac{3}{4}} \quad (4.17) \qquad D = \frac{1}{2}\rho V^2 S C_D \quad (4.18) \qquad C_D = C_{D_0} + \frac{C_L^2}{\pi A e} \qquad C_L = \frac{W}{\frac{1}{2}\rho V^2 S} \quad (4.19)$$

If all these equations are substituted, Equation 4.20 is obtained. The problem is now brought down to a simple root finding problem: for a given altitude and rate of climb, the TAS, V, can be solved for with a root finding function. By repeating this process for all altitudes up to the flight ceiling and a range of ROCs, the plot in Figure 4.6 is obtained. For the aircraft weight, W, the MTOW was taken and for CD_0, the initial value of 0.00671 from the Midterm report was taken.[1] The motivation for this is that the actual converged value for CD_0 gives an unfeasible climb performance diagram since it is likely slightly on the lower side. An explanation for this is presented in Section 5.3.7.

$$0 = \frac{1}{2}\rho V^4 S C_{D_0} - T_0 \left(\frac{\rho}{\rho_0} \right)^{\frac{3}{4}} V^2 + W \cdot ROC_{st} \cdot V + \frac{1}{\pi A e} \frac{W^2}{\frac{1}{2}\rho V S} \tag{4.20}$$

The plot shows that a *ROC* of more than 28 m/s can be achieved at sea level altitude and that the flight ceiling of this aircraft lies at 18 km height at MTOW. Also, the theoretical maximum speed that can be reached is visible: 360 m/s at sea level. However, this value lies above the speed of sound (340 m/s), which implies that the aircraft can fly at supersonic speeds, for which the aircraft is not designed. Clearly, the limits of the model have been exceeded and its assumptions, such as Equation 4.17, are not valid anymore. The inputs and outputs that were used, are shown in Tables 4.7 and 4.8, but the outcomes are not expected to be accurate.

Table 4.7: Inputs of the climb performance diagram

Inputs			
MTOW [kg]	92315	CD0 [-]	0.00671
S [m^2]	510.8	A [-]	4.23
T0 [kN]	284.3	e [-]	0.689

Table 4.8: Outputs of the climb performance diagram

Outputs	
Flight ceiling [km]	18.2
ROCst at sea level [m/s]	>28
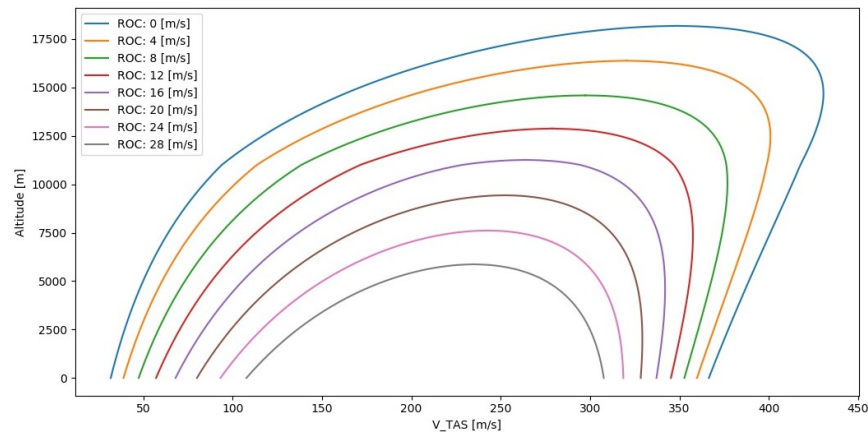
Figure 4.6: Climb Performance at MTOW with CD_0=0.00671

4.2.5. Payload-Range Diagram

To complete the flight performance analysis, the payload-range diagram was created. This was done to verify that the required range can be flown with the design payload of 30 tons, as will be defined in Section 5.1 HPRA-REQ-AWE-1, and to compute the harmonic and ferry range of the Hydrojet. For the construction of the payload-range diagram, firstly the range needs to be defined: the range is the distance travelled by the aircraft at cruise speed and velocity without any head- or tailwind. This means that the distance covered during climb and descent is excluded. The actual distance which the aircraft can travel including climb and descent, is therefore roughly 500 km longer according to some rough calculations based on ROC, rate of descent and airspeed. With this definition set, the range, R, is calculated with the range equation for jet aircraft:

$$R = \frac{V_{C_{TAS}}}{9.80661 \cdot SFC} \left(\frac{L}{D}\right)_{cruise} ln\left(M_{f_{cruise}}\right) \tag{4.21}$$

For this, the TAS in cruise is needed, the SFC, the lift-to-drag ratio in cruise and lastly, the mass fraction during cruise: $M_{f_{cruise}}$ is the ratio between the start and final mass of the cruise phase. This fraction is calculated based on the Class-I mass estimation method presented in the Midterm report and depends on the payload and fuel mass: more range means less payload and vice versa.[1] This relation is perfectly shown in the payload-range diagram in Figure 4.7. Here, also the fuel weight is shown and it can be seen that the fuel weight is not equal to zero for zero range. This is the case since fuel is required for the other phases of flight, namely take-off, climb, descent etc, which all do not count as range.

Point B represents the design point and fulfils both the payload and range requirements: 30 tons of payload can be flown over 4500 km at MTOW. The Hydrojet is able to carry even more payload, but then fuel needs to be traded for this additional payload to stay below the MTOW, as is clear from Figure 4.7. However, at a certain point A, the cargo hold is full and the maximum payload capacity is reached: this point is called the harmonic range, for which the Hydrojet can fly 1125 km with 32.7 tons of fuel. This payload capacity can only be reached with a cargo density of 250 kg/m^3 [4], which is in the high range of typical cargo densities. As becomes clear from the diagram, interchanging fuel for payload is a highly ineffective strategy due to the low gravimetric density of hydrogen: little payload weight is gained and a lot of range is lost.

Instead of decreasing the range, it is also possible to increase the range by lowering the payload. Point C is called the ferry range and is the absolute maximum range the aircraft can fly without any payload, namely 10360 km. This strategy is highly efficient due to the great aerodynamic performance in cruise. As a result of the high lift-to-drag ratio of the BWB design, it is even possible to carry 20 tons of payload over 6450 km. The inputs and outputs that were used, are shown in Tables 4.9 and 4.10.

Table 4.9: Inputs of the payload-range diagram

Inputs			
MTOW [kg]	92,315	SFC [kg/Ns]	5.89E-6
m_{fuel} [kg]	9,396	$V_{C_{TAS}}$ [m/s]	239.6
$m_{payload}$ [kg]	30,000	L/D_{cruise} [-]	25.24
$m_{payload,max}$ [kg]	32,713		

Table 4.10: Outputs of the payload-range diagram

Outputs	
Harmonic range [km]	1,125
Design range [km]	4,500
Ferry range [km]	10,360

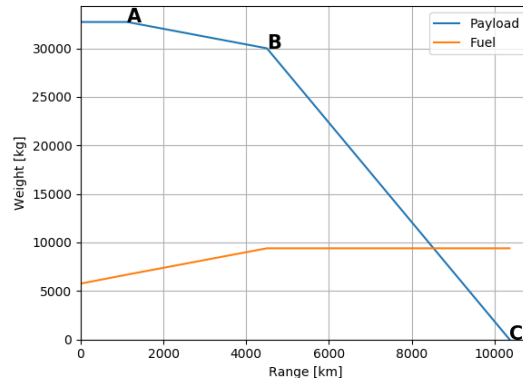[4] https://aerlinesmagazine.wordpress.com/2006/03/13/air-cargo-density-research/ [accessed on 20 June 2020]

Figure 4.7: Payload-range diagram including fuel weight (A: harmonic range, B: Design range, C: Ferry range)

4.3. Verification

In this section, the codes for the wing loading - thrust loading diagram, climb performance diagram and payload-range diagram will be verified. For each these diagrams and the flight envelopes, initial code verification was performed by checking the outcomes with hand calculations. For the wing-/thrust-loading diagram, this meant that the T/W was calculated by hand for every line at $W/S = 1772$ N/m^2, except for the ROC requirement. For the verification of this line, the climb performance diagram was used because in essence, it is the inverse calculation of the ROC requirement. The climb performance diagram was constructed based on a $T/W = 0.1246$, which was taken from Figure 4.3, MTOW and the actual C_{D_0} of 0.003386. From the plot in Figure 4.8, it is then apparent that a maximum ROC of 14 m/s can be achieved, as was set as the ROC requirement. In addition, the cruise requirement was also checked with the climb performance diagram. For this, a T/W of 0.1061, thrust setting of 80 %, C_{D_0} of 0.03387 and a cruise mass fraction of 0.956 of MTOW were taken. The result is shown in Figure 4.9, where the red dot indicates the maximum altitude at which the Hydrojet can fly in the previous mentioned conditions and at the cruise TAS of 239.55 m/s. This altitude lies at 10 km and Figure 4.9 thus proves that the Hydrojet can fly at cruise altitude at cruise velocity. Therefore, the wing-/thrust-loading diagram is verified.
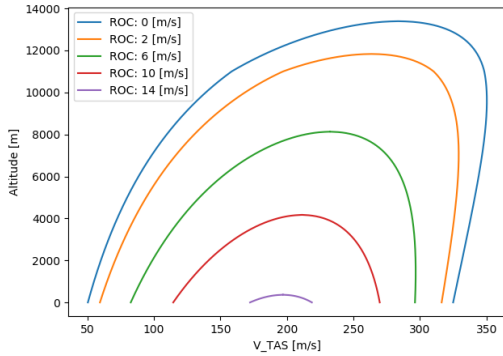

Figure 4.8: Sea level ROC requirement verification at MTOW: $W/S = 1772$ N/m^2, $T/W = 0.1246$, $\tau_{set} = 100\%$, $C_{D_0} = 0.003387$
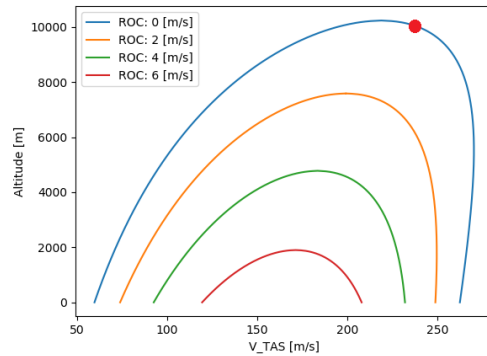
Figure 4.9: Cruise requirement verification: $W/S = 1772$ N/m^2, $T/W = 0.1061$, $\tau_{set} = 80\%$, f$_{cruise} = 0.956$, $C_{D_0} = 0.003386$

Lastly, the payload-range diagram is used for verification of the mass estimation method from Chapter 3. Namely, the mass estimation method has as input that the Hydrojet should fly 4500 km with 30 tons of payload and outputs the MTOW and fuel weight. Now, with the payload-range diagram, it is checked whether this range can be achieved with the design payload and as was discussed in Subsection 4.2.5, this is the case.

4.4. Validation

In this section, the V-speeds, wing-/thrust-loading diagram and payload-range diagram will be validated. First of all, the dry runway speeds V_1, V_R, and V_2 of the A320 were extracted from the Flight Crew Operating Manual (FCOM) and compared to the Hydrojet, see Table 4.11. The V-speeds are of course partly dependent on the aircraft design, but the Hydrojet V-speeds have a similar magnitude as the A320. Although the V_1 and V_2 of the Hydrojet are slightly further apart, their distribution is still similar to that of the A320.

Table 4.11: Most important take-off V-speeds of the Hydrojet and A320 for a dry runway (extracted from the FCOM)

Aircraft	V_1 [knots]	V_R [knots]	V_2 [knots]
Hydrojet	133	136	142
A320	156	157	162

Next, the wing loading - thrust loading of the Hydrojet was plotted in Figure 4.10 and compared to other BWB aircraft. In the Midterm report, it was stated that the Hydrojet had an low wing loading compared to conventional aircraft.[1] The Hydrojet still has the lowest wing loading, but BWBs in general have a low wing loading. This is the case because the wing surface area is relatively large due to the nature of a BWB. Looking at Figure 4.10, a negative relation can be seen between the thrust loading and wing loading: higher wing loading aircraft generally have a lower thrust loading. The Hydrojet has a low wing loading due to the integration of the hydrogen fuel tanks and has a high thrust loading due to the lack of high lift devices. Therefore, the Hydrojet follows the trend and its design point thus seems to be feasible.
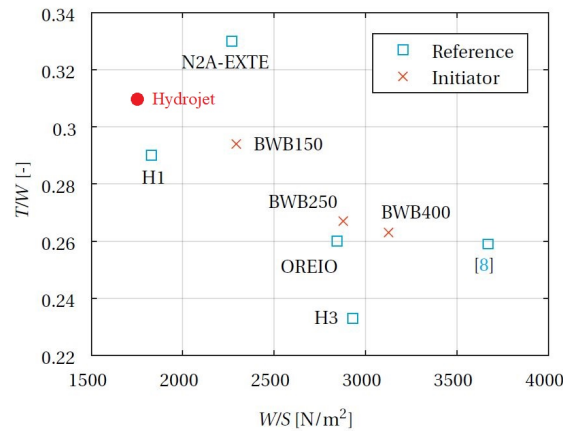
Figure 4.10: Wing loading - thrust loading diagram for reference BWB and the Hydrojet. Edited from: [13]

Lastly, the flight ceiling of typical passenger aircraft lies way below 18 km altitude and therefore, the climb performance diagram is not validated. The fact that the service ceiling of the Hydrojet is so high, can be explained by the high lift-to-drag ratio of the BWB and the incorrect assumptions of the underlying model. Namely, transonic aerodynamics is not taken into account and the decrease of the thrust with altitude is most likely not valid up to these high altitudes.

To conclude, for performance most requirements are met due to the fact that the requirements were directly used in the design process. Only some requirements need more research. Namely, requirement HPRA-REQ-C&M-7 was not considered since the final take-off, V_{FTO}, was left out and for requirements HPRA-REQ-TO-10 and HPRA-REQ-TO-11, more detailed analysis on take-off and landing is necessary.

5
Planform

Now that the performance has been analysed, the planform can be sized to meet the performance requirements. This will be done by first looking at the requirements of the planform in Section 5.1. Next, the planform layout will be discussed in Section 5.2. Since the planform of a blended wing body also needs to be aerodynamically efficient, an aerodynamic analysis is done in Section 5.3. Also, stability and control will be analysed in Section 5.4. In Section 5.5 the structures of the planform will be elaborated upon. Finally, the requirements are checked.

5.1. Planform Requirements

To have an overview of the different requirements the planform needs to be compliant with, the requirements have been listed below. The requirements have been subdivided into separate departments as well.

Planform Requirements

General:
HPRA-REQ-PLF-COS The cost of the planform shall be no more than €63.1 million
HPRA-REQ-AWE-1 The aircraft shall have a minimum payload capacity of 30 000 kg. [14]
HPRA-REQ-AWE-2 The aircraft shall have a cargo capacity of 4512 kg.
HPRA-REQ-AWE-3 The aircraft shall have a cargo volume of at least 28.2 m^3.
HPRA-REQ-AWE-4 The planform shall weigh no more than 21,062 kg.

HPRA-REQ-GAT-1 The wingspan shall be not greater than 65 m.
HPRA-REQ-GAT-4 The aircraft height shall be not greater than 20.1 m.
HPRA-REQ-CAC-1 The aircraft emergency exit configuration shall be designed such that neither the passengers nor the crew members need to make use of the flight deck door.
HPRA-REQ-CAC-6 Between the cabin floor up until 64 cm above the cabin floor, the width of the cabin aisle shall not be lower than 38 cm.
HPRA-REQ-CAC-7 From 64 cm above the cabin floor to the cabin ceiling, the width of the cabin aisle shall not be lower than 51 cm.
HPRA-REQ-CAC-8 The fuselage shall accommodate crew members.

Stability & Control:
HPRA-REQ-PLF-1 The control surfaces shall ensure moment equilibrium in steady flight.
HPRA-REQ-PLF-2 The control surfaces shall enable longitudinal control.
HPRA-REQ-PLF-2.1 The control surfaces shall be able to pitch the nose downward at any point between the trim speed and the stall identification.
HPRA-REQ-PLF-3 The control surfaces shall enable lateral control.
HPRA-REQ-PLF-3.1 The control surfaces shall allow going from a 30 degree banked turn to a 30 degree bank angle in the other direction in 11 seconds at V_2.
HPRA-REQ-S&C-1 The aircraft shall be stable within all operational limits.
HPRA-REQ-S&C-1.1 The aircraft shall be longitudinally statically stable.
HPRA-REQ-S&C-1.2 The aircraft shall be laterally statically stable.
HPRA-REQ-S&C-1.3 The aircraft shall be dynamically stable.
HPRA-REQ-CG-1 The extreme forward and the extreme aft centre of gravity shall not lie beyond the minimum and maximum limitations of the aircraft.
HPRA-REQ-HSU-13 The usage of the hydrogen fuel shall not compromise the stability and controllability of the aircraft during flight.
HPRA-REQ-LOC-2 The aircraft shall have a maximum side slip angle of 15 degrees with a 56 km/h crosswind.

Structures & Materials:
HPRA-REQ-STR-2 Maximum external loads considered to occur on the structure shall be multiplied by a safety factor of 1.5.
HPRA-REQ-STR-5 The structure shall allow for easy access during maintenance.
HPRA-REQ-STR-6 The aircraft shall have protection against catastrophic effects from lightning.
HPRA-REQ-S&M-1 The aircraft's structure shall be able to withstand all loads.
HPRA-REQ-S&M-1.1 The aircraft's structure shall be able to withstand all aerodynamic loads during flight.
HPRA-REQ-S&M-1.2 The aircraft's structure shall be able to withstand all loads during taxi and ground operations.
HPRA-REQ-S&M-3 The fuselage structure shall be able to withstand a pressure difference of at least 8.35.
HPRA-REQ-S&M-4 The fuselage structure shall be able to provide protection against fires.
HPRA-REQ-S&M-5 The fuselage structure shall allow the attachment of undercarriage.
HPRA-REQ-S&M-6 The fuselage structure shall allow space for landing gear (if retracted).
HPRA-REQ-S&M-7 The fuselage structure shall be able to support the stress concentrations due to cut-outs.
HPRA-REQ-S&M-8 The structure shall allow to accommodate 125.8 m^3 hydrogen.

Aerodynamics:
HPRA-REQ-AER-1 The aircraft shall have a lift-over-drag ratio of at least 23.22 change.
HPRA-REQ-AER-2 High lift devices shall be deployed during take off and landing.
HPRA-REQ-AER-3 The aircraft shall provide additional lift during take-off.
HPRA-REQ-AER-4 The aircraft shall provide enough lift during cruise.
HPRA-REQ-AER-5 The aircraft shall be able to slow down during approach.
HPRA-REQ-HSU-10 The size of the aircraft hydrogen tanks shall not result in an unacceptably low aerodynamic efficiency.

5.2. Planform Layout

To find the wing surface area and other relevant geometry input requirements for the Class-II mass estimation and the different engineering departments, an initial planform design has to be made of the blended wing body. This planform design will revolve around the top-level requirement of a capacity of 236 passengers. To start of the planform design, first the cabin will be sized. After this, the cargo will be placed within the inner wing and lastly, the fuel tanks will be sized based on the fuel weight and volume.

5.2.1. Cabin

Starting with the cabin, the first thing to look at is how much space is available for the cabin. Based on the seating configuration shown in the Midterm Report, the cabin will consist of an cross aisle which will be used to board the Hydrojet.[1] After that, a triangular section will start the cabin due to the leading edge sweep angle that will be used. Next, a rectangular section begins where the cabin will have its maximum width. Based on the number of passengers that still need to fit in the cabin, an additional triangular section could be added to the cabin. Also, some space will be left for the toilets and other facilities. This will be located in this cross aisles and at the back of the cabin where the height is less than the aisle height.

Sizing the cabin is not done without defining the constraints. One of the main factors that will constrain the cabin size is the height of the blended wing body at a certain spanwise and chordwise location. This is dependent on the airfoil selected which will be done in Section 5.3. Additionally, for the height of the cabin, at least 1.75 m of height should be available for the aisles.[3] This means that the airfoil needs to have at least a height of 1.75 m at the locations where the cabin will be without insulation and/or panels. For that reason, the cabin will have a height of 1.87 m. This means that the cabin cannot be located directly after the leading edge and will be shifted backward a bit, since space also needs to be reserved for overhead luggage storage. Since the floor of the cabin needs to be a flat surface, the most outward location of the cabin will be used to determine the height from bottom of the blended wing body. Due to the decrease in chord and a constant assumed thickness over chord value, the thickness of the airfoil will decrease when going more outward of the wing. With this it can be seen that the height of the aisle will also shape the cabin in the triangular parts.

For the seating layout, all 236 passengers need to fit inside of the cabin, which is shown in Figure 5.7. This configuration consists of multiple sections within the cabin having either, two or four aisles. The aisles all have a height of 1.87 m and are sized to have a width at least 0.5334 m. The seat pitch used in this configuration is 0.762 m and the seat width is 0.4064 m.

Additionally, behind the cabin there will also be room for toilets and facilities where 1.87 m height is not essential. Note that the space for these facilities has not been indicated in Figure 5.7. The length assumed for this space behind the cabin is 1.5 m. Using the seat width and the aisles width, the total width of the cabin is estimated to be 9.388 m. The length of the cabin can be calculated using the dimensions discussed before and amounts to 17.204 m, as can be calculated based on 5.8.
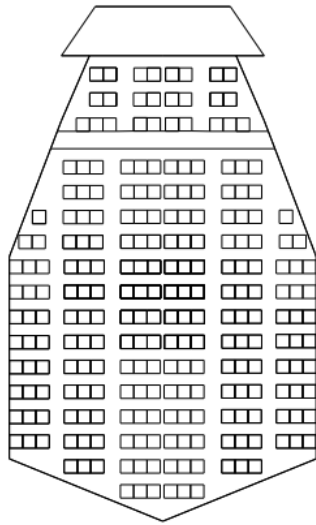

Figure 5.1: Cabin layout of the Hydrojet
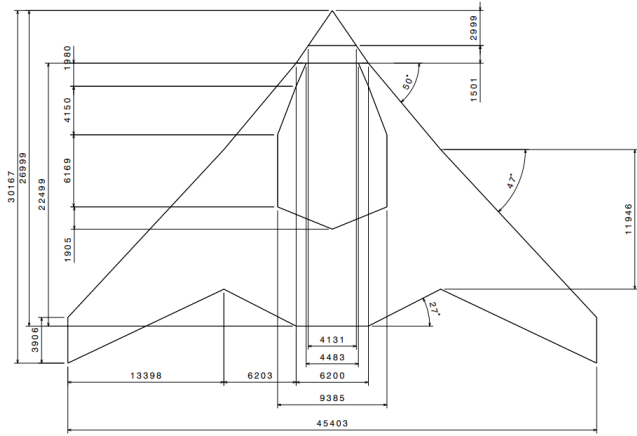
Figure 5.2: Planform of the Hydrojet (dimensions in mm)

5.2.2. Cargo

The passengers will also have cargo to bring on-board. The cargo mass is estimated to be 4512 kg. Using a standard luggage density of 160 kg/m^3, the required cargo volume can be calculated.[15] This resulted in the 28.2 m^3 requirement. For the Hydrojet, the cargo will be placed above the cabin in order to optimally use the volume of the blended wing body and to ensure that the center of gravity location of the Hydrojet will not be shifted backwards too much. Since the mass is not the constraining factor of the cargo but rather the volume, the cargo holds will need to be sized in order to have enough space to hold all cargo. At this point, it is known that the cabin will be placed at the lowest point of the airfoil shape at the chord where the cabin width is maximum, as explained earlier. Added to that value will be the cabin height which will be the lower constraint. The upper constraint is airfoil shape itself. The width of the cargo hold will be 6.2 m as this is the area at which the largest absolute thickness over chord value will be found. Now that every constraint is known, the volume can be calculated in the constraint sizing space. Assuming that the cargo volume could be estimated using the volume of a truncated pyramid, the cargo volume is able to hold 28.9 m^3. This means that solely the space above the cabin is sufficient for storing all cargo.

5.2.3. Fuel tanks

Lastly, the fuel tanks will be added to the design. Since there is not a lot of volume in the outer wings, the fuel will mostly be stored in the inner wing of the blended wing body design. This inner wing of the blended wing body is the inner part up until the bottom kink (see Figure 5.3). Based on the Class-I estimation, the fuel weight is found. Using the density of liquid hydrogen, the required total fuel volume is found which is equal to 138.4 m^3 including 3% boil-off based on duration and flight type.[16] The constraints for the fitting of the fuel tank in the planform are also mostly limited by the height available at the given chord location of the blended wing body. Also, an optimal shape is preferred such as an ellipsoid or a cylinder with spherical end caps. This will be taken into account when sizing the fuel tank. More details about required tank volume, shape and materials are discussed in Section 7.5. Another constraint is the width which will be between the outer kink and the outer wall of the cabin. Now that all constraints have been defined, the fuel tanks can be integrated. For the tank an ellipse is fit within the airfoil shape on the chord where the cabin ends and at the chord where the kink is located. Using a (CATIA) model, the tank has been made on scale and the volume could be calculated. In this model the edges of the tank were rounded to improve its structure for storing the liquid hydrogen. The volume that was calculated by the model was given to be 77.8 m^3 per tank. Since two tanks will be located in the planform, there is no need for additional fuel tanks.

5.2.4. Planform overview

The planform along with the cabin, cargo and fuel tanks can be seen in Figure 5.8 and Figure 5.3. The dimension of the different elements of the planform have been added. The capacity of the cabin, the cargo hold and the fuel tank is, respectively, 236 passengers (pax), 28.9 m^3 and 155.6 m^3. This are all based on the final iteration results from the mass estimation

method and the different engineering compartments. From Figure 5.3 it can be seen that the fuel tanks are well integrated in the aircraft planform, therefore complying with requirement HPRA-REQ-HSU-10. Furthermore, other requirements such as HPRA-REQ-AWE-1 to 3 have all been complied. As well as the wingspan requirement (HPRA-REQ-GAT-1) and the height requirement (HPRA-REQ-GAT-4). Furthermore, the requirements HPRA-REQ-CAC-6 and 7 are not discussed but are assumed to be achievable since the design of the cabin has been done based on CS25 constraints. For HPRA-REQ-CAC-8, the 1.5m cross aisle in the front of the cabin will be used. This fulfills that requirement as well.
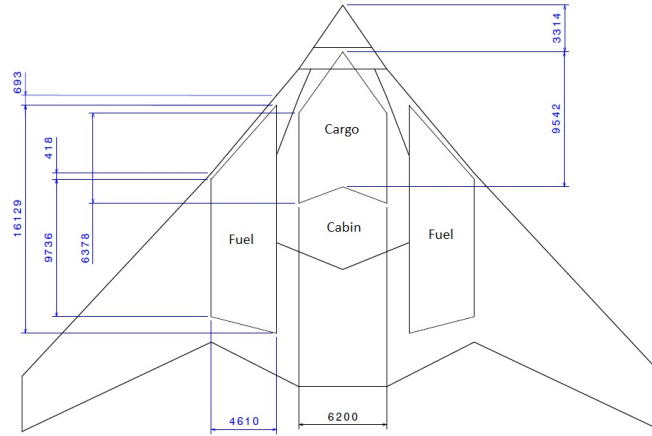
Figure 5.3: Planform layout with the cabin, cargo holds and fuel tanks (dimensions in mm)

5.3. Aerodynamics

With the dimensions of the planform known, the aerodynamic characteristics of the Hydrojet can be assessed. The aerodynamic characteristics of an aircraft have a major influence on the other subsystems which need to be designed in order to fulfil the requirements. Various aerodynamic coefficients such as the maximum lift coefficient, zero-lift drag coefficient, aspect ratio and Oswald efficiency factor have a direct influence on the take-off, climb, and glide performance. The resulting drag forces will define how much thrust is needed, and the lift-to-drag ratio influences the allowable aircraft weight, which in turn affects everything. Hence, the aerodynamics need to be elaborated upon, which is what is done in this section, starting with the selection of airfoils.

5.3.1. Airfoil Selection

To have a trimmed tailless aircraft, the moment coefficient about the wing aerodynamic centre ($C_{m_{ac}}$) should be positive. This is because for the stability criterion it is required that the centre of gravity is located before the aerodynamic centre (which coincides with the neutral point for tailless aircraft), as stated by requirement HPRA-REQ-S&C-1.1 to have a longitudinally stable aircraft.[8] To achieve this, the best option is to select the airfoil based on the following criteria: L/D ratio, $C_{l_{max}}$ and a good thickness for the centre body, with a positive (or not too negative) $C_{m_{ac}}$. The $C_{m_{ac}}$ of the wing is then made positive by applying adequate sweep and washout (negative twist towards the tip). $C_{l_{max}}$ and $(C_l/C_d)_{max}$ are of importance as they represent the aerodynamic performance of the wing. High L/D is needed to comply with requirement HPRA-REQ-AER-1 to have a L/D of at least 23.22. The higher the lift over drag ratio, the lower the fuel consumption because less drag is created for the same amount of lift. Less drag results in less thrust needed to overcome this drag and thus a lower fuel consumption. Secondly, the thickness to chord ratio is very important and has to be high enough such that the cabin can fit in the aircraft, without having to make the aircraft unacceptably long. After the airfoil is selected, it is calculated what the sweep and twist need to be to make the moment coefficient positive. If these values diverge too much from decent values (with respect to drag criteria for example), new airfoils need to be selected and the process is restarted.

In order to not make the washout too high, multiple airfoils have to be selected. The aircraft is therefore divided in two parts: The inner wing, where the passengers and fuel tanks are located, and the outer wing. The different airfoils that have been investigated for the inner and outer wing can be seen in Table 5.1 and Table 5.2.

Table 5.1: Airfoil Inner Wing [17] [18] [19]

Aifoil	$C_{m_{ac}}$	$C_{l_{max}}$	$(C_l/C_d)_{max}$	$(t/c)_{max}$ [%]
LA 2573 A	+0.02	1.43	123	13.2
NACA 23112	+0.03	1.55	100	12
NACA 25112	-0.01	1.5	110	12
Eppler 635	+0.04	1.42	115	11.6

It can be seen that the NACA airfoils outperform the other airfoils in $C_{l_{max}}$ and that within NACA, NACA 25112 has a higher $(C_l/C_d)_{max}$ value. Furthermore, $C_{m_{ac}}$ has a low negative value which can be compensated for by the washout and outer airfoil. To compensate for the negative $C_{m_{ac}}$ of the inner wing, and to not make the washout to high, mostly reflex airfoils (positive $C_{m_{ac}}$) are evaluated. The different airfoils that have been evaluated can be seen in Table 5.2.

Table 5.2: Airfoil Outer Wing [17] [18] [19]

Aifoil	$C_{m_{ac}}$	$C_{l_{max}}$	$(C_l/C_d)_{max}$	$(t/c)_{max}$ [%]
MH 45	+0.0145	1.41	95	9.5
MH 60	+0.0175	1.33	95	10.1
MH 62	-0.004	1.27	93	9.3

From this table, MH 45 is selected. It has the highest $C_{l_{max}}$ and $(C_l/C_d)_{max}$ while having a positive $C_{m_{ac}}$ that is sufficient to have a reasonable washout. In the criteria for the outer wing airfoil, the maximum thickness over chord ratio is included. This ratio is important for the drag divergence mach number (M_{DD}). The drag divergence mach number indicates the speed at which the drag starts to increase significantly. It is thus crucial to fly below this Mach number. M_{DD} decreases with an increasing thickness. As the airfoil of the inner wing has to have a high thickness, the thickness of the outer wings must be low in order to increase M_{DD}. The MH 45 has a low $(t/c)_{max}$ and is thus chosen as the airfoil for the outer wings.

To conclude, for the inner wing of the aircraft, that is where both the passengers and the fuel tanks are located, the **NACA 25112** is selected as airfoil for its high $C_{l_{max}}$ and L/D ratio. The **MH 45** is selected as airfoil for the outer wing for its positive $C_{m_{ac}}$ and high $C_{l_{max}}$ and L/D ratio compared to the other (reflex) airfoils. Now that the airfoils are selected, different aerodynamic characteristics can be calculated.

5.3.2. Lift Coefficient and Stall Angle of Attack

The hydrojet has to be able to produce sufficient lift during flight. The lift coefficient plays a crucial role here. It is designed for three configurations: take-off, cruise and landing. During take-off it has to be high enough to get the aircraft of the ground and to be able to let the aircraft climb to its altitude. During cruise it needs to counteract the weight produced by the aircraft while not making the aircraft climb. At landing the lift coefficient must be high enough to enable the aircraft to reduce speed. Furthermore, the stall angle of the aircraft is crucial for safety aspects. The stall angle for the different configuration is needed to determine the minimum speed at which the aircraft can fly. First, the method of the calculations is explained and afterwards the in-and outputs are given in Table 5.4 and 5.5.

Cruise Lift Coefficient: First of all, the lift coefficient during cruise is estimated. It has to counteract the weight of the aircraft. However, the weight of the aircraft changes during cruise due to the fuel being consumed. Therefore, the lift coefficient that is designed for, counteracts the average weight of the aircraft during cruise. The design lift coefficient is calculated using Equation 5.1.[7]

$$C_{L_{des}} = 1.1 \cdot \frac{1}{\frac{1}{2}\rho V^2} \left\{ \frac{1}{2} \left[\left(\frac{W}{S} \right)_{startcruise} + \left(\frac{W}{S} \right)_{endcruise} \right] \right\} \qquad (5.1)$$

Where the cruise air density and speed ought to be used. The begin and end weights at cruise are defined by predetermined fuel fractions (M_f) that have to be multiplied by the MTOW to attain these weights. These fuel fractions were taken from [1] and are $M_{f_{start}} = 0.97$ and $M_{f_{end}} = 0.92$, respectively. This design lift coefficient during cruise is needed to provide sufficient lift during cruise, as stated by requirement HPRA-REQ-AER-4.

Maximum Clean Lift Coefficient: The maximum lift coefficient in clean configuration at landing and take-off speeds was estimated using the DATCOM (Data Compendium) method from the United States Air Force (USAF), since it is a necessary input for the high lift devices (HLDs) sizing in Subsection 5.3.4. This method makes the distinction between high and low aspect ratio wings. The high aspect ratio method should be chosen with:[7]

$$A > \frac{4}{(C_1 + 1) \cdot cos(\Lambda_{LE})} \qquad (5.2)$$

$$A = \frac{b \cdot (b + 1.9h_{winglet})}{S} \qquad (5.3)$$

Where C_1 depends on the wing taper ratio and can be found in Figure 5.4, and $h_{winglet}$ is the winglet height. For low aspect ratio wings, the three-dimensional effects are so large that the airfoil characteristics do not dictate the wing characteristics that much anymore, since they differ much more from the infinite wing setup for which the airfoil characteristics were determined.[7].
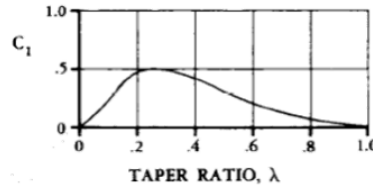

Figure 5.4: C1 Coefficient from Taper Ratio [7]

The aspect ratio of the Hydrojet, corrected for the additional effect of wing tips (Equation 5.3), equals 4.23. The average taper ratio of the Hydrojet equals 0.3847, yielding a C_1 of approximately 0.43. The aspect ratio criteria, using Equation 5.2 and the average sweep angle of 48.5 degrees, amounts to 4.14. Hence theoretically, the high aspect ratio method is to be used, but since the values are so close and depend on the vaguely readable parameter C_1, the low aspect ratio was also considered. The latter however quickly showed to not be applicable due to calculation parameters being out of range, meaning the other method needs to be used. Hence, the high aspect ratio method (HAM) is used. According to the HAM, the wing maximum lift coefficient can be expressed as:[7]

$$C_{L_{max}} = \left(\frac{C_{L_{max}}}{C_{l_{max}}} \right) \cdot C_{l_{max}} + \Delta C_{L_{max}} \qquad (5.4)$$

Since this equation will be evaluated at take-off and landing speed, the latter term can be neglected since it serves to account for the effects of Mach numbers above 0.2. Since the Hydrojet features two airfoil types, Equation 5.4 is evaluated for both airfoils, and the final max clean lift coefficient is found by averaging these two values with their respective wing surface areas. Since the NACA 25112 is the inner aifoil, and the MH45 the outer airfoil, these areas are denoted by S_i and S_o, respectively. The ratio $\frac{C_{L_{max}}}{C_{l_{max}}}$ can be found from Figure 5.5a.
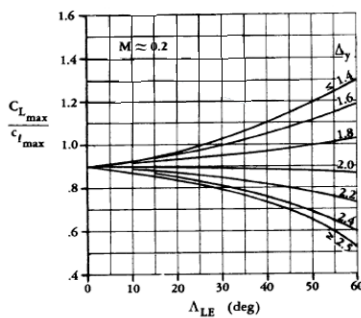
(a) Values For $\frac{C_{Lmax}}{C_{lmax}}$ Depending on Sweep and Airfoil Sharpness
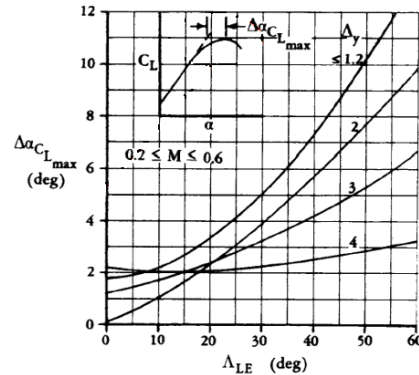
(b) $\Delta \alpha_{C_{Lmax}}$ Depending on Sweep and Sharpness Parameter

Figure 5.5: DATCOM Method for $C_{L_{max}}$ and α_{stall}

The airfoil sharpness parameter Δy can be found by taking the vertical distance of the airfoil edge between 0.15 % and 6 % along the chord. Since the airfoil geometry is known, it is possible to calculate this for both airfoils, and their values are given in the table below:

Table 5.3: Airfoil Sharpness Parameter as Percentage of Chord Length

Airfoil	Δy
NACA 25112	3.12 %
MH 45	3.48 %

Stall Angle of Attack: The stall angle of attack is also estimated according to the DATCOM method. The stall angle is then expressed as:

$$\alpha_{stall} = \frac{C_{L_{max}}}{C_{L_\alpha}} + \alpha_{L=0} + \Delta\alpha_{C_{Lmax}} \quad (5.5)$$

$$C_{L_\alpha} = \frac{2\pi A}{2 + \sqrt{4 + \frac{A\beta^2}{\eta}\left(1 + \frac{tan^2\Lambda_{0.5c}}{\beta^2}\right)}} \quad (5.6)$$

Where $\beta = \sqrt{1 - M^2}$ is the Prandtl-Glauert compressibility correction factor, η the airfoil efficiency factor and can be taken to be 0.95 [7], and $\Lambda_{0.5c}$ the mid-chord wing sweep. The last term in Equation 5.5 accounts for the non-linear increasing part of the lift curve where the lift coefficient reaches its maximum before the flow separates, and can be taken from Figure 5.5b. Again since there are two different airfoils, both of their stall angles are calculated, and now the critical (smallest) value is taken to be the wing stall angle of attack.

The inputs and outputs for each of these calculations are shown in Table 5.4 and 5.5, and will be used to make sure compliance with requirements HPRA-REQ-AER-1, HPRA-REQ-AER-3 and HPRA-REQ-AER-5 is accomplished.

Table 5.4: Inputs of the Lift Coefficient and Stall Angle Calculations

Inputs							
ρ_{cruise} [kg/m^3]	0.41268	MTOW [kg]	90,829.245	λ [-]	0.385	NACA 25112 C$_{l_{max}}$ [-]	1.5
V_{cruise} [m/s]	239.55	FF$_{start}$ [-]	0.97	A [-]	4.23	MH45 C$_{l_{max}}$ [-]	1.41
M_{cruise} [-]	0.8	FF$_{end}$ [-]	0.92	η [-]	0.95	NACA 25112 $\alpha_{L=0}$ [°]	-1.5
$M_{takeoff}$ [-]	0.208	Λ_{LE} [°]	47.5	S_i [m^2]	323.98	MH45 $\alpha_{L=0}$ [°]	-1.02
$M_{landing}$ [-]	0.196	$\Lambda_{0.5c}$ [°]	23	S_o [m^2]	186.863		

Table 5.5: Outputs of the Lift Coefficient and Stall Angle Calculations

Outputs					
$C_{L_{des}}$	0.153	Takeoff C_{L_α}	3.7832 1/rad	Takeoff α_{stall}	24.44 °
Clean $C_{L_{max}}$	0.9536	Cruise C_{L_α}	4.6928 1/rad	Cruise α_{stall}	20.20 °
		Landing C_{L_α}	3.7781 1/rad	Landing α_{stall}	25.36 °

5.3.3. Zero-lift Drag Coefficient Estimation

To estimate the zero-lift drag coefficient, the component build up method is used.[7]

$$C_{D_0} = \frac{1}{S_{ref}} \sum_c C_{f_c} \cdot FF_c \cdot IF_c \cdot S_{wet_c} + C_{D_{misc}} \quad (5.7)$$

Where C_{f_c} is the flat plate skin friction coefficient, FF_c the form factor, IF_c the interference factor and S_{wet_c} the wetted surface area. C_{f_c} is dependent on the type of flow: laminar or turbulent. It is assumed that the first 10 % of the wing is laminar flow and the other 90 % turbulent.[7] For laminar flows, C_{f_c} is defined as follows:

$$C_{f_c} = \frac{1.328}{\sqrt{Re}} \quad (5.8)$$

For turbulent flows, C_{f_c} equals:

$$C_{f_c} = \frac{0.455}{(\log_{10} Re)^{2.58}(1 + 0.144M^2)^{0.65}} \quad (5.9)$$

One parameter is still missing to calculate C_{f_c}: the Reynolds number (Re). The Reynolds number is defined as:

$$Re = \frac{\rho V c}{\mu} \quad (5.10)$$

where ρ is the density, V the flow speed, μ the dynamic viscosity and c the root chord. For c the mean aerodynamic chord (MAC) of the different sections of the wing is taken. The dynamic viscosity is estimated as follows:

$$\mu = \frac{a_0 T^{1.5}}{T + S_c} \tag{5.11}$$

where T is the temperature, a_0 equals $1.47 \cdot 10^{-6}$ kg/ms $K^{0.5}$ and S_c (Sutherland's Constant) equals 113 K. Using these values, the Reynolds number can be calculated. The Reynolds number during cruise is equal to $168 \cdot 10^6$ for the inner wing (from cockpit to the first sweep angle), $120 \cdot 10^6$ for the middle wing (first to second sweep angle) and $58 \cdot 10^6$ for the outer wing.

The next parameter needed for the zero drag coefficient is the form factor (FF_c). In the blended wing design, the different forms are the wing and engines. For the wings the form factor can be calculated using Equation 5.12.

$$FF = \left[1 + \frac{0.6}{(x/c)_m}\left(\frac{t}{c}\right) + \left(\frac{t}{c}\right)^4\right]\left[1.34 M^{0.18}(cos(\Lambda_m))^{0.28}\right] \tag{5.12}$$

where $(x/c)_m$ is the position of the maximum thickness (from 0-1) and Λ_m the sweep angle at the position of maximum thickness. The form factor for the engines (nacelle) can be calculated using Equation 5.13.

$$FF = 1 + \frac{0.35}{f} \tag{5.13}$$

where f is equal to:

$$f = \frac{l}{\sqrt{(4/\pi)A_{max}}} \tag{5.14}$$

with l the length of the nacelle and A_{max} the maximum cross sectional area.

The next component for the zero-lift drag coefficient is the component interference factor: IF. This interference drag is due to the boundary layer interaction when two components interact and when a component is in the region of the velocity of another component. As a consequence, the airflow increases. The value for IF is assumed to be 1.5.[7]

Apart from the component build up drag, drag also occurs due to other miscellaneous components. First of all, there is additional drag during take-off and landing from the landing gear. Based on the dimensions of the landing gear, the drag can be estimated.[7]

$$\Delta C_{D_{LG}} = (0.04955 \cdot e^{5.615 \cdot S_A/(d \cdot w)}) \cdot \frac{S_A}{S_{ref}} \tag{5.15}$$

Here w_{LG} is the width of the landing gear and d the height. S_A is the frontal area.

Next to the landing gear drag, wave drag is also added up to the miscellaneous drag. It is important to know if the aircraft flies below or above the drag divergence number. Therefore M_{DD} is calculated using Equation 5.16.

$$M_{DD} = \frac{k_a}{cos\Lambda} - \frac{[t/c]_{streamwise}}{cos^2\Lambda} - \frac{C_L}{10 \cdot cos^3\Lambda} \tag{5.16}$$

k_a equals 0.87, this is the technology factor of the airfoil which is constant for a given airfoil family. $[t/c]_{streamwise}$ is the thickness over chord ratio in streamwise direction and Λ is the quarter chord sweep angle. Using the correct values, the drag divergence mach during cruise equals 0.876. The Hydrojet flies at a Mach of 0.8 and thus below the drag divergence mach. To determine the amount of wave drag, it must be known if the mach during cruise is higher or lower than the critical mach number (M_{cr}). When the critical mach number is reached, there is a point on the the wing where the speed equals the speed of sound (thus M = 1). The critical mach number is determined using Equation 5.17.[20]

$$\frac{C_{p,0}}{\sqrt{1 - M_{cr}^2}} = \frac{2}{\gamma M_{cr}^2}\left(\left[\frac{2 + (\gamma - 1)M_{cr}^2}{\gamma + 1}\right]^{\gamma/(\gamma-1)} - 1\right) \tag{5.17}$$

$C_{p,0}$ is the minimum pressure coefficient of the airfoil and equals -1.5.[20] From this equation, the critical mach number equals 0.663. Since this is lower than the cruise mach number, the wave drag equals:

$$\Delta C_D = 0.002\left[1 + 2.5\frac{M_{DD} - M}{0.05}\right]^{-1} \tag{5.18}$$

The last additional drag for the zero-lift drag coefficient is due to excrescence and leakage. This is dependent on the type of aircraft. For this aircraft a value of 5 % is taken, as is common with jet aircraft.[7]

Combining all the different components of the zero-lift drag coefficient leads to the values for take-off, cruise and landing configuration shwon in Table 5.6.

Table 5.6: Zero-lift Drag Coefficient during Take-off, Cruise and Landing

	Take-off	Cruise	Landing
C_{D_0}	0.00630	0.00339	0.00630

5.3.4. High Lift Devices

Since the aircraft spends most of its time in cruise flight, the wing is usually designed for this flight phase. This means that the surface area S, maximum lift coefficient $C_{L_{max}}$ and other wing parameters in clean configuration are optimised for cruise. This can have the consequence that the lift required during take-off and landing cannot be achieved at the flight speeds corresponding to those phases. This is why requirements HPRA-REQ-AER-3 and HPRA-REQ-AER-5 have to be specified, and are usually fulfilled with high lift devices (HLDs). For take-off, enough lift should be produced to take off with an acceptable ground roll distance, and for landing the high lift is needed to guarantee a safe (reference) approach speed V_{ref}. This approach speed should be above the reference stall speed V_{SR0} for obvious safety reasons. Furthermore, no excessive angles of attack should be required to attain this high lift in order to guarantee pilot visibility.

Before iterating the design, it was chosen to implement HLDs to make sure the aircraft could slow down to the approach speed at maximum landing weight. This would also be beneficial for the take-off thrust value (which would reduce). The idea was to implement leading edge (LE) slats only, since trailing edge (TE) HLDs rely mainly on increasing the camber of the entire wing to increase the maximum wing lift coefficient.[21] This would decrease the pitch moment coefficient about the wing aerodynamic center significantly, creating the risk that this would drop below zero. If that is the case, the aircraft cannot be trimmed at positive lift, which is not desirable. The reason for the necessity of a positive wing pitch moment coefficient is due to the fact that the Hydrojet is a flying wing (no tailplane), yet this will be discussed in further detail in Section 5.4.

Hence with TE HLDs out of the running, LE slats would be used. These HLDs slide out at the leading edge, yielding the following effects:

- Add a fresh and thin boundary layer on top of the front part of the wing → delaying flow separation
- Increase total lifting surface area → increased lift rate coefficient
- Decrease the effective angle of attack → higher pitch angle needed at landing

The first two are beneficial effects: separation is delayed yielding an extension of the linear part of the $C_L(\alpha)$-curve towards a higher $C_{L_{max}}$ and α_{stall}, and the lift curve slope is increased due to added lifting surface area. The inevitable disadvantage is the higher required angle of attack needed to make these slats effective, probably interfering with pilot visibility during landing (during take-off this is not a problem). Yet the question arises: are these HLDs necessary? After a few weight iterations, the surface area increased, hence requirement HPRA-REQ-AER-2 'High lift devices shall be deployed during take off and landing.' might have become redundant, and had to be investigated. To check if HLDs are needed, it will first be checked if the clean configuration can provide enough lift to maintain a low enough reference landing stall speed, which is required to be (after all iterations) 57.9 m/s. With the clean surface area S, maximum clean lift coefficient $C_{L_{max}}$ and maximum landing weight $W_{landing_{max}}$, the lowest speed that can be achieved is:

$$V_{min} = \sqrt{\frac{2W_{landing_{max}}}{\rho S C_{L_{max}}}} = \sqrt{\frac{2 \cdot 92315.21 \cdot 9.81}{1.225 \cdot 510.8449 \cdot 0.9536}} = 55.10 \text{ m/s} \tag{5.19}$$

Which is below the 57.9 m/s requirement. This is mainly due to the large wing area of the blended wing body design featured by the Hydrojet. Hence for landing, HLDs are not necessary. Let's now consider take-off. The higher the maximum achievable lift coefficient, the lower the needed thrust (as explained in Section 4.2.2). However, since the thrust that would be needed at the current $C_{L_{max}}$ of 0.9536 would not be too high for the two turbofan engines featured on the Hydrojet. Therefore, HLDs are not necessary to fulfil requirements HPRA-REQ-AER-3 and "-AER-5, and hence requirement "-AER-2 is rejected. Not including HLDs in the design has several advantages:

- Reduced complexity of the wing → lower probability of failure

- Reduced wing weight → reduced bending moments → reduced structural weight

- Reduced manufacturing and maintenance costs

- Easier maintenance and accessibility

Now, at the start of this subsection, it was stated that HLDs are required since an optimally designed wing cannot provide sufficient lift at low speeds such as during take-off and landing. So one could raise the question: is the Hydrojet wing-body over-designed now that it does not have any HLDs? To answer this question, it is necessary to understand that an aircraft with an optimal wing has a design lift coefficient which corresponds to the highest clean lift-to-drag ratio. If the actual design lift coefficient is much smaller than the maximum lift-to-drag lift coefficient, its area is too large, and vice versa. To check this for the Hydrojet, its clean drag polar (resulting from the AVL simulation in Section 5.3.5) is plotted below:
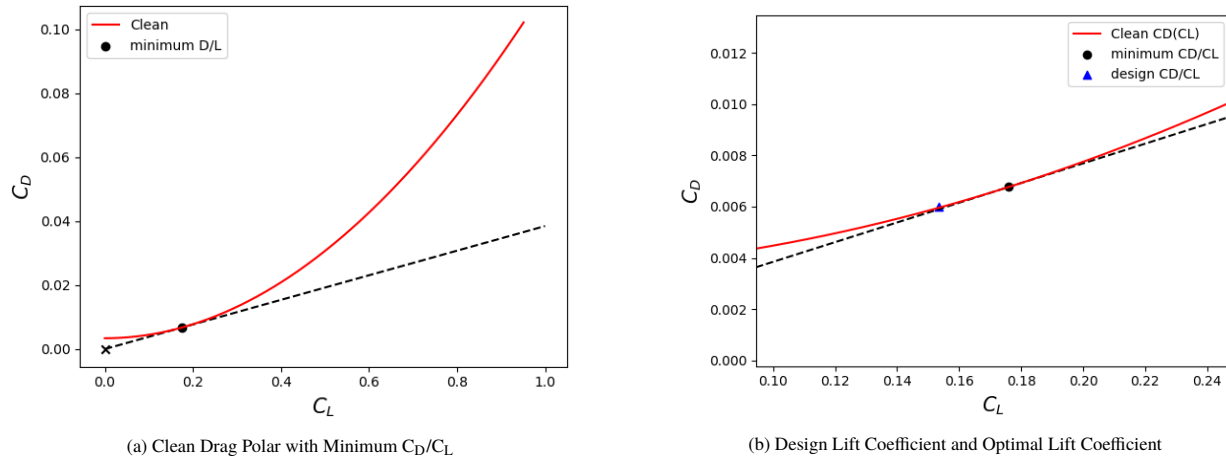

(a) Clean Drag Polar with Minimum C_D/C_L

(b) Design Lift Coefficient and Optimal Lift Coefficient

Figure 5.6: Clean Drag Polar of the Hydrojet

This drag polar yields a maximum C_L/C_D of 26.01 at $C_L = 0.176$. Since it can be seen in Figure 5.6b that the actual design lift coefficient is 0.153 yielding a C_L/C_D of 25.24 (therefore fulfulling requirement HPRA-REQ-AER-1), the wing surface is too big. But how big? It turns out that to get a design lift coefficient of 0.176, the Hydrojet needs a lifting surface area of 451.73 m^2, while the actual lifting surface area is 510.85 m^2. Keeping the air density and flight speed constant, the difference in drag produced can be calculated as follows:

$$\Delta D(\%) = \frac{(S \cdot C_D)_{design}}{(S \cdot C_D)_{optimal}} \tag{5.20}$$

Thus, the drag produced by the current wing is 1.6 % too large, which could still be reiterated on the condition that L/D remains compliant with requirement HPRA-REQ-AER-1. However, due to the crucial influence of the surface area to the planform, thus the fitting of the cabin, cargo and fuel tanks, stability and control etc., and the time constraint, this iteration is kept for future considerations (see Section 14.1 for further details).

5.3.5. Aerodynamic Characteristics from Athena Vortex Lattice (AVL)

To calculate different aerodynamic characteristics of the resulting planform, Athena Vortex Lattice (AVL) is used. AVL is a software tool that uses an extended Vortex Lattice Method (VLM) to analyze aerodynamics of a three-dimensional finite wing with arbitrary geometry at a preliminary level, written by Prof. Mark Drela at Massachusetts Institute of Technology (MIT). The inputs that AVL needs are the following:

- A geometry file defining the complete planform (hence airfoils, sweep/twist angles and dimensions)

- A 'runcase' file specifying flight conditions, operational constraints to be simulated and the zero-lift drag of the aircraft

- An optional mass file defining centroids and mass moments of inertia for more accurate eigenmode analysis

- Specified spanwise and chordwise discretisation patterns to define the panel grid on the geometry

There are many outputs generated after running the AVL simulation, hence only the most relevant data is extracted. This data comprises of the following characteristics:

- Global wing lift and drag coefficients C_L & C_D [-]
- Wing lift rate coefficient C_{L_α} [1/rad]
- Lift distribution along the wingspan $l(y)$ [N/m] for structural calculations (see Section 5.5)
- Induced drag C_{D_i} [-]
- Trim conditions and control derivatives (see Section 5.4)
- Eigenmode analysis to assess dynamic stability (see Section 5.4)

The Vortex Lattice Method and AVL Implementation: It is important to have a thorough understanding of the principles behind AVL and the VLM to make sure this software is valid for the simulation that one wishes to make. The VLM is built upon 'lifting surface' theory, which is an extension on the 'lifting line' theory.[22] This 'lifting line' theory uses potential flow, where the gradient of the (unknown) flow potential Φ equals the flow velocity at a specific point ($\nabla\Phi(x,y,z) = V(x,y,z)$). Potential flow consists of the following important assumptions:

- Steady and uniform flow (constant free-stream velocity and density)
- Subsonic and incompressible flow (Mach numbers < 0.3 for < 10 % density change [20])
- Inviscid and irrotational flow (friction is neglected, and the gradient of the flow velocity is zero)

These assumptions lead to the following equation for potential flow, which is the Laplace Equation:

$$\nabla^2\Phi(x,y,z) = \frac{\partial^2}{\partial x^2}\Phi(x,y,z) + \frac{\partial^2}{\partial y^2}\Phi(x,y,z) + \frac{\partial^2}{\partial z^2}\Phi(x,y,z) = 0 \tag{5.21}$$

By choosing the potential Φ to be a specific function of its arguments, one can construct some elementary flows. For example, the following potentials yield uniform parallel flow, source/sink flow and an irrotational vortex, respectively:

$$\Phi(x) = Ax \tag{5.22} \qquad \Phi(r) = \frac{\pm\sigma}{2\pi} \cdot ln(r) \tag{5.23}$$

$$\Phi(\theta) = \frac{\pm\Gamma}{2\pi} \cdot \theta \tag{5.24}$$

Where A, σ and Γ represent the strength of the flows. The lifting line theory now relies on the superposition of these elementary flows: it superimposes the parallel flow with a vortex to recreate the presence of a lift-generating object (airfoil) in the flow (see Fig **??**). To create a lifting line, many of these vortices are placed spanwise to create 'horseshoe' vortex filaments. These recreate the quarter chord of a finite wing with tip vortices causing induced drag. The more filaments that are included, the more accurate the lift distribution along the simulated wing. The strength of each individual vortex Γ_i is found by solving for them in a system of equations, using the boundary conditions (BCs) that the flow must be tangential to the surface and that far away from the surface the flow should equal the free-stream flow (asymptotic flow).

This method is extended to create a lifting surface by positioning multiple lifting lines of varying span (to account for sweep and taper) behind one another. The result is a surface representing a wing with specific geometry, where horseshoe vortices are positioned spanwise *and* chordwise, to create a so-called vortex lattice (see Fig **??**). It should be noted that as this is a two-dimensional finite wing, the thickness is ignored, hence only thin wings should be analysed using VLM. Camber is taken into account by the calculated vortex strengths however, so any airfoil can be simulated by implementing its camber shape into the flow tangency BC.
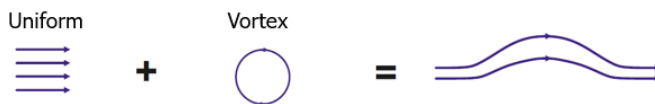

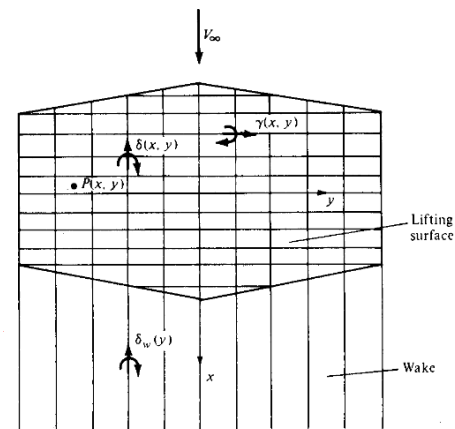Figure 5.7: Superposition of Elementary Potential Flows [23]

Figure 5.8: Vortex Lattice on a 2D Wing [22]

Again, the strengths Γ_i are found by solving the system of equations, which is defined by, in addition to the aforementioned BCs, the Kutta condition (trailing edge BC) and the fact that the lift is zero at the wing tips. This way, any wing can be modelled if the geometry and airfoils are perfectly defined. This is the method that AVL uses, and AVL extends this by adding a model for slender non-lifting bodies and a model for flight-dynamic analysis (eigenmotions, control surface effects and trim conditions). AVL also corrects for compressibility using the Prandtl-Glauert correction factor:[22]

$$\beta = \sqrt{1 - M^2} \tag{5.25}$$

Where M is the (perpendicular) mach number in the compressible regime (M > 0.3). Measurements on airfoil coefficients should be divided by this factor to account for effects of compressibility, then the results are reliable up to M = 0.6.[22] For swept wings however, the perpendicular mach number decreases with increasing sweep angle ($M_{perp} = M cos(\Lambda)$ [1]), hence higher free-stream mach numbers will still yield valid results in AVL if the sweep is sufficiently high. For the Hydrojet, the smallest sweep angle is 45 degrees, yielding a maximum allowed mach number of 0.849. Hence AVL can be used to make a simulation in cruise. Now that the underlying theory and assumptions used in AVL are known, it can be said that the software can be used for:

- Thin lifting surfaces and/or slender non-lifting bodies, such as a blended wing body (all lifting surface)
- Small angles of attack and sideslip (small flow perturbations assumed), such as during cruise
- In case of the Hydrojet, up to M = 0.849 free-stream due to limited implementation of compressibility effects

For aerodynamic characteristics, AVL was thus used to simulate the Hydrojet in trim conditions during cruise. The results are presented in Table 5.7.

These results were obtained using the following panel discretisation: the number of vortices along the chord, N_{chord}, was chosen to be 30, since the maximum length of the aircraft is 27 m (hence less than a meter between two control points). The spacing of these chordwise vortices was chosen to be in a cosine fashion, meaning more vortices concentrated at the leading and trailing edge (start and end points) since at those locations higher gradients in the solution are expected. For the number of spanwise vortices, N_{span}, the default was set to 40 for one half of the span, meaning 80 along the total wingspan. Again the cosine spacing was used to account for gradients at the wing tip and center body. In addition, around the kink (where the sweep angle decreases, the airfoil changes and the thickness decreases), additional vortices (15 on each side) are placed which are also spaced in a cosine fashion to account for the high gradients that are expected there.

Table 5.7: Inputs and Outputs of the AVL Simulations at Cruise (CR), Take-off (TO) and Landing (LD)

Input	CR	TO	LD	Output	CR	TO	LD
$Planform$	Fig. 5.3	Fig. 5.3	Fig. 5.3	α_{trim}	3.159	16.26	16.28
C_{D_0}	0.00339	0.00630	0.00630	C_D	0.00608	0.08637	0.08640
$C_{L_{des}}$	0.153	0.952	0.952	C_{L_α}	4.36	3.36	3.35
M	0.8	0.210	0.198	e	0.689	0.893	0.893
V	239.55	72.0	67.8	L/D	25.24	11.0	11.0
ρ	0.413	1.225	1.225				

The results that are obtained using the above methods can be seen in Table 5.7. The first thing that is noticeable from the output table is the low drag and lift coefficients. The drag coefficient is low due to C_{D_0} and C_L. The drag coefficient consists of two components: the zero lift drag and the induced drag. The induced drag results from the lift coefficient. Therefore, the drag coefficient is also low due to the relation with those two values. The lift coefficient was expected to be on the lower side because of the aircraft's large surface area. From Equation 5.1 it can be seen that a large surface area results in a lower lift coefficient.

Secondly, the Oswald efficiency factor in cruise seems to be accurate, yet the other values seem questionable. More about this is discussed in Subsection 5.3.7.

Next to these values, the lift distribution is also a result that comes from the analysis using AVL. AVL outputs the lift coefficient over the different locations in spanwise direction. Using these values the lift distribution is found. A visual interpretation of the lift distribution can be seen in Figure 5.9. As the downward lift produced seems to be large, it is only at the first point on

---

[1]`http://web.mit.edu/drela/Public/web/avl/avl_doc.txt`[accessed on 12 June 2020]

the wing and thus does not contribute with any significance. The green lines represent the lift distribution, whereas the red lines connect the lift distribution chordwise. The lift distribution is needed for the structural analysis of the Hydrojet. This will be explained in more detail in Section 5.5.
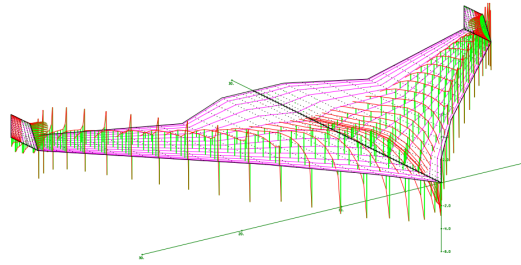

Figure 5.9: AVL Lift Distribution

5.3.6. Verification

As described above, AVL is used to calculate different parameters. In order to check if the correct model is implemented into AVL, the model has to be verified. The AVL geometry is compared with the aircraft drawing that results from the CATIA model. The aircraft implemented in AVL can be seen in Figure 5.10, the aircraft drawing resulting from CATIA in Figure 5.11.
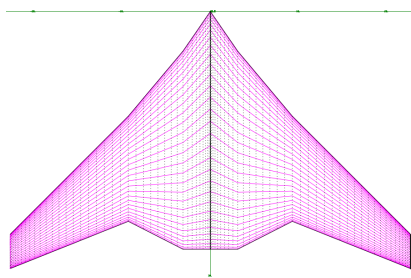

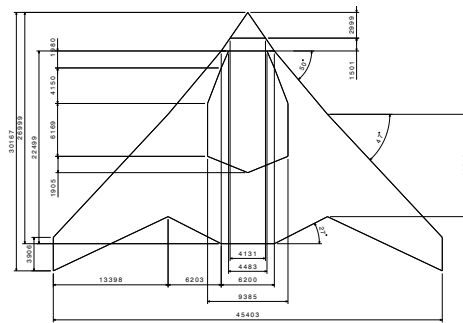Figure 5.10: AVL Aircraft Geometry

Figure 5.11: CATIA Aircraft Geometry

From these two figures it can be seen that the geometry of AVL and CATIA are almost identical. Furthermore, the lengths can be seen in more detail in AVL and they are compared with the lengths in the CATIA drawing. These values are also very similar. From this similarity it is concluded that the model in AVL is correct and is therefore verified.

5.3.7. Validation

AVL Simulation: In the previous section, it was already argued that the AVL software was a suitable model for the simulation purposes: simulating trim at cruise. AVL itself is verified and validated software if used correctly, so the validation will be focused on comparing the AVL outputs to expected outcomes in reality. This will be done in subsequent paragraphs.

Zero Drag Coefficient C_{D_0}: To validate the zero drag coefficient reference values have been searched for to compare with. From [13] and [9] it is estimated that the zero drag coefficient is in the range of 0.0058-0.0068. Compared with the zero drag coefficient during take-off and landing of the hydrojet, 0.0063, this value is a good estimate. The zero drag coefficient during cruise is on the lower side (0.00338). Although [24] states that a value of 0.006 is a good approximation for the zero drag coefficient during take-off and landing, but not for cruise, this value is on the lower side for cruise. The zero drag estimation is based on the component build up method. This method relies mostly on being able to detect the different sections of the aircraft. As the blended wing is only one wing, it is harder to estimate all the different components. Furthermore, during the calculation certain values have been assumed that result from conventional aircraft. This could also result in the zero drag coefficient being on the lower side.

A second method is also used in order to validate the results for the zero drag lift coefficient. This is done because there has never flown a commercial blended wing body aircraft, and thus all data that is gathered is from estimations. The second

method makes used of Equation 5.26.[7]

$$C_{D_0} = C_{f_e} \frac{S_{wet}}{S_{ref}} \tag{5.26}$$

Where C_{f_e} is different for several types of aircraft. For the blended wing it is assumed to be equal to 0.0020.[7] Using the values for the wetted and reference surface area, the zero drag lift coefficient is equal to 0.00413. This result is in between the value found for the zero drag coefficient for take-off/landing and cruise. The reason for this is most likely that the factor C_{f_e} includes both scenarios.

Although C_{D_0} is on the lower side, it is assumed a good value for a first approximation. When more detailed analysis can be done in a later stage, this value will change accordingly.

Oswald Efficiency Factor e: The Oswald efficiency factors that came out of the AVL simulation were 0.689, 0.893 and 0.893 for cruise, take-off and landing, respectively. Let's compare the value for cruise with aircraft of similar (mission) characteristics, seen in the table below:

Table 5.8: Values for e During Cruise of Similar Aircraft, with Related Characteristics [25]

Aircraft	Span [m]	Taper Ratio [-]	Cruise Mach [-]	e [-]
A319	34	0.24	0.79	0.753
A320	34.1	0.24	0.79	0.783
B737-800	34.32	0.219	0.78	0.660
B767-300	48	0.306	0.8	0.670

It can be seen that the value of 0.689 seems to be within realistic bounds, as it lies somewhere between the aircraft with similar missions (A319/320 and B737) as well as aircraft with similar span and taper ratio (like the B767), which influence e. Hence, the value AVL outputs are accepted as valid. The other two seem to be off. As the aircraft does not use HLDs, the Oswald efficiency factor should remain fairly constant across all flight phases, as only those are known to lower the Oswald efficiency factor with about 10 %, which does not explain the value of 0.893, which is much higher than for cruise. The reason why these values are off can be explained by the fact that AVL is not made for simulating high angles of attack. The angles of attack corresponding to take-off and landing can be seen in Table 5.7, and are significantly high. Therefore, AVL results for those cases have to be treated with caution. The high disturbance of the flow during take-off and landing is not modelled with AVL, and therefore the 3D effects, meaning induced drag and thus e, are not accurately represented. These Oswald efficiency factors are thus not considered correct.

Lift Curve Slope C_{L_α}: The lift curve slope from AVL can be directly compared to the value obtained using the DATCOM method, which used Equation 5.6. Looking at Table 5.5, the lift rate coefficient for cruise via the DATCOM method is 4.6928 1/rad, while from Table 5.7 (AVL), a slope of 4.36 1/rad is found. This is a difference of 7.633 %. Since the DATCOM method is specifically made for 3D wings in compressible flows, these values for the cruise lift rate coefficient are accepted as realistic and correct. As for the other flight phases, as aforementioned, the AVL results need to be taken with a grain of salt. In this case, the difference is not that large: DATCOM yields an approximate 3.78 1/rad slope for both take-off and landing while AVL shows a slope of 3.36 1/rad. This is a difference of about 12.5 %, which is already more questionable yet still not dramatic considering the poor performance of AVL in high angle of attack situations. Nonetheless will the DATCOM values be considered to be the valid ones.

5.3.8. Risk
During design different risks are implemented in the aircraft that affects its performance when operating. The different risks that have been identified for the aerodynamics of the planform are:

- Excessive drag leads to a higher fuel consumption
- Not providing sufficient lift during take-off and landing due to the absence of HLDs
- Too high angle of attack which results in 'tail' strike
- Too high angle of attack interferes with pilots visibility

First of all, the drag could be underestimated during the design. Using data from models and software tools during calculation can affect the accuracy. However, as sufficient iterations can improve the accuracy this risk is expected to be minimal. When a scale model is built and analysed more exact values will be known.

During the design no HLDs are implemented, as explained in Subsection 5.3.4. However, all commercial aircraft that fly nowadays make use of HLDs. Omitting the HLDs thus brings a risk as they are not used, even if the analysis is done properly. However, not making use of HLDs also removes the risk of them not working. Further analysis and testing of the aircraft can lower the risk more.

The last risks come from the angle of attack during take-off and landing. A too high angle of attack can interfere with the pilot's visibility. As it is crucial during take-off that the pilot has sufficient visibility this should be designed for properly. During the design, the angle of attack is determined (Section 5.3.2) and from this it can be seen if the visibility is limited or not. Therefore, this risk is mitigated as insignificant. Apart from the pilots visibility, the angle of attack can also cause 'tail' strike. Even though the aircraft does not have a tail, the fuselage should be analysed properly. This can be analysed in detail and this risk is therefore mitigated as improbable.

5.4. Stability and Control

Stability is an important part of characteristic of an aircraft. Therefore, the stability of the Hydrojet will be analysed using the planform and aerodynamic characteristics, starting with longitudinal stability. Next, the wing twist needed in order to be and remain stable is identified. After this, the elevons will be sized. Additionally, directional and dynamic stability of the planform is investigated. Also, the methods used will be verified and validated. Finally, the risks concerning stability and control will be identified and mitigated.

5.4.1. Longitudinal stability

Because a new cabin layout has been defined the centre of gravity (CG) analysis done in the Midterm Report has to be updated.[1] The loading diagram in Figure 5.12 shows the CG at different loading conditions starting from the operational empty weight and ending up at the design maximum take-off weight. On the X-axis is the CG as a fraction of the Mean Aerodynamic Chord (MAC) and on the Y-axis is the aircraft mass at that specific loading condition. From this diagram, after adding a margin of 2 %, the most forward and aft CG can be found. This CG range is dependent on the longitudinal placement of the wing, indicated by the X-location of the Leading Edge of the MAC (XLEMAC), as can be seen in Figure 5.13. To be longitudinally stable, satisfying requirement HPRA-REQ-S&C-1.1, an aircraft has to respond to any difference in angle of attack with an opposite moment, which means that $dC_m/d\alpha = C_{m_\alpha} < 0$. For a tailless aircraft like the Hydrojet Equation 5.27 applies.[8]

$$C_{m_\alpha} = C_{L_\alpha} \frac{x_{cg} - x_{np}}{MAC} < 0 \tag{5.27}$$

Where C_{m_α} and C_{L_α} are the derivatives with respect to the angle of attack of the moment and lift coefficient, respectively. For a tailless aircraft the neutral point (x_{np}) coincides with the aerodynamic centre (x_{ac}), which is assumed to be at 0.25 MAC. With a stability margin of 0.05 MAC [8] Equation 5.27 is satisfied if the most aft CG does not exceed 0.20 MAC. Furthermore, the aircraft should also be trimmable. When an aircraft is trimmed the moment coefficient C_m is equal to zero. For a tailless aircraft Equation 5.28 needs to be satisfied.[8]

$$C_{m_{ac}} = C_L \frac{x_{ac} - x_{cg}}{MAC} \tag{5.28}$$

Due to the stability requirement ($x_{ac} - x_{cg} > 0$) $C_{m_{ac}}$ needs to be positive. Since $C_{m_{ac}}$ is negative for most airfoils $C_{m_{ac}}$ is minimised by choosing the most forward CG to be as close to the aerodynamic centre as possible. With Figure 5.13 an XLEMAC can be chosen that satisfies both these requirements, as can be seen with the black dotted lines. Since the Hydrojet is a blended wing body aircraft, the wing cannot be moved longitudinally like with a conventional aircraft, the wing planform has to be designed such that the chosen XLEMAC is achieved. The outer wing sweep and taper ratio are sized with this in mind. The inputs for the loading diagram can be seen in Table 5.9. This yields the chosen XLEMAC together with the CG range, which can be found in Table 5.10.

Table 5.9: Inputs of the loading diagram

Inputs			
OEW [kg]	52,920	MAC [m]	16.11
W_{fuel}[kg]	9,396	C_r [m]	27
$W_{payload}$ [kg]	30,000	N_{pax} [-]	236

Table 5.10: Outputs of the loading diagram

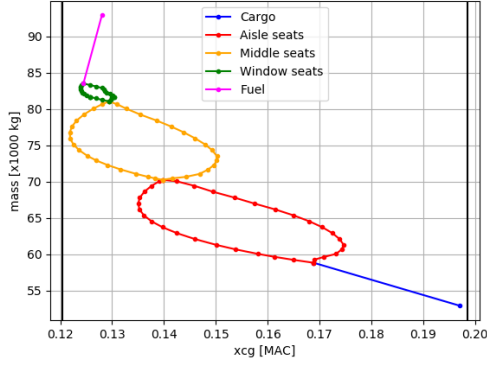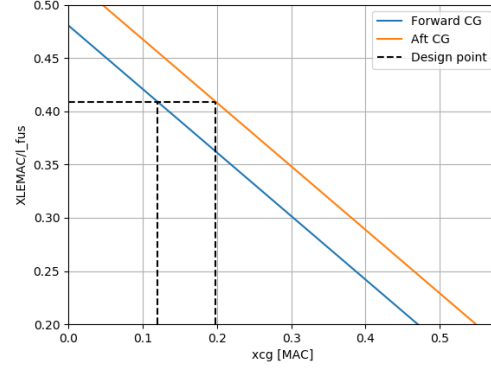| Outputs			
x_{cg} forward [MAC]	0.1201	x_{cg} aft [MAC]	0.1984
XLEMAC [m]	11.04		

Figure 5.12: Loading diagram Hydrojet

Figure 5.13: Centre of gravity as function of wing placement

5.4.2. Wing twist

The controllability requirement from Equation 5.28 requires the moment coefficient around the aerodynamic centre ($C_{m_{ac}}$) to be positive for tailless aircraft, while it is negative for most airfoils. The total $C_{m_{ac}}$ can be made positive by the use of a reflex airfoil or by a combination of wing sweep and a negative twist angle, which makes the wingtips act like a horizontal tail providing negative lift.[8] Since wing sweep is already necessary to fulfil the stability requirements and to allow for more flexibility in the choice of airfoil with regards to aerodynamics, the second option was chosen. To achieve the $C_{m_{ac}}$ as required by Equation 5.28 a suitable twist angle must be chosen. $C_{m_{ac}}$ can be expressed as a function of the airfoil $c_{m_{ac}}$ and lift coefficient as in Equation 5.29.[26]

$$C_{m_{ac}} = \frac{2}{S \cdot MAC} \left(\int_0^{\frac{b}{2}} c_{m_{ac}} c^2 dy - \int_0^{\frac{b}{2}} c_{l_b} c(x - \bar{x}_0) dy \right) \tag{5.29}$$

Where c_{l_b} is the airfoil lift coefficient at $\alpha_{C_L=0}$ or the angle of attack (AoA) at which the total lift is zero. This AoA is found by integrating the lift over the entire wing with Equation 5.30 and using a root finding algorithm to find $\alpha_{C_L=0}$.

$$\frac{L}{\frac{1}{2}\rho V^2} = \int_0^{\frac{b}{2}} c_{l_\alpha}(\alpha_{loc} + \alpha_0) c dy \tag{5.30}$$

Where α_{loc} varies over the span and is a function of the global AoA. The found $\alpha_{C_L=0}$ is then used to calculate c_{l_b} in Equation 5.29. The required twist angle is obtained by iteration with the requirement that the $C_{m_{ac}}$ from Equation 5.29 is equal to or larger than the controllability requirement in Equation 5.28. The calculated twist and the total $C_{m_{ac}}$ together with the important inputs of the calculation can be found in Table 5.11. The outputs can be found in Table 5.12. With these parameters the requirement HPRA-REQ-PLF-1 can be satisfied.

Table 5.11: Inputs of the twist calculation

Inputs			
$\Lambda_{outer\ wing}$ [deg]	45	NACA 25112 α_0 [deg]	-1.5
$\lambda_{outer\ wing}$ [-]	0.4	MH 45 α_0 [deg]	-1.02
NACA 25112 c_{l_α} [1/deg]	0.117	NACA 25112 $C_{m_{ac}}$ [-]	-0.01
MH 45 c_{l_α} [1/deg]	0.114	MH 45 $C_{m_{ac}}$ [-]	0.0145

Table 5.12: Outputs of twist calculation

Outputs	
Twist [deg]	-1.7
$C_{m_{ac}}$ [-]	0.0199

5.4.3. Elevons

To be able to control the aircraft in roll, which satisfies requirement HPRA-REQ-PLF-3, a pair of ailerons are used, which are located near the wing tips to maximise the moment arm. For tailless aircraft these are usually combined with elevators, which enable pitch control, satisfying HPRA-REQ-PLF-2. Placing these so called elevons near the wing tips also increases their pitch control effectiveness as the positive sweep increases the moment arm with respect to the centre of gravity. These elevons can be sized with a roll rate requirement (P) and Equation 5.31.[7]

$$P = -\frac{C_{l_{\delta a}}}{C_{l_P}} \delta a \left(\frac{2V}{b} \right) \tag{5.31}$$

Where δa is the elevon deflection angle and the coefficients $C_{l_{\delta a}}$ and C_{l_P}, which are not lift but roll moment coefficients, are given by Equation 5.32 and Equation 5.33, respectively.

$$C_{l_{\delta a}} = \frac{2 c_{l\alpha} \tau_a}{S_{ref} b} \int_{b1}^{b2} c(y) y \, dy \qquad (5.32)$$

Where c_{l_α} is the airfoil lift slope and τ_a is the aileron effectiveness, which depends on the aileron-to-wing chord ratio as can be seen in Figure 5.14. The bounds of the integral, b1 and b2, are the spanwise locations of the beginning and end of the elevons, respectively.

$$C_{l_p} = -\frac{4(c_{l\alpha} + c_{d0})}{S_{ref} b^2} \int_0^{\frac{b}{2}} c(y) y^2 \, dy \qquad (5.33)$$

Where c_{d0} is the zero-lift drag coefficient of the airfoil and the integral is evaluated over the half span of the wing. The elevon deflection angle (δa), elevon-to-wing chord ratio (c_e/c), and the spanwise position and size of the elevons can be chosen such that the roll rate requirement P is met. The inputs and outputs of these calculations can be found in Table 5.13 and Table 5.14, respectively. For these calculations the roll rate requirement from HPRA-REQ-PLF-3.1 was not used as it required a smaller elevon area or deflection than the roll rate in Table 5.14. For next design phases the elevons can also be checked on pitch control requirements.
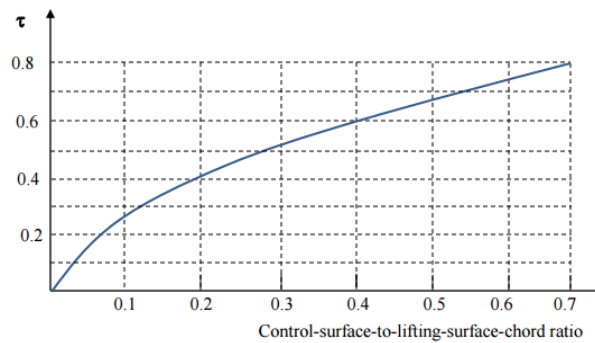

Figure 5.14: Aileron effectiveness parameter[27]

Table 5.13: Inputs of elevons sizing

Inputs			
$\Lambda_{\text{outer wing}}$ [deg]	45	NACA 25112 α_0 [deg]	-1.5
$\lambda_{\text{outer wing}}$ [-]	0.4	MH 45 α_0 [deg]	-1.02
NACA 25112 c_{l_α} [1/deg]	0.117	NACA 25112 $C_{m_{ac}}$ [-]	-0.01
MH 45 c_{l_α} [1/deg]	0.114	MH 45 $C_{m_{ac}}$ [-]	0.0145

Table 5.14: Outputs of elevons sizing

Inputs			
P [7] [deg/s]	20	clα[1/deg]	0.114
τ_a [-]	0.4	cd0 [-]	0.00571

5.4.4. Directional stability
Another important part of static stability is the directional stability (from HPRA-REQ-S&C-1.2), where a change in yaw angle causes a moment in the other direction. Due to the fact that the yaw angle and yaw moment are defined as positive in opposite directions, directional static stability corresponds to a positive yaw moment derivative with respect to the yaw angle ($C_{n_\beta} > 0$). Directional stability in conventional aircraft is usually provided by the vertical tail but since the Hydrojet does not have a tail another solution has to be found. One solution could be to mount vertical stabilisers on the engine nacelles, which would provide sufficient space for them. It would however introduce bending moments to the engine pylons for which it usually is not designed. Another option is to add winglets that are large enough to provide stability. Due to the wing sweep vertical stabilisers on the wing tips will have a larger moment arm, which increases their effectiveness. Additionally, not being mounted on the engines they will not cause as large a roll moment on the wing tips, which reduces the lateral-directional coupling. Having winglets has the additional benefit of reducing the induced drag. With a span of 2 m for each winglet, AVL analysis shows that directional stability is achieved with a C_{n_β} of 0.0142. For the purposes of yaw control rudders will have to be placed on both winglets. In a later design phase these should be sized on directional control, so yaw rate, or directional trim requirements like requirement HPRA-REQ-LOC-2.[27]

5.4.5. Dynamic stability
A statically stable aircraft is not necessarily dynamically stable. Dynamic stability can be described by a set of dynamic eigenmotion: The short period, phugoid, aperiodic roll, dutch roll and the spiral mode. Each of these eigenmotions can

be either stable or unstable, meaning that they are damped or amplified without active control systems. These eigenmodes are analysed with the Athena Vortex Lattice (AVL) software. This software can simulate the different eigenmotions and determine if they are stable by calculating their eigenvalues. These eigenvalues can be seen in Table 5.15. The real part of all the eigenvalues are negative, which indicates that the aircraft is stable for all eigenmotions, which means that HPRA-REQ-S&C-1.3 is satisfied. The real part shows the growth of the motion where positive means that the motion is amplified and negative means that the motions is damped. The imaginary part says something about the periodic nature of the motion. If the eigenvalue has no imaginary part the motion is aperiodic, as is the case with the aperiodic roll and the spiral.

Table 5.15: Dynamic eigenvalues

Eigenmotion	Real part	Imaginary part
Short-period	-0.8758	±2.251
Aperiodic roll	-1.4323	0.0
Dutch roll	$-0.7211 \cdot 10^{-2}$	±0.6187
Spiral	$-0.1728 \cdot 10^{-2}$	0.0
Phugoid	$-0.2244 \cdot 10^{-2}$	$\pm 0.3317 \cdot 10^{-1}$

5.4.6. Verification

In this section the results from stability and control will be verified. This includes the loading diagram, longitudinal stability, zero-lift AoA, wing twist and dynamic stability.

Loading diagram
In the loading diagram the passengers are loaded with the aisle-middle-window order. This order is chosen because it is assumed that the passenger preference would be in that order. This method of finding the CG range is verified by changing this order to see how the CG range changes. While the overall shape of the loading diagram changes the most forward and aft CG do not.

Longitudinal stability: The longitudinal stability is ensured by the fact that C_{m_α} is negative. This can be verified with AVL, which also calculates several stability derivatives. According to the AVL calculations $C_{m_\alpha} = -1.586$, which confirms the longitudinal stability of the Hydrojet.

Zero-lift AoA: The method for finding the zero-lift angle of attack α_0 was verified by comparing the result with the α_0 of both airfoils of the wing. The α_0 of the wing should be close to those of the airfoils while also being slightly higher due to the negative twist. For the chosen airfoils NACA 25112 and MH 45 α_0 is approximately -1.5 and -1.02 degrees, respectively. Comparing this to the α_0 of the wing, -0.00518 degrees, this meets the expectations.

Wing twist: The script calculating the $C_{m_{ac}}$ of the wing and the required wing twist for controllability was verified by checking its behaviour when changing certain parameters. The sweep of the wing has an effect on the moment arm of the outer wing. A higher sweep angle would increase the moment arm and therefore increase the effect the outer wing has on the total $C_{m_{ac}}$. Since the airfoil of the outer wing has a positive $C_{m_{ac}}$ and since the outer wing produces negative lift at α_0, a higher sweep angle should increase the total $C_{m_{ac}}$ and decrease the required twist. This was confirmed by the $C_{m_{ac}}$ script. The same is true for the outer wing taper ratio, a higher taper ratio increases the $C_{m_{ac}}$ and decreases the required twist angle.

Dynamic stability: Verifying the eigenvalues calculated by AVL is difficult without numerically solving the equations of motion. For this a lot of stability derivatives are needed, some of which have been calculated in previous sections and others are difficult to estimate especially for a blended wing body aircraft. This will be done in the next phase of the design. The eigenvalue of the aperiodic roll however, is mostly dependent on one stability derivative, C_{l_p}, which was estimated for the sizing of the elevons.[26] In that section the C_{l_p} was estimated to be -0.012, so negative, which agrees with the aperiodic roll stability predicted by the eigenvalue.

5.4.7. Validation

Validation for stability and control was done by comparing the results obtained from the models with other designs and common practices in aviation. The assumed OEW centre of gravity for the Hydrojet of 52.7 % of the body length was compared to a few concepts like in [28], which had its OEW centre of gravity at 57.5 %. Another BWB concept, the SAX-29, had it at 59 % [29], both of which are close but further back. The wing twist for aircraft usually are under 5 degrees and for the purposes of avoiding tip stall have to be negative.[7] The wing twist of -1.7 degrees obtained from this analysis was therefore deemed to

be realistic.

5.4.8. Risk
Due to the novelty of the Hydrojet planform shape there is a lot of uncertainty with regards to stability and control. The stability of blended wing bodies, due to the fact of not having a tail, can be difficult to analyse. This means that there are some risks involved in the design, some of which are:

- Wrong assumption of a.c. location
- Inaccuracy of the dynamic stability analysis

The aerodynamic centre (a.c.) of the wing was assumed to be at 25 % of the MAC. If this assumption is incorrect the aircraft may not be longitudinally statically stable. This risk has been decreased with the stability margin of 5 % and it may be decreased even more with a detailed calculation of the a.c. position.

The dynamic stability was assessed with the eigenvalues calculated with the AVL software. Some of these eigenvalues were very close to 0 and a positive eigenvalue would mean instability in that particular eigenmotion. Instability in the spiral would not be a big problem as the pilots have enough time to correct but for other eigenmotions active control systems have to be in place to stabilise the aircraft.[30] Next to active control, further analysis should be done on the dynamic stability by for example verifying the AVL analysis with the calculation of the necessary stability derivatives to simulate the dynamic eigenmodes.

5.5. Structures
The size of the aircraft has been determined now, based on the general, stability & control and aerodynamics requirements in Section 5.1. Next, structural analyses are performed in order to assess the structural characteristics of the Hydrojet. The structure of an aircraft is a vital component, because it sustains all the loads experienced during a mission and functions as an attachment frame for all the (sub)systems. It is therefore important that the structure of an aircraft is designed accordingly. Furthermore, to align with the Strategic Research and Innovation Agenda (SRIA) objectives, the structure of the aircraft will be designed to incorporate structural health monitoring (SHM) concepts. This will be done using non-destructive testing (NDT) techniques in order to promote the damage tolerance design philosophy [2].

For the analysis, the aircraft structure is split up into the inner wing and the outer wing, and only the lift loads are analysed to have a more conservative approach.

5.5.1. Outer wing
In Figure 5.15 the wing-box of the outer wing can be seen, which is used for the analyses. The following assumptions are made for the analyses of the wing-box:

1. The wing is modeled as a beam.
2. The cross-section of the wing-box is assumed to be rectangular.
3. The shear center and centroid are located in the center of the cross-section.
4. The lift acts at the quarter chord.
5. The effects of the taper on the normal stresses are neglected.
6. The front and aft spar are located at 3.5% and 85 % of the chord respectively to allow for the hydrogen tank integration.
7. The stringers are modeled as point masses on the skin of the wing-box.
8. Ribs are placed at a spacing of $61cm$. [31]

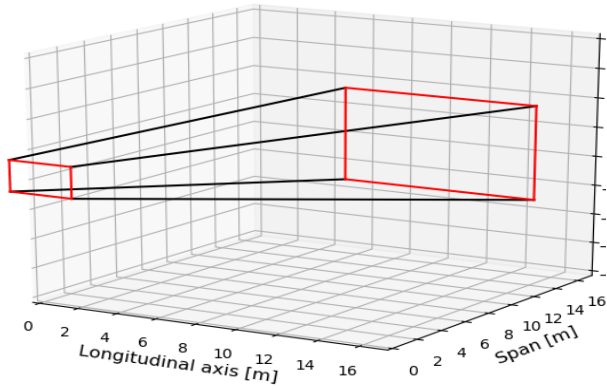[2]http://www.clean-aviation.eu/[accessed on 28 May 2020]
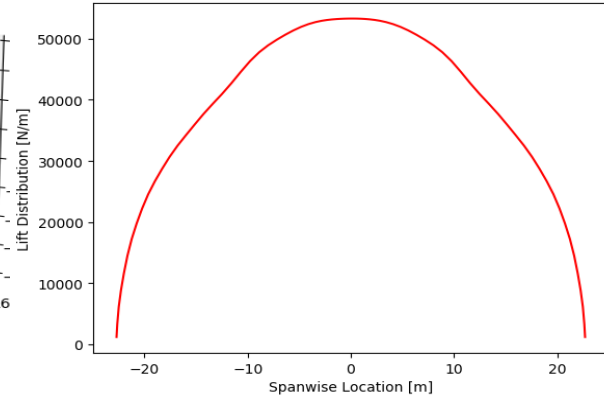
Figure 5.15: Wing-box model

Figure 5.16: Spanwise Lift Distribution during cruise

The lift distribution utilised for the computations is retrieved from AVL and can be seen in Figure 5.16. This distribution is integrated once to get the shear (V_{shear}) distribution and twice to get the moment (M) distribution in spanwise direction. The following boundary conditions are used to determine the integration constants:

$$V_{shear}(tip) = 0 \qquad (5.34) \qquad\qquad M(tip) = 0 \qquad (5.35)$$

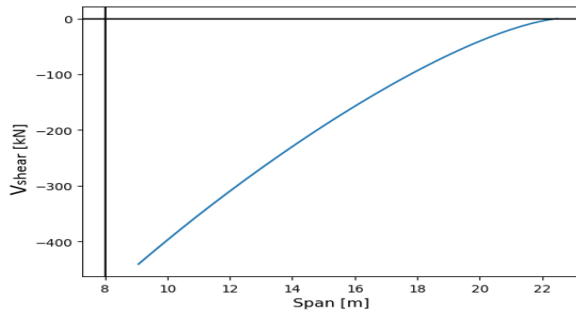The resulting graphs can be seen in Figure 5.17 and Figure 5.18.
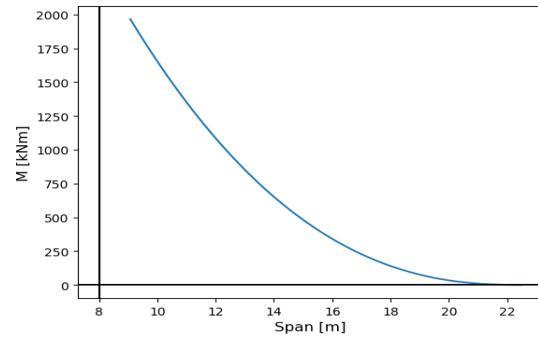

Figure 5.17: Spanwise shear force

Figure 5.18: Spanwise moment

The torque at the root of the outer wing, which is needed for the calculations of the bending stresses in the inner wing, is determined as well. Subsequently, the normal stresses are calculated using Equation 5.36. The moment of inertia is calculated using standard formulas for thin-walled cross-sections as described by the book "Aircraft Structures for Engineering Students".[32]

$$\sigma_n = \frac{M_{xx} \cdot y}{I_{xx}} \qquad (5.36)$$

The retrieved span-wise stress distribution is multiplied by the ultimate load factor. The latter is found by multiplying the critical load factor retrieved from Figure 4.5 in Chapter 4 by 1.5 (requirement HPRA-REQ-STR-2).

The maximum stress is at the root of the outer wing, as expected. This maximum stress should not exceed the yield stress of Glass-Epoxy, which is 504Mpa. The stress is lowered by increasing the moment of inertia, which is done by increasing the skin thicknesses and adding stringers. Typical stringers used for a wing box are: Z-, J-, Y-, I-, T- and hat-stringers. Z- stringers are chosen for the wing-box of the outer wing, because of their relatively high structural efficiency and ease of assembly.[33]

Multiple iterations are performed to match the yield stress of Glass-Epoxy and the updated stress distribution can be seen in Figure 5.19. The new geometrical characteristics can be found in Table 5.16.
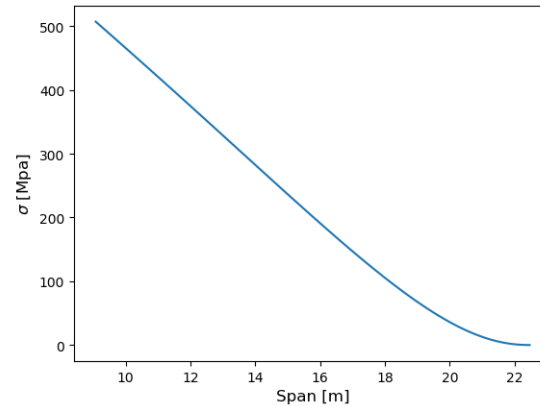
Figure 5.19: Normal stress distribution outer wing

	First value [m]	Optimised value [m]
Skin thickness	0.001	0.0014
Spar thickness	0.001	0.01
Stringer		
Top skin	0	8
Bottom skin	0	5
Thickness	-	0.004
Height	-	0.055
Width	-	0.033

Table 5.16: Characteristics wing-box

5.5.2. Inner wing

Prior to the structural analysis of the inner wing, a cabin cross-section design must be chosen. Three fuselage concepts, mentioned in the Midterm Report, can be seen in Figure 5.20.[1]
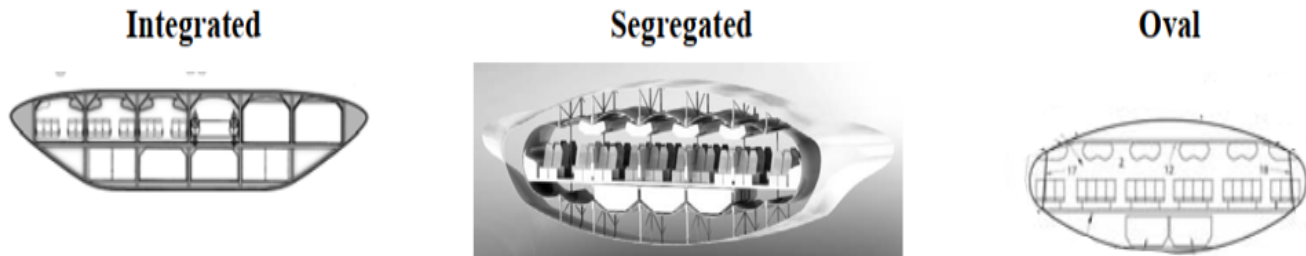

Figure 5.20: Fuselage concepts BWB [34]

The 'integrated concept' contains a sandwich structure, which carries both pressurisation and aerodynamic loads. Due to the non-circular cross-section of the fuselage, pressurising the cabin will primarily result in bending stresses instead of skin-membrane stresses. Sandwich structures have a high bending stiffness and are therefore used to cope with these bending stresses.

The 'segregated concept' on the contrary is a double-skin concept. The inner skin carries the pressurization loads, while the outer skin carries the aerodynamic loads. According to some, this concept is lighter and superior due to its load diffusion and fail-safe characteristics. However, others argue that in case of rupture of the inner skin the pressurisation loads need to be carried by the outer shell, which, therefore, needs to be designed accordingly. The latter adds extra weight.[34]

The 'oval concept' is a relatively new concept. The pressurisation of this cross-section will only result in in-plane stresses, hence bending moments due to the pressurisation of the cabin will be absent. Furthermore, the horizontal members of the

cabin are loaded in compression and the vertical in tension. For this concept the wasted pressurised space is larger compared to the other concepts. When increasing the radii of the fuselage panels, the weight of this concept becomes relatively larger.[34]

The chosen concept for the Hydrojet is a combination of the integrated and segregated concept. The oval fuselage would be the best to withstand the pressurisation loads and keep the weight low, but the height of the fuselage is larger compared to the integrated fuselage. The same also holds for the segregated cross-section. The height of the fuselage is limited by the t/c ratio of the chosen airfoil for the center body. Therefore, the integrated concept is deemed to be the only applicable option. This is modified by integrating the multi-arched inner skin of the segregated concept, to deal with the cabin pressure.

The cross-section can be seen in Figure 5.21. The arcs are modelled as triangles (depicted in green) to simplify the calculations for cross-sectional properties. This was also done to decrease the difficulty of generalising the cabin to contain more bays, and/or aisles, during the design process.
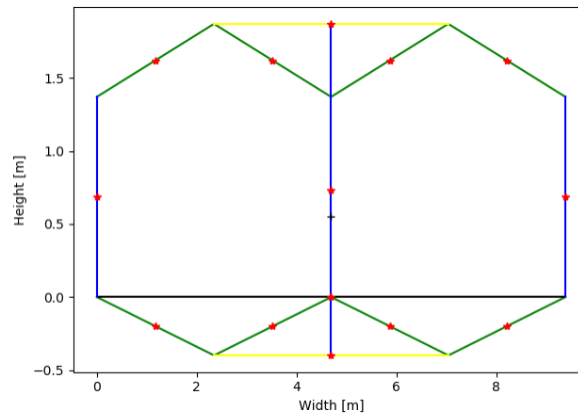

Figure 5.21: Cabin cross-section

The aft part of the aircraft should also be built to cope with the cabin pressure, however, this will result in a heavy structure and wasted pressurised space. For these reasons an aft bulkhead is placed at the end of the cabin, in order to seal the pressurised part and support the pressurisation loads. This aft bulkhead is aligned with the rear spar of the outer wing to create a continuous load path and a more efficient structure. Furthermore, keel beams will be used to optimise the structure.

The following assumptions are made for the analyses of the inner wing:

- The arcs are modelled as triangles for the moment of inertia computations.
- All the lift forces are carried by the cabin structure.
- The lift distribution of the inner wing is constant along the length.
- The cross-section of the cabin is constant.
- The cabin floor does not carry any bending loads caused by aerodynamic forces.

The lift distribution along the length of the fuselage is found by integrating the span-wise lift distribution of the inner wing and dividing this by the length of the cabin. Again, this distribution is integrated once to retrieve the shear distribution and twice to obtain the moment distribution. The obtained graphs can be seen in Figure 5.22 and 5.23. It can be noticed that both diagrams are not zero at the end of the cabin. This is caused due to the constant lift distribution assumption. For a BWB the lift is not constant length wise, because the reference area varies over the length of the aircraft and the airfoil camber as well.
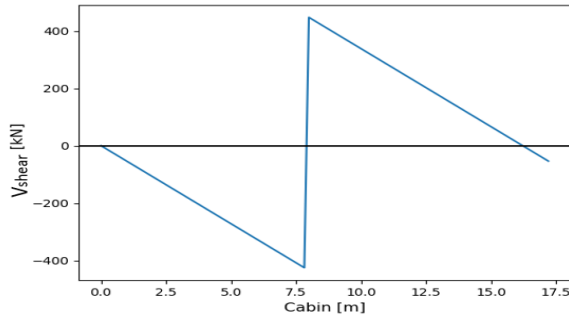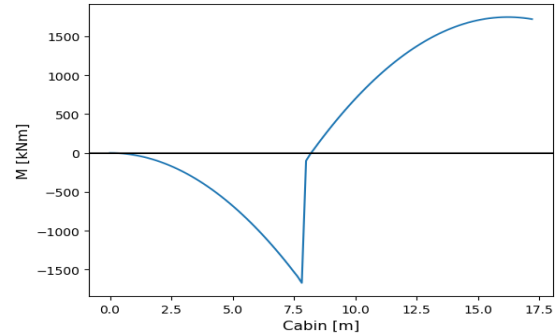
Figure 5.22: Cabin shear force diagram

Figure 5.23: Cabin moment diagram

The moment of inertia is calculated using a python script. First the geometry of the cross-section is generated and the center of gravity is found, then the moment of inertia is calculated for each section and summed up. The normal stress is calculated using Equation 5.36 and Equation 5.37. The latter is the axial stress due to the pressure difference between the cabin and the ambient environment. A pressure difference of 57571.22 Pascal is used, which is the same as the Boeing 737-900 [3]. The obtained stresses are subsequently multiplied by the ultimate load factor as was done for the outer wing.

$$\sigma_{\text{axial}} = \frac{\Delta p R}{2t} \tag{5.37}$$

An attempt was also made to match the yield stress of the cabin material, which is also Glass-Epoxy. However, the yield stress would only be reached for skin thicknesses below 1mm and would not be resistant against impacts. For this reason, a skin thickness of 1mm has been chosen. The wall thickness has been chosen the same as the spar for the outer wing. The resulting stress distribution can be seen in Figure 5.24. It can be seen that the shape of the diagram is similar to the one of the moment distributions, this is due to the constant moment of inertia throughout the length of the cabin. Furthermore, a peak is located at the end of the cabin. The latter is caused by the continuous lift distribution. In the actual situation the lift distribution would be higher at the front of the fuselage near the aerodynamic center. This would move the peak somewhere close to the center of the cabin. The cross-sectional properties can be found in Table 5.17.
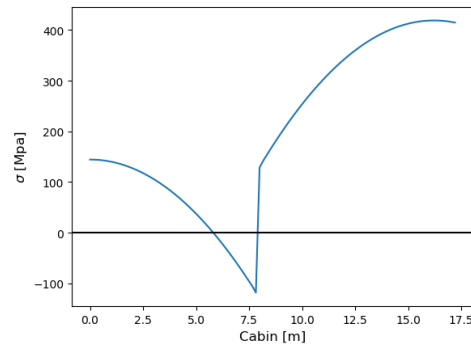
Figure 5.24: Normal stress distribution along the cabin length

Table 5.17: Characteristics cabin

	First value [m]	Optimised value [m]
Skin thickness	0.002	0.001
Wall thickness	0.005	0.01

5.5.3. Flutter
A phenomenon that can occur during an aircraft mission is flutter and can be described as dynamic instability of an elastic body in an airstream. This occurs at the flutter speed (V_f) when the unsteady aerodynamic loads caused by the oscillation

---

[3]`http://mrcabinpressure.com/aircraft.htm`[accessed on 5 June 2020

matches the structural vibration. Below this speed, the oscillations of the structure will be stable and above V_f the oscillations will diverge (unstable).

A system with one degree of freedom can generally not be unstable, unless it contains unusual characteristics. On the contrary, a system with two or more degrees of freedom can be unstable without having any unusual characteristics. The forces related to the different degrees of freedom can interact, resulting in unstable oscillations for particular phase differences. For an aircraft wing, these are bending and torsion.

In a pure bending or pure torsional motion, the aerodynamic forces generated by the effective wing incidence oppose the motion. Hence, pure bending or pure torsional oscillations converge. This is not the case for a combined oscillation with a 90 degree phase difference, in other words maximum bending occurs at zero twist and vice versa. The latter can be seen in Figure 5.25. At zero bending twisting of the wing creates a positive geometric incidence for an upward movement of the wing, thus the lift force will not oppose the motion. For a downward movement of the wing a reversed situation exists. This time a negative geometric incidence is created, and again the lift force is in the same direction as the motion. The effective wing incidence on the contrary always generates aerodynamic forces which damp the motion. At velocities above V_f the destabilization forces become larger than the damping forces and the oscillations diverge.
The forms of coupling that can occur are:

- **Inertial**: The CG is located ahead of the flexural axis. Due to an upward movement of the wing a moment is created around the flexural axis by the weight acting in the CG. The latter causes the wing to twist. So, a twisting motion is caused by a vertical motion.

- **Aerodynamic**: A change in incidence angle of the wing (rotation) results in change of lift, which causes a translation. While a translation changes the effective incidence, which results in a lift that causes a rotation. These oscillating aerodynamic forces act through the center of independence. The latter is similar to the aerodynamic center in steady motion.

- **Elastic**: For elastic coupling translation and rotation are coupled via the elastic stiffness of the wing. The spring force acts in the flexural axis and rotation is created around the center of independence.
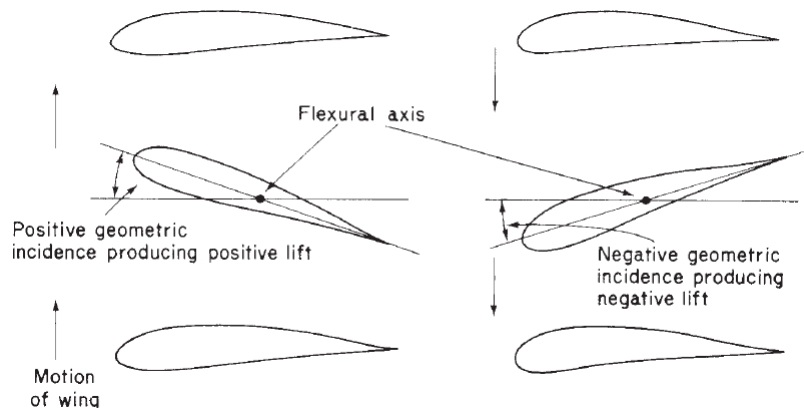

Figure 5.25: Coupling of bending and torsional oscillations

So, flutter can be prevented by decoupling the two motions. So, the inertial coupling can be prevented by making the CG coincide with the flexural. Aerodynamic coupling can be prevented by making the center of independence coincide with the flexural axis. The latter also prevents elastic coupling. It should be noted, however, that in practical circumstances, the CG and center of independence do not coincide with the flexural axis.
The flutter analysis can be done using advanced aeroelasticity simulation tools or by testing. The problems can then be solved by adjusting the stiffness and/or mass of a part, and limiting the flight envelope (avoid V_f).

5.5.4. Verification and Validation
Verification and validation is an integral part of the design process, thus needs to be done for the structures model as well. Verification is done by testing the computer model(code) for programming mistakes. This is done by performing unit testing for each function in the Python script, which is followed by integral and system testing.

Verification outer wing script: First, the geometry of the inner wing is implemented in python. Verification for this function is done visually, by plotting the geometry. The next function calculates the moment of inertia. This is verified by comparing the python results with values obtained from two online calculators[4] [5]. Both online calculators gave exactly the same results and were within 5 % of the python results. This discrepancy is caused, because the online program does not apply the thin walled assumption.

Next the load distributions are generated. The verification of this function is done by using Equation 5.38 as input for the lift distribution and checking the outcomes against analytical solutions. The results are given in Table 5.18. The obtained distributions were the same. As mentioned before, the shear force (V_{shear}) distribution was found by integrating the lift distribution once and the moment (M) distribution was found by integrating the lift distribution one more. The latter was also noticeable in the graphs, as the V_{shear} graph was quadratic and M graph was cubic.

For the torque calculations the resultant shear force was computed and multiplied by the distance to the shear center. This is verified by comparing the results with analytical solutions and is also given in Table 5.18.

As can be noted, all the errors are smaller than 1 %. These discrepancies can be caused by rounding errors.

$$L(x) = 10 \cdot x \tag{5.38}$$

Table 5.18: Verification of load distributions

	Analytical	**Python**	**Error [%]**
V_{shear}	2,155.9 N	2,155.6 N	<1
M	17,187.9 Nm	17,188.8 Nm	<1
σ_n	539 Mpa	542Mpa	<1
Torque	1,380,447.4	1,379,849.8	<1

Unit testing has been completed now and integral testing can be done. Integral testing is done to check whether the functions are connected in the right way. Some functions use the output of another function as input and even though the functions themselves are implemented correctly; the wrong input will result in faulty outcomes. Integration testing is done using the debug command of Pycharm python Integrated Development Environment (IDE). [6] An example is given in Figure 5.26. The red dot indicates the line that will be debugged. It can be noticed that all the inputs and outputs are displayed, thus wrong inputs/outputs will immediately be detected.

Figure 5.26: Integral testing Pycharm

After integral testing, system testing can be done, which involves testing the entire program. This is done by changing input parameters and checking whether the output changes in an expected way. The performed tests can be seen in Table 5.19. $L(x)$ in test one and two is the lift distribution function. The second test is also verified analytically. For test four and five, the skin thickness is increased and decreased respectively. This results in a larger and smaller Ixx respectively. A larger Ixx will result in a smaller σ_n, as can also be concluded from Equation 5.36. For the second test the shear force distribution looks like a step function, first it is equal to one and after that it increases due to the contribution of the wing. Furthermore, it is also checked if the increase is indeed equal to the shear force at the root of the outer wing.

Verification inner wing: First the cabin geometry is implemented into python, this is verified visually, by plotting the cross-section. The cabin cross-sectional properties were verified by hand, the total area had an error of 1.25%, the centre of gravity in the z direction had an error of 5.96% and the moment of inertia had an error of 8.4% compared to the program. These are mostly analytical continuation calculation errors, however some of the error is caused because of the thin-walled assumption

---

[4]https://www.johannes-strommer.com/english/calculators/area-moment-of-inertia-and-section-modulus/ [accessed on 12 June 2020]
[5]https://calcresource.com/moment-of-inertia-rtube.html [accessed on 12 JUne 2020]
[6]https://www.jetbrains.com/pycharm/ [accessed on 12 June 2020]

Table 5.19: System tests outer wing

Test #	Test	Result	Expected effect
1	L(x) =0	Only loads due to the outer wing	Same as results
2	V_{shear} =1	linear shear force and quadratic moment distribution	Same as results
3	t_{skin} = 10*t	σ_n decreases	Same as results
4	doubling differential pressure	σ_n increases	Same as results
5	Increasing the cabin length	all loads increase	Same as results
6	Decreasing the cabin length	all loads decrease	Same as results

used for the analytical calculations.

The load calculation functions used for the outer wing, were also used for the inner wing. So, unit testing is not performed again. Integral testing is also done in the same way as for the outer wing. When it has been completed successfully, system testing is done. The performed tests can be seen in Table 5.20.

Table 5.20: System tests inner wing

Test #	Test	Result	Expected effect
1	L(x) =0	No Loads	Same as results
2	L(x) =1	linear shear force and quadratic moment distribution	Same as results
3	t = 10*t	σ_n decreases	Same as results
4	t = t/10	σ_n increases	Same as results
5	Increasing the span	all loads increase	Same as results
6	Decreasing the span	all loads decrease	Same as results

Considering the successful completion of all the systems tests for both scripts the program is deemed verified.

Validation: Validation is done to prove that the considered model accurately represents the real-life situation. For the structures model validation is done by comparing the obtained results with reference aircraft data. Data is retrieved from relevant papers and conventional aircraft. Due to the novelty of the design, data from physical tests and similar aircraft is not available. First of all, the load diagrams are compared visually. For the outer wing, the shape of the bending and shear load diagrams are compared with the diagrams for the various distributions from [7]. The diagrams of the Hydrojet have the same shape as the ones used for the validation.

For the inner wing, the diagrams are compared visually with the diagrams produced by Pan et al [35]. which are depicted in Figure 5.27 and 5.28. The shear force diagram is very similar except of the small steps in the plot. These are caused by the weight of different subsystems in the aircraft. The latter is not included for the Hydrojet computations. The moment diagram is a bit different. The step in the moment diagram of the Hydrojet is not present in Figure 5.28. This is because the moment caused by the wing is not added to the cabin moment distribution of Pan et al. Furthermore, it can be observed that the bending moment diagram goes to zero at the end of the fuselage. This is not the case for the Hydrojet, because a rectangular lift distribution was assumed for the inner wing, which only holds for a conventional aircraft. For a BWB the surface area of the inner wing (fuselage) varies along the aircraft, thus the lift distribution will not be even.

---

[7]`http://ciurpita.tripod.com/rc/rcsd/bendMom/bendMom.html` [accessed on 13 June 2020]
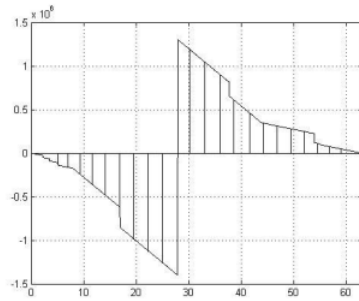
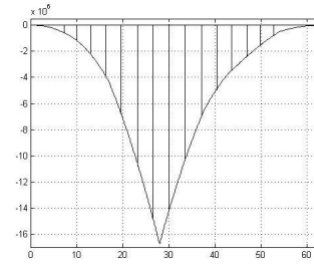Figure 5.27: Shear diagram for CJ828 Structure

Figure 5.28: Bending diagram for CJ828 Structure

As a final step for the validation of the structures model the obtained thicknesses of the skin and stringers are compared with existing aircraft. The skin thicknesses for the B737 and B747 aircraft can be seen in Table 5.21.[36]

Table 5.21: Skin thicknesses

Aircraft	t [mm]
B737	1-1.6
Hydrojet	1-1.4
B747	1.8-2.2

It can be noticed that the results of the Hydrojet are somewhat in between the values for these two reference aircraft. The B747 has a higher skin thickness range, due to its larger size and weight. The values of the Hydrojet are close to the ones of the B737, which has a similar size. For the stiffeners validation, the paper of Chintapalli et al. [37] was used. They have two wing-box models, one with 17 stringers and one with 15 stringers. Furthermore, the top skin also has more stringers than the bottom skin. The optimal dimensions according to the report of Mikulik et al.[36] for a Z profile stringer is: a height around 30 mm, a thickness around 2 mm and a width of approximately 15 mm. These are smaller than the ones of the Hydrojet, because during the design of the wing-box it was opted for a thicker skin with less stringers which have a larger size. All things considered the structures model can be deemed valid.

5.5.5. Additional Structural Remarks
Some parts of the BWB need additional reinforcement, because they need high load bearing capabilities or are a weak point. Some of these are addressed in this section.

The hydrogen tank will be placed between the cabin wall and the outer wing root. This section of the structure needs to allow for the tank placement and also needs to withstand additional loads, since the tank will not be a load bearing structure. Thus, additional reinforcement will be added around the tank. A rib will be placed at the outer wing root, extra stiffeners will be added and the thickness of the skin will be increased.

If windows will be added on top of the cabin, cut-outs will be needed in the structure which creates stress concentrations. Since the top of the fuselage experiences large loads during a flight, additional reinforcements need to be added at these locations to prevent failure of the structure. An example of such a reinforcement is a window frame. Adding cameras and LED screens is also a possibility and will be evaluated in the post-DSE phase.
The engines of the Hydrojet will be attached on top at the back of the blended wing body. The structure should also allow for the mounting of the engines. This will be done by attaching the structure of the pylons to the longerons, which will be running along the length of the aircraft. Longitudinal and circumferential stringers will also be placed for additional reinforcement.

5.5.6. Risks
There are no comparable operating existing BWB aircraft. Thus, the different structures design concepts are still unproven. The optimal design configurations for the structure of a BWB aircraft have only been analysed so far and testing still needs to be done. Some of the risks related to the structure of the aircraft are:

- The front spar is too close to the leading edge of the outer wing.

- Under estimated pressurisation loads.

- Other loads are critical.

- High stress intensity factor, K_I.

- High loads induced by the winglets.

- Large design changes to fulfil all the requirements.

The leading edge spar is usually placed at 20 % in order to allow for the placement of leading edge high lift devices. However, the Hydrojet has no leading edge high lift devices. The leading edge spar is placed at 3.5 % of the chord to accommodate the hydrogen tank. At this location of the chord the airfoil has a lower height and consequently the wing-box as well. The reduced height leads to a less stiff structure, which is more prone to flutter. To be certain of the wing-box design a more detailed analysis, such as finite element method (FEM) needs to be performed.

The cabin does not contain the most optimal cross-section, which is circular, to withstand the pressure loads. The cross-section is split up into two bays with an arched structure in order to reduce the out-of-plane stresses. The pressurisation loads are, however, modelled for a circular cross-section. Thus, the loads are a bit under estimated. A more advanced model needs to be created in order to have a higher accuracy.

Only bending and shear are considered for the analysis. Torsion and buckling also need to be considered to make the analysis complete. The latter can require the addition of more ribs and/or stiffeners. However, the chances are small due to the short outer wing and the thick centre body of the Hydrojet. To confirm these expectations a complete analysis will be done in the post-DSE events.

If K_I is higher than the fracture toughness K_{Ic} of the chosen material, the skin cannot sustain the maximum stress with a crack of a detectable size present. To solve this complication the stress needs to be lowered. The latter can be done by increasing the skin thickness, amount of stringers or stringers area. The crack analysis will be done in the post-DSE design phase.

The winglets have not been considered in the structural analysis of the outer wing. The vertical stabiliser placed on the winglets can induce additional forces on the outer wing. These need to be analysed in more detail so that the structure can be designed accordingly.

Most of the structure requirements still need to be attained. This needs to be done once all the loads have been analysed and the exact structural arrangement is known. If it turns out that a requirement cannot be fulfilled, design modifications are required. These adaptions can for instance cause substantial weight changes which will require reiterations of the complete design.

6
Landing Gear

The dimensions of the Hydrojet have been determined now and the undercarriage sizing can begin. This chapter focuses on the landing gear design and sizing. First, the requirements of the undercarriage are introduced in Section 6.1. Next, the landing gear layout will be considered in Section 6.2. After that the landing gear will be positioned in Section 6.3. In Section 6.4, the tyres will be selected. Additionally, the shock absorber will be discussed in Section 6.5. Next, the materials and recyclability will be elaborated on in Section 6.6. After that, verification and validation is performed in Section 6.7. Finally, the risks of the landing gear will be identified in Section 6.8 and the compliance with the requirements is checked in Section 6.9.

6.1. Requirements

The undercarriage allows for ground manoeuvres of the aircraft and also absorbs the shocks of landing. Additionally, the landing gear should also provide braking capabilities and prevent damage of the ground surface. The sizing of the undercarriage should be considered early on in the design, since the aircraft should allow for storing the landing gear and a load path must be created to direct the loads into the airframe. For the successful completion of these functions some requirements have been generated and are listed below. These requirements will drive the design and sizing of the landing gear.

Landing Gear Requirements

General:
HPRA-REQ-LG-COS-1 The landing gear shall weigh no more than 3439 kg.
HPRA-REQ-LG-COS-1 The cost of the landing gear shall be no more than €2.4 million.
HPRA-REQ-LAN-6 The landing shall be made without excessive vertical acceleration, tendency to bounce, nose over or ground loop.

Stability & Control:
HPRA-REQ-LG-1 The landing gear shall provide a scrape angle such that a sufficient AoA can be achieved to generate 90 % of the maximum lift in take-off configuration with deflated struts.
HPRA-REQ-LG-2 The landing gear shall provide a tipback angle with respect to the most aft operating CG of at least 15 deg and larger than the scrape angle with extended struts.
HPRA-REQ-LG-3 The landing gear shall provide an overturn angle of at most 55 deg with respect to the most forward CG to prevent lateral tip over.
HPRA-REQ-LG-4 The landing gear shall provide an engine/tip clearance angle of at least 5 deg, taking into account the effect of wing sweep, with tyres and struts deflated.
HPRA-REQ-LG-5 The nose landing gear shall carry at least 8 % of the aircraft weight for the most aft operating CG.

Airport:
HPRA-REQ-LG-4 The landing gear shall protect the runway.
HPRA-REQ-LG-4.1 The number of main landing wheels for regional jets shall comply with $N_{mw}=MTOW/120000$.
HPRA-REQ-LG-4.2 The number of main struts shall equal 2 for $N_{mw} < 12$ and 3 or 4 for $N_{mw} > 12$.
HPRA-REQ-LG-4.3 The tyre pressure p_w shall comply with $p_w = 430 \ln(LCN) - 680$ for paved surfaces, where $10 < LCN < 100$.
HPRA-REQ-LG-5 The main gear span shall be not greater than 15 meters.
HPRA-REQ-GRO-1 The aircraft shall enable visual inspection.
HPRA-REQ-GRO-2 The aircraft shall enable accessibility for maintenance.
HPRA-REQ-GRO-3 The aircraft shall be able to provide ramp service.

Structures & Materials:
HPRA-REQ-LG-1 The landing gear's structure shall be able to withstand all loads during landing.
HPRA-REQ-LG-1.2 The landing gear's structure shall be able to withstand all loads during taxi and ground

---

> operations.
> **HPRA-REQ-LG-2** The landing gear tyres shall be able to be rethreaded.
> **HPRA-REQ-LG-3** The landing gear structure shall comply with the safe-life philosophy.

6.2. Landing Gear Layout

Prior to the sizing of the landing gear, it needs to be determined whether the landing gear will be retractable or fixed. The fixed landing gear remains deployed during all phases of the flight and is common for small aircraft with low cruise speeds. Fixed landing gear is less complex, lighter and easy maintainable compared to a retractable one. However, fixed landing gear is not favourable for cruise speeds above 278 km/h due to the excessive gear drag penalty.[38] Since the cruise speed of the Hydrojet is 862 km/h, the retractable gear is the only viable option besides its disadvantages.

Next, the landing gear configuration is chosen. The possible configurations are: tricycle, bicycle, tailwheel. The first configuration has the third wheel in the front of the fuselage, while the tail wheel configuration has the third wheel in the aft part. The bicycle configuration is less widely used and has two main centered wheels, one at the nose of the fuselage and one in the middle, with one smaller wheel attached to each wing. The tricycle gear layout is widely applied in the aircraft industry and is also chosen for the Hydrojet, because of:

1. Good over the nose visibility during ground operations.
2. Good ground loop stability.
3. Good steering capabilities.
4. Levelled cabin floor while on the ground.

Hence, requirement HPRA-REQ-LAN-6 is met.

6.3. Landing Gear Positioning

Landing gear positioning is done using the method for conventional aircraft, as described by Roskam.[38] This approach is applicable for the BWB, because the landing gear needs to perform the same functions. The landing gear positioning is done based on the the stability and control landing gear requirements.

First the main gear is placed using the tip-back and scrape angle definitions in Figure 6.1, the aft CG, and the center body airfoil geometry. The aft CG location is retrieved from Section 5.4 and is 14.24m. The position is determined graphically, in compliance with requirement HPRA-REQ-LG-2, and the results are given in Table 6.1. The obtained height is sufficient to fulfil requirements HPRA-REQ-GRO-1, HPRA-REQ-GRO-2 and HPRA-REQ-GRO-3.

Table 6.1: Main gear positioning

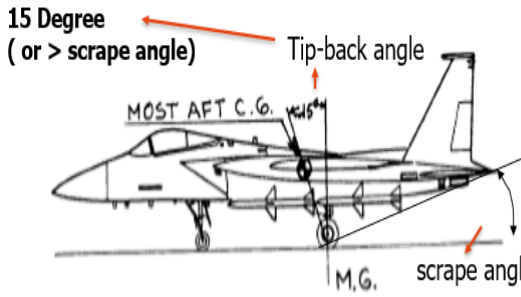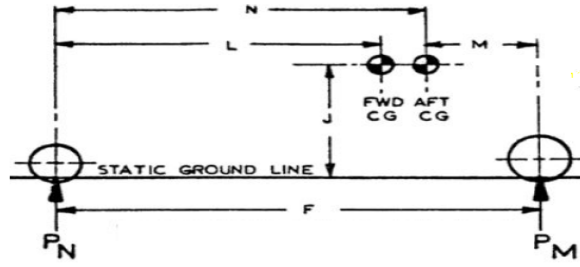| Parameter	Value
Scrape angle [deg]	13.5
Tip back angle [deg]	15
Gear height [m]	1.9
Main gear position [m]	14.85

Figure 6.1: Tip back and scrape angle

Figure 6.2: Landing gear diagram

The position of the main gear is now known and the location of the nose gear can be determined. The latter is done by considering the following criterion: for the most aft position of the CG the weight on the nose gear should not be less than 0.08MTOW (requirement HPRA-REQ-LG-5). Using this criterion and the definitions in Figure 6.2, Equation 6.1 is derived and the nose gear position is determined. This is found to be 7 m (N) from the aft CG and 7.24 m from the nose.

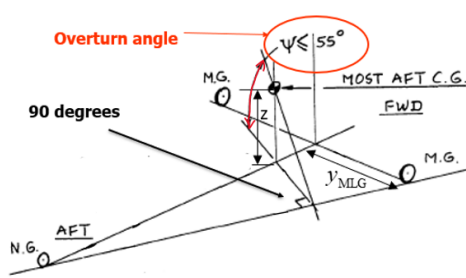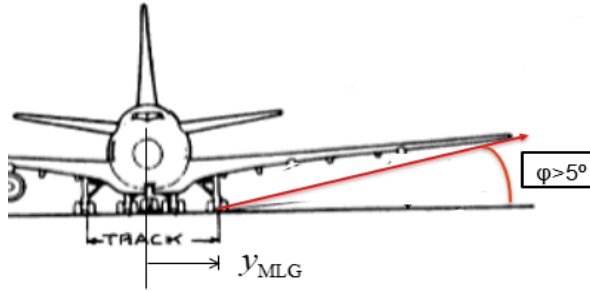$$N = (M_{MW} \cdot 0.92)/0.08 \tag{6.1}$$

Figure 6.3: Overturn angle

Figure 6.4: Tip clearance angle

Finally, the lateral stability and clearance are assessed to determine the width of the landing gear track (y_{MLG}). For the stability, Equation 6.2 is used. The overturn angle, ψ, can be seen in Figure 6.3 and should not exceed 55°. "z" in this equation is the height of the CG and is assumed to be 3.15m. Once the track width has been determined, the lateral clearance is checked. For lateral clearance the tip clearance angle (phi) should be at least five degrees and is depicted in Figure 6.4.

An iterative process is used to obtain a y_{MLG} that meets both criteria. The final results are a overturn angle of 53°, tip clearance angle of 6.5° and a track with of 2.9 m. It can be noticed that requirement HPRA-REQ-LG-3, HPRA-REQ-LG-4 and HPRA-REQ-LG-5 are met.

$$y_{MG} = \frac{N + M_{MW}}{\sqrt{\frac{N^2 \tan^2 \Psi}{z^2} - 1}} \tag{6.2}$$

6.4. Tyre Selection

With the configuration and the position of the landing gears, the sizing and selection of the tyres can be done accordingly. The landing gear sizing is also done using the methodology described by Roskam.[31]

First the number of wheels is determined. For the nose wheels a standard of two is used. The number of main wheels is determined by Equation 6.3 which follows from requirement HPRA-REQ-LG-4.1. Here MTOW is the maximum take-off weight in Newtons. The result in rounded to the nearest multiple of 4, with a minimum of 4. Using the MTOW obtained from the Class-II weight estimation in Section 3.2, 8 is obtained for the number of main gears. So, the main gear will consist of two bogies with four wheels each, also known as the dual tandem layout, and is in line with requirement HPRA-REQ-LG-4.2.

$$N_{mw} = \frac{MTOW}{120000} \tag{6.3}$$

Next, the maximum static load on each tyre is determined. For the main gear this is calculated using Equation 6.4 and for the nose gear Equation 6.5. The factor 1.07 is required for FAR 25 certification and 1.25 is used to account for weight growth of the aircraft. 0.92 and 0.08 are the weight fractions.

Additionally, for the nose gear, the dynamic load is determined as well. This value is divided by 1.5 and compared to the static load. The highest value is used for the the nose tyre selection. The dynamic load is calculated using Equation 6.6. In this equation $\frac{a_x}{g}$ is the maximum deceleration and is equal to 0.45 according to Roskam. n_t is the number of nose tyres and is equal to two. The other symbols are defined in Figure 6.2. The results for the load calculations are given in Table 6.2. It can be noticed that the dynamic load for the nose gear is higher than the static load, thus the former will be used for the tyre selection.

$$P_m = (0.92 \cdot MTOW \cdot 1.07 \cdot 1.25) \cdot 10/8 \qquad (6.4) \qquad P_m = (0.08 \cdot MTOW \cdot 1.07 \cdot 1.25) \cdot 10/2 \qquad (6.5)$$

$$P_{n_{dyn}} = MTOW \cdot \frac{(M_{MW} + \frac{a_x}{g} \cdot J)}{n_t \cdot (M+N)} \qquad (6.6)$$

The pressure of the tyres needs to be determined as well for the tyre selection and is done using Equation 6.7, which follows directly from requirement HPRA-REQ-LG-4.3. LCN in this equation is the load classification number, which is equal to 50. This value is obtained from the Boeing 757-200 aircraft. The pressure is also given in Table 6.2.

$$p = 430\ln(LCN) - 680 \qquad (6.7)$$

As a final step for the tyre selection, the maximum operating speed for the tyre, $V_{tyre-max}$ is determined. The latter is obtained by taking the largest value from Equation 6.8 and 6.9. As can be seen from the results in Table 6.2, $V_{tyre-max}$ is equal to 80 m/s.

$$V_{landing_{tyre-max}} = 1.2 \cdot V_{landing} \qquad (6.8) \qquad V_{take-off_{tyre-max}} = 1.1 \cdot V_{Take-off} \qquad (6.9)$$

Table 6.2: Tyre Characteristics

Parameter	Value	Parameter	Value
P_n [kN]	49.4	$V_{landing_{tyre-max}}$ [m/s]	80
P_n [kN]	142	p(pressure) [psi]	145
$P_{n_{dyn}}$ [kN]	81.9	$V_{Take-Off_{tyre-max}}$ [m/s]	76

The loads, pressure and maximum operating speed of the tyres are now known and the selection can be done accordingly. Goodyear's data base[1] is used for the tyre selection. The selected tyres are presented in Table 6.3. The dimensions are defined as follows: outer diameter (D_0) x width - inner diameter.

Table 6.3: Tyre specifications

	Dimensions [m]	Static load [kN]	Maximum operating speed [m/s]	Tyre Pressure [Psi]	Loaded radius [m]
Nose gear	0.86x0.23-0.46	87.9	101	213	0.37
Main gear	1.04x0.38-0.46	142.4	101	190	0.44

6.5. Shock Absorber

As mentioned before, shock absorption is one of the main functions of the landing gear. To allow for shock absorption, shock absorbers are incorporated in the undercarriage. The following types of shock absorbers can be distinguished:

- Steel springs or rubber disks (solid systems): They are a simple system, have a high reliability and a low cost. Disadvantages are: the very high weight and low absorption efficiency. Solid systems are used for general aviation.

- Oleo-pneumatic: This type is most widely applied currently for transport aircraft. They have a low weight and the highest efficiency. They have a good energy dissipation as well, which means the absorbed energy is released gradually. Spring absorbers, on the contrary, release all their energy instantly.

- Liquid absorbers: This type is as reliable as the oleo-pneumatic one. However, it has a low efficiency and high weight. They are compact and have good a fatigue life and are, therefore, sometimes used on small aircraft.

---

[1]https://www.goodyearaviation.com/resources/pdf/tire-specifications-6-2018.pdf[acessed on 15 June 2020]

- Pneumatic or gas: This type has been used in the past, but are not used anymore these days. This is because of their high weight, and low reliability and efficiency relative to oleo-pneumatic absorbers.

Based on these characteristics, oleo-pneumatic is the feasible one for the Hydrojet undercarriage.

With the type of shock absorber known, the sizing can be done accordingly. This is done using the methods described by Roskam[38] and Curry[39].

The shock absorber stroke for the main gear is calculated using Equation 6.10. V is the sink speed and is equal to 3.048 m/s accoring to EASA CS-25. For the landing load factor (N) 1.2 is mostly used.[40] S_t is the tyre deflection and is calculated using Equation 6.11. The tyre efficiency η_t has a value of 0.47.[40] Oleo-pneumatic shock absorbers have an efficiency η_s of 0.8 according to Roskam.[38]

$$S_{ch} = \frac{\frac{V^2/2g}{N} - S_t \eta_t}{\eta_s} \qquad (6.10) \qquad\qquad s_t = D_0 - 2 \cdot (loaded - radius) \qquad (6.11)$$

The shock absorber of the nose gear is comparable to the one of the main gears, however it only absorbs the shock of the nose gear loads instead of the complete aircraft. Consequently, for the nose gear Equation 6.12, adapted from Roskam and Curry, is used for the calculation of the shock stroke of the nose gear.

Furthermore, [38] advises to add 1 inch (2.54 cm) to the computed values. Finally, the diameter of the shock absorber can be computed using Equation 6.13.[38] Here P is the maximum static load on each strut in lbs. The output of the equation is in ft. The dimensions for the shock absorber can be seen in Table 6.4.

$$S_{ch} = \frac{\frac{2Pn \cdot V^2}{2g} - S_t \eta_t \cdot N \cdot 2P_{n_{dyn}}}{N \cdot \eta_s \cdot 2P_{n_{dyn}}} \qquad (6.12) \qquad\qquad d_s = 0.041 + 0.0025(P)^{1/2} \qquad (6.13)$$

Table 6.4: Shock absorber dimensions

	Length [m]	Diameter [m]
Main gear	0.42	0.28
Nose gear	0.25	0.16

6.6. Materials and Recyclability

As mentioned before, the landing gear needs to withstand some high impacts during landing. Additionally, the undercarriage will also encounter moments due to the friction between the runway and the wheels during braking. Thus, the material of the struts must be of high strength (requirement HPRA-REQ-LG-1 and HPRA-REQ-LG-1.2). In the Midterm Report two candidates, Titanium 10V-2Fe-3Al and Steel 300M, were identified to be suitable for the landing gear.[1] Both materials have a high strength, but they have some drawbacks. Titanium has the best strength-to-weight ratio, but is much more expensive than Steel. Since the struts will only be a small part of the aircraft weight, Titanium 10V-2Fe-3Al is opted for. Other promising characteristics for this material are the good fatigue life and recyclability.[1]

The tyres of an aircraft have rubber as base material and are also recyclable. In the past old tyres were shredded and destroyed in cement. However, these days they can be recycled and turned into profitable solutions such as anti-vibration pads for rail, castings for the building, and mulch for playgrounds and sports fields. [2] [3] A new method for the recycling of aircraft tyres is called chemical scissors. This method is capable of breaking the strong bonds in the aircraft tyre and dissolving the rubber. [4]

6.7. Verification and Validation

The computations for the landing gear positioning are done analytically. These calculations are verified by checking the units and doing them for a second time. Furthermore, it is also checked whether the outcomes are in the right order of magnitude.

For the tyre selection and shock absorber sizing the formulas are implemented in a python script. Verification is done by checking the order of magnitude and checking the units. Integration testing and system testing are not performed, because the

---

[2]https://www.rubbergreen.eu/en/recycling[accessed on 16 June 2020]

[3]https://www.liligo.com/travel-edition/what-really-happens-to-old-airplane-tires-3495.html[accessed on 16 June 2020]

[4]https://aviationtribune.com/featured-content/aircraft-tires-innovation-exists-in-synergy-with-recycling/[accessed on 16 June 2020]

formulas are simple and coding errors can immediately be detected.

The validation is done by comparing the obtained results with other concepts. The Master thesis paper of Ikeda is used for this.[41] The landing gear layout is similar compared to the design of Ikeda. The only difference is the number of wheels. For the main gear there are two bogies of six wheels and for the nose gear one with four wheels. This can be explained by the fact that Ikeda's concept is designed for 555 passengers and has a weight of 428,140 kg. Thus, more wheels are needed to carry all the load.

The tyre dimensions are validated using conventional reference aircraft, due to the lack of data for BWB aircraft. The tyre dimentions for two reference aircraft can be seen in Table 6.5. It can be noted that the tyre sizes are close to the one of the Hydrojet. The Hydrojet is heavier compared to these aircraft and also shorter. The weight on the nose gear is thus higher and consequently the size is larger. The size differences can also be explained due to the different manufacturers.

Table 6.5: Tyre dimensions of reference aircraft [5]

	A321 NEO	B737 max9
Main gear	50x18-22	44.5x16.5-21
Nose gear	30x8.8-15	27x7.75-15

6.8. Risks

Although the methods described by Currey and Roskam are widely used for a preliminary sizing of the undercarriage, there are still risks involved due to the distinctive design. Some of the risks involved with the landing gear design and functioning are outlined in this section. The following risks are identified:

- Wrong CG range or unexpected CG travel
- Flaws of the methodology
- Not compatible with the electric motor

If the CG range has not been determined accurately, CG travel during ground activities can result in higher loads than expected. The latter can make maneuvering difficult and also cause failure of the strut. This risk can be reduced by applying a safety factor and allow for weight growth as Roskam suggests.[38]

The applied methodology is based on conventional aircraft. This method is deemed applicable, because of the same requirements of the Hydrojet undercarriage compared to conventional aircraft. Since there are no comparable BWB aircraft operational, the results can only be validated using conventional reference aircraft. There might be some problems that occur during testing, which are not anticipated for during the design. Thus, a more thorough analysis needs to be done, using a simulation model.

As mentioned in Chapter 7, an electric motor will be used for taxiing. This motor will be mounted on the nose landing gear. For the design of the landing gear a conventional method is used which does not take this motor into consideration. To be sure that the electric motor complies with the conventional undercarriage design method, the possible effects of mounting the motor needs to be evaluated. This will be done in the post- DSE phase of the design.

6.9. Compliance with Subsystem Requirements

Most of the undercarriage requirements presented in the first section are met. The ones that still need to be attained are: HPRA-REQ-LG-1, HPRA-REQ-LG-2T and HPRA-REQ-LG-3. The first requirement was not discussed in the preliminary sizing method of Roskam.[38] To check the compliance of this requirement with the design an additional analysis will be performed in the next design phase. The second requirement, HPRA-REQ-LG-2T, is related to the retraction mechanism of the landing gear and will be designed in the next design phase as well. The final requirement states that the landing gear structure will comply with the safe-life philosophy. This means that the landing gear structure should not fail during the operational life-time of the aircraft. This requirement will be fulfilled by choosing materials with a good fatigue life, which is already done for the strut. Furthermore, a simulation will be done in the post-DSE phase to verify the requirement.

---

[5]`https://www.bridgestone.com/products/speciality_tires/aircraft/products/applications/pdf/tire_applications.pdf`[accessed on 15 June 2020]

7
Power and Propulsion

With the planform design and its performance characteristics being determined, the Power and Propulsion subsystem can be sized. This will be done by first introducing the different requirements of the power and propulsion subsystem and its accompanying elements in Section 7.1. After that, the power system will be discussed in Section 7.2. The power usages are necessary to be able to size the turbofan and fuel cell. Next, the turbofan system has been analysed and sized in Section 7.3. As the turbofans produce some pollutants, an emission analysis is performed next to the overall performance. Additionally, the fuel cell system is discussed in Section 7.4. In Section 7.5, the fuel tanks will be designed. The required fuel and fuel rates are now known. This makes it possible to size the fuel tanks and the fuel system. Furthermore, in Section 7.6, verification and validation is performed for the different sections to examine all used methods and programs. Next, the risks of this subsystem are identified and mitigated in Section 7.7. Finally, a compliance matrix is created to see if all requirements are fulfilled in section 7.8.

7.1. Subsystem Requirements

Before any meaningful sizing can be performed for the power and propulsion subsystem, requirements must be set which can describe the limits and the essential needs of the subsystem. These requirements are stated below. Several of these requirements have been derived from the CS-25 requirements.

Power and Propulsion

Powerplant - General:
HPRA-REQ-PRO-COS-1 The power and propulsion system shall weigh no more than 7737 kg.
HPRA-REQ-PRO-COS-1 The cost of the power and propulsion system shall be no more than €9.3 million.
HPRA-REQ-PGE-1 The powerplant shall be constructed and installed to allow for inspection.
HPRA-REQ-PGE-2 The powerplant shall be constructed and installed to allow for maintenance.
HPRA-REQ-PGE-3 All powerplants shall be isolated from each other.
HPRA-REQ-PGE-4 The powerplant shall allow for in-flight restarting of the engine.
HPRA-REQ-PGE-5 The powerplant shall provide a means to remove hazardous ice accumulations on the engine.
HPRA-REQ-S&C-5 The pilot shall have information on the engines available during operation.

Powerplant - Turbofan:
HPRA-REQ-TUR-1 The engines shall use hydrogen based fuel.
HPRA-REQ-TUR-2 The engines shall be able to provide a maximum thrust of at least 284.27 kN.
HPRA-REQ-TUR-4 The engines shall provide the required power when the fuel cell is not operating
HPRA-REQ-TUR-5 The engine shall not provide reverse thrust in case of an engine malfunction.
HPRA-REQ-TUR-6 All the temperatures in the different stations shall be lower than the limits of the materials
HPRA-REQ-TUR-7 The engine shall show a decrease of emissions of 99 % w.r.t. to conventional fuel turbofans for civil aviation.

Powerplant - Fuel cell:
HPRA-REQ-POW-1 The fuel cell shall be able to generate at least 301 kW.
HPRA-REQ-POW-2 The power bus shall provide power to each subsystem relative to their respective needs.
HPRA-REQ-POW-3 The required hydrogen and air shall be provided under optimal conditions.
HPRA-REQ-POW-4 The created water shall be collected and stored in an on-board tank.

Powerplant - Integration:
HPRA-REQ-PIN-1 The nacelles in which the engines are mounted shall be able to withstand all of the loads which can be encountered during flight.
HPRA-REQ-PIN-2 The pylons which will connect the nacelles with the fuselage shall be able to withstand all of the

---

load which can be encountered during flight.
HPRA-REQ-PIN-3 The fuel cell system shall be designed such that it fits in the reserved space.

Powerplant - Fuel tank:
HPRA-REQ-PFT-1 Each fuel tank shall be able to withstand the structural loads acting on the system.
HPRA-REQ-PFT-2 Each fuel tank shall be able to withstand the vibrational loads acting on the system.
HPRA-REQ-PFT-3 Each fuel tank shall have an expansion space of at least TBD % of the tank capacity.
HPRA-REQ-PFT-4 There shall be no ignition source present in the fuel tank or fuel tank system.
HPRA-REQ-PFT-5 Each fuel tank shall have an access point for refueling.
HPRA-REQ-PFT-6 The access point for refueling shall allow a rate of refueling of 1.162 kg/s.
HPRA-REQ-PFT-7 Each fuel tank shall be insulated to prevent rapid boil-off.
HPRA-REQ-PFT-8 Each fuel tank shall have measures to prevent sloshing.

Powerplant - Fuel System:
HPRA-REQ-PFS-1 Each fuel system shall be able to ensure a continuous fuel flow rate.
HPRA-REQ-PFS-2 Each fuel system shall supply the engine or the fuel cell independently of other fuel systems.
HPRA-REQ-PFS-3 The fuel system shall prevent the ignition of fuel during a lightning strike.
HPRA-REQ-PFS-4 Each fuel system shall provide 100% of the required fuel under each intended operating condition.
HPRA-REQ-PFS-5 The fuel system shall show no difference in performance when operating in hot weather.
HPRA-REQ-PFS-6 Each fuel system shall be able to withstand the structural loads acting on the system.
HPRA-REQ-PFS-7 Each fuel system shall be able to withstand the vibrational loads acting on the system.
HPRA-REQ-PFS-8 The fuel shall be transformed to the ideal engine and fuel cell conditions before being injected.

Powerplant - Cooling:
HPRA-REQ-PCO-1 The powerplant cooling shall keep the temperatures within the limits of the materials.
HPRA-REQ-PCO-2 The cooling system shall only cool those parts in need of cooling.

Powerplant - Fire Protection:
HPRA-REQ-PFP-1 Each component that transports or carries a flammable fluid shall be fire resistant.
HPRA-REQ-PFP-2 No tank or reservoir that does not add safety and carries a flammable product shall be placed in a designated fire zone.
HPRA-REQ-PES-3 Each powerplant installation shall be able to be shut off.
HPRA-REQ-PES-4 The combustion equipment shall be isolated by firewalls from the rest of the aircraft.
HPRA-REQ-PES-5 Each engine shall be equipped with a fire detection and extinguish system.

7.2. Power System

The power system enables the aircraft to be completely functional. It ensures the operation of the electrical network, communication, landing gear propulsion and all other non-propulsive power systems. Therefore, it is important to identify all these components and associated power usage such that a detailed budget breakdown can be constructed. As this breakdown depends on the flight phase, it will be constructed for the phases which are consuming the most power. Afterwards, this information can be used as input for the fuel cell sizing and power-off take of the turbofan.

7.2.1. Avionics and Actuation

The avionics of the aircraft, running on electrical power, includes the display units and monitoring elements of the cockpit, the navigation beacons and communication systems, sensors and safety systems to prevent collisions and the pumps and valves that are required for transferring the hydrogen and air to its desired location. As all these elements are general needs for commercial aircraft, they are more or less aircraft independent, making it possible to use reference values from other aircraft to estimate the power usages. For this design the A320 NEO will be used because of two reasons: First of all, the aircraft is the precursor of the direct competitor (A321 NEO) which makes the values valid. Secondly, extensive documentation was available for this aircraft.

For the actuation system (actuators and stabilisers) the Hydrojet will differ from conventional technology. All hydraulic systems of the aircraft will be replaced by electrical systems. The conventional technology has reached its saturation point, making it impossible to attain large additional improvements. Furthermore, eliminating the hydraulic power systems has

multiple advantages. First of all, higher efficiencies can be reached because of the absence of conversion losses. Secondly, the overall system mass will reduce and finally the maintenance and operating costs will drop as well.[42] Typical values for these electrical elements in aircraft were found through research and are summarised in Table 7.5.[43]

7.2.2. Commercial Cabin Equipment

The cabin environment encompasses all power systems relating passenger comfort in the cabin. This means the lighting system, in flight entertainment and all equipment to prepare food and drinks. As airlines main intentions are to minimise operational cost, they want minimal consumer loads in the cabin. On the other hand they want to maximise the passenger experience during the flight, which accompanies an increase of power levels. Consequently, decisions need to be made to find the necessary power levels.

Since the Hydrojet is a regional, mid-range aircraft with focus on sustainability while offering quality and comfort for its passengers, there is opted for a LED full mood lighting system. This system has very good performance and reliability and uses the newest LED technology, which results in a power consumption of 2.25 kW for typical mid-range aircraft. [1].[43] Furthermore, the in-flight entertainment system will be limited to a shared system consisting out of a few screens because of the short flight times, resulting in values of around 5 kW. As the kitchen equipment consumes a lot of power during the cruise phase and with an eye on green flying, it is chosen to use the most recent, efficient ovens and kettles to reduce the consumption as much as possible. Typical values in the range of 35-45 kW are found to be realistic.[43]

7.2.3. Landing Gear System

The landing gear system of the Hydrojet consumes power derived from three sources: First of all, the retraction and deployment of the landing gear after take-off and before landing, executed by electrical actuators, consuming of about 5.7 kW. Secondly, the ability to brake which will be carried out by an electro-magnetic system. These systems are extremely efficient and have the opportunity of a regenerative braking mechanism. Analysis shows power needs of about 5 kW for the whole system. [43]

Compared with conventional aircraft, the landing gear of the Hydrojet will have a third function. It will be exploited as propulsion system during taxi. This is to have zero harmful pollutants. This means that an electrical motor will be mounted on the nose landing gear which will provide the necessary thrust. An advantage that comes with this design is that the aircraft will be able to pushback by itself, reducing the turnaround time. In order to design this motor properly and to find the maximum required power, constraints have to be identified. According to the International Civil Aviation Organisation (ICAO), following taxi requirements needs to be fulfilled [44] [45]:

- **HPRA-REQ-TAX-1** The aircraft shall be able to reach 10 knots in 20 seconds.
- **HPRA-REQ-TAX-2** The aircraft shall be able to reach 20 knots in 90 seconds.
- **HPRA-REQ-TAX-3** The acceleration performance shall be the same for both dry and wet surface.
- **HPRA-REQ-TAX-4** The acceleration is limited by the maximum friction force identified on the nose landing gear.

The power consumed by an electrical motor can be found in Equation 7.1. Here, T_q represents the torque exerted by the motor and ω the angular velocity of the landing gear. Changing this coordinate frame to a linear system results in a second equation where the power is a function of the total propulsive force, F_{tot}, velocity of the aircraft, V, and landing gear radius r.

$$P_M = T_q \cdot \omega = F_{tot} \cdot r \cdot \frac{V}{r} \tag{7.1}$$

Analysing this equation shows that at constant torque the power will increase to unacceptable levels as the aircraft is accelerating. At constant power the torque and acceleration will decrease as function of the velocity. Therefore, to minimise the necessary power, one needs to maximise the torque acceleration right from the start while keeping a constant power, large enough to fulfil the performance requirements. The relation of the total propulsive force and acceleration of the aircraft can be found in Equation 7.2. The total force is reduced by the aerodynamic drag and the rolling resistance force acting on the main landing gear, which equals the rolling resistance coefficient of 0.015 times the weight carried by the main landing gear.[46]

$$M_{aircraft} \cdot a = F_{tot} - (\mu_{crr} \cdot W_{mlg}) - \frac{1}{2} \cdot \rho \cdot S_{ref} \cdot C_{D_{to}} \cdot V^2 \tag{7.2}$$

As already said the net force is limited by the maximum friction force which is expressed in Equation 7.3. This force is mainly dominated by the traction coefficient, which equals 0.4 in the critical situation of a wet surface.[46]

---

[1]https://www.aviationbusinessnews.com/cabin/cabin-lighting-passenger-comfort/

$$F_{net} \leq \mu_{traction} \cdot ng_\% \cdot W_{aircraft} \tag{7.3}$$

With this being defined, the necessary power can be calculated. This is done by increasing the power gradually until the point that all performance requirements are met, taking into account this maximum net force. All inputs and output for these calculations can be found in Table 7.1 and 7.2, respectively.

Table 7.1: Inputs for sizing landing gear taxi system

Table 7.2: Inputs for sizing landing gear taxi system

Inputs			
MTOW [kg]	92,315.21	$\mu_{traction}$ [-]	0.4
NG [%]	13	μ_{crr} [-]	0.015
MG [%]	87	S_{ref} [m^2]	510.84
ρ [kg/m^3]	1.225	$C_{D_{TO}}$ [-]	0.08637

Outputs	
P_{max} [kW]	132.33
a_{max} [m/s^2]	0.51

7.2.4. Ice Protection System and Cooling

As aircraft are flying at high altitudes, they are encountering low temperatures of about 220 - 230 K. This gives rise to the accumulation of ice around the edges of the planform and the engine inlets. Therefore an ice protecting system needs to be designed to keep all these surfaces above freezing temperatures such that there is no major loss in the performance of the aircraft, leading to an extreme malfunctioning or a crash.

In conventional aircraft this protection system is covered by blowing hot bleed air derived from the engines through small piccolo tubes along these surfaces. This is a highly inefficient method as valuable energy is wasted. Furthermore, it adds significantly to the total weight of the power system. Therefore it is decided to use an electro-thermal system on the Hydrojet. This system consists out of resistive electrical circuits, installed underneath the aforementioned surfaces, producing heat for anti-icing and deicing. This means that instead of bleed air, electrical power is extracted from the engines. Furthermore, all heated regions can be controlled separately which optimises the power consumption. The required power levels for the different flight stages can be found in Table 7.5 and were retrieved through research.[47]

Besides the cold regions, the turbofan also has some extremely hot zones that needs to be cooled. Downstream the combustion chamber, temperatures of about 1500-2000 K are no exception. However, as these temperatures often exceed the melting temperature of the turbine blade and vane material, cooling is necessary. For the turbofans of the Hydrojet, external film cooling will be employed. This means that pressurised bleed air is taken from the compressor stages at a temperature of about 900 K and is injected through small holes enclosed in the material of the blades and vanes of the turbine.[48] This then creates a thin insulation layer, lowering the skin temperatures to none critical values. Internal cooling, which would be another solution is discarded because it is less effective and the gradual temperature gradients can cause thermal stresses and cracking. Both techniques are visualised in Figures 7.1 and 7.2. As the functioning of both mechanisms are only dependent on moving a small amount of compressor energy to the turbine, without really extracting it, it can be assumed that the change in performance can be neglected, which induces no extra need for external power.

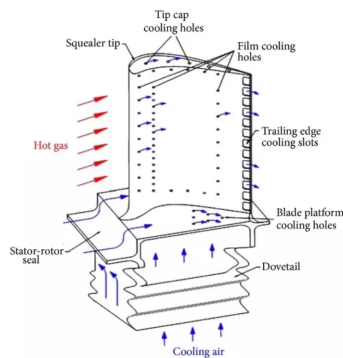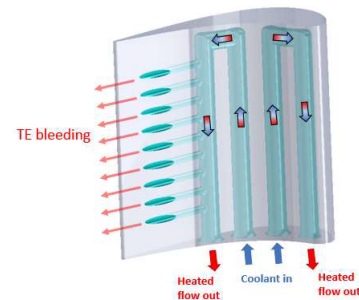Figure 7.1: Visualisation of Film Cooling Technique [49]

Figure 7.2: Visualisation of Internal cooling channels [50]

7.2.5. Environmental Control system (ECS)

This system is responsible for the cabin experience of the passengers as it includes the pressurisation, cooling and ventilation of the cabin. This means that fresh, pressurised cold air (bleed air) needs to be supplied continuously to the cabin mixer unit.

This unit on his turn then combines the bleed air with the part of the filtered, recirculated air that is not removed from the aircraft before been blown into the cabin. For now, the power usages to produce this bleed air will be analysed.

In a conventional aircraft this bleed air is simply provided by the engines. This could be adopted for the Hydrojet flight as well, but as the ground operations are carried out by a fuel cell, without an operating turbofan, an additional electrical compressor supplied with ram air is always required such that the ECS is never interrupted. Furthermore, the fuel cell requires ram air for its own operation as well. Therefore, the Hydrojet will be designed with a system which can be used during the whole flight and which integrates both systems into one. This system will be powered by the turbofan during flight and by the fuel cell during ground operations.

The total system can be seen in Figure 7.3. The working mechanism is quite straightforward. Ram air is supplied through a variable opening (ability to change air flow) in the aircraft. This happens by itself, due to the velocity of the aircraft or by the sucking power of the fan. The fan is thus included to assure a constant air flow during taxi and standstill aside from its pressurisation function. The air is then guided to a compressor where it is pressurised to its optimal condition, following the ECS system requirements. During ground operation, the valve will be opened. This to initiate an air flow to the fuel cell which is necessary for the operation of it. As the optimal condition of the fuel cell requires pressurised air, it is first guided through a pump.[51] The final aspect that needs some attention is the temperature. Following this system, the temperature still needs to be corrected. This will be done by exchanging heat with the hydrogen fuel, which is explained in Section 7.5.3.
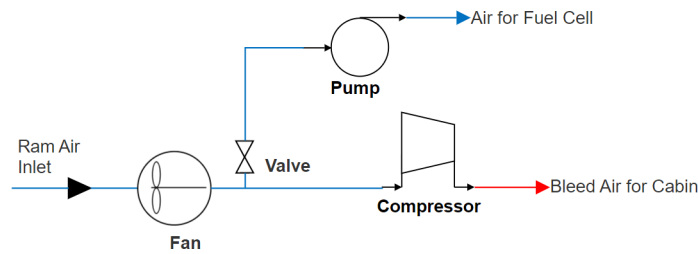

Figure 7.3: Ram Air Inlet System

With all this being defined, the power usages can finally be calculated. This starts by finding the required pressure ratios. For the fan, analysis shows that the ratio needs to be as low as possible without compromising a stable air flow. Therefore the lower limit of 1.2 is assumed.[51] Analysis of ECS systems shows that most commercial aircraft have an entry pressure of about 2.82 Bar.[52] Fuel cells operate optimally at a pressure of 10 Bar.[51] Adopting these numbers together with the ambient conditions of air, Equation 7.4 results in the required pressure ratios.

$$P_2 = \Pi \cdot P_1 \tag{7.4}$$

Then Equation 7.5 can be used to find the energy that is added to the flow, taking into account the different system efficiencies.

$$T_2 = T_1 + \frac{T1}{\eta_{fan}} \cdot [\Pi^{\gamma-1/\gamma} - 1] \tag{7.5}$$

Finally, Equation 7.6 is used to calculate the total work once the mass flows are known. As the A320 ECS system requires 0.75 kg/s of air for 190 passengers. The assumption that these numbers scale linearly gives a necessity for 0.93 kg/s air flow to the Hydrojet.[43]

$$W_{req} = \dot{m} \cdot C_p \cdot (T_2 - T_1) \tag{7.6}$$

To give a clear overview of all different inputs and outputs together with their values, Table 7.3 and Table 7.4 are constructed, respectively.

Table 7.3: Inputs ECS System

Inputs			
Π_{Fan} [-]	1.2	P_{FC} [bar]	10
$\dot{m}_{ECS}$ [kg/s]	0.93	η_{Fan} [-]	0.88
P_{ECS} [Pa]	281418	η_{Com} [-]	0.92
P_{TO} [Pa]	101325	P_c [Pa]	26429.7
T_{TO} [K]	288.15	T_c [K]	223.15

Table 7.4: Outputs ECS System

Outputs			
$\Pi_{Com_{TO}}$ [-]	2.31	Π_{Com_c} [-]	8.87
$W_{Fan_{TO}}$ [kW]	15.41	W_{Fan_c} [kW]	11.93
$W_{Com_{TO}}$ [kW]	82.35	W_{Com_c} [kW]	204.28

7.2.6. Power Breakdown

With all the power subsystems being defined and analysed, it is possible to make a power budget breakdown. The results are presented in Table 7.5. From this table, the total maximum power levels can be identified for the crucial flight stages. This means that the fuel cell will need to be designed such that it can generate a minimum of 300.36 kW. The power-off take from the turbofan is crucial at cruise and equals 318.85 kW.

Table 7.5: Power Breakdown Hydrojet

System Description				Amount of Power [kW]				
Power Source	System	Symbol	Subsystem	Taxi-out	Take-off	Cruise	Landing	Taxi-in
Electrical [kW]				**197.715**	**96.22**	**140.49**	**80.61**	**197.72**
	Avionics	AV		**40.92**	**31.56**	**32.67**	**45.92**	**40.92**
			Navigation	2.27	1.24	1.24	2.27	2.27
			Communication	7.35	7.35	7.35	7.35	7.35
			Monitoring	9.69	9.69	9.69	9.69	9.69
			Fuel Systems	17.77	10	10	10	17.77
			Collision & Avoidance	1.91	1.66	1.66	1.66	1.91
			Aircraft Management	1.93	1.62	2.73	14.95	1.93
	Cabin Equipment	CCE		**7.25**	**7.25**	**47.25**	**7.25**	**7.25**
			Lights	2.25	2.25	2.25	2.25	2.25
			Entertainment System	5	5	5	5	5
			Kitchen Equipment	0	0	40	0	0
	Actuation & Control	AFCS		**12.89**	**43.48**	**34.28**	**16.74**	**12.89**
	Landing Gear	LG		**132.33**	**5.7**	**9**	**10.7**	**132.33**
			LG Actuation	5	5.7	0	5.7	5
			LG Taxi System	116.5	0	0	0	116.5
			Motor Efficiency [95%]	5.82	0	0	0	5.82
			Braking System	5	0	0	5	5
	Ice Protecting System	IPS		**4.33**	**8.23**	**26.29**	**0**	**4.33**
Pneumatic [kW]				**102.65**	**102.65**	**178.36**	**102.65**	**102.65**
	Environmental System	ECS		**102.65**	**102.65**	**178.36**	**102.65**	**102.65**
			Ram Air Fan	15.41	15.41	11.93	15.41	15.41
			Compressor	82.35	82.35	157.94	82.35	82.35
			Motor Efficiency [95%]	4.89	4.89	8.49	4.89	4.89
TOTAL POWER [kW]				**300.36**	**198.87**	**318.85**	**183.26**	**300.36**

7.2.7. Electrical Block Diagram

The electrical block diagram of the Hydrojet is presented in Figure 7.4. In this diagram, the flow of current is shown from the generators to the different loads which are present in the breakdown. Three different circuits can be distinguished. The red line represents the circuit when the aircraft is at the gate, consuming external electricity. When the aircraft want to initiate its pushback, it opens the fuel cell valves which then starts to produce electricity. After some time the fuel cell will become self-sustainable. Hence, the grey circuits takes over the electrical functions and the external power line is pulled out. When the taxi procedure is almost finished, the turbofan power switch will be closed such that the turbofans can be started. This will be done by guiding electrical energy towards the compressors to initiate the rotations and the air flow followed by combustion. When this is completed, the fuel cell valves will be closed and the turbofan will take over the functions of it (green circuit).
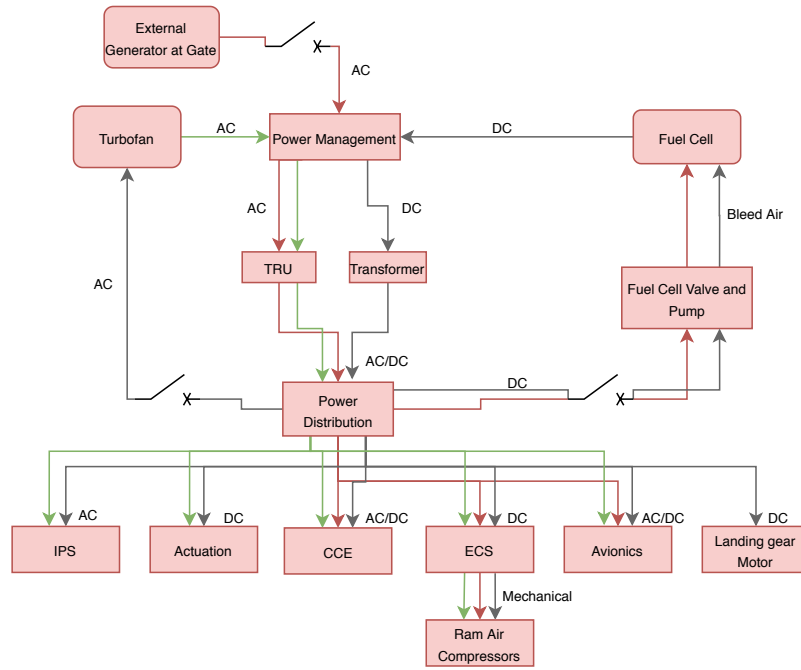
Figure 7.4: Electrical Block Diagram of the Hydrojet

7.3. Turbofan System

The goal for the design of the turbofans is to reduce the thrust specific fuel consumption (TSFC) together with the elimination of NO_x emissions. The reason why only NO_x emissions are considered, is due to the mechanism behind hydrogen combustion, which is elaborated upon in Subsection 7.3.6. Thus, trying to achieve this, requires an optimisation of the parameters influencing these design variables. For this matter following objective functions are defined [53]:

$$EI_{NO_x} = f(FPR , CPR , \Phi , \tau , TIT , COMD)$$
$$TSFC = f(FPR , CPR , \Phi , \tau , TIT , BPR) \tag{7.7}$$

In general, all of the parameters that are considered to affect either the fuel usage, or the NO_x emissions in gram per kg of fuel (EI_{NO_x}) are: the fan pressure ratio (FPR), the compressor pressure ratio (CPR), the residence time τ of the combustion, equivalence ratio Φ, the combustor chamber design (COMD), turbine inlet temperature (TIT) and the bypass ratio (BPR).

Thus, in order to optimise the design variables, at least seven other parameters must be optimised. In order to solve this problem, the following methodology was adapted. First, the TIT and Φ were determined based on which give the lowest amounts of NO_x emissions empirically. This is chosen as starting point such that the emission variable is eliminated as much as possible, right from the start. Then, as the BPR only determines the thrust specific fuel consumption, it was selected based on current limitations. Using these numbers, as well as the known thrust, an optimum can then be found for the FPR and CPR by calculating all of the different stages within the turbofan. Once these are determined, also the τ can be found by analysing the combustor itself.

7.3.1. TIT and Equivalence Ratio

Analysing the historical trend of turbine inlet temperatures shows a logarithmic increase over the years. Nowadays, engines are made with a TIT above 2000 K.[54] This number is still increasing as it has a positive effect on the total efficiency of the engine. The only limiting factor, slowing down this growth, is the material properties. The best turbine blade materials (single crystal) start to melt at about 1200 K. Therefore, active cooling is required. Unfortunately, this trend has the opposite effect on NO_x emissions: Higher combustion temperatures result in more energy, causing more NO_x to be formed. Lowering this temperature is thus the solution, at least till a certain point induced by the maximum attainable overall pressure ratio. Analysis of optimised designs, taking into account all these elements, show most favourable effects around 1600 K.[53] A value which will be used for the Hydrojet design as well.

Combustion is a very complex chemical process which relies on the interaction between oxidant and fuel fractions, in this case hydrogen and air. Obviously, different fractions will result in different outcomes. Therefore, this ratio is often used to

characterise a typical combustion. For this design, the equivalence ratio will be adopted. This ratio is shown in Equation 7.8 and represents the actual fuel to air ratio to the stoichiometric fuel to air ratio. A ratio smaller than one implies a lean combustion where there are more air molecules compared to hydrogen molecules following the stoichiometry of the reaction. A ratio larger than one implies a rich combustion, where the opposite is true. One main effect can be identified when changing this ratio, namely the total amount of energy that is released. This mainly determines the total thrust and flame temperature which in its turn then has an influence on the NO_x production. This effect is the same for all fuels, but is visualised in Figure 7.5 for the case of kerosene.

$$\Phi = \frac{F/A}{(F/A)_{stoic}} \tag{7.8}$$

Thus, to minimise both TSFC and NO_x emission, this ratio should be minimised as much as possible. However, the lower limits need to be taken into account. This means avoiding the blow out region where too much air causes the combustion to stop, which is equal to 0.1 for hydrogen.[55] Additionally, there is also the point where not enough thrust is generated anymore. At this stage, it is quite difficult to predict this second value. Therefore, enough margin is taken and an equivalence ratio of 0.3 is assumed, as this is the most common ratio for commercial aircraft at take-off. During the simulation this value will be changed to find the lowest possible condition.
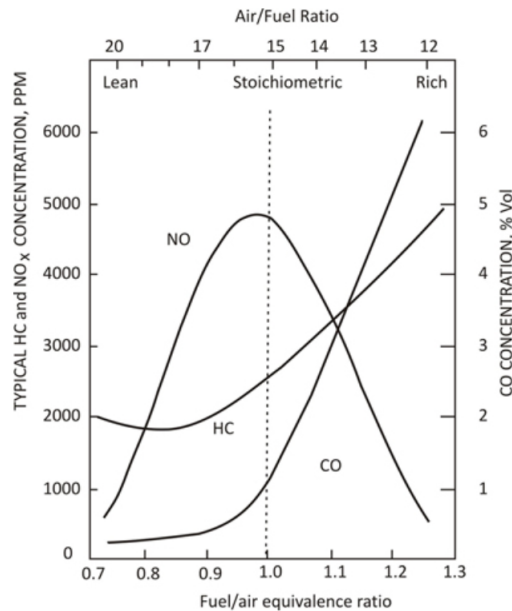

Figure 7.5: Combustion Products of Kerosene versus Equivalence ratio [56]

7.3.2. Bypass Ratio
Next, the BPR must be established. It is known that a larger BPR is more fuel efficient, and as far as TSFC is concerned, one would preferably pick the largest possible BPR.[57] However, there are of course certain limitations. First of all, because a higher BPR will also cause a bigger diameter for the same amount of thrust, the engine nacelle will then also be heavier and cause extra drag.[58] Secondly, when one has a larger bypass ratio, the tip speed of the fan will also increase, which can become limiting as well.[57] Because of these limitations, the best achievable BPR is currently 12-15, where the highest BPR in use is 12.5, on the PW1100G engine.[58] Taking all of this into account, it has been chosen to use a BPR of 12, as this is clearly feasible, and will also have a large positive effect on the TSFC.

With this being defined, a first estimation of the mass flow can be established using Equation 7.9. Here, T_{TO} represents the take-off thrust which is determined in Chapter 4. N is the number of engines, a_0 the speed of sound at sea level. BPR is another expression for the bypass ratio. G is the gas parameter constant of turbofans. η_{nozzle} and η_{tf} are turbofan efficiencies for which typical values are used.[59]

$$\dot{m} = \frac{T_{TO}}{N \cdot a_o} \cdot \frac{1 + BPR}{\sqrt{5\eta_{nozzle} \cdot G \cdot (1 + \eta_{tf} \cdot BPR)}} \qquad (7.9)$$

$$G = \frac{TIT}{600} - 1.25 \qquad (7.10)$$

Table 7.6: Inputs for the calculations used to obtain the relevant mass-flows.

Inputs			
T_{TO} [kN]	284.265	BPR	12
N [-]	2	TIT [K]	1600
η_{nozzle} [-]	0.98	a_0 [m/s]	340
η_{tf} [-]	0.735		

Table 7.7: Inputs for the calculations used to obtain the relevant mass-flows.

Inputs			
$\dot{m}$ [kg/s]	657.71	$\dot{m}_{core}$ [kg/s]	50.93
$\dot{m}_{bypass}$ [kg/s]	607.12		

7.3.3. Turbofan Lay-out
As all stations within a turbofan are related to each other, only a few variables are required to calculate its overall performance. In this case the above defined variables, take-off thrust and flight conditions are already enough to find the optimal design.

For the Hydrojet design a two spool, geared turbofan with two supplementary modifications will be used. With this is meant that the conventional design will be changed by installing a intercooler between the core and the bypass flow. The main reason for this is the additional efficiency. Furthermore, heat will be exchanged between the exhaust gases and the hydrogen fuel before it is injected in the combustion chamber. This is necessary as it is stored at 22K. Hydrogen has large viscosity and density fluctuations at those low temperatures, making the combustion unstable. Obviously, this exchange will cause the efficiency to drop. Therefore the absolute minimum of 150 K is assumed as injection temperature.[60] A sketch of the design together with the official numbering can be found in Figure 7.6.

To analyse the individual effects of those modifications, three simulations will be made: One with the conventional design during take-off, one with the intercooler, also during take-off, and finally one with the complete design for both take-off and cruise.
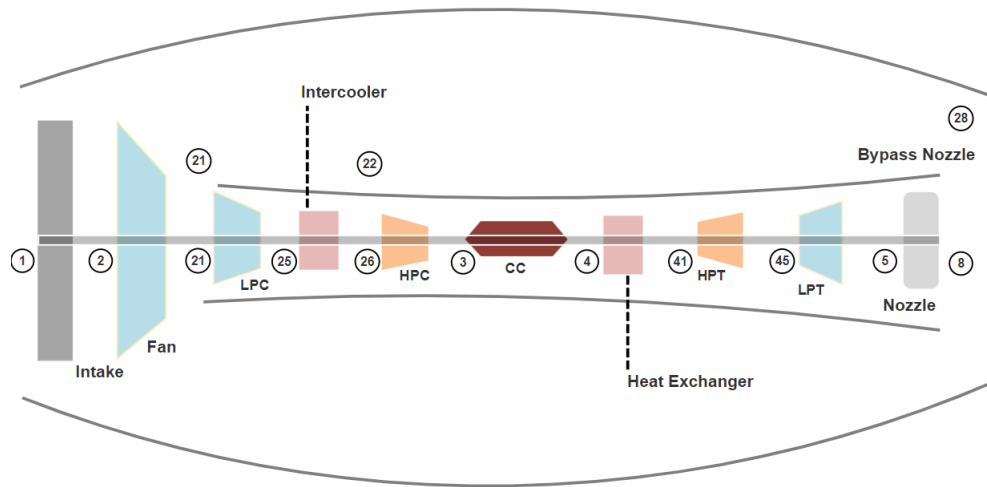
Figure 7.6: Station Numbering Turbofan

7.3.4. Turbofan Calculations and Pressure Ratios
To find this optimal design point, one needs to define the final unknown values that are left (the pressure ratios). For the Hydrojet, three types of pressure ratios are taken into account, namely those of the fan, the low pressure compressor (LPC) and the high pressure compressor (HPC). Pressure ratios are fixed for a given turbofan condition and throttle setting. Since take-off is the most limiting case with respect to thrust generation, they will thus first be calculated for take-off.

The first simulation, the conventional turbofan, thus starts by establishing equations relating the generated thrust, given in Equation 7.11, with the compressor pressure ratios.[59] For simplicity, this equation will be further analysed in three parts, the

first part giving the bypass thrust, the second part giving the core thrust and the third part representing the potential chocked flow thrust.

$$T = [\dot{m}_{bypass} \cdot (V_{28} - V_0)] + [\dot{m}_{core} \cdot (V_8 - V_0)] + [A_{bypass} \cdot (P_{28} - P_0) + A_{Core} \cdot (P_8 - P_0)] \tag{7.11}$$

Bypass Thrust: The first element $\dot{m}_{bypass}$ is already determined above. Therefore, only the exhaust velocity, V_{28}, needs to be expressed differently. This can be done with the temperature relation, resulting in the following equation:

$$T_{bypass} = \dot{m}_{bypass} \cdot (V_{28} - V_0) = \dot{m}_{bypass} \cdot \sqrt{2 \cdot C_{P,a}(T_{21} - T_{28})} \tag{7.12}$$

In Equation 7.12, T_{21} is the temperature after pressurisation by the fan. This value is related with the inlet condition via the temperature in combination with the pressure ratio of the fan. T_{28} is the exhaust temperature which is linked with the pressure release during expansion, P_{21}, which is on its turn related with the inlet conditions. All this can be combined into one equation, presented below. Here, the thrust is only a function of the fan pressure ratio.

$$T_{bypass} = \dot{m}_{bypass} \cdot \sqrt{2 \cdot C_{P,a} \cdot [T_2 + \frac{T_2}{\eta_{fan}}(\Pi_{fan}^{\gamma-1/\gamma} - 1)] \cdot [\eta_{nozzle} \cdot (1 - (\frac{P_{28}}{P_2 \cdot \Pi_{fan}})^{\gamma-1/\gamma})]} \tag{7.13}$$

Core Thrust: The same principle can be applied for the core thrust. However, one main difference is present: The core thrust is not only a result of pressurisation. More stations are involved, thus it requires more relations. Equation 7.14 gives the starting point for the analysis.

$$T_{core} = \dot{m}_{core} \cdot \sqrt{2 \cdot C_{P,g}(T_5 - T_8)} \tag{7.14}$$

In Equation 7.14, T_5 gives the temperature after the high pressure turbine. To relate this with its previous stations, the turbine works needs to be included. As both are expressions of energy, this relation is quite straightforward. For T_8 the pressure release ratios are again used, just as with the bypass thrust. Filling in these relations results in Equation 7.15.

$$T_{core} = \dot{m}_{core} \cdot \sqrt{2 \cdot C_{P,g} \cdot [T_4 - \frac{\dot{W}_{LPT} + \dot{W}_{HPT}}{\dot{m}_{core}C_{P.g}}] \cdot \eta_{nozzle} \cdot (1 - \frac{P_8}{P_5})^{\gamma/\gamma-1}} \tag{7.15}$$

The two unknown work rates in Equation 7.15 can be defined as they need to be equal to the total work of the compressors plus the power-off take for the cabin. Furthermore, compressor works can be related with the temperature differences over that station, which is in his turn then connected with the pressure ratio. An expression for this description is given below

$$\dot{W}_{HPT} = \frac{\dot{m}_{core} \cdot C_{P,a} \cdot \left[[T_2 + \frac{T_2}{\eta_{fan}} \cdot (\Pi^{\gamma-1/\gamma} - 1)][1 + \frac{1}{\eta_{LPC}} \cdot (\Pi_{LPC}^{\gamma-1/\gamma} - 1)]\right]}{\eta_{mech_H}} \tag{7.16}$$

$$\dot{W}_{LPT} \cdot \eta_{mech_L} = \frac{\dot{m}_{core} \cdot C_{P,a} \cdot T_2 \cdot [\Pi_{fan}^{\gamma-1/\gamma} - 1]}{\eta_{gear} \cdot \eta_{fan}} + \frac{\dot{m}_{core} \cdot C_{P,a} \cdot \left[T_2 + \frac{T_2}{\eta_{fan}}[\Pi^{\gamma-1/\gamma} - 1]\right]\left[\Pi_{LPC}^{\gamma-1/\gamma} - 1\right]}{\eta_{LPC}} \tag{7.17}$$

Chocked Flow Thrust: When the pressure build up in the turbofan is too high, the flow will not be able to reach the ambient pressure as it reaches the nozzle. Therefore, the chocked flow thrust is defined, given in Equation 7.18. To find the required areas, Equation 7.19 can be used.

$$T_{chocked} = A_{bypass} \cdot (P_{28} - P_0) + A_{core} \cdot (P_8 - P_0) \tag{7.18}$$

$$\dot{m} = \rho \cdot A \cdot V \tag{7.19}$$

This last relation concludes the analysis of the different stations. The total thrust is now only a function of the compressor pressure ratios, which makes it possible to calculate the optimal values. To do this, two ranges of sensible LPC and fan compression ratios were taken, and for each relative combination of the two, the HPC compressor ratio could be calculated. For the fan, a compression ratio range of 1.0 to 2.0 was chosen and for the LPC compressor, a range of 1.0 to 4.0.

Note that the mass flow is estimated at first. Then, once calculations are done, all of the unfeasible combinations are filtered out and from the remaining combinations, the one with the highest produced thrust is chosen. Note that this thrust could be higher or lower than the required take-off thrust. Thus, the preliminary estimated mass flow can be adjusted such that the output thrust matches the required thrust, and in this manner the exact mass flow can be found. This can be done since it is found that mass flow will only affect the total generated thrust - and the required engine size later on, - if all the rest is kept constant.

For the second and third simulation the exact same procedure is applied after adding the additional station and element.

7.3.5. Turbofan Overall Performance
The final values representing the overall turbofan performance during take-off can be found in Table 7.8. From these values some important conclusions can be made.

First of all one can see the positive effect of the intercooler. Heat is exchanged between the core flow and the bypass flow. This causes the bypass thrust to increase, which means that a lower core thrust is required. The effect of this is a lower equivalence ratio and thus fuel flow.
In general: the intercooler causes the TSFC to drop without compromising the thrust. Secondly, simulation three shows an reduction in overall performance when compared with the second one. This was expected as energy is extracted to pre-heat the hydrogen. Inspecting the temperature and pressure differences at station 5 confirms this. Thus, the thrust is a little bit lower for the same overall parameters.
In general: The heat exchange extracts energy which causes the efficiency to decrease a bit.

Note that the complete system performs quite well. The required thrust is generated for a small amount of fuel. The equivalence ratio is low, which limits the production of NO_x. The overall pressure ratio equals 30.39 which is lower than the turbofans used in conventional aircraft. This implies a higher TSFC but lower NO_x emission compared with those aircraft.[53] High temperatures are encountered in the turbine stages, thus cooling as described in Subsection 7.2.4 is required.

Table 7.8: Results Take-off performance

Take-off Performance: [Values for one engine]			
Parameter	Simulation 1	Simulation 2	Simulation 3	Unit
T	141.4	143.0	141.3	kN
Π_{fan}	1.4	1.4	1.4	-
Π_{LPC}	1.3	1.6	1.6	-
Π_{HPC}	8.0	13.6	13.6	-
Φ	0.31	0.28	0.28	-
$\dot{m}_{fuel}$	0.4605	0.4159	0.4159	kg/s
TSFC	$3.25595 \cdot 10^{-6}$	$2.90959 \cdot 10^{-6}$	$2.94288 \cdot 10^{-6}$	kg/s·N
P022	1.43	1.43	1.43	Bar
T022	321.8	325.8	325.8	K
P03	14.84	29.44	29.44	Bar
T03	657.4	738.8	738.8	K
P05	1.25	1.36	1.29	Bar
T05	915.6	801.2	787.9	K

For cruise, the final design is analysed as well. The final values can be found in Table 7.9. As drag equals thrust during cruise, only 36.775 kN or 13% of maximum thrust is required. To obtain this thrust the compressors will run much slower, having a smaller overall pressure ratio. Furthermore, the fuel flow will lower. This all results in a equivalence ratio of 0.14. An optimal number as this is extremely low but still higher than the critical limit for blow out which equals 0.10. However, the TSFC is increased as both thrust and fuel do not scale linearly.

Take-off Performance: [Values for one engine]		
Parameter	**Simulation 3**	**Unit**
T	18.8	kN
Π_{fan}	1.12	-
Π_{LPC}	1.28	-
Π_{HPC}	8.14	-
Φ	0.14	-
$\dot{m}_{fuel}$	0.20798	kg/s
TSFC	$1.1055 \cdot 10^{-5}$	kg/s·N
P022	0.44	Bar
T022	264.3	K
P03	4.34	Bar
T03	480.6	K
P05	0.50	Bar
T05	571.5	K

Table 7.9: Results Cruise Performance

There is, however, one last phenomenon to take into account, which is boundary layer ingestion (BLI). BLI occurs when an engine is mounted near the trailing edge of an airfoil - or in the case of a BWB also the fuselage, - and the engine ingests a fraction of the boundary's kinetic defect. This effect is beneficial for TSFC.[61] On the other hand, when the engine inlet is large enough, the viscous boundary can cause non-homogeneous inlet conditions, which in turn cause fan distortion effects that can reduce fan efficiency.[62] The extent to which these two phenomenons affect the total efficiency has not been calculated, as this is outside the scope of this report.

7.3.6. Combustion Chamber Design and NO_x Emissions

The main goal of the turbofan design was described as minimising the TSFC and eliminating the NO_x emissions, this is in order to be compliant with the crucial requirement HPRA-REQ-TUR-7: 'The engine shall show a decrease of emissions of 99 % w.r.t. to conventional fuel turbofans for civil aviation.' As the overall performance is now defined, their contribution to this requirement cannot be changed anymore. Therefore, it is time to look into the combustion chamber design and residence time as they are the final variables influencing the NO_x emissions. Afterwards a thorough engine emission analysis has to performed to see if the requirement is fulfilled.

Burning hydrogen promises to greatly reduce combustion emissions, as the theoretical chemical reaction between hydrogen (H2) and oxygen (O_2) only produces water (vapour):

$$2H_2 + O_2 \rightarrow 2H_2O \tag{7.20}$$

However, since a turbofan is an 'air-breathing' engine, it relies on the supply of oxygen from the surrounding air in the atmosphere. This air is a mixture of mainly nitrogen gas (N_2) and O_2, which make up about 78 % and 20 % of the constituents of ambient air, respectively. Therefore, N_2 also enters the core flow of the engine, and can react with O_2 in various ways to create NO_x. It is therefore necessary to explore these formation mechanisms to get a better view of the creation process.

NO_x Formation Mechanisms

There are four main pathways that allow for the creation of NO_x during combustion[53]:

- Thermal NO_x
- Prompt NO_x
- Fuel NO_x
- The N_2O pathway

The most dominant source of NO_x emissions is due to so-called thermal NO_x. This is NO_x that is created by allowing an endothermic reaction with O_2 due to the high amount of heat present in the combustion chamber. This reaction works as follows:

$$N_2 + O_2 + heat \rightarrow 2NO \qquad (7.21) \qquad\qquad 2NO + O_2 \rightarrow 2NO_2 \qquad (7.22)$$
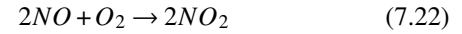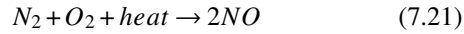
The chemical reaction 7.22 occurs when the NO molecules leave the exhaust and get in contact with the oxygen in the atmospheric air. Thermal NO_x accounts for about 85 % of all NO_x emissions.

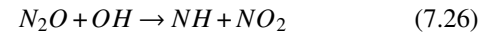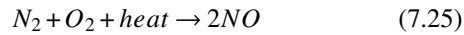If N_2 reacts with a free hydrocarbon radical, it is said to create prompt NO_x. When organically bound nitrogen present in a fuel is oxidised, it is classified as fuel NO_x. Both prompt and fuel NO_x are only relevant when hydrocarbon-based fuels (such as kerosene) or fuels containing organically bound nitrogen are used, in combination with low temperature and fuel-rich combustion.[53] These are thus neglected (eliminated) by designing the combustion chamber for high temperature and fuel-lean burning, which will be elaborated upon later in this subsection.

Finally, the N_2O pathway is facilitated in high pressure and lean-fuel burning conditions creating the N_2O, which is applicable to the combustion chamber featured in the turbofan of the Hydrojet. Lowering the pressure ratios over the compressors would lower the effectiveness of this NO_x creation mechanism. Yet this in turn would be detrimental to the specific fuel consumption. Therefore, an optimisation has to be performed while designing the combustion chamber. The reactions that can take place via the N_2O pathway are:

$$N_2O + O \rightarrow 2NO \qquad (7.23) \qquad\qquad N_2O + H \rightarrow NO + NH \qquad (7.24)$$

$$N_2 + O_2 + heat \rightarrow 2NO \qquad (7.25) \qquad\qquad N_2O + OH \rightarrow NH + NO_2 \qquad (7.26)$$

NO_x that is created this way accounts for the remaining 15 % of all NO_x creation. It should be noted however that about 98 % of the NO_x emissions consist of NO, and thus NO_x only makes up a tiny 2 %.[63] Now that it is known how NO_x is produced in detail, the combustion chamber can be designed based on optimising the Specific Fuel Consumption (SFC) and NO_x emissions.

Combustion Chamber Design: The combustion chamber can be designed in various ways. Every small element can be changed as well as the complete working mechanism. Therefore, a schematic overview, as can be seen in Figure 7.7, is made to find a relation between the combustor design and the mechanisms of NO_x production.
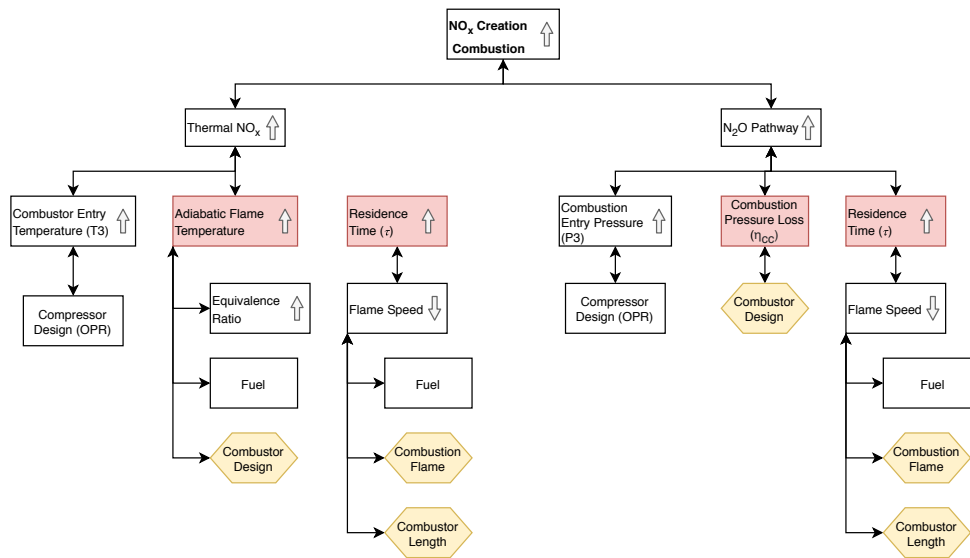
Figure 7.7: NO_x Production Parameters

From this figure follows that additional NO_x emissions are always the result of an increase in combustion entry temperature and pressure. This was found earlier and is thus already optimised. Furthermore, the emissions are a result of a higher flame temperature as more heat is available. Therefore, the combustion chamber needs to be designed to minimise this. Additionally, it is influenced by the combustion pressure loss, which is neglected due to its minor effect.[53] Finally, it is also a result of a longer residence time. Thus the combustor needs to accommodate a short residence time.

On top of all this, another still adjustable variable was found. Namely the combustion flame. During normal combustion two different type of flames can be identified: a diffusion flame and a premix flame. The former is visualised as a yellow and reddish flame. The burning is stable, slow, flashback free (flame propagates back to the tank) and reliable in terms of ignition. A premix flame on the other hand is volatile, which causes the burn rate to be very high, reducing the residence time. However, this flame is prone to instabilities and flashback, which poses a risk for safety. When choosing this flame, safety has to be taken into account.[56]

In the case that no changes would be made to the combustor design, hydrogen would burn completely differently compared to kerosene. First of all, hydrogen has much more energy stored for the same amount of mass. Thus the adiabatic flame temperature will be higher for the same equivalence ratio. Luckily, hydrogen has a much wider flammability or operating range. This makes it possible to run the combustion extremely lean which implies a lower flame temperature and thus lower NO_x emissions. Secondly, the chemical properties of hydrogen ensure a flame speed which is seven times higher than with kerosene. The effect of this property is a lower burn time which means a shorter residence time and thus also a shorter combustion chamber length. To conclude, hydrogen combustion itself already offers multiple opportunities to reduce NO_x emissions significantly without changing the design.[64]

Significant changes are not enough. The objective for Hydrojet is set, thus that changes need to be made. Research was performed and one concept was deemed feasible based on performance and effects, namely lean direct injection (LDI) in combination with micromix combustion.[60] This method relies on premixing the fuel combined with a typical mechanism of fuel injection and ignition. Premixing is chosen above the conventional design, even with the extra risk of auto ignition and flashback as it induces a high flame speed. Furthermore, analysis shows the possibilities to mitigate the risks by keeping the mixing area and time short.[60] Beside of this, micromix and LDI can only be used with premixed fuels which immediately makes the conventional design unacceptable.

To premix the fuel, an injector needs to be designed, This will be a LDI system. Such a system consist out of multiple injection holes with a specific geometry to create vortices which mixes the fuel. Research showed an optimal design created by NASA where the fuel is mixed radially at an angle upstream the flow at 7 different points.[60] When this is completed the gas needs to be ignited. This will be done by adopting the micromix system. This means that many ignition switches are created to form multiple miniaturized flames instead of a few big flames. In this way the hot flame regions and temperatures are minimised hence the reduced NO_x emissions.[64]

NO_x Emission Rate of the Hydrojet: Now that the turbofan and specifically its combustion chamber are designed, it is possible to run an analysis on the amount of NO_x that is produced per kilogram of used fuel. Several different methods were found to estimate the NO_x emissions of a turbofan. All containing the same variables but different constants and exponents as those depend on the combustor design and geometry. However, research from NASA already revealed more general expressions where the constants are a function of the design. Therefore, their estimation method will be used.[60] The final equations can be found below:

$$PPM_{NO_x} = A^* \cdot (P_3)^a \cdot \Phi^b \cdot \tau^c \cdot exp(T_3/d) \cdot \frac{\Delta P^e}{P} \quad (7.27) \qquad EI_{NO_x} = \frac{PPM_{NO_x}}{630} \cdot \frac{1+f/a}{f/a} \quad [g/kg fuel] \quad (7.28)$$

Here P_3 represents the combustion entry pressure, $\Delta P/P$ the percentage of pressure loss due to the fuel flow injection. Φ and f/a represent the fuel flow properties being equivalence ratio and fuel to air ratio respectively. τ is the residence time and T_3 the combustion entry temperature. As can be seen, all previous mentioned variables are included in these equations. The constants A, a, b and d serve as correction factors to the fuel injection method. For the Hydrojet, this means numbers that correspond to lean direct injection. The combustion flame and thus flame speed is hidden in the constants c and e. Note that all these numbers are calculated with US customary units.

It should be noted that P_3, Φ and T_3 vary with the thrust setting. These exact relations are quite complex, thus to quantify the effect of the thrust setting, which varies during flight, a statistical relation was set up using regression. The engines used to derive this relation are:

- The LEAP engine familiy (1A, 1B and 1C); on the Boeing 737 MAX family and the Airbus A320
- CFM56-7B familiy (26, 27); on the Boeing 737-400
- PW4056; on the Boeing 747 and the Airbus A330

The statistical relation that was found using these engines between the thrust setting (TS, in %) and NO_x emissions (EI_{NO_x}, in g/kg) for conventional engines is as follows:

$$EI_{NO_x} = 4.6047 \cdot exp(0.0176 \cdot TS) \tag{7.29}$$

Since this exponential behaviour is the same for any turbofan, the Hydrojet turbofan will be assumed to exhibit this relation as well, yet the first constant is different: filling in Equation 7.27 and 7.28 for take-off (i.e. TS = 100%), results in the following value for NO_x emissions per engine: 1.8608 g per kg of fuel. Hence for the Hydrojet, the equation becomes:

$$EI_{NO_x} = 0.3201 \cdot exp(0.0176 \cdot TS) \tag{7.30}$$

All that is left to make the analysis is determining the variation of the thrust setting throughout the flight. To make the analysis representative, the flight profile is the same for the Hydrojet and the comparing conventional jet, meaning that each TS for both cases have equal duration. The following flight profile is used, with a total flight time of 312 minutes (5.2h):

Table 7.10: Flight Profile and Thrust Settings

Flight Phase	Thrust Setting Conventional [%]	Thrust Setting Hydrojet [%]	Duration [min]
Take-off	100	100	5
Climb	85	85	30
Cruise	15	80	242
Descent	15	20	30
Landing	30	30	5

Using these values, and Equation 7.29 and 7.30 yields the following per-flight average emission rate: for the Hydrojet: 0.54 g/kg, and for conventional: 17.76 g/kg. Hence the Hydrojet has a NO_x emission rate that is 96.96 % lower than current turbofan engines.

7.3.7. Engine Noise

Production of engine noise can often pose problems for regulations, and must thus be minimised. Turbofans are known to have two main sources of noise, namely fan induced noise and jet induced noise. Jet noise is the most dominant source of noise, and thus one should focus on this type of noise when aiming to reduce overall noise. Jet noise, in turn, is caused by a combination of turbulent mixing noise and imperfect shock noise. The latter should not be significant if the nozzle is not choked and/or well designed. And indeed, in practice often turbulent mixing noise is the dominant source of noise, and thus must be reduced. This type of noise occurs when the jet exhaust has significantly higher velocity and temperature than surrounding flow.[65] To reduce this type of noise, three measurements were taken.

First of all, having a high BPR makes sure most of the energy is already extracted out of the core mass flow before it is exhausted. This lowers the jet exhaust velocity and temperature, and thus also noise. Moreover, having the exhaust of the fan surround the exhaust of the jet, where the fan exhaust has a temperature and velocity higher than ambient conditions, but lower than those of the jet exhaust, the different will then be more gradual, and thus noise is even further reduced. Because the chosen design for the Hydrojet has a BPR that is very high on the current commercial spectrum of BPRs, in this respect it will most likely have relatively low noise.

Secondly, it is chosen to integrate a category B type of nacelle. This means the exhaust of the jet is pre-mixed with the fan exhaust right before both are exhausted together. This again has positive effect for noise reduction, and even for thrust generation.[66]

Finally, it is also chosen to use chevrons on both the fan and jet exhausts. Chevrons are saw-tooth like indents on the exhausts, which give extra vorticity to the flow, and thus make mixing of the flow easier, reducing noise produced by turbulent mixing noise. Chevrons do, however, slightly reduce thrust generation because energy is lost to this vorticity. For a thrust loss of roughly 0.50%, chevrons offer about a 2.5 dB decrease in effective perceived noise level.[67]

7.3.8. Engine Materials and Dimensions

As the turbofan performance and relating parameters are known, the final items that are left are the dimensions of the turbofan, as well as the materials used for each part. First, some semi-empirical relations from Torenbeek [66] will be used to determine the dimensions, after which a material will be chosen for each part.

First, in order to obtain the total nacelle length, Equation 7.31 is used. The mass flow is calculated using Equation 7.9 and for a type B nacelle, meaning one with a mixer, C_l equals 9.8 and Δl equals 0.10. Furthermore, the highlight diameter is assumed

to be equal to the inlet diameter. To obtain this diameter, Equation 7.32 is used, where φ equals 1. For a type B engine, this maximum is located at roughly 35 % of the total nacelle length. Lastly, the exit fan diameter can be calculated using Equation 7.33. In Table 7.11 and 7.12, the various inputs and outputs are presented.

$$l_n = C_l \left(\sqrt{\frac{\dot{m}}{\rho_0 a_0} \frac{1+0.2BPR}{1+BPR}} + \Delta l \right) \tag{7.31}$$

$$D_n = D_i + 0.06\varphi l_n + 0.03 \tag{7.32}$$

$$D_{ef} = D_n \left(1 - \frac{1}{3}\varphi^2 \right) \tag{7.33}$$

Table 7.11: Inputs for the dimensions of the turbofan engine

Inputs			
$\dot{m}$ [kg/s]	657.71	C_l [-]	9.8
ρ_0 [kg/m^3]	1.225	BPR [-]	12
a [m/s]	340	Δl [-]	0.10
φ [-]	1		

Table 7.12: Outputs for the dimensions of the turbofan engine

Outputs			
l_n [m]	7.28	D_n [m]	2.54
D_{ef} [m]	1.69		

Now, to finalise the design of the turbofan, for each part an elaboration of the material choice will be given.

Fan: For the fans of the turbofan engine, titanium will be used because of its high strength to weight ratio, its corrosion and fatigue resistance and its ability to withstand bird strikes. The temperature stays below 423.15 K so Ti-10V-2Fe-3Al is suitable.

Compressor section: In the compressor, the pressure of the air flowing through it can be raised up to 30 times and the temperature can rise to 820 Kelvin. The materials must therefore, have high strength at high temperatures, they must resist fatigue, cracking and oxidation and they must also withstand creep. If creep occurs, the material will slowly change shape when it is stressed at a high temperature. The material will be an alloy as no single metal would have all the properties desired. Superalloys are alloys that can resist very high temperatures and they are generally nickel, cobalt or iron based. For extra strength, aluminium and/or titanium is added. Recycling nickel alloys are most meaningful if they are recycled into the same alloy again[2]. Hence, for the compressor section a nickel based alloy called Inconel[3] (nickel-chromium-iron) will be used.

Combustion chamber: Temperatures in the combustion chamber are 1600K and superalloys are used. Refractory metals that have very high resistance to heat, corrosion and wear are often added to a superalloy. These metals are only in alloy form as they are very dense and the weight has to be kept down. Ceramics are also feasible options due to their high resistance.

Turbine: The first set of turbine blades are in the highest pressure and hottest part of the gas flow. Therefore, they are made with either a nickel-based superalloy or ceramic blades. More so, unheated outside air is circulated to keep them from melting. After the first set of turbine blades, the temperature is cooler and stainless steel can be used.

Exhaust material: For the exhaust of the turbofan, Inconel alloys are again used because of their strength, thermal expansion properties and corrosion resistance even under extremely high temperature conditions where aluminium and steel would creep because of thermally induced crystal vacancies.

Casing: The materials used for the casing do not have to withstand such high temperatures, but they do need to be strong enough so in case a blade breaks off, it would be stuck in the casing instead of entering the aft-center body and causing damage to the APU, as an example. Aluminium or polymer matrix metals are used as engine casings. Hence, Al 2024-T4 will be used.

7.4. Fuel Cell System

In this section the design of the fuel cell will be explained. The fuel cell will have two functions: It will function as an APU in case of engine failure and it will power the engines in the landing gear during taxiing. First a general explanation is given about the type of fuel cell. Then it is explained how the design point was chosen. Finally, the output parameters are presented in a table and the results are verified and validated.

---

[2]https://www.corrotherm.co.uk/blog/can-you-recycle-nickel-alloys [accessed on 21 June, 2020]
[3]https://www.altempalloys.com/inconel-alloys.html [accessed on 21 June, 2020]

7.4.1. Type of Fuel Cell

There are two types of fuel cells that make use of hydrogen as fuel, namely the solid oxide fuel cell (SOFC) and the proton exchange membrane fuel cell (PEMFC). Requirement HPRA-STK-SUS-1 states that the aircraft shall emit zero emissions. The SOFC emits carbon monoxide and carbon dioxide during operation, restricting the use of this type of fuel cell. Therefore, the PEMFC was chosen as a starting point. The PEMFC only emits water and has other favourable properties such as high reliability and fast start up in case of emergency. In Figure 7.8, the fuel cell is shown. It is based on an electrolyte that allows positively charged hydrogen atoms to pass through while the electrons have are not. This mechanism creates the electric current. Only hydrogen and oxygen (provided by an airflow) is needed to power the fuel cell. The emissions only consist of water, air, and a small portion of the hydrogen.
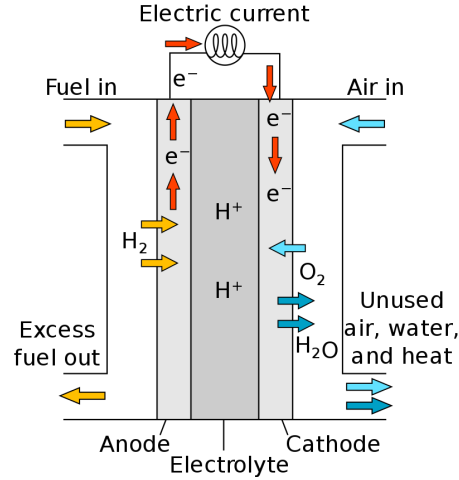
Figure 7.8: Diagram of a PEM Fuel Cell

7.4.2. Fuel Cell polarisation curve

In order to design the fuel cell, a polarisation curve is necessary. This curve relates the voltage provided by one cell to the current or current density i $[A/cm^2]$. The ideal voltage of a single fuel cell is around 1.2 V. However, there are three factors that decrease the voltage. These are all influenced by the current density. They are shown in Equations 7.34, 7.35 and 7.36.[68] Where R is the universal gas constant, T_{OP} the operating temperature, α is the charge transfer coefficient, F the Faraday coefficient and n the exponential concentration loss coefficient, i_0 the exchange current density r_{ohmic} the ohmic loss coefficient and i_Δ. The polarisation curve following from these equations is shown in Figure 7.9. The arrows point out the different voltage losses, as explained before.

$$V_{act} = \frac{R \cdot T_{op}}{\alpha \cdot n \cdot F} \cdot \ln\left(\frac{i}{i_0}\right) \quad (7.34) \qquad V_{ohmic} = i \cdot r_{ohmic} \quad (7.35) \qquad V_{conc} = \frac{R \cdot T_{op}}{n \cdot F} \cdot \ln\left(1 - \frac{i}{i_\Delta}\right) \quad (7.36)$$

After determining the polarisation curve, one could calculate the properties of the engine including the current density, cell voltage and fuel flow. In order to make the fuel cell efficient, it would have to minimise fuel flow. Therefore, for every current density the fuel flow was computed. For this, the number of cells in a stack (placed in series) was calculated by dividing the voltage needed, which is 270 V in this case, by the voltage per cell. The current is computed using Formula 7.37 where I is the current, P_{req} is the required power and V_{req} is the required voltage. Subsequently one can find the area needed per stack (A_{stack}) and the number of cells needed per stack using Formulas and 7.38 7.39.[68]

$$I = \frac{P_{req}}{V_{req}} \quad (7.37) \qquad A_{stack} = \frac{P_{fc}}{V_{stack} \cdot i} \quad (7.38) \qquad m_{stack} = \frac{A_{stack}}{A_{cell}} \quad (7.39)$$

All parameters required for computing the fuel mass flow at maximum operating power, are available now including the number of cells in series n_{stack}, number of cells per stack m_{stack}, the stack current I_{stack}, the hydrogen stoichiometry λ_{H_2}, molar mass of hydrogen M_{H_2} and the Faraday constant F. Using Formula 7.40 the mass flow of hydrogen is finally calculated for each current density setting. [68]

$$\dot{m}_{H_2} = \frac{n_{stack} \cdot m_{stack} \cdot I_{stack} \cdot \lambda_{H_2} \cdot M_{H_2}}{2 \cdot F} \quad (7.40)$$
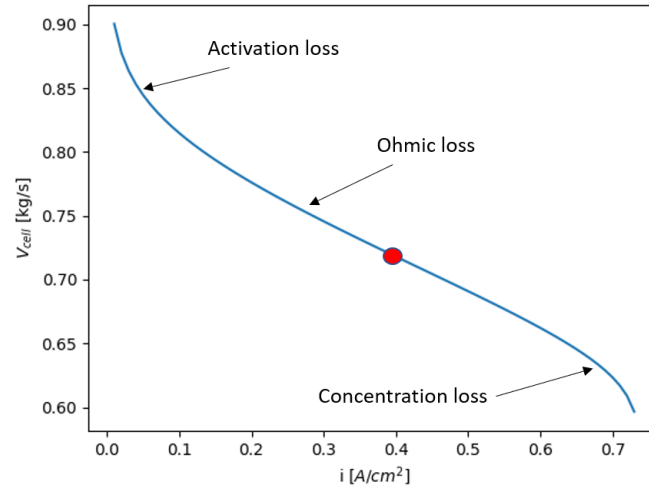
Figure 7.9: Polarisation Curve fuel cell

The minimum fuel flow is reached at the highest cell voltage, which implies at the lowest current density. Therefore, choosing the lowest fuel flow will result in an unusable design point. However, it does point out that minimising current density is desirable. Still, lowering the current density poses the problem of increasing total electrode area and therefore increasing the weight as well as the cost of the material, due to the high cost of platinum. As the total area increases exponentially with lower current densities, current densities below 0.2 A/cm^2 are unsuitable. Finally, a current density of 0.4 A/cm^2 was chosen because a higher density will not result in a significantly lower weight and the effect on the cell voltage is reasonable. This point is shown as a red dot in Figure 7.9. In addition to the hydrogen mass flow, there is also an airflow needed and a mass flow of water out of the system. These were important for the compressor and for the emissions respectively. These were calculated using relations in what ratio oxygen and hydrogen are used and then corrected for their molar mass. In Table 7.13 and 7.14, the final parameters are shown. The fuel cell mass and fuel cell volume were computed using the relation for PEMFC of 650 W/kg and 1100 W/L.[69]

Table 7.13: Input Fuel Cell

Inputs			
P_{req} [kW]	319	A_{cell} [cm^2]	780
V_{req} [V]	270	r_{ohmic} [Ω/cm^2]	0.15
η_{fc} [-]	0.6	i_Δ [A/cm^2]	0.74
V_{cell} [V]	0.7	i_0 [A/cm^2]	0.0004

Table 7.14: Output Fuel Cell

Outputs			
Current Density [A/cm^2]	0.4	Stack Current [A]	1196
Cell Voltage [V]	0.71	Fuel Cell Mass [kg]	496.6
Stack Voltage [V]	270	Fuel Cell volume [L]	293.5
Oxygen Mass Flow [kg/s]	0.53	Water Mass Flow [kg/s]	0.05
Hydrogen Fuel flow [kg/s]	0.0093	n_{stack} [-]	376

7.5. Fuel Tanks

In this section, the fuel tanks will be discussed. First the amount of necessary fuel will be explained. Then, the tank structure and materials will be chosen. Next, the fuel system will be described and lastly, the fuel system layout will be given.

7.5.1. Amount of Fuel

After iterating the design, the final value for the fuel weight came out to be 9395.6 kg. This is the amount of fuel that is used by both turbofans and the fuel cells combined during a flight of 4500 km at maximum payload, as per requirement HPRA-REQ-PER-2. To achieve an acceptable storage density, hydrogen has to be stored in liquid form, requiring cryogenic tanks due to its very low boiling point of -252 °C at 1 atm. Liquid hydrogen (LH2) is stored at 70 kg/m^3. Therefore, a required volume storage of 134 m^3 follows. However, since the tanks will feature passive thermal control with insulation materials, there will be passive heat flow across the surface of the tank. This will result in LH2 heating up past its boiling point, creating the so-called boil-off effect: a fraction of the stored LH2 will vaporise, making this portion of hydrogen unsuitable for usage, as the fuel and propulsion system are not designed to transport gaseous hydrogen. In addition, this boil-off gas builds up possibly dangerous amounts of pressure in the tank.

To correct for this loss of hydrogen, studies performed during the Cryoplane Project suggest a 3 % boil-off fraction of the total stored hydrogen.[16] Research performed by NASA suggests a 2 % gaseous fraction [16], thus the most critical value of 3 % is taken. This leads to a new fuel weight of 9395.6/0.97 = 9686.19 kg. This in turn yields a final total fuel volume of 138.4 m^3.

7.5.2. Tank Structure and Materials

The tank has to allow for this 138.4 m^3 to fit, in addition to being able to keep the fuel at cryogenic temperatures and cope with the increased pressure due to boil-off. Therefore, the shape of the tank and the materials it is made of, need to be determined. This will be done now.

Tank Shape: The shape of the tank depends on various aspects. The main factors are the available space inside the airframe, whether or not the tanks have to carry external loads (and if so, how high?), and the necessity to minimise passive heat flow over the tank surface. During the design, it was first assumed that it would be sufficient to have the tanks fit inside the two-dimensional planform (aircraft top view), and that the body would accommodate for sufficient tank height. In addition, the tanks would not be integrated into the load-bearing structure, to not apply too many constraints on their design and potential volume (which is very much needed). It should be noted however, that from a weight standpoint, an airframe-integrated tank is the superior option.[16]

With the above assumptions in mind, the tank was initially planned to be an elliptical cylinder with elliptical end caps. To minimise the passive heat flow, or in other words to minimise tank surface area for available storage volume, a completely spherical tank is optimal. This was already known from [16], yet was confirmed during design. After basic calculations, two spherical tanks to account for the 138.4 m^3 would be too large in height and therefore a cylindrical tank with circular end caps was selected to have the tanks adapted more to the shape of the fuselage-wing-body and thus decreasing the height. When the dimensions for this tank shape were optimised to have minimal surface area, the cylindrical (straight) part reduced to zero. Hence, it was consequently chosen to drop the minimum ratio of surface area-to-storage volume and mainly adapt the tank geometry to fit it inside the aircraft. The penalty of added passive heat flow, is paid with more insulation.

The shape of the tank was thus decided to have the general shape of an elliptical cylinder with elliptical end caps, the dimensions and the elliptic ratios would all be variables during design. This seemed to be the most promising method to design the tanks (adopted from [70]), as now the aforementioned variable could be tweaked in order to make the tanks fit whilst providing sufficient fuel volume. The main geometry of the fuel tanks is described in Figure 7.10. In Figure 7.11, three possible tank shapes are described, by varying the parameters defined in Figure 7.10. Note how flexible this approach of tank sizing is.
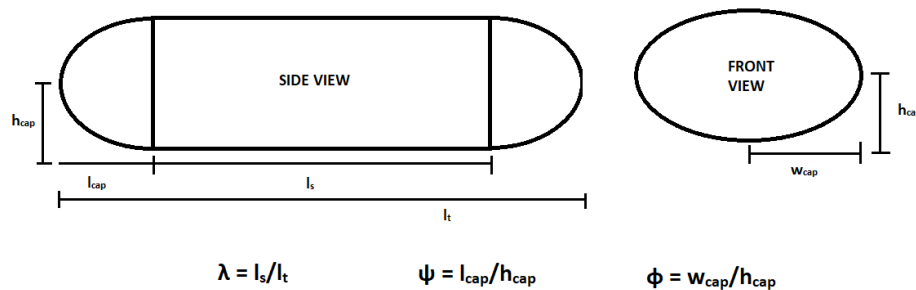

$$\lambda = l_s/l_t \qquad \psi = l_{cap}/h_{cap} \qquad \phi = w_{cap}/h_{cap}$$

Figure 7.10: Definition of the Tank Geometry

(a) Fuel Tank: $\lambda = 0.68$, $\phi = 1$, $\psi = 1$

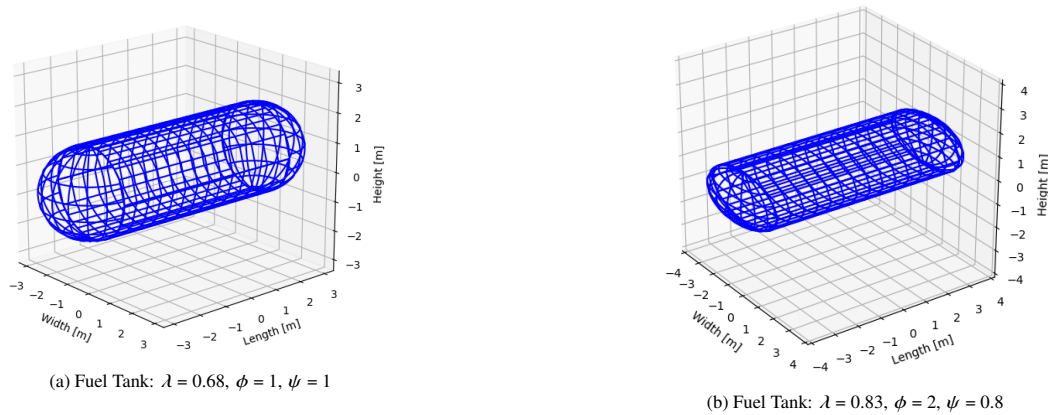(b) Fuel Tank: $\lambda = 0.83$, $\phi = 2$, $\psi = 0.8$

Figure 7.11: Various Tank Shapes Using Different Geometry Inputs

The tank in Figure 7.11a resembles the simple cylinder with spherical end caps, while the tank in Figure 7.11b is a better representation of what the actual fuel tanks would look like: two of which would be positioned on either side of the cabin along the length of the aircraft. In this case, the height can be limited according to any constraints resulting from the airfoil. Adopting this method has the advantage of the research performed in [70], which performed a mechanical and thermal analysis and could give values for the tank mass, insulation thickness and gravimetric efficiency (fuel weight over total fuel tank weight), depending on the chosen values for λ, ϕ and ψ. From their results, it was noted that $0 < \lambda < 1$ always holds, and it was suggested that ψ should equal 1 and ideally $1 < \phi < 1.5$.

There is however a risk involved with this approach: what if the tank does not fit after all? The best option is to make it fit, and with that is meant to alter the shape around the tank (affecting the airfoil and planform), yet this takes time. This time was unfortunately no longer available when it was seen that the tanks would indeed not fit. Due to the airfoil shape of the fuselage, towards the end of the aircraft, the height available became too small, as the tanks would bulge out about 30 cm at rear. Due to the width and length constraints, it was not possible to alter the tank geometry further to make it fit. Adding an additional fuel tank behind the cabin and/or splitting up the volume in smaller tanks did not solve the problem either. This is a risk that was identified during the concept selection, yet the tanks can still fit inside the blended wing-body, albeit resorting to a more general geometry to most efficiently use the space available. This will be shown now. The disadvantage of such a tank is that it is much harder to size correctly: mechanical and thermal analysis cannot be adopted from literature due to the very specific shape of the available space provided for the tanks in the Hydrojet Design.

As a last resort, CATIA was used to shape the fuel tanks such that they fit inside the aircraft and are big enough to store the required LH2 volume of 138.4 m^3. The process was started using the geometry of the wing sections that would contain the tanks, which is the section between the cabin and the outer wings. The two sides of the tanks were made as elliptical as possible while still following the outer NACA 25112 airfoil shape, so that an elliptical cylinder approximation could be used to perform an independent mechanical and thermal analysis, which was now required. The final result of the fuel tank shape (two in total) is shown in the figure below:
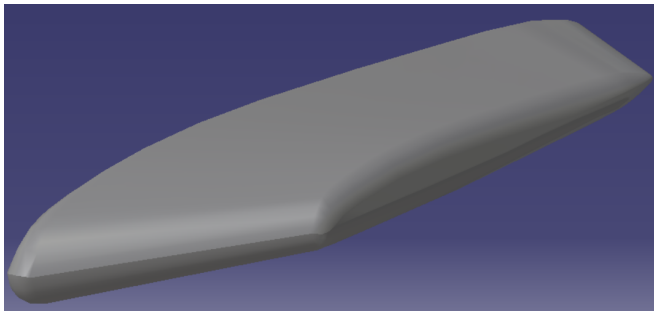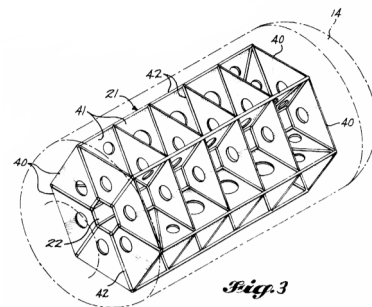

Figure 7.12: One of Two Fuel Tanks

Figure 7.13: Internal Tank Baffle Structure to Reduce Sloshing [71]

Note how the tank nicely follows the airfoil and both the LE and TE sweeps. Using CATIA, an internal volume of 77.8 m^3

was found for each of the two tanks, yielding a total possible fuel storage volume of 155.6 m^3 which easily accommodates the fuel needed to achieve the range of 4500 km at the design payload. Additionally, it allows for an internal structure to prevent excessive sloshing (see below). The space taken up by the tank wall and its insulation is also taken into account and fits into the aircraft. Per tank, the total available volume equals 95.94 m^3, which again perfectly accommodates for the wall and insulation thicknesses, which will be discussed subsequently.

Sloshing: As the fuel inside the tanks is depleted during flight, the liquid has more free space to move around. This can cause wave motion and fluid separation. These in turn poses unforeseen dynamic forces and dangers regarding aircraft stability and tank rupture.[71] Sloshing dynamics are quite complex and are usually analysed using Computational Fluid Dynamics (CFD) simulations, which are out of the scope of this project. Therefore, a quantitative analysis is not performed. Rather, measures that have been proven to work, are implemented into the fuel tank, such as baffle structures seen in Figure 7.13. Since the tank can contain more fuel volume than necessary, this baffle structure can be flexibly designed without compromising the fuel storage. In addition, it is secured to the tank wall, and due to the external insulation, this baffle structure does not cause boil-off.

Insulation Type: Since the fuel will need to be insulated to maintain a temperature below -252 °C, the main design choice that arises is whether the insulation is located on the inside or outside of the tank wall. Internal insulation has its advantages compared to the other option, but comes with challenges. The main advantages are:

- Tank walls remain at the ambient temperature of the primary structure and aircraft skin, hence;
- Minimal to no thermal expansion encountered, hence;
- Attachment to and support from the primary structure is not compromised

These advantages simplify the further mechanical design of the tank. However, there is one rather large drawback: the insulation material should be impervious to gaseous hydrogen (GH2). At the moment, this is a deal-breaker since there are hardly any materials or liners providing good insulation and being impermeable to GH2. When GH2 is diffused from the insulation into the tank wall, the thermal conductivity of the insulation material would be compromised.[16] It is therefore chosen to implement insulation on the exterior of the tank, meaning extra consideration needs to go into the effects of thermal expansion. In addition, now the insulation material has to be impervious to air, to again conserve its effectiveness.

Insulation Methods: There exists two methods of insulation which are feasible for cryogenic pressure vessels; vacuum-jacketed systems and foam-based insulation. The insulation is necessary to reduce the heat transfer as stated previously which consequently reduces the boil-off rate. Concurrently, the frost build-up is also reduced, which can otherwise hinder the ability to fly. Heat transfer to the tank occurs from the temperature of the surroundings from convection and radiation, this heat is then transferred through the insulation into the tank via conduction, as can be seen in Figure 7.14.
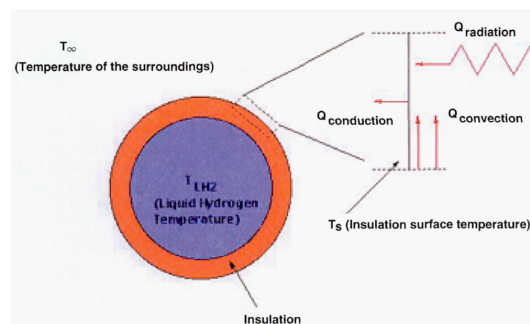
Figure 7.14: Heat transfer. [72]

Vacuum-jacketed insulation, or multi-layered insulation (MLI), have near zero thermal conductivity, but they both have a high vacuum requirement. This means that a double wall would be needed which is heavier. The main drawback to the vacuum-jacketed insulation is that if the vacuum is lost, the insulation will fail, causing a rapid boil-off of liquid hydrogen.[16] The foam type insulation is much more resistant to catastrophic failure than the vacuum-jacketed type of insulation. However, the density and thermal conductivity of the foam insulation is greater. Besides this, the foam needs to be protected using a fairing and also from hydrogen embrittlement. The offset of two relatively thick walls for the MLI might offset the disadvantage of the thicker insulation needed by the foam which has a higher thermal conductivity. Moreover, the rapid boil-off in case of a vacuum loss is unacceptable for an aircraft application, hence foam will be chosen. The foam material was chosen to

be an open cell due to its ability to insulate complex shapes better and it is an excellent option for aircraft because of their excellent cyclic behaviour. Subjecting polyurethane foam to 4000 thermal cycles, which is around 14 years of lifetime (typical for aircraft fuel tanks), caused no mechanical or thermal degradation of the polyurethane.[73] The recycling of polyurethane foam is only possible with chemical recycling and the details are given in section 11.3.

Tank Wall Materials and Thickness: For the tank wall, three main considerations due to the effects of hydrogen must be addressed. Firstly, the permeability of hydrogen is discussed. Between metals and composites, metals have a much lower hydrogen permeation rate. A liner used on a composite would also work. However, due to the thermal expansion differences, separation of the liner can occur, hence a metal shall be used. The second consideration is hydrogen embrittlement, which can cause cracking at stress levels below the yield stress. The material used for the tank wall must be resistant to hydrogen embrittlement. Hence, a high strength steel or aluminium should be used. Aluminium shows minimal possibility of hydrogen embrittlement due to the face-centered cubic structure, which minimises the solubility of hydrogen and reduces its movement through the lattice. Problems arising due to hydrogen embrittlement throughout the aircraft's lifetime can be resolved by baking the absorbed hydrogen out of the material.[74] Thirdly, the material should "retain satisfactory ductility and fracture resistance at cryogenic temperatures".[75]

The material selection for the tank wall is done by finding the material with the minimum thickness and low cost/weight between Al 5083-O and Al 2219-T87. These two materials are evaluated because they have good fracture toughness from their great ductility (no ductile to brittle transition) as it is annealed. This leads to lower chances of failure. Furthermore, they are both very commonly used cryogenic aluminium alloys.[76] After doing analysis on the mass and cost of their respective usage, the chosen material for the on-board cryogenic fuel tank is Al 2219-T87. It had considerably lower thickness, for a small added weight and cost. The analysis was done by assuming the fuel tank is a cylinder, using the largest radius of the actual fuel tank, and the entire length and area found in CATIA. The pressure used, P_{LH2}, was the pressure that the hydrogen is pumped into the tank with during refuelling. A safety factor of 1.5 was added. In order to find the thickness of the wall, the thin-walled assumption was applied. Equation 7.41 was solved as the hoop stress is the most critical stress, where R_{LH2} is the largest radius of the liquid hydrogen tank and t_{LH2} is the thickness of the liquid hydrogen tank. The hoop stress is the most critical stress, since the radial stress is negligible for thin-walled vessels, and the axial stress is half the the hoop stress. The inputs for the equation can be found in Table 7.15, and the outputs in Table 7.16.

$$\sigma_\theta = \frac{P_{LH2}R_{LH2}}{t_{LH2}} \tag{7.41}$$

To calculate the minimum thickness of non-circular shapes, ASME rules for Construction of Pressure Vessels gives the correct method.[77] However, the method used previously is assumed to be conservative, because the radius is larger than needed throughout the tank, and the rules can be applied in a future design phase to make the tank more lightweight.

Table 7.15: Inputs for liquid hydrogen tank wall thickness.

Inputs			
Largest radius [m]	8.0645	Thickness volume [m^3]	0.709
Volume [m^3]	95.936	Safety factor [-]	1.5
Pressure [Pa]	241,317	Wall materials	List of values
Area [m^2]	143.68	Material densities [kg/m^3]	List of values
Length [m]	4.61	Yield Strength [Pa]	List of values
Volume [m^3]	95.936	Price [Euro/kg]	List of values

Table 7.16: Outputs of liquid hydrogen tank wall.

Outputs	
Material chosen	Al 2219-T87
Material yield stress [MPa]	366
Material density [kg/m^3]	2870
Material price [€/kg]	2.53
Tank wall thickness [m]	$8.00 \cdot 10^{-3}$
Tank wall mass [kg]	$2.03 \cdot 10^3$
Tank cost [Euro]	$5.15 \cdot 10^3$

Insulation Thickness: To determine the thickness of the insulation, a paper by NASA is followed which takes into account all three forms of heat transfer, namely, convection, conduction and radiation. In the verification, a first-order analysis using convection and conduction is done to make sure the results used in the paper make sense. In order to account for the added heat transfer through the supports, connections, and piping, a 30% margin is added to the heat transfer.[75] It is expected that the radiation will decrease the insulation surface temperature and thereby increase the boil-off rate. Hence the first order analysis will need a higher insulation thickness than necessary. In order to calculate the insulation thickness, first the maximum allowable boil-off mass in the flight was calculated, which was boil-off mass of 254.5kg using the 3% loss. This corresponds to a boil-off rate of 0.01kg/s for a total duration of 7 hours. Then applying the method shown next, the boil-off rate for many thicknesses are found by first solving for the temperature at the insulation surface numerically. Finally, the thickness associated with the maximum boil-off rate allowed was then chosen to be the final insulation thickness. The inputs for the equations can

be found in Table 7.17 and the final outputs can be found in Table 7.18.

The heat transfer to the insulation comes through convection of the air surrounding the tank and radiation into the surface, which can also be seen in Figure 7.14. The heat transfer to the tank is given in Equation 7.42. The heat transfer through the insulation and into the tank is given by Equation 7.43.[72]

$$Q_{in} = Q_{convection} + Q_{radiation} = h(T_\infty - T_S) + \epsilon \sigma_{sb}(T_\infty^4 - T_S^4) \tag{7.42}$$

$$Q_{out} = Q_{conduction} = \frac{K(T_S - T_{LH2})}{t_{ins}} \tag{7.43}$$

The symbols are as follows: h is the convection coefficient for the air surrounding the tank. It is assumed the tank does not have blowing air around it.[72] This coefficient h is found using Equation 7.45. T_∞ is the temperature at cruise, T_s is the insulation outer surface temperature, ϵ is the insulation surface emissivity, σ_{sb} is the Stefan-Boltzmann constant, K is the thermal conductivity of the insulation, T_{LH2} is the hydrogen storage temperature and finally, t_{ins}.[72]
Then Equation 7.42 is set equal to Equation 7.43 in order to solve for T_s, as shown in Equation 7.44. This is done numerically using the nsolve function from a python library called Sympy[4]. The starting solution is set close to the predicted solution which is close to the cruise temperature.

$$Q_{in} = Q_{out} \tag{7.44}$$

$$h = \frac{N_{UD} K_G}{D_{LH2}} \tag{7.45}$$

Where N_{UD} is the Nusselt number and is dependent on the geometry of the tank, which is cylindrical in this case. The Nusselt number is found using Equation 7.46. K_G is the thermal conductivity of the air, and finally, D_{LH2} is the liquid hydrogen tank diameter.

$$N_{UD} = \left[0.60 + 0.387 R_{ad}^{1/6} / \left[1 + (0.559/0.5 P_{LH2} D_{LH2})^{9/16} \right]^{8/27} \right]^2 \tag{7.46}$$

The Rayleigh number, R_{ad}, is given by Equation 7.47 in which g is the gravitational acceleration and β_t is equal to the inverse of the cruise temperature since an ideal gas is assumed.[72]

$$R_{ad} = g \beta_t (T_\infty - T_s) D_{LH2}^3 / (v_{gas} \alpha_{gas}) \tag{7.47}$$

Finally, the gas diffusivity and viscosity, α_{gas} and v_{gas}, respectively, are found using a curve fit for air on different temperatures and is calculated using Equation 7.48 and Equation 7.49 found from [72].

$$\alpha_{gas} = -3.119 \times 10^{-6} + 3.541 \times 10^{-8} T_\infty + 1.679 \times 10^{-10} T_\infty^2 \tag{7.48}$$

$$v_{gas} = -2.079 \times 10^{-6} + 2.777 \times 10^{-8} T_\infty + 1.077 \times 10^{-10} T_\infty^2 \tag{7.49}$$

After numerically solving for T_s, the boil-off rate, $\dot{M}_{boil}$, of liquid hydrogen can be calculated using Equation 7.50. This is done using an energy balance between the heat flow through the insulation and the energy needed to boil the liquid hydrogen, which is the latent heat of vaporization of liquid hydrogen, h_{fg}, which in this case h_{fg} = 446592. J/kg.[72]

$$\dot{M}_{boil} = \frac{K A (T_s - T_{LH2})}{t_{ins} h_{fg}} \tag{7.50}$$

Protection for foam insulation: The foam has to be protected from hydrogen embrittlement, the outside air and from external damage. Therefore, the structure consisting of some layers developed by [75] will be used as this satisfies the requirements. The structure consists of two MAAMF vapour barriers, MAAMF is a multilayer sandwich and MAAMF stands for the different materials used in each layer. The MAAMF vapour barrier consists out of the following layers: A Mylar layer, adhesive, aluminium foil, adhesive, aluminium foil, adhesive, Mylar and finally a Dacron or glass net fabric.[16][75] The MAAMF has a surface density of 0.225 kg/m^2 and a thickness of 1.524 · 10^{-5} m.[75] Lastly, a fairing is applied at the outer surface to protect the foam from external damage. This fairing has a surface density of 1.304 kg/m^2 and a thickness of 0.0157 m.[75]
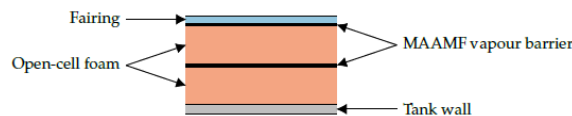

Figure 7.15: Structure for the fairing[70]

---

[4]https://docs.sympy.org/latest/modules/solvers/solvers.html [accessed on 21 June, 2020]

Table 7.17: Inputs to find the insulation thickness

Inputs					
R_{GH2} [m]	8.0645	Foam materials	Polyurethane	σ_{sb} [W/(m²K⁴)]	$5.67 \cdot 10^{-8}$
Inner Volume [m³]	95.936	Foam densities [kg/m³]	32.1	g [m/s²]	9.80665
R_{LH2} [Pa]	241317	Foam K [W/(mK)]	0.0112	h_{fg} [J/kg]	446,592
Area [m²]	143.68	T_∞ [K]	223.15	K_G [W/(mK)]	0.02
Length [m]	4.61	T_{LH2} [K]	20	Flight duration [s]	25,200
Thickness volume [m³]	0.709	T LH2 boiling point [K]	22	Allowed boil-off mass [kg]	253.63
Safety factor [-]	1.5	ε[W/(m²K⁴)]	0.05		

Table 7.18: Outputs for insulation thickness

Outputs	
Insulation material chosen	Polyurethane
Insulation thickness [m]	0.08
Insulation mass [kg]	$3.7 \cdot 10^2$
Insulation cost [Euro]	$2.04 \cdot 10^3$
Insulation outside surface temperature [K]	191.8
Boil-off mass rate [kg/s]	0.01

Total Liquid Hydrogen Tank specification: The total tank thickness, including the tank wall, the tank insulation and the fairing with the MAAMF vapour barriers adds up to 0.104 m, with a mass of $2.4 \cdot 10^3$ kg and a cost of €$7.18 \cdot 10^3$. The additional weight to the inner wing structure is $1.54 \cdot 10^3$ kg.

7.5.3. Fuel system
The fuel system of the Hydrojet will consist out of a ground operations fuel system, a flight operation fuel system and a refuelling system.

For this former past, the systems works as follows: fuel will be taken from the the first hydrogen tank while keeping the same fuel masses in both tanks via the transfer line. This fuel then goes through a pump where it is pressurised up to 10 bar. This to increase the vapour pressure of hydrogen, inducing more safety. Additionally, 10 bar is the optimal working pressure of hydrogen in the fuel cell.[78] Next the fuel will be pumped to a heat exchanger where heat is exchanged with the bleed air required for the air conditioning and pressurisation of the cabin (ECS). An increase in temperature from 20 K to 353.15K is obtained, the optimal temperature for fuel cells. This is also the moment for the phase change to occur, so extra heat is exchanged to make the hydrogen gaseous. The air which is required for the operations of the fuel cell comes from the outside ram air. After pressurisation and separation this air is guided to a heat exchanger and a filter system to make the fuel cell run reliably. At the end, the air will enter the fuel cell at 3 bar with a temperature of 380K, which, again, are the optimal conditions for the working of air in the fuel cell.[78] Water will be created during electrolysis. This water will be stored in a tank after it has been used to cool down the heat exchanger. Finally, bleed air for the ECS system, which is already explained in Subsection 7.2.5, is included in the layout as it needs to be cooled down before entering the mix manifold. This can be done with the extremely cold fuel as explained above, so both fuel and bleed air support in each other functions.

For the flight operations system, the working mechanism is more or less the same. Fuel is pumped from the tanks to a heat exchanger to the turbofan. As more mass flow is present now the bleed air will not be able to increase the temperature up to 150K which is the injector temperature, described in Subsection 7.3.6. Therefore the flow will be heated once more at the exhaust gases of the turbofan. The ECS system works exactly the same as above.

The last system is the refuelling system at the airport. To ensure comparable turnaround times with respect to reference aircraft, the on-board hydrogen tanks will have at least one inlet for the liquid hydrogen (per tank). The inlet will be placed at the bottom side of the fuel tank. Furthermore, the tanks will also have an outlet at the top of the tank for gaseous hydrogen that is formed during refuelling.

7.5.4. Fuel System Layout
A simplified configuration of the fuel system described above is given in Figure 7.16. Note that the real system is one, complete system. They are represented as two different systems here for convenience.
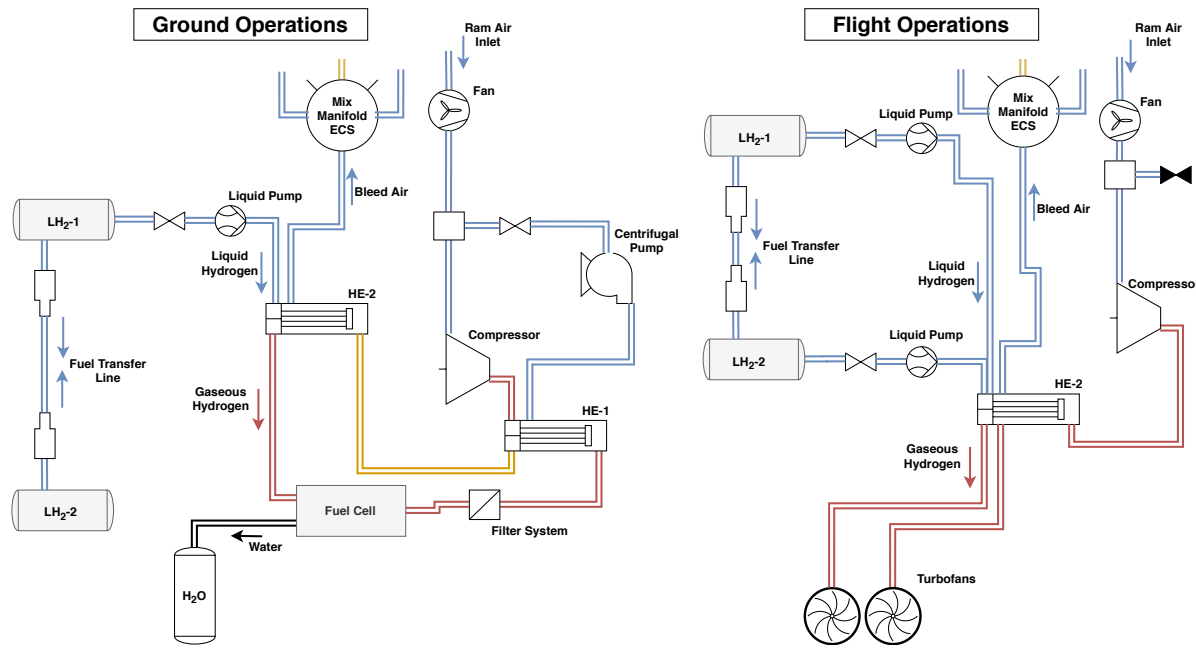
Figure 7.16: Fuel System of the Hydrojet during Ground and Flight Operations

7.6. Verification and Validation

To verify and validate the complete system of power and propulsion, there will be two separate verification and validation methods used for each subsystem. Namely, one for the turbofan itself, and one for the fuel cells. One other verification method is given for the insulation thickness of the cryogenic liquid hydrogen tank.

Verification for the turbofan engine is done using the gas turbine calculation program 'Gasturb', and giving it the same inputs as were used to calculate the results for take-off as are given above. Gasturb is a suitable program for this purpose as it is a verified and validated program itself. Note that the mass flow will now be given as additional input, instead of the take-off thrust, as Gasturb does not take thrust as input. Once the correct inputs are given, Gasturb will provide the total temperature, total pressure and mass flow at each station, as well as the generated thrust. By comparing the parameters at each station, verification can be performed. Moreover, by comparing also the generated thrust, the whole system can be validated.

To verify the thickness of the insulation a first order estimation of the overall heat transfer is made using conduction and convection. This was done using the same equations as before, however $Q_{radiation}$ is removed. The results for a boil-off mass of 0.01004 kg/s are as follows: The temperature T_s is 214.8K and the thickness is 0.094m. As was predicted, neglecting radiation increases the surface temperature and therefore the boil-off rate is also increased, which in turn increases the insulation thickness required for maintaining the allowed boil-off rate. For the final insulation thickness, the method presented by [72] will be used as it is more representative of reality. Furthermore, the effect of increasing the insulation thickness has the effect expected on the boil-off rate as can be seen in Figure 7.17. Validation was done by comparing insulation thickness with other aircraft. In [75] an insulation thickness of 0.076mm presented the minimum weight, hence the insulation thickness is validated as it is in the correct range for liquid hydrogen tanks.

Figure 7.17: Effect of insulation thickness on boil-off rate after 7 hours.

The verification of the fuel cell consisted of unit tests, integration tests and system checks. The unit tests were performed by using hand calculations for every step. For the integration testing two or more functions were combined and cor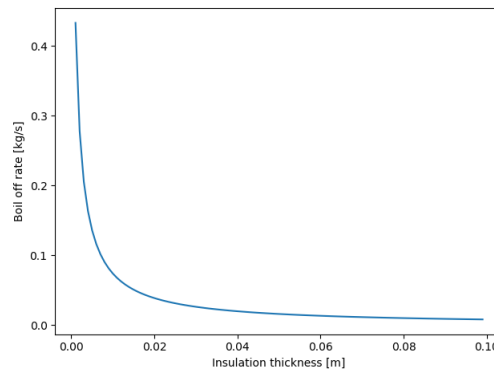rected if the results were unreasonable. The system test used a master thesis from TU Delft.[68] Several graphs were plotted including the polarisation curve and also weight vs current curve. These curves were than compared to the curves in the thesis. In this case some of the shapes were not comparable and therefore the code had to be changed.

Validation was performed using a consisting fuel cell and comparing the numbers. In this case a the PowerCell MS-100 was used for validation. This cell has a power of 100 kN with a weight of 170 kN. This gives a specific power of 580 kW/kg. Efficiency of the fuel cell is 58 %. Furthermore, operating voltage is between 250 and 500 V. Due to the fact that the current density used for the design point is set the number of cells in a stack (m_{stack}) and in series (n_{stack}) is known. The voltage range can be calculated. It was found to be between 230 and 340 V. This is a bit of a lower range but it does serve as prove that it converges. The specific power and efficiency is a bit lower in the PowerCell but it must be taken into account that the fuel cell technology is a field where a lot of progress can still be made. In the 20 years the fuel cells are expected to have twice as much specific power and an efficiency of 75 %. Therefore, assuming these factors to be a little higher in a few years when the production of the Hydrojet will start seems reasonable.[68] [79]

7.7. Risk

In order to increase the chance for a successful power and propulsion system, the possible risks to the system must be identified such that they can be anticipated and mitigated. In this section, first the risks will be identified. These risks will then be mapped into a risk map, such that the more critical ones are identified and a mitigation plan can be made for them. Finally, a mitigated risk map will be presented. Note that for power and propulsion, a more expansive risk analysis is performed, as hydrogen powered propulsion and storage is known for higher risks.

7.7.1. Risk Identification

The following possible risks to the power and propulsion system are listed below. Note that only those risks that are relevant to this and the following design phase are listed.

Power and Propulsion Risks

General risks:
Risk-CON3&4-4.1 The propulsion system weight is more than accounted for in the Class-II mass estimation.
RISK-PROP-GEN-1 The power and propulsion system becomes much more expensive than was accounted for.

Turbofan risks:
RISK-PROP-TURB-1 During testing, the engines are not capable of producing the required thrust
RISK-PROP-TURB-2 During testing, the engines produce more than the allowed amount of emissions.
RISK-PROP-TURB-3 The failure rate of the engines is too high to comply with regulations.

Integration risks:
RISK-PROP-INT-1 During testing, the pylon and/or nacelle plastically deforms/fails under maximum loads that can be encountered.

RISK-PROP-INT-2 During a later design phase, the fuel cell cannot be fitted anymore withing the planform.

Fuel cell risks:
RISK-PROP-CELL-1 The fuel cell is not capable of delivering the required power output.
RISK-PROP-CELL-2 The fuel cell is not capable of converting chemical to electrical energy with the required efficiency.
RISK-PROP-CELL-3 The water tank is not large enough to hold all of the dispose water.

Fuel tank risks:
RISK-PROP-TANK-1 The fuel tank degrades too fast under given cyclic loads.
RISK-PROP-TANK-2 The fuel tank fails under maximum encountered loads.
RISK-PROP-TANK-3 Heat diffusion along the walls of the fuel tank is more than was accounted for.
RISK-PROP-TANK-4 There is more boil-off than was accounted for.
RISK-PROP-TANK-5 Hydrogen evaporates from the fuel tank into the cabin.

Fueling system risks:
RISK-PROP-FUEL-1 Under extreme conditions, such as a high load factor within a turn, the fuel system is not capable of delivering 100 % of the required fuel to the engines and/or fuel cell.
RISK-PROP-FUEL-2 Hydrogen evaporates from the fuel system into the cabin.

Taxiing system risks:
Risk-CON3-4.2 The electric motor in the main landing gear results in too heavy landing gear for retraction.
Risk-CON3-4.3 The electric motor in the main landing gear contributes to more drag than anticipated.
Risk-CON3-4.4 The electric motor in the main landing makes the aircraft slip.

7.7.2. Risk Mitigation

Assessing both the probability and the impact of these risks, the estimation of this can be seen in Figure 7.18. All of the risks on the diagonal above the centre diagonal and above are considered critical risks, and require mitigation. This mitigation is presented below.
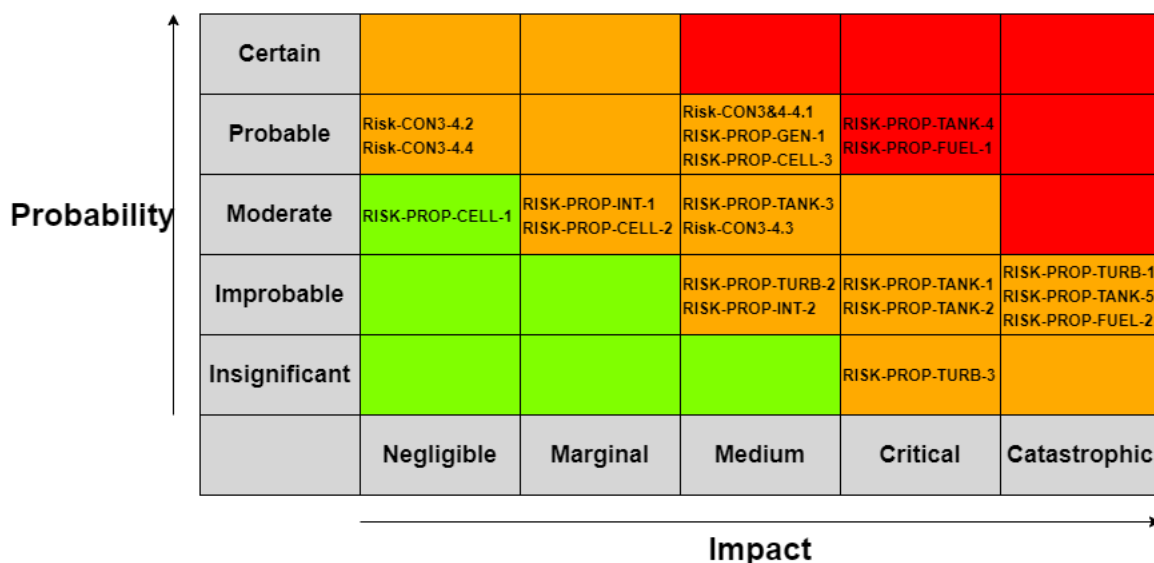
Figure 7.18: Risk map for the propulsion system without mitigation.

Risk-CON3&4-4.1 By using a contingency plan for the propulsion system weight, the probability of this risk occurring can be lowered.
RISK-PROP-GEN-1 By using a contingency plan for the cost of the propulsion system, the probability of this risk occurring

can be lowered.

RISK-PROP-TURB-1 Once a more detailed design on the turbofan will be performed, a contingency plan should be made for the thrust as well, such that the probability of this risk occurring can be lowered.

RISK-PROP-CELL-3 Any excess of water can fed into the toilet disposal system, or perhaps fed to the propulsion system, as this is known to decrease NOx emissions. However this does decrease thrust level. It could also be dumped in the atmosphere.

RISK-PROP-TANK-4 A small space of a few millimeters can be left during design. If indeed boil-off is too much, an extra layer of insulation can be added to reduce this impact.

RISK-PROP-TANK-5 This subsystem must have larger safety margins than others, and go through rigorous testing, in order to reduce the chance of this occurring.

RISK-PROP-FUEL-1 A large safety margin must be placed on the design for the fuel pump in order reduce the chance of this occurring.

RISK-PROP-FUEL-2 This subsystem must have larger safety margins than others, and go through rigorous testing, in order to reduce the chance of this occurring.

With the mitigation plan applied, the resulting risk map is presented in Figure 7.19.

Figure 7.19: Risk map of the propulsion system once a mitigation plan is applied.

7.8. Compliance with Subsystem Requirements

Now the compliance of the designed power and propulsion system with the identified requirements as stated in Section 7.1 must be checked, such that the extent to which this system has been successful can be assessed.

It is found that all of requirements that have set numerical constraints have been met. These are those requirements like HPRA-REQ-TUR-7, or HPRA-REQ-POW-1. Some of the other requirements have been met as well. However, the following requirements have not yet been met: HPRA-REQ-PGE-1-2-4, -TUR-5, -PIN-1-2-3, -PFT-2-4, -PFS-3-6-7 and -PFP-1-2-3-5. This is because these requirements can only be met once a much more detailed design has been performed. Thus, as of now, the power and propulsion systems seems to be successful in its design, and is ready for further design.

Ground Facilities

The subsystems of the aircraft have been designed now and this is followed by the design of the ground facilities. This is a crucial part for the operation of the Hydrojet, due to its unconventional design and distinctive fuel. To design it, first its requirements will be listed in Section 8.2. The compressor and cooler will be elaborated upon in Section 8.3. Furthermore, the availability and tank specifications will be investigated in Section 8.4 and Section 8.5, respectively. Additionally, the energy iteration can be found in Section 8.6. Next, verification and validation of the process and results will be discussed and the energy iteration can be found in Section 8.7. Moreover, the risks coming with the ground station will be identified in Section 8.8. Also, a final overview will be given in Section 8.9. To conclude the compliance with the subsystem requirements will be checked in Section 8.10.

8.1. Preliminary Sizing Recap

From the Midterm Report it is known that the ground station will consist of a Proton Exchange Membrane (PEM) electrolyser, which will produce green gaseous hydrogen from water at the ground facilities which can be either located on site or at a remote location. The fact that the hydrogen should be green and not grey or blue, means that the ground facilities will be powered by green energy sources such as wind turbines and solar panels (Grey means that the hydrogen is produced from fossil fuels and blue makes use of carbon capture). This will ensure that the production of the hydrogen will be completely based on sustainable energy which fits the sustainability goals of the Hydrojet. Furthermore, the oxygen produced will be sold to certified medical or educational oxygen distributors. The hydrogen gas will be stored in underground Type IV spherical pressure vessels under a pressure of 700 bar and 0 degrees Celsius.[80] [81] By adapting the existing gas pipeline infrastructure in Europe, the gaseous hydrogen will be transported from the remote or on site ground facilities to the airport.[82] At the airport a compressor will be stationed in order to liquefy the gaseous hydrogen before it will be tanked into the aircraft. The energy consumed for the production of hydrogen and the amount of wind turbines or solar panels needed, have already been calculated in the Midterm report.[1] A quick overview of the results of the Midterm report is given in Table 8.1.[1] A picture of the ground station can be seen in Figure 8.1.

Table 8.1: Ground facility properties know from Midterm Report [1]

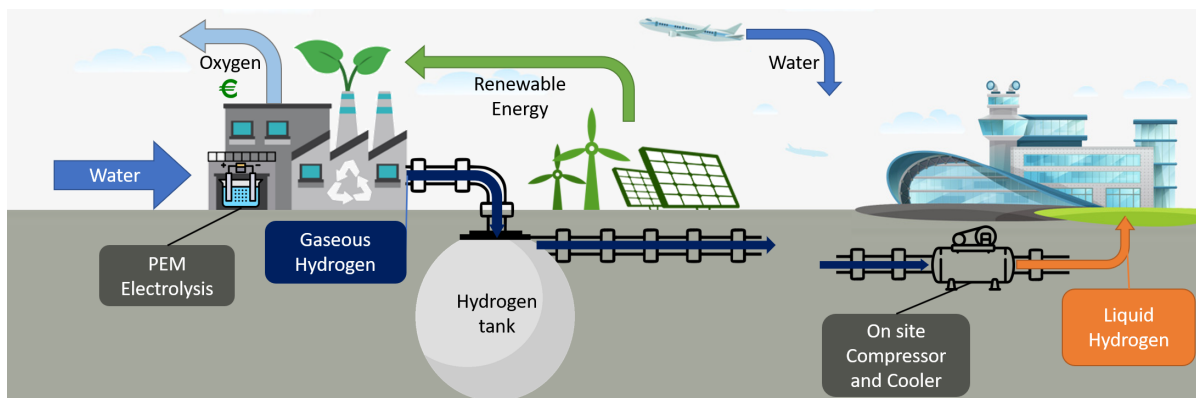| Ground fuel [kg]	Moles H_2 & H_2O	E_{in} needed [J]	P_{in} (24 hours) [W]	Turbines needed	P_{in} (12 hours) [W]	Solar panel area [m^2]	Water needed [kg]	Volume [m^3]	Radius tank [m]
88,010	$4.37 \cdot 10^7$	$1.25 \cdot 10^{13}$	$1.45 \cdot 10^8$	2.1	$2.89 \cdot 10^8$	$3.75 \cdot 10^6$	$7.87 \cdot 10^5$	2,256.67	8.14

Figure 8.1: Sketch of the ground facilities[1]

For the ground facilities, many aspects have already been determined as can be seen in Table 8.1. However, the compressor and cooler located at the airport still need to be discussed. Next to this, the fuel availability and tank specifications will also

be looked at. Also, an energy iteration will be present to size the ground facilities optimally.

8.2. Ground Facilities Requirements

Before going into more detail of the ground station, it is important to keep an overview of the requirements. That is why the subsystem requirements have been identified and are show below. The ground station will be designed based on these subsystem requirements.

Ground Facilities

Hydrogen Production:
HPRA-REQ-HPR-1 The production of hydrogen shall not cause any emissions destructive towards the environment.
HPRA-REQ-HPR-2 The production of hydrogen shall be conducted in a safe manner.
HPRA-REQ-HPR-3 The production cost of hydrogen shall not compromise the ability for hydrogen powered regional air travel to compete with its conventional counterpart.
HPRA-REQ-HPR-4 The production of hydrogen shall rely on renewable sources.
HPRA-REQ-HPR-6 The hydrogen needed for a fleet of 10 aircraft shall be produced within 24 hours.
HPRA-REQ-HPR-7 The hydrogen shall be converted from gas to liquid state before entering the aircraft tanks.

Hydrogen Ground Storage:
HPRA-REQ-HSU-1 There shall be safety protocols and systems to ensure safe hydrogen refuelling.
HPRA-REQ-HGS-1 The location of the ground facility shall not compromise safe and efficient operation.
HPRA-REQ-HGS-2 The ground storage facility shall safely store hydrogen.
HPRA-REQ-HGS-3 The ground storage tanks shall ensure a TBD energy efficiency use for cooling.
HPRA-REQ-HGS-4 The ground storage facility shall ensure safe handling of hydrogen fuel to the aircraft.
HPRA-REQ-HGS-5 The fuelling system shall accommodate at least 6 aircraft simultaneously.
HPRA-REQ-HGS-6 The fuelling system shall be able to service a fleet of 10 aircraft.
HPRA-REQ-HGS-7 The fuelling system shall accommodate a fuel flow of at least 1.16 kg/s.
HPRA-REQ-HGS-8 The ground storage facility shall include safety systems for hydrogen leaks.
HPRA-REQ-HGS-9 The ground storage facility shall enable visual inspection.
HPRA-REQ-HGS-10 The ground storage facility shall enable accessibility for maintenance.
HPRA-REQ-HGS-11 The ground station shall be able to transport the produced hydrogen to the tank and refuelling point at the airport.
HPRA-REQ-HGS-12 The ground facilities shall have at least 3 separated hydrogen storage tanks.
HPRA-REQ-HGS-13 The ground storage tanks shall be recyclable at End-of-Life.
HPRA-REQ-HGS-14 The ground storage tanks shall be able to withstand a pressure of 700 bar.
HPRA-REQ-HGS-15 The ground storage tanks shall be able to operate at 0 degrees Celsius.

8.3. Compressor and Cooler

Since the hydrogen will be delivered in gaseous form to the airports, the gaseous hydrogen will need to be liquefied before it can be tanked into the aircraft. Therefore, a compressor and cooler will be present on the airport which will convert the gaseous hydrogen to liquid hydrogen. The design for the compressor and cooler that will be used for the implementation at the airport is taken from IDEALHY.[83]

This compressor and cooler design have the ability to more efficiently convert gaseous hydrogen to liquid hydrogen compared to other existing hydrogen converters. The energy to convert the gaseous hydrogen to liquid hydrogen is equal to 6.4 kWh/kg liquid hydrogen. Since the total amount of fuel is already known from the mass estimation in Chapter 3, the total energy needed for conversion can be calculated. Additionally, a value of 6.67 kWh/kg liquid hydrogen was assumed for the inclusion of both the conversion energy and the energy for the plant itself. Thus, now an estimate can be made for the complete energy consumption of the ground facilities. In the conversion process, some losses occur. For 1 kg liquid hydrogen output, a total of 1.017 kg gaseous hydrogen will be needed as input, meaning that the conversion has an 98.3% efficiency. This is also taken into account for the conversion energy. Next to the newly produced hydrogen, there is also boil-off gaseous hydrogen left in the tank of the Hydrojet after it has completed a flight. This boil-off gaseous hydrogen will be collected and put into the compressor as well, liquefying the gaseous hydrogen again. By implementing this smaller hydrogen loop into the system, less hydrogen is wasted. Therefore, less hydrogen has to be produced and the excess of green energy can be delivered to the regular

power grid. Multiple compressors might be needed for the airport to facilitate all the aircraft at the same time. However, using careful airport planning, the number of compressors needed can be reduced.

8.4. Fuel availability

To ensure that there will always be liquid hydrogen available for the Hydrojet to tank, the operational cycle of the Hydrojet is analysed. For the maximum range, a five hour flight time is assumed based on the range and cruise speed given. For the time needed to refuel the aircraft, the fuel massflow can be calculated for regular kerosene pumps. As a reference, the Boeing 747-400 ER has been taken. This conventional kerosene aircraft has a fuel volume of 246,150 L or 246.150 m^3.[84] The Boeing 747-400ER is fully tanked within 53 minutes with 4 nozzles pumping at a pressure of 35 psi[1]. Using this information, the massflow can be calculated as shown in Equation 8.1. Now, using a density of 70 kg/m^3 for the liquid hydrogen, the massflow can be calculated.

$$\dot{m} = \rho \cdot \frac{dV}{dt} + \frac{d\rho}{dt} \cdot V = \rho \cdot \frac{dV}{dt} \tag{8.1}$$

This resulted in a massflow of 1.1622 kg/s per nozzle. The dV/dt is assumed to be constant in order to build upon the existing pumps used in current aviation. If the fuel mass is then divided by the massflow, the time to refuel the aircraft with one nozzle is obtained. The refuelling time was found to be 8083.9 seconds or 134.7 minutes, using only one nozzle. Since two fuel tanks are located on each side of the cabin, two refuelling nozzles with a pressure of 35 psi will be used to refuel the Hydrojet. The maximum fuel capacity is than reached within 67.4 minutes. Finally, the boarding of passengers and the loading of the cargo is assumed to take one hour. This adds up to about seven hours before the aircraft needs to be refuelled again. It is assumed that the destination reached after a five hour flight, will have hydrogen ground facilities as well. The aircraft will need to be refuelled again after 14 hours at the same ground station. This means that the production of hydrogen needs to be improved, since the aircraft now needs to be refuelled after 14 hours instead of the assumed 24 hours from the Midterm report.[1]

8.5. Storage Tank Specifications

Not only one tank, but three tanks will be used for hydrogen ground storage. This is due the applied strategy that one tank will always be in use, one tank will be on stand-by, ready to be switched on, and one tank will be in maintenance. Next to this, the risks will also be spread over multiple tanks, when there is for instance a leakage or other complications with one tank. Additionally, the tank material and thickness will also be sized.

8.5.1. Tank Safety and Maintenance Features

The safety features that the spherical tank will have, are leak before burst and safety valves. Leak before burst dictates that the pressure vessel should be designed such that a crack will grow, allowing the fluid to escape and thereby reducing the pressure, prior to growing large enough to cause fracture at operating pressure. This is important as the operating pressure is quite large and any fracture at that pressure would create considerable damage to the surroundings. Secondly, safety valves should be implemented to ensure that the operating pressure is never exceeded in operation.

The maintenance features will include pressure vessel closures that are held back by the internal pressure. These closures will be designed such that quick access to the pressure vessels is allowed by maintenance personnel.

8.5.2. Tank Materials and Thickness

The tanks are spherical, as this is the theoretically ideal shape for a pressure vessel that resists internal pressure. The tank wall is assumed to be thin walled. It will be checked if $D/t > 20$. If this is not the case, then a different calculation must be used. A safety factor of 2 is taken, as weight is less important on the ground, and the failure of the weld holding the two halves of the spherical vessel has to be reduced using a safety factor. A spherical pressure vessel is held together against the gas pressure due to tensile forces of the walls. The stress in a thin-walled spherical pressure vessel can be found using Equation 8.2.

$$\sigma_\theta = \sigma_{long} = \frac{P_{GH2} R_{GH2}}{2 t_{GH2}} \tag{8.2}$$

Where σ_θ is the hoop stress and σ_{long} is the stress in the longitudinal direction, P_{GH2} is the internal gauge pressure, R_{GH2} is the inner radius of the sphere and t_{GH2} is the thickness of the wall. The inputs for finding the gaseous hydrogen tank wall thickness can be found in Table 8.2. Rearranging the equation and solving for t, using the yield stresses of different materials with a safety factor of 2, leads to Table 8.3. The mass is found by calculating the volume of the skin, $V_{thickness}$ and multiplying

---

[1]http://www.boeing.com/assets/pdf/commercial/airports/acaps/7474sec5.pdf [accessed on 9 June, 2020]

it with the density of the material. The volume of the thickness is found using Equation 8.3.

Table 8.2: Inputs for finding wall thickness.

Inputs			
Radius [m]	7.24	Possible materials	list of values
Volume [m3]	1590.02	Material densities [kg/m3]	list of values
Pressure [MPa]	70	Material yield stresses [Pa]	list of values
Safety factor [-]	2	Material price [euro/kg]	list of values

$$V_{thickness} = \frac{4}{3} \cdot \pi \cdot ((R_{GH2} + t_{GH2})^3 - R_{GH2}^3) \tag{8.3}$$

Table 8.3: Wall specification per material

Output				
Material	Steel 300M	Al 2024 T4	Titanium	Carbon Composite
Density [kg/m^3]	7870	2800	4670	1610
Yield stress [MPa]	690	330	1100	1900
Price [€/kg]	.993	2.36	22.3	50
Tank wall thickness [m]	0.734	1.54	0.461	0.267
Diameter/thickness ratio [-]	21.7	11.4	33.4	56.3
Tank wall mass [kg]	$4.21 \cdot 10^6$	$3.48 \cdot 10^6$	$1.51 \cdot 10^6$	$2.93 \cdot 10^5$
Tank material cost [€]	$4.18 \cdot 10^6$	$8.2 \cdot 10^6$	$3.37 \cdot 10^7$	$1.47 \cdot 10^7$

Out of the different materials, Steel 300M was the least expensive option and will therefore be chosen. The thin walled assumptions hold as D/t is 21.7, which is larger than 20. Since Steel 300M has a CO2 emission of 2.5 kg per kilo of steel produced, producing one tank will emit at least $1.05 \cdot 10^7$ kg of CO2. Using recycled steel, the CO2 production is 0.703 per kilo steel produced and $2.96 \cdot 10^6$ kilos of CO2 is produced for one tank. Therefore, recycled steel will be used as the properties are the same.

Polymer liners of type IV pressure vessels will be obtained by blow molding. Polyethylene terephthalate will be blow molded on top of the tanks. Due to the large thickness of the tank, the liner will be very thin. It is assumed the cost and mass is negligible compared to the wall cost and mass.

8.6. Energy Iteration

Now, taking the compressor, cooler, availability and tank specifications into account, the ground facilities can be reiterated and the amount of green energy needed, can be updated. Currently, the amount of ground fuel is determined based on the assumptions that the fleet of 10 aircraft will fly continuously over the maximum range. However, after a more thorough analysis, it is concluded that 85 % of the aircraft fly at a lower range, and thus need less fuel. 15 % of the aircraft fly at the maximum range.[85] Furthermore, the amount of on-board fuel is updated based on more detailed analysis done in Chapter 3. Based on the number of aircraft with a different range and the on-board fuel, the total amount of ground fuel is calculated. When the amount of ground fuel is known, the energy that is needed can be calculated. This energy also includes the energy that is needed for conversion and cooling, as explained in Section 8.3.

As the goal of this project is to design a sustainable aircraft, where the fuel is produced by means of green energy, solar panels and turbines are used. To minimise the area needed for the renewable energy sources, the wind turbines and solar panels are combined. The results can be seen in Table 8.4.

Table 8.4: Sizing of Renewable Energy Sources

Ground fuel [kg]	Total E$_{in}$ needed [J]	Turbines needed	Solar panel area [m^2]	Solar panel length [m]	Solar panel width [m]
62,011	$1.18 \cdot 10^{13}$	3	$1.65 \cdot 10^6$	2,055	801.1

The solar panel length is determined based on the distance between all of the turbines. The diameter of the turbine is 137 m. From [86], the space needed between two wind turbines is equal to $7 \cdot D_{rotor}$. Based on this, the total length of the three turbines, and thus the solar panels, equals 2,055 m. The amount of energy produced by the turbines is subtracted to determine the energy needed to be produced by the solar panels. From this energy, the total solar panel area is calculated. Since the solar panel's length and area are known, the width can be easily calculated and equals 801.1 m.

8.7. Verification and Validation

For the ground facilities design, most of the elements used are based on currently available elements. These elements are the PEM electrolyser and the wind turbines and solar panels. For validation of the energy that will be used, the ground facilities themselves will have to be built and see what the energy consumption is, based on a full time work load. Additionally, the energy consumption of the ground facilities can be compared with other hydrogen plants. However, since this information is not available at the moment, the verification will be postponed to the post DSE activities.

Only the structure can be verified in some ways. Pressure vessels have a minimum mass, since it scales with the pressure and volume it contains and is inversely proportional to the strength to weight ratio of the material used. For a spherical vessel the minimum mass, M_{GH2}, is Equation 8.4.

$$M_{GH2} = \frac{3}{2} p_{GH2} V_{GH2} \frac{\rho}{\sigma_y} \tag{8.4}$$

Using this equation with the data for the tank, V_{GH2} is the volume of the tank and ρ the material density. A minimum mass of $1.9 \cdot 10^6$ kg is found for steel 300M. This is 2.2 times smaller than the mass calculated previously. The difference comes primarily from the safety factor. Hence, the tank mass is verified to be larger than the minimum required.

8.8. Risk

To assess the risks of the ground facilities itself, a risk analysis is performed. This will start by identifying the different design and operational risks. Furthermore, the mitigation measures for the identified risks will be described as well.

All the risks resulting from the design and operations of the ground facilities have been identified. These are listed in below:

- The tank is not strong enough to uphold 700 bars of pressure over a lifetime of 25 years.
- Leakage and failure of the tank is hard to detect since the tank is placed underground.
- The gaseous hydrogen tanks are not able to supply a fleet of 10 aircraft simultaneously.
- The tank will not be 0 degrees Celsius at all times.
- The green energy delivered to the ground facilities is insufficient to make the ground facilities carbon neutral.
- Energy cannot be delivered at all times due to the natural energy sources used.
- Leakage and losses occur in the pipeline infrastructure.
- Leakage and losses occur during the liquefaction of hydrogen.
- Water is not always available for hydrogen production.
- PEM Electrolyser yield is lower than expected.
- A wind turbine malfunction causes a shortage of green energy.
- Solar panel efficiency will reduce over time.

Using mitigation measures, the probability and impact of the risks can be reduced. The mitigation measures for each risk are described below.

For the first risk, the lifetime of the tank is questioned. Using a safety factor when designing the tank, the life time could be increased for lifecycles and wear and tear of the tank. The second risk describes some implications with the use of underground tanks. Using a monitor system to maintain the tanks at all time, will mitigate this risk until this becomes improbable. Thirdly, the needs of the aircraft may exceed the supply of the tanks. These tanks have been sized based on flight statistics. However, with the use of three tanks, there will always be enough fuel. This risk is thus considered negligible. The fourth risk is about the storage temperature in the tank. The tank may have a slightly higher temperature when the tank is not completely full. However, since this will be monitored by the monitoring system, the impact is assumed to be marginal.

For the fifth risk, additional solar panels and wind turbines could be installed to eliminate this risk completely. Also, the sixth risk is eliminated completely due to the connection of the main power grid as well. The seventh risk is about the infrastructure that will be used to transport gaseous hydrogen. If leaks and losses occur at an identified point in the infrastructure, the route could be closed temporarily in order to repair the leakage. To identify where the leakage and losses occur, a system will need to be designed in order to do so. Moving on to the eighth risk, the production is influenced by the amount of water available. By implementing a water reservoir at the ground facilities, this risk can be mitigated completely. Furthermore, operation risks such as the ninth and tenth risk, can be mitigated by scheduling maintenance on a regular basis and cleaning the solar panels too.

8.9. Final Overview

Since every aspect of the ground facilities has been discussed, a final overview is given here. The ground facilities will convert water into hydrogen gas using PEM electrolysis. The pure oxygen that is also produced by this process, will be collected and sold to licensed oxygen distributors for medical and educational use. This is done to eliminate any waste. The ground facility will be entirely powered by three onshore 3 MW wind turbines and a solar panel area of 2,055 m by 801.1 m. The green energy sources will also be used to provide energy for the converter and cooler located at the airport. This will be done by connecting the green energy sources to the power grid providing it with green electricity. This electricity is then taken up again from the main power grid located at the airport. This will ensure that the ground facilities work entirely on green sustainable energy, which fits the sustainable goals of the Hydrojet. For storage of the gaseous hydrogen, three spherical, steel 300M, underground tanks will be used, each with a thickness of 0.753 m and a radius of 7.24 m. Using three tanks will ensure that there will always be hydrogen available for refuelling the aircraft by including redundancy. However, since the tanks will be located underground, an additional monitoring system will be installed to ensure safety at all time. The gaseous hydrogen will be transported using underground pipelines to the airport. The compressor and cooler will be available there, converting the gaseous hydrogen to liquid hydrogen consisting of both boil-off gaseous hydrogen from the aircraft and newly produced gaseous hydrogen. The final values of the sizing of the ground facilities can be seen in Table 8.5.

Table 8.5: Final specification of the ground facilities

Ground Facilities Specifications			
Ground fuel [kg]	62,011	Water needed [kg]	$5.54 \cdot 10^5$
Total Energy needed [J]	$1.18 \cdot 10^{13}$	Water cost per tank [€]	473.8
Wind Turbine	GE 3 MW onshore wind turbine platform	Tank Material	Steel 300M
Turbines needed [-]	3	Tank Volume [m^3]	1,590
Turbine diameter [m]	137	Tank Mass [kg]	$5.5 \cdot 10^6$
Solar panel area [m^2]	$1.65 \cdot 10^6$	Tank wall thickness [m]	0.753
Solar panel length [m]	2,055	Tank cost [M€]	5.44
Solar panel width [m]	801.1	Number of tanks	3

8.10. Compliance with Subsystem Requirements

Now that, the final subsystem layout is known, it can be assessed whether the requirements of Section 8.2 are met. Taking everything into account, all requirements for the hydrogen production are fulfilled. Note that proper safety requirements for the production of hydrogen will always be valued. The cost estimation of the hydrogen production is, at this stage of the project, difficult to estimate due to the many unknowns present for the realisation costs of the ground facilities in its entirety. Moving on to the hydrogen storage, almost all requirements have been fulfilled. Since the hydrogen tank underground will operate at 0 degrees, an active cooling system is required. This will be done in further post-DSE iterations of the ground facilities and requirement HPRA-REQ-HGS-3 is considered as ongoing. The efficiency of the cooling will be done at this stage as well. The fuel flow of the hydrogen ground facilities depends on the available pipeline infrastructure and needs to be analysed as well. Requirement HPRA-REQ-HGS-7 is considered as ongoing as well. The design and sizing of the ground facilities at this phase of the design, is completed now.

Final Design

Now that every subsystem has been designed and analysed in detail, the final design will be given in this chapter. To start off, it is explained how the iterations have progressed in Section 9.1. Additionally, the results of the converged iteration will be given including the interface diagrams in Section 9.2 and Section 9.3, respectively. Furthermore, a final design portrait will be given in Section 9.4. Furthermore, a sensitivity analysis will be done on the iteration process in Section 9.5. Lastly, the risks are identified and mitigated in Section 9.6.

9.1. Progression over Iterations

In this section, the progression over the iteration process, as defined in Section 2.5, is explained. During aircraft design the so-called snow ball effect is a result from iterations and parameters changing. Most parameters within the design of the aircraft are interrelated. Therefore, when a parameter changes, it will influence other parameters directly or indirectly. It is thus crucial to determine all parameters that will be affected such that updates can continuously take place. These updates (iterations) will continue until every parameter converges. Convergence is assumed when all parameters differ less than 1% from their previous value, as explained in Chapter 3. When all values have converged, one more iteration is done to make sure that all values stay converged. In Figures 9.1 and 9.2, the convergence of some of the most important parameters such as L/D and MTOW can be seen.
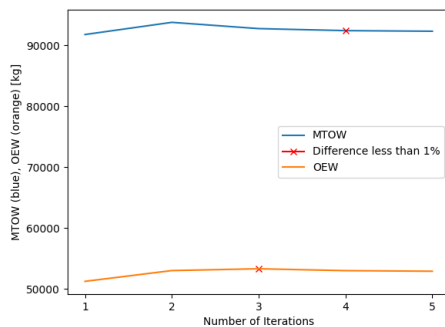
Figure 9.1: MTOW and OEW during Iterations
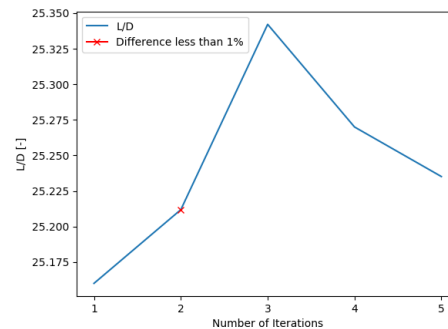
Figure 9.2: L/D during Iteration

Four iterations were necessary to let all parameters converge. An additional fifth one is done as a check to see that all parameters stay converged. After the last iteration all parameters of the design are final. The results of the parameters can be seen in the chapters above. All these parameters make up the total design of the aircraft. The most important parameters of the Hydrojet can be seen in the next section.

9.2. Resulting Parameters

In Table 9.1 the most important parameters of the different departments are presented. These values give an overall impression of the size of the final design.

Table 9.1: Final Results Hydrojet Design

Values from Final Design					
Department	**Parameter**	**Value**	**Department**	**Parameter**	**Value**
Planform Layout	Total length cabin [m]	14.2	**Turbofan system**	Thrust at take-off [kN]	284.3
	Cabin top width [m]	9.39		Number of turbofans [-]	2
	Cabin top height [m]	1.87		Turbofan diameter [m]	2.54
Aerodynamics	Total surface area [m^2]	510.85		Turbofan length [m]	7.28
	Wingspan [m]	45.4		Cruise TSFC [kg/s/N]	$1.1055 \cdot 10^{-5}$
	AR [-]	4.23	**Fuel Cell system**	Stack voltage [V]	270
	L/D [-]	25.24		Stack Current [A]	1196
	L [kN]	928		Fuel cell mass [kg]	496.6
	$C_{L_{cruise}}$ [-]	0.1534		Fuel cell volume m^3	293.5
	e_{cruise} [-]	0.689		Max power fuel cell [kW]	319
	α_{trim} [deg]	3.159	**Hydrogen tanks**	Total hydrogen mass [kg]	9686.19
Stability and Control	Forward CG limit [MAC]	0.1201		Fuel tank mass [kg]	2403.63
	Aft CG limit [MAC]	0.1984		Fuel tank volume m^3	138.4
	XLEMAC [m]	11.04		Fuel tank efficiency [-]	0.8
	Wing twist [deg]	-1.7			
Landing Gear	Nose gear location [m]	7.24			
	Main gear location [m]	14.85			
	Height [m]	1.9			

9.3. Interface Diagrams

In this section the different system interfaces of the final design will be showed and elaborated. The system diagrams consist of a hardware/software and data handling block diagram and a communication flow diagram.

9.3.1. Hardware and Software Block Diagram

To get an overview of the different hardware and software elements, a hardware and software block diagram has been made. The hardware part, indicated in red in Figure 9.3, with the different hardware components along with the pilot and their relation are shown. For the software block diagram, indicated in yellow, the same has been done.
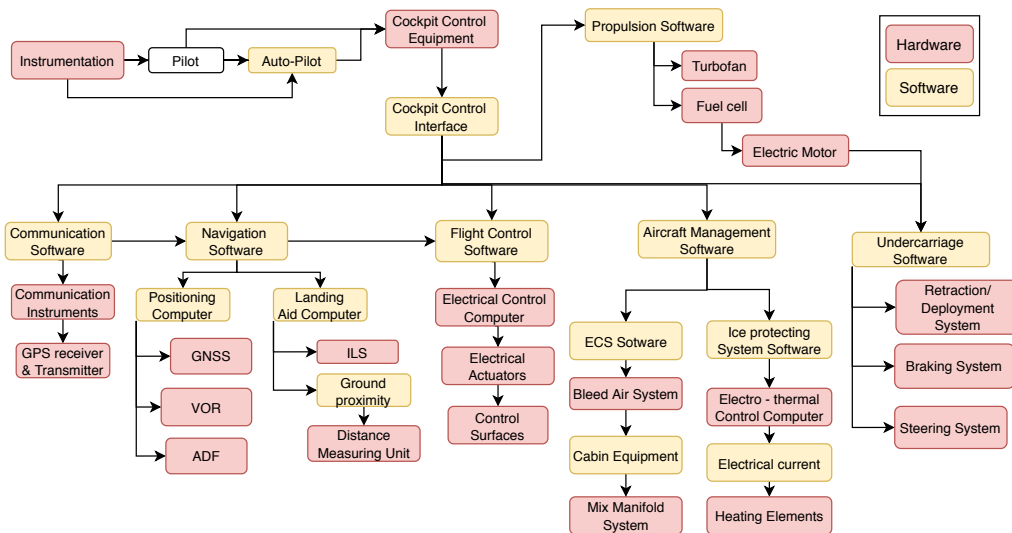

Figure 9.3: Hardware and Software Block Diagram of the Hydrojet

9.3.2. Data Handling Block Diagram

An overview of the data handling is shown in Figure 9.4. As can be seen multiple components of the aircraft will be feeding data to the Flight Data Unit. All these components are the Global Positioning System (GPS) for the current aircraft position,

the Ground Radio Service (GRS) for communication with the ground, the Garmin Display Unit (GDU) and Flight Management System (FMS) which will show the data output to the pilots and the GDC is the air data computer. Lastly, a magnetometer (the GMU) will distribute information about the magnetic field. The Flight Data Unit will send the data to the flight memory unit which is the black box of the aircraft. Also, using a data link, data will be send from the Flight Data Unit to the ground platform. The content of the data can be seen in the flow of the block diagram as well.
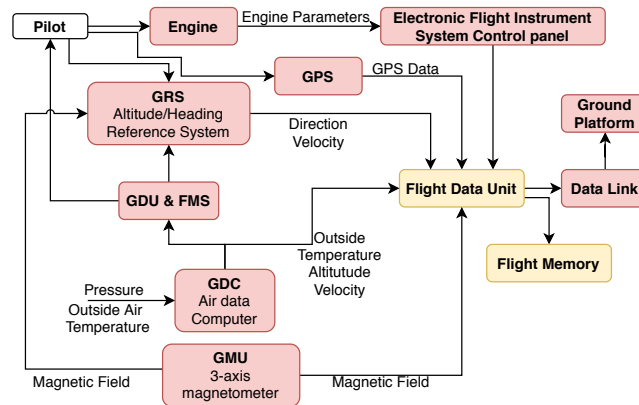
Figure 9.4: Data Handling Block Diagram of the Hydrojet [87]

9.3.3. Communication Flow Diagram

The communication flow diagram can be seen in Figure 9.5. This diagram shows the communication of the aircraft system with the environment. This starts with the data from other aircraft and the data from the ground being received by the ADS-B In component. This stands for the receiver of the Automatic Dependent Surveillance–Broadcast (ADS-B). The weather condition will go to the pilot while the neighbouring aircraft positions will go to the Traffic Alert and Collision Avoidance System (TCAS). This will feed the traffic data to the navigation display which the pilot can see. Furthermore, the aircraft's GPS will also feed its position to the navigation display. Lastly, the attitude of the aircraft is determined using a gyroscope. This information will be sent to the attitude indicator. The GPS location and attitude of the aircraft will also be sent out by the ADS-B Out component to other neighbouring aircraft and ground platforms.
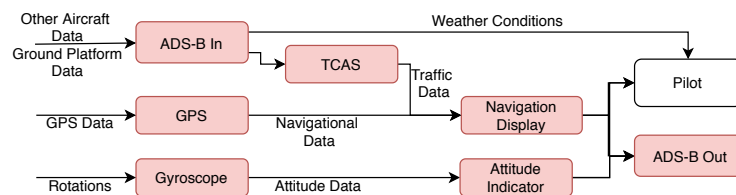
Figure 9.5: Communication Flow Diagram of the Hydrojet

9.4. Final Design Portrait

As already said in the Section 9.1, the convergence of the iteration process concludes the technical part of the design. The ultimate configuration of the Hydrojet is now determined and fixed. To give an impression of this design and its complete integration, a top level portrait is presented in Figure 9.6.

Figure 9.6: Final Design Portrait

The final design of Hydrojet comprises a blended wing body aircraft which uses hydrogen powered turbofans and a fuel cell to foresee in the required power and propulsion. A design has been established by focusing on the main goal of this complete design project, namely the creation of a new, commercially feasible aircraft which produces zero harmful emissions and which is 90 % recyclable.

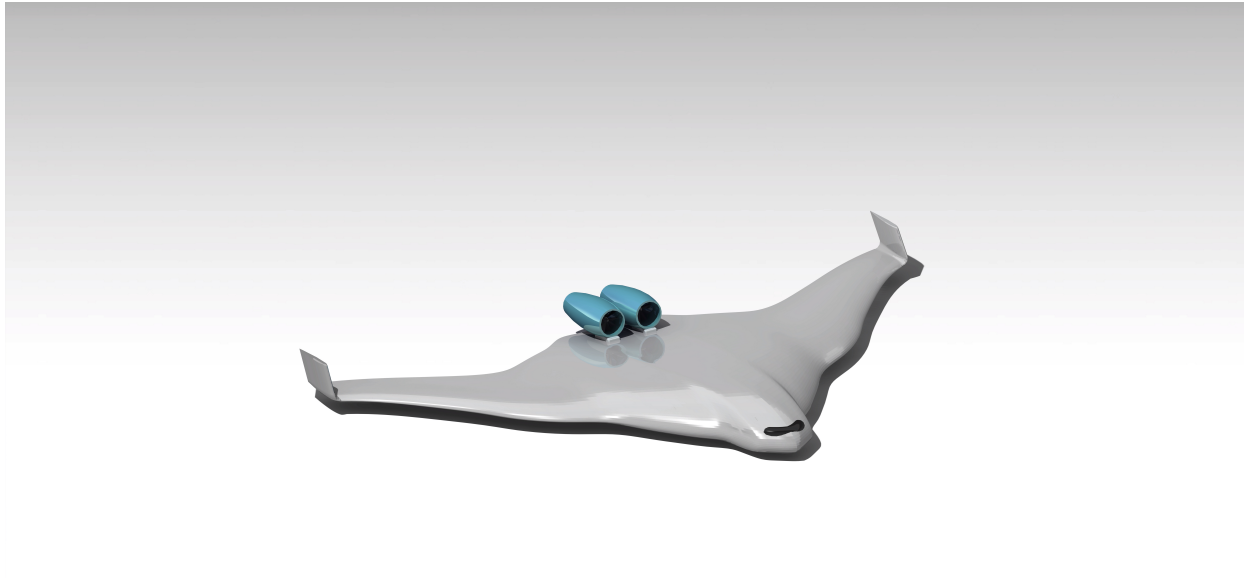The blended wing body, which is a challenging design, was chosen above all other designs as it has optimal aerodynamic performance and fuel storage capabilities.
As the power and propulsion subsystems are the key elements in the production of harmful emissions they needed to be designed and sized carefully. Eventually, the turbofan in combination with the fuel cell was adopted as it has the best performance characteristics in relation with the zero production of harmful pollutants. The hydrogen powered turbofans are capable of producing the required thrust at take-off and cruise while the fuel cell is very effective in producing moderate power levels to fulfil the needs for the ground operations. All this while emitting negligible harmful emissions. Finally, it was chosen to place the turbofans on top of the blended wing as this would make it possible to increase the efficiency through boundary layer ingestion.

9.5. Sensitivity

To investigate the robustness of the design solution and its feasibility, a sensitivity analysis is performed on the iteration process. This will reveal which parameters are critical for converging to the solution of the iteration process. First, the method of the sensitivity analysis will be elaborated. Then, the results of the sensitivity analysis for Class-I and Class-II will be given.

9.5.1. Method

The sensitivity analysis will be performed by determining the growth factor (GF) of an input parameter. The formula for the growth factor is seen in Equation 9.1, where Sc_{i+1} is the parameter value where the weight of the criterion is changed by 1 %. Sc_i is the unchanged parameter value. Additionally, there will also be looked at the shrink factor (SF). This works on the same principle as the growth factor only now the Sc_{i+1} becomes Sc_{i-1}. The formula for the shrink factor is seen in Equation 9.2

$$GF = \frac{Sc_{i+1} - Sc_i}{Sc_i} \cdot 100 \qquad (9.1) \qquad\qquad SF = \frac{Sc_{i-1} - Sc_i}{Sc_i} \cdot 100 \qquad (9.2)$$

For the iteration, three parameters have been identified in order to assess the sensitivity. These parameters are the MTOM, OEM and the Fuel mass. The inputs of the Class-I and Class-II mass estimation method will be increased by one percent. This will result in a deviation. This deviation gives the growth and shrink factor explained in Equation 9.1 and Equation 9.2.

9.5.2. Results

For Class-I and Class-II, the inputs have been identified in Section 3.1 and Section 3.2. By increasing or decreasing the inputs by 1 %, the difference in MTOM, OEM and Fuel weight is given. The results can be seen in Table 9.2 for Class-I and Table 9.3. The climb mass fraction is the mass fraction determined for climb based on the latest performance parameters.

Table 9.2: Sensitivity analysis of the Class I inputs

Inputs	Growth Factor			Shrink Factor		
	MTOW	OEW	Fuel	MTOW	OEW	Fuel
$m_{payload}$	0.81	0.70	0.81	-0.81	-0.70	-0.81
v_{cruise}	0.72	0.62	0.32	-0.72	-0.62	-0.32
Cruise range	0.81	0.69	0.79	-0.81	-0.69	-0.79
Loiter range	0.81	0.70	0.81	-0.81	-0.70	-0.81
SFC	0.93	0.80	1.40	-0.93	-0.79	-1.39
L/D_{cruise}	0.83	0.71	0.90	-0.83	-0.71	-0.90
L/D_{loiter}	0.81	0.70	0.81	-0.81	-0.70	-0.81
E_{loiter}	0.83	0.71	0.90	-0.83	-0.71	-0.90
Gravimetric ratio H_2	0.83	0.71	0.90	-0.83	-0.71	-0.90
Climb mass fraction	-1.25	-1.08	-9.90	1.31	1.12	10.18

Table 9.3: Sensitivity analysis of the Class II inputs

Inputs	GF			SF			Inputs	GF			SF		
	MTOM	OEM	Fuel	MTOM	OEM	Fuel		MTOM	OEM	Fuel	MTOM	OEM	Fuel
v_{cruise}	-3.44	-5.90	-3.76	-4.20	-6.07	-3.87	location front spar/chord	-3.37	-5.80	-3.70	-4.26	-6.17	-3.94
$Range_{cruise}$	-3.44	-5.90	-3.76	-4.20	-6.07	-3.87	location rear spar/chord	-3.26	-5.62	-3.59	-4.37	-6.34	-4.05
AR	-3.34	-5.75	-3.67	-4.29	-6.22	-3.97	$S_{outer\ wing}$	-2.66	-4.67	-2.98	-4.97	-7.28	-4.64
n	-2.79	-4.89	-3.12	-4.83	-7.07	-4.51	$S_{inner\ wing}$	-2.64	-4.64	-2.96	-4.99	-7.31	-4.66
S	-2.71	-4.76	-3.04	-4.92	-7.19	-4.59	c_{root}	-2.55	-4.50	-2.87	-5.07	-7.44	-4.75
ρ	-3.13	-5.42	-3.46	-4.50	-6.54	-4.17	c_{tip}	-2.53	-4.47	-2.85	-5.09	-7.47	-4.76
S_{fin}	-3.13	-5.42	-3.46	-4.50	-6.54	-4.17	$MAC_{inner\ wing}$	-2.53	-4.47	-2.85	-5.09	-7.47	-4.76
Q_o	-3.13	-5.42	-3.46	-4.50	-6.54	-4.17	$MAC_{outer\ wing}$	-2.53	-4.47	-2.85	-5.09	-7.47	-4.76
τ	-3.19	-5.50	-3.51	-4.44	-6.45	-4.12	MAC	-2.61	-4.60	-2.94	-5.01	-7.34	-4.69
$\tau_{outer\ kink}$	-3.19	-5.51	-3.51	-4.44	-6.45	-4.12	$w_{inner\ wing}$	-2.68	-4.71	-3.01	-4.94	-7.23	-4.61
$\tau_{inner\ wing}$	-3.20	-5.53	-3.53	-4.43	-6.43	-4.10	$AR_{inner\ wing}$	-2.68	-4.71	-3.01	-4.94	-7.23	-4.61
$\tau_{outerwing}$	-3.19	-5.51	-3.51	-4.44	-6.45	-4.12	$AR_{outer\ wing}$	-2.68	-4.71	-3.01	-4.94	-7.23	-4.61
τ_{root}	-3.19	-5.51	-3.52	-4.44	-6.44	-4.11	$\Lambda_{LE_{inner}}$	-2.58	-4.56	-2.91	-5.04	-7.38	-4.71
Q_i	-3.19	-5.51	-3.52	-4.44	-6.44	-4.11	$\Lambda_{LE_{outer}}$	-2.47	-4.37	-2.79	-5.15	-7.56	-4.82
n_{pplant}	-3.19	-5.51	-3.52	-4.44	-6.44	-4.11	λ_{inner}	-2.46	-4.36	-2.78	-5.16	-7.57	-4.83
n_{MG}	-3.18	-5.49	-3.51	-4.45	-6.46	-4.12	λ_{outer}	-2.43	-4.32	-2.76	-5.18	-7.61	-4.86
P1	-3.18	-5.49	-3.51	-4.45	-6.46	-4.12	b_{outer}	-2.16	-3.90	-2.49	-5.44	-8.01	-5.11
P2	-3.18	-5.49	-3.51	-4.45	-6.46	-4.12	$c_{kink_{outer}}$	-2.16	-3.90	-2.49	-5.44	-8.01	-5.11
P3	-3.18	-5.49	-3.51	-4.45	-6.46	-4.12	$c_{kink_{inner}}$	-2.25	-4.04	-2.58	-5.35	-7.88	-5.03
Y1	-3.18	-5.49	-3.51	-4.45	-6.46	-4.12	S'_{outer}	-2.21	-3.98	-2.54	-5.39	-7.93	-5.06
Y2	-3.18	-5.49	-3.51	-4.45	-6.46	-4.12	$c_{kink_{inner}}$	-2.21	-3.98	-2.54	-5.39	-7.93	-5.06
Y3	-3.18	-5.49	-3.51	-4.45	-6.46	-4.12	S_{cabin}	-2.15	-3.88	-2.47	-5.45	-8.03	-5.12
A_{bar}	-3.27	-5.64	-3.60	-4.36	-6.32	-4.03	S_{aft}	-2.13	-3.85	-2.46	-5.47	-8.06	-5.14
T_{TO}	-3.12	-5.40	-3.45	-4.51	-6.56	-4.18	λ_{aft}	-2.13	-3.84	-2.45	-5.47	-8.07	-5.15
Mff	-3.12	-5.40	-3.45	-4.51	-6.56	-4.18	$N_{cabin\ crew}$	-2.13	-3.84	-2.45	-5.47	-8.07	-5.15
N_{pax}	-2.97	-5.16	-3.29	-4.67	-6.80	-4.34	l_{cabin}	-2.12	-3.83	-2.44	-5.48	-8.08	-5.16
N_{eng}	-2.88	-5.02	-3.20	-4.75	-6.94	-4.43	$n_{containers}$	-2.12	-3.83	-2.44	-5.48	-8.08	-5.16
N_{pilots}	-2.87	-5.01	-3.20	-4.76	-6.94	-4.43	m_{ULD}	-2.12	-3.83	-2.44	-5.48	-8.08	-5.16
p_{cabin}	-2.87	-5.01	-3.20	-4.76	-6.95	-4.43	m_{bgge}	-2.12	-3.83	-2.44	-5.48	-8.08	-5.16
m_{pax}	-2.87	-5.01	-3.20	-4.76	-6.95	-4.43	BPR	-2.14	-3.87	-2.47	-5.46	-8.04	-5.13

Now from Table 9.2, it can be seen that a critical factor is the Climb mass fraction. This fraction will increase the fuel mass by 10.18 % when it is decreased by one percent and decreases the fuel mass by 9.9 % when the value is increased with one percent. All the mass fraction used in the Class-I mass estimation are a fraction of the MTOM. This means that when the climb mass fraction is increased by 1% actually the whole MTOM is increased by 1 percent. And when this increase in absolute weight is then compared to the fuel mass, this results in the large increase. Also the fuel fraction is calculated with the climb mass

fraction. This will also add to the already large contribution of the MTOM scaling. The rest of the inputs show an expected behaviour when increasing or decreasing its value. For the Class-II inputs, the sensitivity analysis does not conclude in one or several clearly critical input parameters. The percent deviation is around the same for every input value. This is expected due to the complex relations between the mass and the geometry of the planform.

As can be seen from the Class-II, the values will converge to an arbitrary value over the iteration process. This results approaching the most optimal values for the MTOM, OEM and fuel mass with the given requirements for range, cruise speed and payload mass. Since these inputs are either direct requirements or directly derived from the requirements, the feasibility of the design using this method is proven.

9.6. Risk

In this section the risks of the final design will be assessed. Risks during the design process and operation can have a large effect on the design choices. It is therefore an important part of engineering design and a thorough risk analysis is needed. In previous reports a number of risks have already been identified and assessed.[1] The relevant ones and some additional risks found during the design process are listed in this section. After that those risks are assessed on their probability of occurrence and on their potential impact, which can be seen in Figure 9.7. Subsequently mitigation plans are presented for the most important risks, that either were used during this design phase or should be taken into account in future design phases. The risks are assessed again with the mitigation plans in mind, this can be seen in Figure 9.8.

9.6.1. Risk Identification

Design Risks

Risk-01 The weight estimation methods for BWB aircraft are not accurate enough leading to the predicted weight being too low and the aircraft being under-designed.
Risk-02 The production of hydrogen is more expensive than predicted resulting in the operational costs being too high.
Risk-03 The cabin planform of the Hydrojet makes evacuation more difficult.
Risk-04 Fuel leakage endangers the safety of the passengers.
Risk-05 Failure of the ground hydrogen storage prevents aircraft from being refuelled.
Risk-06 The aircraft is not able to operate at many small airports due to the hydrogen facilities needed.
Risk-07 Due to the complex structure the structural analysis is not accurate enough causing it to be too heavy.
Risk-08 Inaccuracy of the stability analysis for BWB aircraft causes the aircraft to be unstable in certain conditions.
Risk-09 Passengers are uncomfortable in the Hydrojet due to the absence of windows on the sides.
Risk-10 The manufacturing costs of the aircraft exceed the requirement.
Risk-11 Periods of low power generation by the wind turbines and solar panels make it impossible to produce enough hydrogen.
Risk-12 The hydrogen tanks on the aircraft explode, endangering the passengers.

Project Risks

Risk-PR01 The production costs of the BWB turn out to be too high to make it a competitor on the civil aviation market.
Risk-PR02 Passengers do not trust the inclusion of two new technologies, namely hydrogen and blended wing body
Risk-PR03 The costs for training the crew for the operation of blended wing body are too high for airliners.
Risk-PR04 Airports are unwilling to make the investment into hydrogen production.
Risk-PR05 Investments for the next phase off the project are too low to continue the project.
Risk-PR06 Due to COVID-19 the demand for new aircraft decreases resulting in a lower amount of Hydrojets sold.
Risk-PR07 Due to COVID-19 the emissions have decreased such that emission free aircraft are less needed.
Risk-PR08 No existing engine company is willing to make the investment into production of hydrogen turbofans.
Risk-PR09 Countries with a lower capacity for sustainable energy are not able to produce enough electricity for hydrogen production.
Risk-PR10 New propulsive technologies or planform designs are researched that may prove to be better or more efficient than hydrogen turbofan and BWB respectively.

9.6.2. Risk Mitigation

Risk-01 A safety factor could be applied to the weight to decrease the risk of under-designing. In later design phases more detailed weight estimation methods could be used, like estimating the weight of parts or sub-assemblies.

Risk-02 Putting a safety factor on the predicted production cost could decrease the chance of the cost becoming too high. Centralising the power generation and hydrogen production could also reduce the cost.

Risk-03 Apart from the exits at the front, additional emergency exits can be placed at the back and on the floor of the cabin. The amount and type of emergency exits should conform to safety regulations.

Risk-04 The tanks are designed taking into account the fact that hydrogen leaks occur faster than other gases. Additionally, detection systems could be put in place near the tanks and in the cabin that detect hydrogen leaks and warn the crew. This way, if a leakage were to occur measures to evacuate the passengers or to fix the leakage could be taken on time.

Risk-05 Additional hydrogen tanks are present as a back-up. There are three tanks. There will always be one in use, one as back-up and the third one can be in maintenance. Regular maintenance will also reduce the probability of failure.

Risk-06 As was discussed earlier, airports that do not have the space for all the facilities involving hydrogen production could get their hydrogen from a centralised production facility. The hydrogen would only have to be received and liquefied at the airport.

Risk-07 In further design stages more accurate structural analysis could be done, such as implementing FEM. At a certain point parts of the aircraft could even be manufactured and tested.

Risk-08 In later design phases stability should be analysed with more accurate methods. Furthermore, active control systems could be used to stabilise the aircraft and also to further dampen certain eigenmotions.

Risk-09 Screens with live feed cameras of the outside will be placed. In this way, passengers are able to look outside. If it is feasible, windows could also be added to the roof.

Risk-10 Also here there should be a safety factor to the manufacturing cost.

Risk-11 During peak power periods more hydrogen will be produced than necessary, which will be stored in the back-up tanks. This reserve fuel can then be used during periods of power shortage. When the reserve tanks are filled, the excess power is supplied to the power grid. During times of power shortage at the ground station, power can be provided by the grid instead. As long as the energy provided to the grid does not exceed the energy taken from it, the hydrogen production can be considered carbon neutral.

Risk-12 The fact that the hydrogen in the tanks is cryogenic and that no oxygen is present in the tanks reduces the chance of an explosion. The insulation of the tanks also reduces the boil-off to make sure that the hydrogen in the tanks stays liquid.

Risk-PR01 In case of increased probability for too high costs, an application for government grants could be filed, for example at the EU level or even the Clean-Sky project. Furthermore, the airliners could be convinced to invest a little more because costumers are willing to pay more.

Risk-PR02 Public advertisements could be placed online or at airliners websites that ensures the safety of the new technologies and emphasises the benefits.

Risk-PR03 Pilot trainers as well as trainers of flight attendants, could be informed early to implement BWB training into their program . This will decrease the probability of this risk, as the effort required to retrain the crew for the BWB will be lower for airliners.

Risk-PR04 With the help of airliners that already purchased a Hydrojet, airports could be convinced to make the investment. Maybe also local governments can be convinced to invest, especially if the noise levels are lower for the Hydrojet than kerosene powered aircraft. In a further market analysis it should be assessed how willing airports are to make the investment in order to have good information on what airliners will be more suitable for selling the Hydrojet.

Risk-PR05 In case of hesitance by investors, the government could maybe help by giving grants or maybe the Clean-Sky project could help. The government could also insure investors in case of a loss on the investment. Furthermore, a lot of effort from the project should be used to find sufficient funds to continue the project. Especially now with COVID-19.

Risk-PR06 This poses a big problem for the project. However, due to government saving big airliners and demanding greener aviation, this will improve the demand for the Hydrojet. In order to amplify this response, the airliners should be made aware that the time to change the emissions in aviation and make it greener is now.

Risk-PR07 This risk is not very critical. Greener aviation is an ongoing process that is only being accelerated. However, it must be made clear to passengers and airliners that all emissions are negative even if they are lower.

Risk-PR08 This risk is catastrophic for the project. Without the infrastructure of a big engine company, a hydrogen engine will not be available. It could be useful to have a few securities from airliners that they will purchase aircraft in order to convince the engine companies to collaborate. In case of a real danger to the project other options should be researched including building the engine with a new team, or including green aviation organisations with knowledge about propulsion.

Risk-PR09 This risk's probability cannot be lowered. In order to bring the Hydrojet into operation the hydrogen will have to be produced. The aircraft will have to be filled with as much hydrogen as possible on green airports in order to use the least amount of unsustainable hydrogen at these airports.

Risk-PR10 This risk would be quite critical. However, upcoming technologies will have to be monitored during the project to see if they could end up being more suitable. Yet entirely new technologies will need more years to develop while the Hydrojet could already be in production. In order to keep the Hydrojet competitive even after several years in service new versions will probably have to be made. Updating certain components such as the fuel cell could be done.
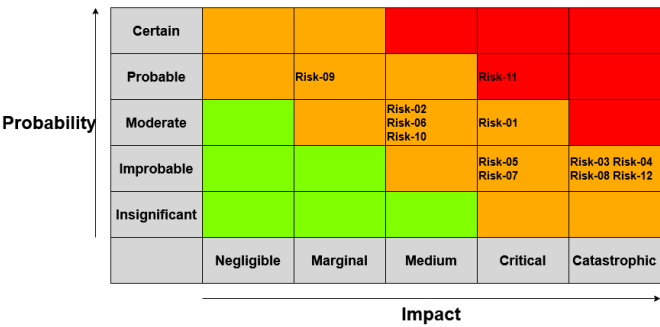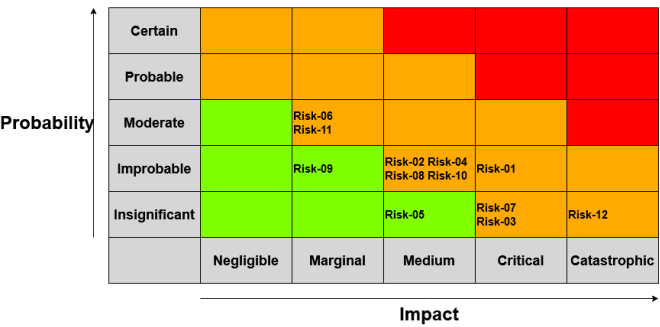

Figure 9.7: Risk map before mitigation
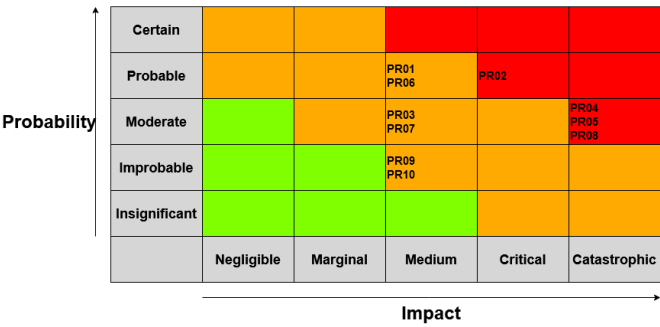

Figure 9.8: Risk map after mitigation

Figure 9.9: Project risk map before mitigation

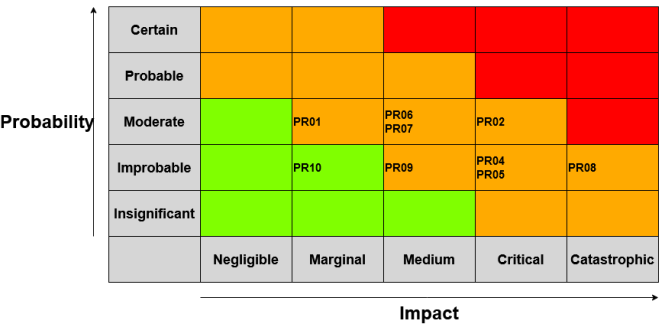Figure 9.10: Project risk map after mitigation

<div align="right">

10

</div>

<div align="right">

Operations

</div>

In this chapter, the operations of the final product will be described now that its design has been concluded. There are some uncommon operational procedures for the Hydrojet due to the unconventionality of the design. First, the ground facilities operations will be described in Section 10.1. Next, the aircraft operations will be elaborated in Section 10.2. Finally, the RAMS (Reliability, Availability, Maintainability and Safety) characteristics will be analysed in Section 10.3.

10.1. Operations Ground Facilities

The hydrogen ground facilities are responsible for the production, transport, conversion and refuelling. To get an overview of the ground station, see Chapter 8. This section will elaborate on the different aspects of the operation in the order described before.

10.1.1. Production Operations

The hydrogen will be produced using PEM electrolysis until the underground storage tanks are completely full. The hydrogen will be produced from normal water and the oxygen produced with the electrolysis will be collected and sold to licensed oxygen distributors for medical and educational use. The energy used for the electrolysis is produced using solar panels and onshore wind turbines. When the underground gaseous hydrogen tanks are full, there is no need for energy to be produced. This is when the energy will be routed to the power grid. This will continue as long as the gaseous hydrogen tanks remain completely filled. Since solar panels are being used, the peak production will be achieved during the day. The wind turbines can operate during the day and night depending on the surrounding of the wind turbines. Furthermore, the ground station is able to completely fill the hydrogen tanks within 7 hours. The produced hydrogen will go directly from the electrolysis process to the underground storage tanks.

10.1.2. Transport Operations

Transporting the hydrogen will consist of transporting the gaseous hydrogen to the underground storage tanks and from the underground storage tanks to the compressor located on the airport. Then from the compressor the liquid hydrogen will need to go to the airport refuelling point and the boil-off gaseous hydrogen back to the compressor.

Starting with the transport from the PEM electrolyser to the underground storage tanks, the gaseous hydrogen will be lead through pipelines which will be connected with the underground storage tanks. This will be a relatively short distance since the underground storage tanks are located close by. Next, the gaseous hydrogen will need to be transported from the underground storage tanks to the airport where the compressor is located. This can be done by adapting the existing pipeline structure for gaseous hydrogen use.[82] However, some countries are not able to setup a pipeline infrastructure due to cost constraints. As a short term (or emergency) solution, liquid hydrogen should be made and transported using cryogenic hydrogen trailers. There are at least 3 liquid hydrogen trailers needed to completely fill both tanks of aircraft.[88] Lastly, the hydrogen will go from the compressor to the refuelling point of the aircraft in liquid form. This will be done by using on site trailers. These trailers will be transporting the liquid hydrogen over a short distance. Furthermore, the trailers will also transport the boil-off gaseous hydrogen back to the compressor to liquefy it again. The inlets on the bottom of on-board tanks will be used to pump the fuel into the aircraft. The outlets on top of the on-board fuel tanks will be used to extract the gaseous hydrogen during the refuelling process. After this, the trailers will head back to the compressor again with the gaseous boil-off hydrogen.

10.1.3. Conversion and Refuelling Operations

The gaseous hydrogen is converted using a compressor and cooler to a cryogenic state. This will be done at the airport itself in order to ensure that the least boil-off will occur. As was described before, the boil-off hydrogen gas will be recycled by liquefying it again. This is also helpful for venting the hydrogen tank and ensuring that the on-board tank is cooled as much as possible at the start of the service time.

10.2. Aircraft Operations

The Hydrojet will perform multiple flights a day. Every aircraft has a different destination and thus a different flight time. To give an overview of the aircraft operations, two different scenarios are discussed: a flight with the maximum range and a short haul flight (maximum 3 hours).

First of all, a visual check of the aircraft is performed. The aircraft is fuelled while loading the passengers and cargo on board. The pilots works through the mandatory paperwork before going on to the take-off phase. When air traffic control gives permission, the Hydrojet will taxi to the runway. When at the runway the aircraft takes off. Loading, refuelling and performing checks on the aircraft will take about one hour for the short haul flight and 1.5 hours for the maximum range flight. After take-off the aircraft flies to its destination in three to five hours. When at the destination it will taxi to the gate. When at the gate the passengers and cargo are loaded off the aircraft. Taxiing takes 20 minutes and unloading both passengers and cargo takes 40 minutes. After that, visual inspection and refuelling will be done again and the same process starts over. For maximum short haul flight, the whole process takes about five hours, for maximum range flights it takes around 8 hours. Depending on the type of flight, short haul or long range, there can be two, three or four flights a day.

10.3. RAMS Characteristics

The operational performance of the Hydrojet needs to be evaluated as well, especially due to the novelty of the design. This can be done by assessing the the RAMS (Reliability, Availability, Maintainability and Safety) characteristics of the aircraft. These are defined as follows:

- Reliability is the probability that the system will function in an acceptable way for a given period of time when used under the specified operating conditions.
- Availability is the percent or probability that a system will be ready when needed for use.
- Maintainability is the ease, accuracy and safety of performing maintenance actions.
- Safety is protection from hazards to people and other equipment.

All these aspects are related to each other as can be seen in Figure 10.1. A good reliability improves the availability and the maintainability. The latter in turn enhances the availability as well and the safety. Furthermore, safety and reliability are highly correlated. A reliable system is a safe system and vice versa.
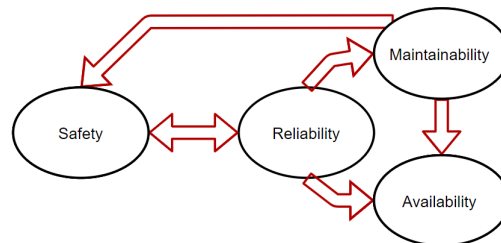
Figure 10.1: RAMS Relations

10.3.1. Reliability

For the reliability, only the unconventional systems are analyzed, because of their relatively low technology readiness level (TRL). These subsystems are identified to be: the engines, the hydrogen tank and the fuel cells. The other subsystems are assumed to be reliable due to their extensive application in the aviation industry.

Engines: There are no existing aircraft which are propelled by turbofan engines running on hydrogen. This leads to a decrease in reliability of the aircraft, because unexpected failures can occur during flight testing. It should be noted that these failures will be minor, because the engine functions in the same way as a conventional turbofan. The major difference is found in the combustion process. There will be hydrogen entering the combustion chamber instead of kerosene. So, if the combustion process occurs in the way it should, the engine will not fail more often than kerosene engines.

Fuel Cells: As of now, fuel cells are only used for small electric air planes. There are no operational comparable aircraft using fuel cells as the main power source. In other words: the concept is unproven for large aircraft. The other revolutionary concept is the use of the fuel cell for taxiing as well as APU. The fuel cell used in automotive has shown that failure rate is low due to

the limited number of parts. Furthermore if one cell fails only the cells that are positioned in the same stack will be useless. As the fuel cell in the Hydrojet will have several stacks placed in parallel a failure of one fuel cell will not be catastrophic, it will only reduce the current by a certain fraction, in this case 1/4 as there are 4 stacks. Furthermore a dynamically used fuel cell, a fuel cell which is turned on and off all the time, has a lifetime of around 5000 hours. If the APU is used for 30 minutes each flight during taxiing and occasionally during flight it will be able to serve around 10000 flights. With 3 flights a day the fuel cell should last almost 10 years. The 5000 hours is much shorter than 90000 hours for a stationary fuel cell as it will have more cycles because it is not used constantly.[89]

Hydrogen Tank and Distribution System: The hydrogen tank design is unconventional, even for a hydrogen tank. The optimal shape for a pressurised tank is a sphere or a cylinder with spherical end caps as mentioned before in Section 7.5. The hydrogen fuel tank for the Hydrojet is not shaped optimally. The latter can lead to unexpected failures which only occur in operational conditions of the aircraft. This decreases the reliability of the aircraft. The hydrogen distribution system also needs to be designed to cope with the low temperatures and high pressures. The material and the insulation are chosen in Section 7.5, such that they can withstand these extreme conditions. However, their application in the aviation industry is still limited and failures can occur. The latter also decreases the reliability of the aircraft. Hydrogen detection sensors will be placed near the hydrogen tanks and pipelines. These sensors need to function properly, and the accuracy should be consistent. If such a sensor malfunctions at a certain location, a small leak can increase over time which can have severe consequences. Sensors for similar systems have been applied in the space industry, but are still unproven in the aviation sector.

The Hydrojet: The Hydrojet is a state-of-the-art design, because of its blended wing shape and hydrogen propulsion system. Some blended wing body aircraft, such as the Lockheed SR-71 Blackbird[1] and Northrop Grumman B-2[2], already have been produced. However, these are not for civil transport. For transport BWB no full scale models have been produced yet. Only some small prototypes for transport purposes, like the Boeing X-48[3] have been built. Furthermore, the research done on Hydrogen BWB aircraft is limited as well.

10.3.2. Availability

"Aircraft availability is a key indicator to monitor aircraft performance, as a complement to operational reliability, and can be employed to optimise the profitability of an airline."[90] This availability is influenced by different operations which can be split up in two categories, operational and non-operational. The division of the various tasks is shown in Figure 10.2. The operating time is split up in service time and standby time. The non-operating time is split up into maintenance, which is also divided into planned and unplanned maintenance, and other non-maintenance tasks. Based on this overview, it can be seen that in order to assess the availability, the non-operating time will be divided by the operating time. From the top-level requirements (HPRA-STK-SR-1) at least an availability of 50 % should be achieved for the Hydrojet.
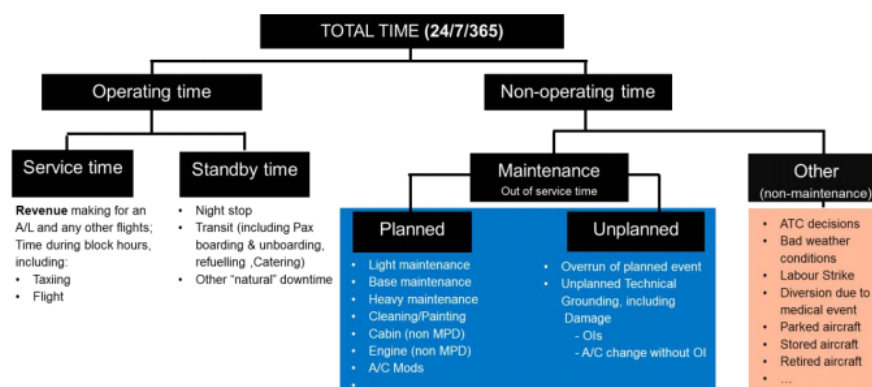
Figure 10.2: Division of operational and non-operational tasks in the lifetime of aircraft.[90]

The service time was already calculated in Section 8.4. The service time for one continuous full range flight was approximately 7 hours, meaning that the aircraft cannot fly this range more than twice a day. After this, the aircraft will be refuelled and the visual inspection of the aircraft components will begin. If needed, some light maintenance will be done as well and a

---

[1]https://www.lockheedmartin.com/en-us/news/features/history/blackbird.html [accessed on 14 June 2020]

[2]https://www.northropgrumman.com/air/b-2-spirit-stealth-bomber/ [acessed on 14 June 2020]

[3]https://www.aerospace-technology.com/projects/boeing-x48-unmanned-aerial-vehicle/ [accessed on 14 June 2020]

maximum of two hours is estimated for this task. After this the passengers will be able to board and this will take around 1 hour. The refuelling of an empty fuel tank will take about one hour as well. This means that the turnaround time of the aircraft is estimated to be one hour since refuelling and boarding will be done at the same time.

Maintenance will also take up time in the lifetime of aircraft and thus will be taken into account for determining the availability of the aircraft. Each maintenance process will be elaborated in the Maintenance subsection seen below. For line maintenance, about twelve hours per week is assumed. This is standard for most aircraft[4]. Additionally, the type A check will be performed which will take about 10 man-hours. A type B maintenance check takes about 6 to 24 hours. This type B check happens every eighteen months to six years depending on the age of the aircraft. The C check happens every eighteen months to two years, which takes around three to seven days. A type D check will be done once in every twelve years of the aircraft lifetime. This set standard was six years previously, however, for new aircraft, twelve years can be applied[4]. This is estimated to take around 6 weeks.

Now that the service time and the maintenance time of the aircraft are explained, an estimation for the availability can be done. This estimation will be made using the shortest reoccurring maintenance times. This results in one aircraft having 81.37 % availability during the entire lifetime of the aircraft. This does not include the unforeseen maintenance and the other non-maintenance aspects shown in Figure 10.2.

10.3.3. Maintainability

The maintenance of the aircraft is a crucial part in the aircraft availability. The more maintenance there is on the aircraft, the less flights it can perform. Both the maintenance and the fact that it does not fly increases the cost and reduces the profit. However, aircraft maintenance is necessary in order to ensure safe travel. Aircraft maintenance is split into three parts: line maintenance, base maintenance and defect rectification. Detect rectification is done during either line or base maintenance. Within these three there are different checks that are performed. The different checks are Line check, type A, B, C and D.

Line Maintenance: Line maintenance is defined as any maintenance task that can be done either outside of a hangar (open sky), or when the weather does not permit it in a hangar. Line maintenance is done by local maintenance providers which are hired by the airline. Most of the aircraft require line maintenance on a regular basis. It typically includes a daily check. Some components are specified as line replacement units. These units can be replaced during line maintenance. However, oversimplification of replacement units should be noted. For example, the engine is considered as line replacement units. When this component gets damaged by for instance a bird strike, it is allowed to be replaced during line maintenance. However, it would be better to do this during base maintenance such that sufficient resources can investigate and replace the engine.

Base Maintenance: This are all activities that are related with heavy checks and repairs. All maintenance that does not fall under line maintenance is considered base maintenance. During base maintenance, both major and minor systems are investigated. Time consuming labour like refurbishing the interior, corrosion prevention, structural work and many other tasks are done during base maintenance. As opposed to line maintenance, base maintenance cannot be done by any operator. Regulations require the operator to have a contract for every aircraft.

Defect Rectification: Defect rectification is defined as resolving a defect of the aircraft. It is obvious that this should be done as soon as possible to reduce the aircraft's immobilisation. However, the question arises if it should be done during either line or base maintenance. If the aircraft should be put in line or base maintenance depends on how severe the defect is. Generally, when the defect is small and it can be resolved easily, it can be done by line maintenance. However, line maintenance has certain restrictions based on regulations. They are not allowed to repair any damage. The decision to let the aircraft go to line or base maintenance is done based on regulations and the ability of the line maintenance team. Furthermore, it can also be done that the aircraft is released into service (for a limited amount of time) based on the severeness of the defect.

In order for maintenance to take place, the aircraft has to be accessible. During maintenance, parts of the aircraft have to be visually inspected. This means that accessibility for either direct visual inspection or by means of equipment to aid visual inspection (indirect) should be taken into account. Tools used for indirect visual inspection are magnifiers, borescope, etc. A new technology that is being used for maintenance recently are drones. Drones are equipped with cameras that capture high resolution images. These images are transferred to another facility where they are analysed. The images can be compared to previous images to improve the quality of visual inspection. This is only done in facilities outside of the area of the airport as

---

[4]https://www.qantasnewsroom.com.au/roo-tales/the-a-c-and-d-of-aircraft-maintenance/#:~:text=Heavy%20maintenance%20happens%20every%2018,the%20aircraft%20type%20and%20age.&text=Happens%20every%2018%20months%20to%20two%20years%20(depending%20on%20type,aircraft)%20and%20takes%20three%20weeks. [accessed on 18 June 2020]

they are not allowed neither on the airport nor in a hangar at the airport. By making use of drones, the aircraft's immobilisation gets reduced.[5]

As maintenance is a time consuming activity and the time spent on it should be reduced as much as possible, while keeping it safe, detailed planning of the maintenance activities is necessary. The time spend on the maintenance task is dependent on the type check that is performed. There are five types of checks: Line/transit, A, B, C and D.[91] Line check is done at the gate and on a daily basis. It has to be done before the first flight of the day and during each stop when in transit. It consists of a visual inspection of the fluid levels, wheels and brakes, and emergence equipment.

Routine light maintenance and engine inspection happens during a type A check. It is performed at the gate and has a duration of one shift (approximately 10 hours). This check can happen overnight. The last check at the gate is the type B check. It is similar to a type A but with different tasks. The duration can range from ten hours to one day. Type C and D checks take place at a hangar because of their longer duration. During the type C check, a structural inspection of the airframe is performed. Access panels are opened, routine and non-routine maintenance is performed as well as run-in tests. As these tasks are more labour intensive, the duration ranges from three days to one week.

Lastly, the most heavy maintenance check is the type D. After paint removal, major structural components such as engines, landing gear, flaps, electronics, etc are removed and investigated. The duration of a type D check can range from three to six weeks. However, the time spend on every check is dependent on the task. Depending on the type of defect, it can take more or less time. As these checks are important for the availability of the aircraft, a detailed planning must be made to ensure minimal ground time and optimal safety considerations. For the Hydrojet, a planning of the maintenance activities that require a long duration can be seen in Figure 10.3.
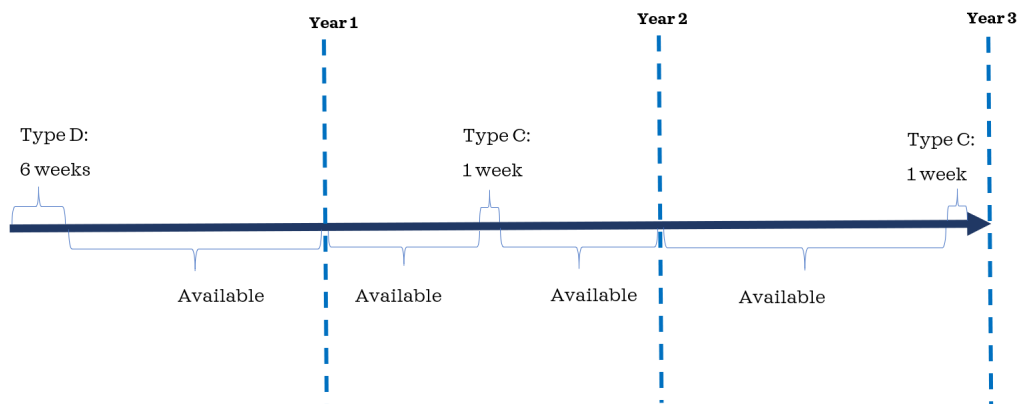
Figure 10.3: C and D type maintenance of the Hydrojet over three years

Line maintenance, type A and type B checks are not shown in the figure as they happen very frequently. Based on the maintenance schedule, the availability is calculated which can be seen in Subsection 10.3.2. From the figure it can be seen that the availability is highly dependent with the time spend on maintenance. From the airline point of view, it is preferred to have a maximal availability time. A coupled analysis of the maintenance time and availability is needed to accomplish this.

10.3.4. Safety

During the design of an aircraft, safety has to be implemented at many different stages. Both during the design of subsystems, such as the fuel tank and engine, and the system, the overall aircraft, safety has to be implemented. An aircraft has to comply with many different regulations, most of which are based on safety. It is therefore crucial to implement safety into the design to create a feasible result.

Fuel Tanks: The design of the fuel tanks is a delicate task. As hydrogen is highly flammable, sufficient safety should be implemented during the design. The form of hydrogen on board is liquid. Liquid hydrogen does not require high pressure storage. However, during the storage of hydrogen, boil-off can occur. This boil-off results in an increased pressure in the tanks. To safely cope with the pressure of the fuel tank, pressure valves have been installed. In addition, not one but two valves per

---

[5]https://www.airbus.com/newsroom/press-releases/en/2018/04/airbus-launches-advanced-indoor-inspection-drone-to-reduce-aircr.html

tank are installed to ensure redundancy in case of failure.

Apart from the pressure that can increase during flight as boil-off occurs, the fuel tank is also designed for countering sloshing. During flight fuel is consumed, which lowers the mass of the fuel in the fuel tanks. As the mass of the fuel is reduced, more space is created in the fuel tank. This can result in uncontrolled motion of the fuel. The motion of the fuel can affect the aircraft dynamics. To cope with sloshing, so called baffles are included in the fuel tank, a explained in Chapter 7. Fuel flows from the fuel tanks towards the engine. As the liquid hydrogen is contained at cryogenic temperatures, it is important to keeps this separate from any other instruments. The fuel pipes are therefore placed in such a way that it has no contact with any other system. Lastly, as hydrogen is highly flammable, the situation when impact happens should be investigated precisely. Hydrogen as fuel has the perception to be more flammable than other fuels. However, compared to any other fuel it is just as flammable.[92] From Figure 10.4 it can be seen that the danger zone of other fuels are many times greater than the danger zone of hydrogen.
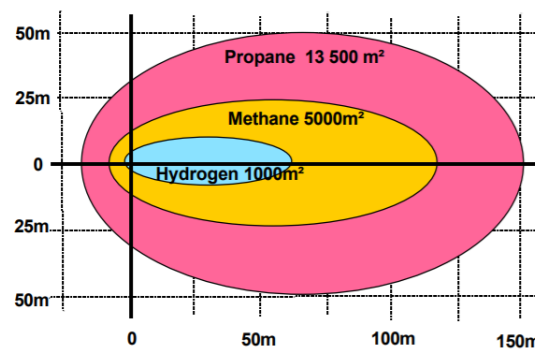
Figure 10.4: Danger Zones of Liquefied Gases[93]

Furthermore, hydrogen burns at concentrations that are significantly lower than the limit for detonations. To explain further, when burning and in contact with air it will burn at lean concentrations and not explode.[94] This means that in case of fire, hydrogen will keep burning until it runs out of fuel. There shall be no detonation in case of fire. This is often misconceived due to historic events. For example many people see the incident with the Hindenburg as one big fireball. However, it burned for one minute without any explosions occurring.[93] Although this was with gaseous hydrogen, liquid hydrogen will also not cause any explosions. The Hydrojet can therefore also help to change the misconception people might have about hydrogen, pushing forward to change from kerosene to hydrogen, from environmental destructive to green flying.

Overall Aircraft: Although the aircraft is designed precisely to ensure a safe flight, an emergency landing and/or evacuation should always be designed for. In the event of an evacuation, all passengers should be able to be evacuated in not more than 90 seconds[6]. To meet this evacuation time, an evacuation plan should be made in detail. Sufficient emergency exits have to be implemented to keep the evacuation time below 90 seconds. Based on the CS 25.807 requirement there should be two type I and six type III emergency exits.[95] The location of the different emergency exits and the emergency pathways can be seen in Figure 10.5. The front two emergency exits are type I, the six behind are type III exits.

---

[6]https://www.express.co.uk/travel/articles/850701/flight-secrets-cabin-crew-emergency-evacuation-time#:~:text=One%20aviation%20expert%20on%20Quora,take%2090%20seconds%20or%20less%E2%80%A6 [accessed on 19 June 2020]

Figure 10.5: Emergency Exits and Pathways

In case of an emergency evacuation passengers can go through the emergency exits on to the wings. To get down from the wing (either on the ground or on water), multiple slide rafts are placed on the wings. There is one slide located on the front of the cabin, one on the front of the wing and two on the back of the wing, all on each side of the aircraft. The slide rafts can be seen in Figure 10.6 and 10.7.
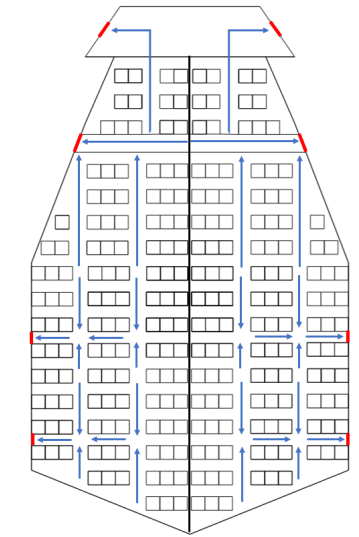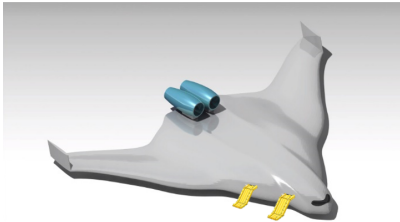

Figure 10.6: Front Slide Rafts
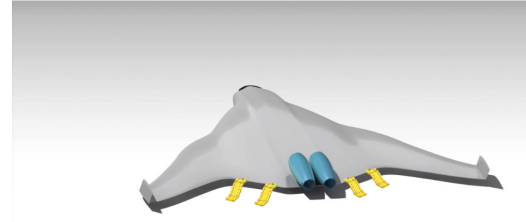
Figure 10.7: Back Slide Rafts

In case of emergency landing on an airport, the Hydrojet has to be refuelled. However, as not every airport shall have a hydrogen storage facility, an alternative must be found. A solution for the need of liquid hydrogen is by transporting it with lorries. One trailer can contain a maximum amount of hydrogen of 4,000 kg.[88] The maximum range of the Hydrojet is 4,500 km, therefore the maximum range for a flight back in case of emergency is 2,250 km. For this range, a total of 4698 kg is needed on board the aircraft. This results in a maximum of 2 trailers that needs to be transported to the airport where the Hydrojet has landed.

Hydrogen Loss: Hydrogen loss can occur during the flight. This can happen due to a malfunction of the fuel tank. The action on what to do when there is a hydrogen loss is dependent on the moment the loss is detected. First of all, when hydrogen loss is detected very early, this can be either during take-off, climb or at the beginning of cruise, the aircraft has to turn around and perform an emergency landing on the airport where it took off. Secondly, hydrogen loss can be detected in a later stage of the flight. When this happens, all fuel from the tank that is leaking is pumped into the other second fuel tank to minimise the fuel loss. Depending on the amount of fuel that is lost, the aircraft can either continue its regular flight or change its setting towards gliding. Changing the setting to gliding is done to ensure that the aircraft can land at its destination.

As mentioned, the hydrogen leaks are assumed to be detected. For this a detection system is developed. Different temperature sensors are placed around the fuel tank structure. In case of leakage, the sensors detect the temperature decrease since the liquid hydrogen is stored at cryogenic temperatures. The sensor will send the information to the cockpit which will be seen by the pilot. This system also offers the advantage that in case of leakage, it can be exactly determined where on the tank the leakage occurs. This can then be resolved during maintenance. However, the influence of the temperature decrease should be investigated carefully. The temperature decrease could block the actuators and stop them from working. A solution for this could be to install heating systems.

11
Sustainability

The final design of the Hydrojet is merely one piece of the entire system, which includes the production, operation and retirement of the Hydrojet. It is of importance that this entire system is sustainable, considering the top-level requirements as well as the long-term future of aviation. Therefore it is necessary to dive into the sustainability aspects corresponding to production, operation and retirement. This will be done in this chapter. It is first discussed how sustainability is implemented during the production phase. Then, in Section 11.2, the fuel economy, emissions and other operational aspects w.r.t. sustainability are discussed. Section 11.3 discusses the recyclability rate of the Hydrojet and the corresponding processes. Then finally, the option for carbon neutrality is explored in Section 11.4.

11.1. Sustainable Production of the Hydrojet

Sustainability will be implemented throughout the production process of the Hydrojet. This will be done by means of reducing the emissions during the production, minimising waste and energy usage.

The amount of hazardous air pollutants will be minimised during the production process. This will be done by using green energy sources, such as solar energy and wind energy. The emissions for manufacturing processes will also be reduced. The latter can be done by filtering the exhausts of systems, such as ovens and autoclaves. The use of these devices will also be limited due to their high energy consumption. Emissions during the transport of parts will also be reduced. This will be done by building the manufacturing site in a central location. This will allow to transport the parts easily from an airport, a dock or a train-station.

The lean philosophy will be applied to reduce waste. In order to have an ideal lean manufacturing process, waste of all forms needs to be eliminated. Waste can be defined as anything that utilises resources, but does not add value to the product or service for the parties of interest. The following actions can be distinguished in the production process [96]:

1. Actions that create value for the customer

2. Actions that do not add any value, but cannot be omitted immediately.

3. Actions that do not add value, and can be eliminated immediately.

For the waste reduction, actions of type three need to be eliminated first. This is followed by type two. It should be noted, however, that not all the actions of type two can be eliminated. An example of this is the transportation of parts. Excessive energy usage is also a form of waste and should be minimised. This can be done by using machines with a high energy consumption only when necessary or using energy efficient alternatives.

To calculate the total carbon emission during production, the amount CO_2 per system is estimated. This is estimated by using CO_2 emission fractions of kg CO_2 per kg of material used. The different fractions per material can be seen in Table 11.1. These values come from CES EduPack[97], unless otherwise noted.

Table 11.1: Emission and Energy Usage per Material for Production.[97]

Material	CO_2 production [kg/kg]	Embodied energy production [MJ/kg]
Al 2024-T4	13.7	204
Steel 300M	2.5	33.9
Al 2219-T87	13.3	206
Al 5083-O	15	214
Ti-10V-2Fe-3Al	55.4	920
Electronics [98]	39	-
S-glass QI	7.8	106
Carbon epoxy QI	52.34	723

Furthermore, since the mass fraction of each system in function of the OEW is known, the total fraction of kg CO_2 per system can be calculated. Multiplying by the OEW results in the CO_2 emission per system, the total amount of CO_2 per system can then be calculated for the production of the Hydojet. The CO_2 emission per system is an average between materials if more than one material is present in the system. The amount of carbon dioxide emission per system can be seen in Table 11.2.

Table 11.2: Emission per System for Production

System	Materials used	CO_2 [kg]
Wing	S-glass QI, Al 2024-T4	136,533
Empennage	Carbon epoxy QI	2,770
Fuselage	S-glass QI, Al 2024-T4	143,359
Landing Gear	Ti-10V-2Fe-3Al	10,319
Installed Engines	Titanium, Steel 300M, Al 2024-T4	268,775
Electronics	Electronics	220,834
Payloads	Textiles	11,536
Total		794,126

11.2. Sustainable Operation of the Hydrojet

The operation of the Hydrojet is the most important phase, since it will continue for about 25 years per unit. All the resources that are used during operation such as fuel and other energy sources, materials, food and packaging have to be taken into account for sustainability.

11.2.1. Fuel Provision and Economy

A central aspect in the operation of an aircraft is its energy source, or fuel. For the provision of fuel to be sustainable, its creation should be able to continue indefinitely. This is one of the main reasons hydrogen is chosen as the energy source: using Proton Exchange Membrane (PEM) electrolysis - mentioned in Chapter 8, - hydrogen fuel can be created using water and renewable energy, such as wind and solar. The working of PEM electrolysis is visualised in Figure 11.1. Hence, by supplying power to the PEM setup, hydrogen is produced. This yields a great security of fuel provision, while featuring a renewable creation process. The provision of fuel is, however, just one part of the sustainable story for the fuel. The other part is about how much of it an aircraft needs per flight, which should also be optimised. This can be captured by the so-called fuel economy (FE).
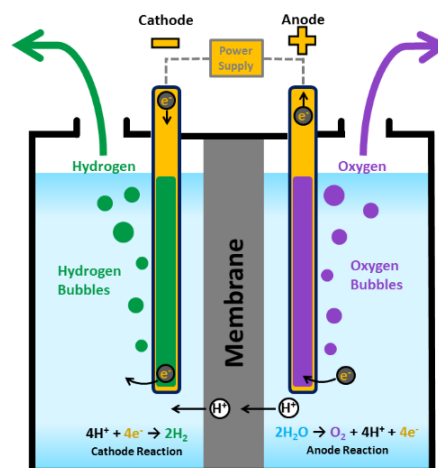
Figure 11.1: PEM Electrolysis of Hydrogen [99]

The FE of an aircraft is a very important and useful parameter to quantify how efficient that aircraft is in fulfilling its primary purpose. For a passenger aircraft such as the Hydrojet, this purpose would be to transport civilian passengers and their luggage from one location to another, requiring minimal energy. This is beneficial both for the environment and the economy, since per flight less hydrogen has to be produced, saving water and energy, and bought by the airlines, saving money. The FE of passenger transport aircraft is given by convention in amount of fuel used in liters per 100 km per passenger (L/100km/pax). The FE is determined by four main aspects [100]:

- Aerodynamic efficiency - Lift-over-drag ratio (L/D)

- Engine efficiency - Thrust specific fuel consumption (TSFC)

- Weight efficiency - OEM-over-MTOM ratio (OEM/MTOM)

- Seating density - Amount of passengers on board (pax)

This is since L/D dictates how much drag there will be for a certain lift, which needs a certain thrust. This in turn defines the TSFC. The weight efficiency also influences the needed lift and thus the resulting drag. These are the relative parameters, yet the total fuel consumption is defined by how much mass has to be transported in the end, namely the amount of passengers and their luggage.

For the seating density, pax was set to a maximum of 236 as a top-level requirement. The OEW/MTOW ratio was determined from the Class-I mass estimation in Chapter 3, which used data from existing aircraft, and is found to be 0.573. Hence the two main factors that could be influenced during the design were TSFC and L/D. To have a high value for the L/D, an aerodynamic design is crucial. For that reason, the blended wing-body design was chosen, yielding an impressive L/D during cruise of 25.24. The turbofan engine was also optimised to have an optimal TSFC of $1.1055 \cdot 10^{-5}$ kg/Ns during cruise. These design specifications should result in a promising fuel economy.

To compare the FE of the Hydrojet to existing competitors however, all values should be converted to MJ/100km/pax due to the volumetric energy density difference between hydrogen and conventional jet fuel. The Hydrojet stores 8.4 MJ/L of hydrogen, while conventional fuel is stored at 35 MJ/L. In addition, the FE changes if different missions are flown, i.e. a different range and payload (pax and mass/pax). Hence the distinction is made between short-to-mid range missions and upper range missions. For flights in the short-to-medium-to-upper range for the Hydrojet missions, the data in Table 11.3 for comparison is used. All found FE (in L/100km/pax) are multiplied by 35 MJ/L.

In the extreme case, the Hydrojet will fly at its maximum range of 4500 km at 236 pax, needing a fuel amount of 138.4 m^3, which equals 1,162,560 MJ. The corresponding FE achieved is 109.47 MJ/100km/pax. Comparing this to the industry average value of 93.83 MJ/100km/pax, at first glance the Hydrojet seems less fuel efficient. This does not really make sense, since the point of a blended-wing-body is to increase fuel efficiency. Yet for the Hydrojet, the payload mass per passenger - person and luggage mass, - is taken to be 127 kg/pax. This is a much higher value than the one used by the industry, which is about 105 kg/pax.[14]

Therefore the FE needs to be corrected once more to get to the standardised unit of MJ/100km/kg (energy used per 100 km travelled per kilogram of payload transported). Then the Hydrojet has a fuel economy of 0.861 MJ/100km/kg and the current industry an average of 0.894 MJ/100km/kg. Hence the Hydrojet is 3.6 % more fuel efficient. Considering that the Hydrojet is a raw design compared to current operational passenger aircraft, which are approaching their maximal achievable total efficiency, this is very promising. Adjusting the combination of range and payload for the Hydrojet will increase this fuel economy even further, and in the long term, technological improvements in hydrogen powered, blended-wing-body aircraft will also contribute in continuing improvement of fuel economy. This is why the Hydrojet is an extremely strong candidate considering long-term sustainable (civil) aviation.

11.2.2. Emissions

With global warming playing an ever increasing role in today's world, it leads to pressing responsibilities to reduce the anthropogenic output of greenhouse gases in virtually every industry where they are produced. Aviation is one of them, and burning conventional aviation fuel leads to large amounts of mainly CO_2 and water vapour being emitted in the atmosphere. More specifically, CO_2 makes up about 72 % of the total emissions of conventional jet engines, and water vapour about 27 %.[114] CO_2 contributes for 20 % to forced global warming.[115] These emissions will remain regardless of the overall efficiency of aircraft, unless disruptive fuel technologies and propulsion concepts are used. They are the only options that can save the industry from contributing to the destruction of the environment. This is another core reason why hydrogen fuel is a promising approach.

In Section 7.3.6 it was already stated that burning hydrogen fuel, besides water (vapour) only leads to the emissions of NO_x. This already means a significant improvement compared to the burning of conventional aviation fuels. However, from a long-term perspective it is still necessary to strive for complete zero-emission aviation, and limiting the NO_x emissions as much as possible without having any other harmful exhaust gasses is a great leap in the right direction. To minimise the detrimental effects of NO_x effectively, however, it is necessary to have an understanding of how it contributes as a harmful emission. Water vapour (contrails) are left out of the analysis, due to top-level requirement HPRA-STK-SUS-1, yet for other

Table 11.3: Comparison Data at Various Missions within the Hydrojet Range

Aircraft	Mission [km]	# Seats	FE [MJ/100km/pax]
A319neo [101]	1100	144	102.2
A319neo [102]	1220	124	98.7
A319neo [103]	1900	136	67.55
A320 [104]	1900	150	91.35
A320 [105]	3984	150	85.05
A320neo [102]	1220	154	78.75
A321 [104]	1900	180	87.5
A321neo [102]	1220	192	76.65
A321neoLR [106]	6300	154	85.05
A330-200 [104]	1900	293	82.95
A330-200 [107]	5600	241	108.85
A330-300 [107]	5600	262	104.3
B737-300 [108]	939	126	121.1
B737-600 [109]	930	110	125.65
B737-600 [109]	1900	110	110.25
B737-700 [109]	930	126	111.65
B737-700 [109]	1900	126	97.65
B737-700 [104]	1900	128	94.85
B737 MAX7 [102]	1220	128	96.95
B737 MAX7 [102]	1100	144	102.55
B737 MAX7 [101]	1900	140	67.9
B737 MAX8 [103]	1220	166	79.8
B737 MAX8 [102]	1900	162	85.4
B737 MAX8 [110]	6300	168	74.55
B737 MAX9 [111]	1220	180	79.8
B737 MAX9 [102]	1900	180	70.7
B737 MAX9 [110]	6300	144	88.55
B757-200 [106]	930	200	101.85
B757-200 [112]	1900	190	105.7
B757-200 [106]	6300	158	105
B767-200ER [113]	5600	224	96.25
B767-300ER [105]	3984	218	108.15
B767-400ER [113]	5600	245	103.25
AVERAGE	2712	169	**93.83**

projects concerning dismantling aircraft emissions, the effect of water vapour should be taken into account.

NO_x emissions play a role both on the ground and in the upper troposphere/lower stratosphere, where commercial aircraft cruise and thus spend the most time. On the ground, NO_x emissions contribute to the creation of smog and acid rain.[116] These in turn can damage vegetation and cause respiratory health problems as well as heart diseases in case of long exposure. This, however, is mainly a concern in big cities due to emissions of ground vehicles and power plants.[116] For aircraft, only the airport and its direct neighbourhood are affected by NO_x emissions. To mitigate this, the fuel cell designed in Section 7.4 acts as the APU and also powers the electrical motor in the landing gear, achieving actual zero-emission taxiing.

Aircraft NO_x emissions in the upper troposphere and lower stratosphere play a role in various chemical interactions which have the net result of increasing ozone (O_3) levels and decreasing methane (CH_4) levels in those altitudes.[117] This process due to NO_x is primarily present in the northern mid-latitudes, which covers (among others) virtually all of Europe, making it especially relevant for the Hydrojet considering the top-level requirements. Both O_3 and CH_4 are greenhouse gasses, yet CH_4 is a more aggressive greenhouse gas than O_3.[118] Furthermore, it is known that O_3 increases at cruising altitudes, due to fact that NO_x emissions stay concentrated around the flight routes they originate from, in this case over Europe. The decrease in CH_4 that are caused by the NO_x emissions, however, extend globally. This has the main effect of cancelling out the added greenhouse effect due to aircraft NO_x emissions on a global scale, yet locally increase it in the northern mid-latitudes.[117] It is therefore still necessary to limit those emissions at cruising altitudes, which was done by designing the turbofans of the Hydrojet and specifically their combustion chamber in a particular way that minimises NO_x emissions (details found in Section 7.3.6).

It is now time to compare the emissions of the Hydrojet to those of current aviation. Table 11.4 shows the type and quantity of constituents of harmful conventional fuel exhaust emissions, not considering water vapour.[1]

Table 11.4: Harmful Combustion Products of Conventional Jet Engines

Emission Type	CO_2	NO_x	CO	UHC	soot
Fraction [%]	99.4475	0.4641	0.0652	0.0221	0.0011

It was also shown in Section 7.3.6 that the Hydrojet turbofans emit NO_x at a per-flight average rate of 0.54 g/kg, and conventional turbofans emit NO_x at 17.76 g/kg. This means a reduction of 96.96 % in NO_x for the Hydrojet compared to its conventional counterparts. To summarise, the Hydrojet eliminates CO_2, CO, UHC (unburned hydrocarbons) and soot emissions, and reduces NO_x emissions with 96.96 % compared to current civil aviation. This yields a total reduction from 100 % harmful emissions to 0.014 % harmful emissions w.r.t. current civil aviation. This finally means that the Hydrojet realises *a total reduction of 99.986 % in harmful emissions* compared to current aviation standards, which is a phenomenal improvement, and also results in the compliance with requirement HPRA-SUS-1.

11.2.3. Other In-service Sustainability

Minimising fuel consumption and harmful emissions of the aircraft is not the only objective during the aircraft operations. Emissions from ground systems such as shuttles, luggage vehicles etc, should be either minimised or compensated. By switching to electrically propelled ground vehicles, this could be achieved, yet it is a call that is made by the airports, and can only be encouraged. Thus, to make sure the corresponding carbon emissions are cancelled out, policies are made in Section 11.4. To minimise aircraft noise, as explained in Section 7.3.7, the turbofans will feature a high bypass ratio to form a cold stream of air around the hot and fast jet stream, as well as a Type B nacelle which premixes these two flows. One additional feature are the chevrons present at the nacelle and jet exhaust, visualised in Figure 11.2[1]. As aforementioned, these decrease noise by 2.5 dB whilst creating an insignificant 0.5 % thrust loss.

Figure 11.2: Chevrons on the Nacelle and Jet Exhausts

11.3. Sustainable Retirement of the Hydrojet

The top level requirement of sustainability HPRA-STK-SUS-2 states that 90% of the aircraft shall be recyclable by weight. In the sustainable retirement of the Hydrojet, this requirement must be met. Furthermore, the CO2 associated with the recycling of the materials and the energy required or obtained from its recycling is presented.

Recycling of metals: In the midterm report[1], metals were found to be more sustainable and less energy intensive to produce using recycling than by producing it from the ore itself. This can be verified by looking at the CO2 produced and the energy needed to produce the metals in Table 11.1. While recycling the metals, a certain amount of energy is needed and a certain amount of CO2 is released. The embodied energy is the energy required to recycle 1kg of the metal. As a consequence of recycling 1kg of the metal, the CO2-equivalent mass (kg CO2e), in kg, is produced and released into the atmosphere. The values for the recycling of the metals used in the Hydrojet are shown in Table 11.7.

Recycling of Glassfibre-epoxy and Carbon-epoxy: Recycling of composites that use epoxy was seen to have processes to enable them to be completely recycled in [1], even though they are thermosetting polymers. For example, mechanical grinding

---

[1]https://www.adviationonline.com/aerodynamics-an-ace-up-the-sleeve/ [accessed on 20 June, 2020]

glass of fibres is a very mature process and for carbon fibres pyrolysis is the most mature.[119] Glass-epoxy is recyclable, both the fiber fraction and the resin fraction.[120][121] If mechanical recycling is not possible due to no economic incentive, as the glass fibres retrieved are more expensive to retrieve than if bought as virgin fibres, chemical recycling can be used. Chemical recycling, of which pyrolosis is the most common form thereof, is seen to play a vital role in the extraction of value from waste plastic[2]. Pyrolysis is a two-step process which is a viable way to recover valuable materials and also produce fuel and chemicals. In Table 11.8 heat of combustion is the amount of energy released when the material fully combusts. The net amount of energy retrieved is found by finding the difference of the heat of evaporation for water from the measured heat of combusting the material in an oxygen bomb calorimeter and bringing all combustion products, including water vapor, back to the pre-combustion temperature.

Recyclability fraction of aircraft subsystems: In [1], a recyclability percentage of 90% was found using OEW factions per system from statistics and a recycling fraction for the materials selected per system. Using the same procedure, but with OEW sytem fractions from the class II weight estimations leads to the same recyclability percentage of 90%. The recycling fractions for each primary component is explained in [1], in short for all components a base 0.03 recycling loss penalty is chosen because of human error or major issues with materials. The composites have a 0.92 recyclable fraction, and the metals have 0.97 recyclable fraction. 87% of e-waste is recycled in the Netherlands.[122]

Table 11.5: Recyclable fraction per component

Component	Wing	Empennage	Fuselage	Landing gear	Installed engines	Systems	Payloads
Weight fraction	0.24	0.001	0.252	0.078	0.214	0.107	0.109
Material used	Al 2024-T4, Glass/epoxy	Carbon/epoxy	Glass/epoxy	Steel 300M	Inconel, Steel 300M, Al 2024-T4	Electronics	Various
Recyclable fraction	0.92	0.92	0.92	0.97	0.92	0.84	0.77

A more in detail recyclability percentage can be found by looking at the subsystems OEW fractions, also found from the class II weight estimation. In Table 11.6 the recyclability fraction per subsystem is presented. The final total recycling percentage of the Hydrojet is thus 91.3%.

Table 11.6: Recyclable fraction on subsystem level

Component	Weight fraction	Material used	Recyclable fraction
Covers	0.096	Glass-epoxy	0.92
Ribs	0.034	Al 2024 T4	0.97
Secondary weight penalties	0.072	Glass-epoxy	0.92
Fuselage	0.135	Glass-epoxy	0.92
Wing	0.156	Glass-epoxy	0.92
Vertical tail	0.001	Glass-epoxy	0.92
Landing gear	0.078	Steel 300M	0.97
Engine	0.214	Inconel, Steel 300M, Al 2024-T4	0.97
Fixed equipment	0.107	Electronics	0.84
Operational items	0.109	Textile	0.77

CO2 associated with recycling

In Table 11.8 the CO2 associated with recycling the composites used in the Hydrojet are shown. Similarly, in Table 11.7 the CO2 associated with recycling the metals are shown. In the next section the CO2 produced during retirement is calculated.

Table 11.7: Emission per Metal for Retirement. Values are from CES EduPack[97].

Material	CO2 footprint recycling [kg/kg]	Embodied energy recycling [MJ/kg]
Al 2024 T4	2.75	35
Steel 300M	0.703	8.96
Al 2219 T87	2.77	35.3
Al 5083-O	2.85	36.3
Ti-10V-2Fe-3Al	8.63	110
Electronics	19.5[98]	-

---

[2]https://www.chemanager-online.com/en/whitepaper/science-enable-sustainable-plastics [accessed on 20 June, 2020]

Table 11.8: Emission of Composites for Retirement and Production. Values are from CES EduPack[97].

Materials	S-glass QI	Carbon epoxy QI	Polyurethane foam
Combustion CO2[kg/kg]	1.02	3.33	2
Heat of combustion (net) [MJ/kg]	12.6	32.9	22.3

11.4. Carbon Neutral Approximation

The carbon emission of the total product can be calculated by combining the emissions of the different phases of both the aircraft and the ground facilities. These emissions can be countered using different methods which will be discussed below.

11.4.1. Carbon Dioxide Component Build Up

The total emission of the aircraft is constructed by combining the emission of all the different components. These components include the production of both the Hydrojet and the hydrogen, the operation, and retirement of the hydrojet. The Hydrojet retirement CO2 production is calculated by multiplying the OEW fractions of each system with the CO2 produced in each system with the recyclability fractions for systems and finally, with the OEW. The contribution of each individual component can be seen in Table 11.9.

Table 11.9: Emission per Component over the Lifetime of the Hydrojet

	CO_2 [ton]
Hydrojet Production	$7.94 \cdot 10^5$
Hydrogen Production	0.0
Hydrojet Operation	0.0
Hydrojet Retirement	$1.87 \cdot 10^5$
Total Emission	$9.81 \cdot 10^5$

From this table it can be seen that the total amount of CO_2 is $9.81 \cdot 10^5$ kg. In addition to this, the amount of CO_2 needed to produce 3 hydrogen ground storage tanks equal $8.88 \cdot 10^6$ kg. Thus, to make a fleet of 10 Hydrojets and 1 ground station with 3 ground storage tanks, $18.69 \cdot 10^6$ kg are produced.

11.4.2. Countering Emissions

Although the goal of this project is not to design a carbon neutral aircraft. It is beneficial to investigate how close the design is, and what could be done in order to become carbon neutral. As is concluded in the previous section, $18.69 \cdot 10^6$ of CO_2 should be removed from the complete process to become carbon neutral. Several actions can be done for this.

First of all, it is chosen that the catering on board of the aircraft will contain vegetarian, vegan and meat meals. There will be multiple options for vegetarian and vegan meals and only limited options for meat meals. It is assumed that 50 % of the passengers choose for a vegetarian of vegan meal. On average, to produce meat meals, 3 kg of CO_2 is needed, for vegetarian meals this equals 0.9kg. For vegan meals this lowers to 0.75 kg.[123] This results in a CO_2 reduction of 159.3 kg per flight. The number of flights of the aircraft during its lifetime is estimated to be 31,000. It is assumed that half of these will contain catering service. This number is based on the maximum short haul flight as not all flights will do maximum long range or minimal short haul flights. This number of flights results in a total carbon dioxide reduction of 2,469 ton. Due to the fact that this is compared to a conventional aircraft, where most meals are with meat, a second option must be found to make the Hydrojet carbon neutral.

The second option for reducing the emission is to increase the number of turbines and/or solar panels that are used to provide energy to produce the hydrogen. This extra energy that is being provided from the turbines and solar panels is supplied to the electrical grid. Due to its sustainable nature, less electricity needs to be produced from for example a gas plant. A natural gas electricity site is, apart from renewable energy, the most climate friendly method to produce electricity. For every kWh produced, the natural gas produces 0.572 kg of carbon dioxide.[124] This results in a total of $38.5 \cdot 10^{12}$ J that needs to be produced by the wind turbines and solar panel area. The same values for the wind turbines and solar panels are used as in Chapter 8, as well as the idea to minimise the area needed. This results in an increase of 18 wind turbines and 115,455 m^2 of solar panel area.

By implementing a more wider variety of vegetarian and vegan meals, by increasing the number of turbines with 18 and by increasing the solar panel area with 115,455 m^2, the complete process of the Hydrojet can be made carbon neutral.

12

Financial Analysis

In this chapter the final steps of the detailed design phase will be discussed. This will start off with the production plan, assembly logistics and flight certification method which will be given in Section 12.1. Next, the cost breakdown of the design will be given in Section 12.2. After that, a market analysis is performed in Section 12.3. Furthermore, the return on investments will be investigated in Section 12.4.

12.1. Production Plan, Assembly Logistics and Flight Certification

Before the Hydrojet's position in the market can be analysed, the production plan and the logistics of the assembly must first be described as this influences the production cost. The process of certifying the aircraft is also explored as is influences the development costs and the time it takes to put the Hydrojet on the market.

12.1.1. Production Plan

After detailed design, the production process can start. The Hydrojet consists of many parts which can be subdivided into even smaller parts. These parts are called assemblies and sub-assemblies respectively. For aircraft production typically assembly lines in series are being used. The assembly process for the Fokker F18 is depicted in Figure 12.1. It can be observed that there are several branches connected to a final assembly line. These branches produce sub-assemblies, which are transferred to the final assembly. A similar procedure will be used for the Hydrojet. The tail-cone in this figure will represent the aft body of the blended wing. There will also be no tail branch, because the Hydrojet does not have one. Furthermore a hydrogen tank branch will be added. This sub-line will be connected to the main line prior to adding the outer wing, since the tank will be placed between the cabin and the outer wing root.

Each (sub)assembly line will have working stations. At each station the same crew will perform the same tasks for each aircraft. The time allocated for each station is fixed and when the time has passed all aircraft will move to the following station. This time is also known as the "delivery interval".[96] The parts for each branch will be produced at workshops using the appropriate manufacturing processes and half-fabricates (sheets, plates, bars, and blocks). The finished parts will be delivered to a warehouse for short-term storage or directly to the assembly site.It should also be noted that not all the the sub-assembly lines are at one factory. Some of the sub-assemblies are also produced at factories of partners. These will be electronics, like flight deck instruments, the fuel cell system , the turbofan engines and the landing gear motor system.

The assembly method increases the production efficiency by splitting the work up in portions, thus reducing the delivery time. Furthermore, the size of tools and half-fabricates are also limited. Hence, large parts such as skin panels cannot be manufactured in one go. Using divisions increases the accessibility and ease of production. The following two types of divisions will be used in the Hydrojet:

1. Mounting divisions: These are needed for movable parts like doors, hatches, control devices and high lift devices. Additionally, also for parts that need to be exchangeable and inspectable.

2. Manufacturing or production divisions: these are required for structural and manufacturing reasons such as: Inner wing - outer wing divisions, cabin divisions, divisions where different materials meet and divisions for fail-safe reasons, for example crack stopping division.

The lean philosophy, as already mentioned in Chapter 11, will also be applied throughout the production process of the Hydrojet. The lean philosophy will increase the production efficiency and decrease the manufacturing costs. The latter is defined as follows: "Lean thinking is the dynamic, knowledge driven, and customer-focused process, through which all people in a defined enterprise continuously eliminate waste with the goal of creating value."[96] Lean manufacturing will also be applied for the production of the Hydrojet by using the "5S" approach and the "Just-in-Time" (JIT) principle. The former consists of five steps, also known as the 5 S's, which are: Sort, Simplify, Standardise and Sustain. These steps should not be seen as a list of actions. Instead, it has to be carried out like daily activity, which demands concentration, dedication and devotion for maintaining it and eventually making it a culture company-wide [1]. The JIT principle focuses on producing and

---

[1]https://www.isixsigma.com/tools-templates/5s/practical-approach-successful-practice-5s/[accessed on 17 June 2020
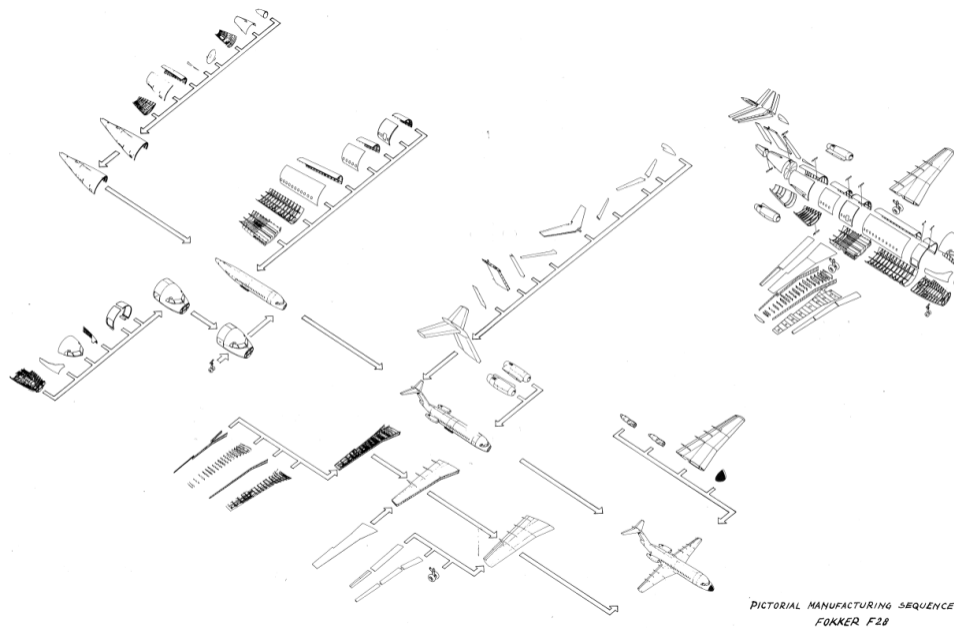
Figure 12.1: Manufacturing Sequence [96]

delivering the correct items, at the correct time and in the correct amounts. By organising the logistics and the layout of the factory in this way the production process can take place continuously and efficiently. The lean principle will also minimise the costs and promote the sustainability aspect of the Hydrojet.

As mentioned in Section 5.5, structural health monitoring (SHM) will be integrated in the aircraft structure by means of non-destructive testing (NDT). SHM not only needs to be done for the final product, but it also needs to be done throughout the production process, starting with the half-fabricates. This is also known as SHM level 0: Good Quality Control of the Condition of the Starting Structure.[125] This is done to detect damage that can occurs during quality checks in the factory, transportation, installation, and production and transit of the half-fabricates. Detecting defects at an early stage can prevent growth of the defects and waste of a part. The latter can occur when a part does not pass the final quality check and needs to be discarded.

12.1.2. Logistics
The aircraft will be produced and assembled at multiple different sites. Usually, by definition of the lean manufacturing principles, transport does not add any value to the product. However, past experiences of aircraft manufacturers have shown that distributing the production and assembly lines will have a positive economic impact compared to the centralised production and assembly of an aircraft.[96] The Hydrojet production and assembly chain will also consist of the separated production and (sub) assembly sites and will result in the final aircraft being assembled at a centralised site in the end. The logistics of the parts can be split up in two categories, the logistics within the site itself and the logistics between different sites.

At the site itself,transportation of products should be kept to a minimum, meaning that the work stations should be located close to each other. This will ensure that no time is wasted and that the production time for parts and components is minimal. Additionally, the parts should be easily disconnected from machinery and jigs. The line production used at the production site will need to follow the JIT principles. This means that the parts will be stored minimally and that the production line will run smooth and continuously. For logistics between the different sites, transport is also needed. For relatively short distance (within a country) the Tesla Semi will be used to transport the different parts between sites. However, limiting factors for transporting arises from weight and size (volume) of the produced parts. Tesla Semi is used to reduce the environmental impact during transport of parts. If the parts are too large to transport easily with the Tesla Semi or when the distances are too long, transport aircraft such as the Airbus Beluga aircraft or the Boeing 747 Dreamlifter will be used for transportation of the different parts and assemblies. The final assembly will be done on a centralised site between every (sub) assembly site in order to have minimal transportation time losses.

12.1.3. Flight Testing & Certification

When the Hydrojet is assembled flight testing and certification will be done. This will be done mostly by conducting tests on the aircraft such as a flight test to determine the stability, or an evacuation test to check the safety standards of the aircraft. Tests will be conducted to the extent that the aircraft will comply with all European standards. Some of the tests that need to be performed, especially due to the distinctive design of the Hydrojet, are:

- Water Intake Testing: The runway covered with water on which the aircraft has to take off. Minimal water may enter the engine. Furthermore, aircraft taxi is tested on the wet runway.

- Temperature and Altitude Testing: The aircraft is brought to extremely hot/cold climates or very high/low altitudes to check for normal functionality.

- Velocity Minimum Unstick Test: During this test the aircraft minimum take-off velocity is determined. The aircraft scrapes the runway to allow for maximum angle of attack.

- Brake testing: The aircraft is first loaded to its maximum take-off weight with worn-out brake pads. It is then brought to take-off speed on the runway before stopping. With the high heat that occurs at the brakes the wheels should deflate. There is a soft metal in the plugs that will melt first to ensure safe deflating. Emergency crews have to wait for five minute after which they can check the aircraft to see if the fire has spread to the aircraft's body.

- Noise Test: The noise level of the aircraft is tested at three different stages. First of all the highest noise is measured anywhere within 450 m of take-off. Secondly, it is measured when the aircraft has covered a distance of 4.5 km from the runway, when it is at the start of roll. And lastly, during approach 120 m below the aircraft when it is 2 km from the runway.[2]

- Flight Test for Stability and Controllability: During this flight test the aircraft's attitude, angle of attack and side slip angle are tested. Furthermore, there are accelerometers placed at different positions on the aircraft to measure the acceleration of the aircraft in all six degrees of freedom.

- Evacuation Test: A simulation is made of an emergency landing where all passengers and crew have to evacuate within a certain time frame.

As requirement HPRA-STK-SR-2 states that the aircraft has to comply with all European aviation standards, all these test have to be performed before the aircraft can be sold to any airline.

12.2. Cost Breakdown

The profitability of the Hydrojet highly depends on the costs that are associated with it, which consists of the development cost and the production cost. These costs influence the price that must be set on the aircraft and affect how many units can be sold. In this section the development and production costs are estimated per subsystem.

12.2.1. Development Cost

The development costs consist of all the costs due to developing the actual product. This includes the engineering of the product itself, engineering of the manufacturing (ME), manufacturing tools design, fabrication costs of the tools, and some miscellaneous costs. Markish [126] states an overview of the estimated amount of dollars per pound for these different development costs, relatively. Converting these values to euros per kilogram, and also taking into account inflation - as this report was made in 2002, - Table 12.1 is obtained. The weights used are derived from the final iteration of the Class II weight estimation, where "Systems" is a combination of m_{covers}, m_{ribs}, $m_{fixed\ equipment}$ and $m_{secondary}$. The "Payload" weight was then taken as $m_{operational\ items}$. It is then found that the total development costs is about €4215 million, or €4.2 billion. It should be noted, however, that these numbers are based on the development of a conventional aircraft, and since the Hydrojet incorporates numeral novel technologies, it may turn out costlier than projected here.

12.2.2. Production cost

The production costs are the costs of manufacturing the aircraft per unit. Similarly to the development cost, they are divided in cost per subsystems, each with its own specific cost (in USD/kg).[126] With the subsystem weights from the Class II weight estimation the total production cost can be estimated. After accounting for inflation and multiplying it with the exchange rate from USD to EUR of 0.91 (20 June 2020), the total unit production cost amounts to 108.6 million euros.

12.3. Market Analysis

In this section the market analysis is performed. First, the operational costs are investigated. Next, the added value of the Hydrojet and a SWOT analysis will be presented. After that, the pricing for the Hydrojet will be determined. Additionally, the

---

[2]https://www.airportwatch.org.uk/briefings/how-aircraft-are-certified-for-noise/

Table 12.1: Breakdown of estimated cost per system per development cost.

	Engineering [€/kg]	ME [€/kg]	Tool design [€/kg]	Tool fabrication [€/kg]	Miscellaneous [€/kg]	Weight [kg]	Total [M€]
Wing	20180.05	5044.30	5297.51	17556.90	2369.94	12716.09	641.47
Vertical Tail	59353.76	14839.86	15579.58	51637.94	6973.26	90.83	13.48
Fuselage	36522.11	9129.82	9587.87	31776.54	4290.36	13261.07	1210.82
Landing Gear	2842.22	711.27	745.41	2472.36	332.87	4087.32	29.06
Installed Engines	9892.29	2472.36	2597.54	8606.32	1160.79	10990.34	271.75
Systems	39042.83	9761.42	10247.93	33967.24	4586.25	20527.41	2003.59
Payloads	12248.01	3061.29	3214.92	10657.62	1439.60	1453.27	44.50
Total							**4214.68**

Table 12.2: Breakdown of unit production costs

	Weight fraction [-]	Specific cost [€/kg]	Production cost [M€]
Wing	0.24	2507.58	31.84
Vertical Tail	0.001	6494.64	0.3437
Fuselage	0.252	2719.33	36.26
Landing Gear	0.078	615.75	2.542
Installed Engines	0.214	1042.04	11.80
Systems	0.107	1259.36	7.131
Payloads	0.109	1571.42	9.064
Final Assembly	1	181.10	9.584
Total			**108.6**

competition and magnitude on the aviation market will be investigated, as well as, the market share within sustainable aviation. Finally, this section will conclude by exploring the possibilities on other markets.

12.3.1. Operational Costs
The operational costs of an aircraft have an effect on how attractive it is for airlines. For the purpose of this analysis the Direct Operational Cost (DOC) will be estimated per flight with the design range of 4500 km. One component of the DOC is the cost of operating an aircraft during flight, which includes the crew wages, fuel, oil and lubricants, landing and navigation fees, and maintenance. The rest of the DOC consists of the insurance, financing and depreciation.[127]

The cost of the hydrogen fuel was based on a rate of 1.7 cts/MJ[3] (USD), while the crew, landing and navigation fees, and maintenance were calculated using semi-empirical methods relating them to MTOW, maximum thrust and other specifications.[16] The rest of the components were expressed as a percentage of the total DOC.[127] After accounting for inflation and converting the costs to Euro this method gives a total DOC of around € 58,000 per flight of 4500 km, the breakdown of all the components can be found in Table 12.3. The cost per available seat mile (CASM) amounts to 7.8 euro cents, which is comparable to the CASM of the B737-700/LR flown by Alaska Airlines, 7.6 euro cents, and of the A320 flown by United, 7.7 euro cents.[4] This also meets the requirement of the CASM not exceeding 13 euro cents.

12.3.2. Added Value Hydrojet and SWOT Analysis
In order to better understand the position of the Hydrojet within the current market, the strengths of the Hydrojet with respect to conventional aircraft must be analysed, as well as the weaknesses, possible opportunities, and threats. This then leads into a SWOT diagram.

The most obvious strength of the Hydrojet is its emissions. It has no CO_2, CO, SOx, HC, PM or soot. The only pollutant emitted by the Hydrojet is NOx. However, during taxiing there is none at all, and during cruise NOx emissions are reduced by 99.96 % with respect to current aircraft. Moreover, the energy used to produce the hydrogen itself will be generated by sustainable means such as wind or solar energy. Finally, the Hydrojet will be 90 % recyclable. This means that, in summary, the complete life-cycle of the Hydrojet is sustainable, which grants it a unique position within the current market for eco-friendly alternatives to conventional flight.

---

[3]http://www.renewableenergyfocus.com/view/3157/hydrogen-production-from-renewables/ [accessed on 29 April 2020]
[4]https://www.planestats.com/bhsn_2014dec [accessed on 19 June 2020]

Table 12.3: Direct operational costs

Service	Operational cost	
	[€/flight]	[%]
Crew	20,334	35.1
Fuel	19,167	33.0
Oil and lubricants	1,160	2.00
Landing & navigation fees	3,674	6.33
Air-frame maintenance	1,827	3.15
Engine maintenance	814	1.40
Insurance	580	1.00
Financing	5,799	10.0
Depreciation	4,640	8.00
Total	**57,995**	**100**

There are also some financial benefits to the Hydrojet. First of all, because of the electrical motor in the landing gear, the aircraft is capable to deliver its own push-back. This reduces required man-hours. Furthermore, the Hydrojet will not - or nearly - have any emissions related fees, because of its very low levels of emission. There is even a possibility of receiving funds or subsidies for the development of this aircraft by governments, in order to reach the green-house gas goals they have set. And lastly, as oil reserves will become depleted in the near future, this will most likely also cause kerosene prices to greatly increase, making Hydrojet the cheaper alternative as well.

It should also be noted that since out-of-factory cost as well as operational costs are about the same as competitor aircraft, this is neither a weakness nor a strength.

There are, of course, also some weaknesses to the Hydrojet concept. First of all, the aircraft requires new ground facilities, such as large hydrogen tanks and even on-site hydrogen production methods. Also, since the Hydrojet is a novel design, integrating not only a blended wing body, but a hydrogen powered propulsion system as well, the development time will most likely take longer, and cost more, than a new conventional kerosene powered aircraft. Furthermore, hydrogen being highly flammable as well as having a very low viscosity causing for example a boil-off effect - this technology will most likely be more difficult to get through safety regulations, again possibly increasing development cost and time.

And finally, it is always a possibility for a competitor to also develop a hydrogen powered aircraft, or another sustainable alternative, like an electric aircraft, which perhaps has even better strengths and marketability than the Hydrojet. If this is the case, and the competitor out-competes the Hydrojet once both aircraft hit the market, this can become a great financial threat. It can also happen that once the Hydrojet is ready for operations, some failure, scandal, or other form of bad press causes the public to distrust hydrogen fuel, making it unmarketable and thus causing great financial loss as well.

In Figure 12.2 a SWOT analysis is presented, summarising the strengths, weaknesses, opportunities and threats as are discussed above in one diagram.

12.3.3. Hydrojet Competitive Pricing

The Hydrojet is able to fulfil a need that no other aircraft on the market can fulfil right now: it will provide sustainable and zero-emission regional air travel. This means that it can be priced higher than its competitors that are currently on the market, since the Hydrojet will enter the sustainable aviation market. Still, the Hydrojet cannot be too expensive: it must be priced competitively such that airlines are willing to purchase the Hydrojet over conventional aircraft.

In the Baseline report, a unit cost of €119.6 was found to be the competitive price for 236 passengers, as shown in Table 12.4. This value was based on five direct competitors, namely the A321-NEO (LR), B737 MAX 10, A310-200, E195-E2 and the CRJ900. These are all conventional aircraft, since the prices of sustainable zero-emission aircraft are not known at this moment. The price was calculated in the following way: Of the number of passengers (PAX) and unit cost of each aircraft, a weighted average was taken such that the total averages were close to the requirements, namely 232 passengers and €99.9 million. Based on those weights, then the unit cost per passenger was computed of each aircraft and those values were multiplied by 236; the number of passengers that the Hydrojet will carry. From this, the unit price of each aircraft was found if they would have carried 236 passengers. By again taking the weighted average of those unit prices, the competitive unit price

INTERNAL

strengths
- Very low emissions
- No emissions during taxiing
- High recyclability
- Hydrogen itself also sustainably produced
- No external push-back needed

weaknesses
- Relatively long development time
- Higher development costs
- Requires completely new ground facilities in order to be operated
- More difficult to pass safety regulations

POSITIVE

NEGATIVE

opportunities
- Lower emission taxes
- Possibility for government funding
- Kerosene becomes substantially more expensive than hydrogen

threats
- Competitor also develops hydrogen powered aircraft
- Competitor develops another sustainable technology capable to compete with Hydrojet
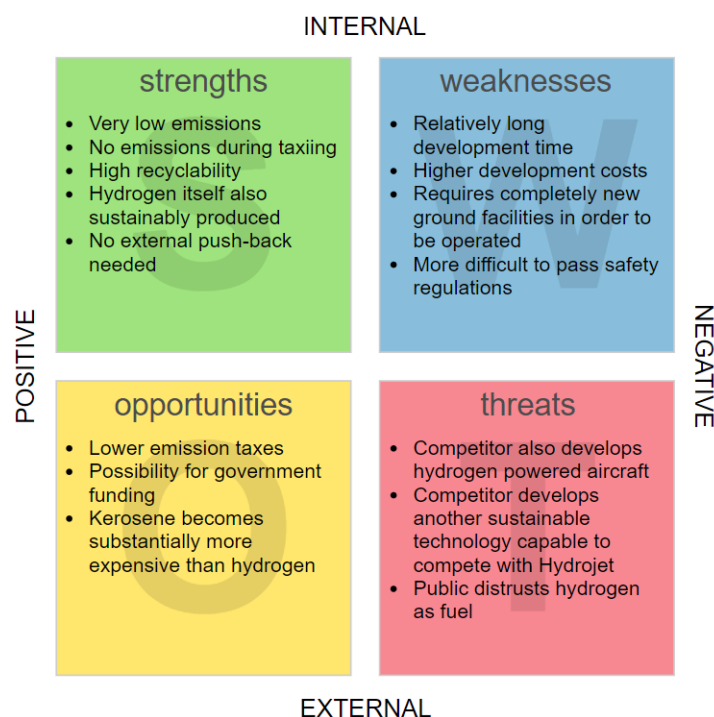- Public distrusts hydrogen as fuel

EXTERNAL

Figure 12.2: SWOT analysis for the marketability of the Hydrojet

of €119.6 was found.

Table 12.4: The competitive price estimation for the Hydrojet based on the weighted average of five reference aircraft [2]

Aircraft	PAX [-]	Unit Price [M€]	Cost per passenger [M€]	Unit cost for PAX 236 [M€]
A321-NEO (LR)	244 (33.3%)	118.7 (25%)	0.486 (25%)	114.7 (25%)
B737 MAX 10	230 (33.3%)	123.6 (25%)	0.537 (25%)	126.8 (25%)
A310-200	220 (33.3%)	107.3 (25%)	0.488 (25%)	115.1 (25%)
E195-E2	132 (0.0%)	55.8 (12.5%)	0.422 (12.5%)	99.8 (12.5%)
CRJ900	76 (0.0%)	44.4 (12.5%)	0.608 (12.5%)	143.5 (12.5%)
Weighted Average	232	99.9	0.506	**119.6**

The conclusion is that the Hydrojet will have a similar unit cost compared to its conventional competitors if the aircraft is sold at the competitive price. However, if the Hydrojet is slightly more expensive, it will still be purchased by the airlines due to the added value of the design.

12.3.4. Competition and Magnitude Aviation Market

Boeing and Airbus are market leaders when it comes to civil aircraft sales. In 2018 they produced 806 and 800 aircraft respectively. In 2019, due to the B737 MAX issue, Boeing only produced 345 aircraft in 2019 in contrast with the 863 aircraft delivered by Airbus.[5] A big airline like KLM solely already bought 64 aircraft between 2015 and 2019. This only shows the amount of aircraft sold and the potential of the Hydrojet[6]. In order to find a good estimation on how many Hydrojets could be sold the future market will have to be investigated on.

First of all it will be most likely that the bigger airlines will lease the Hydrojets as they have the most money and resources to invest in the change to hydrogen powered aircraft. Of these airlines the budget airlines will most likely not be interested except for if the Hydrojet offers much lower operational costs. The Hydrojet's operational costs will be comparable to conventional aircraft. Smaller airlines with no real home country have difficulties to survive due to COVID-19 and will probably not focus on sustainability the next few years. The bigger airlines that will most likely receive government grants will actually have to reduce CO_2. For KLM the exact values of this reduction are not published. However for Air France the emissions will have to

---

[5]https://www.forbes.com/sites/greatspeculations/2020/01/06/how-airbus-has-grown-over-the-years-to-dethrone-boeing-as-the-largest-com #518fbbd43a59 [accessed on 17 June 2020]

[6]https://www.klm.com/travel/nl_en/images/KLM-Jaarverslag-2019_tcm542-1063986.pdf [accessed on 17 June 2020]

Table 12.5: List of suitable customers with their fleet size

Airline	Number medium range aircraft
KLM	100
Air France	184
Lufthansa	193
Swiss Air	69
British Airways	187
Austrian Air	58
Transavia	79
Total	**870**

Table 12.6: Table of sale opportunities for different future aviation industry situations by 2030

Emission Reduction / Industry Growth	10 %	20 %	30 %
1 %	415	350	267
2 %	445	375	286
3 %	476	402	306
4 %	509	430	328
5 %	545	**460**	350
6 %	582	491	374

be reduced with 50 % in 2030 compared to 2005[7]. This number of 50 % in 2030 is asked of more airlines in other countries including Austrian Air[8]. Some simplifications should now be made with regards to how many emission free aircraft are needed in several cases. In case of no reduction in emissions for kerosene powered aircraft up to a reduction of 30 %. First, a list is made of airlines that will likely have to reach this 50 % goal and the current size of their fleet. This list can be found in Table 12.5. Alitalia is also receiving government grants, however they will significantly reduce the fleet in the next few years and are just trying to stay in business[9].

The airlines that will most likely be interested in the Hydrojet together have 870 aircraft with a range between 3000 and 7000 km in their fleet. For this analysis it is assumed that the fleets could have different efficiencies in the future ranging from 10 % to 30 %.[10] Furthermore aviation is expected to be at the same level as before COVID-19 in 2023[11]. It is assumed that aviation would grow with about 4.9 % if COVID-19 did not happen. A range of growth rates is suggested ranging from 1 % to 6 % per year within the aviation industry after 2023. 6 % might be optimistic, however this growth rate will only happen after 2023. Until 2023 no growth is assumed so potentially the growth could be explosive after COVID-19. This growth will directly be shown in growth of aircraft. Furthermore it is assumed that the 50 % will only be accomplished for medium haul aircraft. CO_2 emission of long haul aircraft, which is not the area of the Hydrojet, will not be regarded for the emission count. From these assumptions the calculation of potential sales for each situation is shown and can be found in Table 12.6. The most likely situation with a growth of 5 % and an increase in efficiency of 20 % 460 zero emission aircraft could be sold by 2030.

In Europe the concerns for emissions are bigger than in other parts of the world. However it could be useful to investigate other markets like Asia, Australia and North America. Asia seems to be the least interesting market to the Hydrojet. In Asia concerns for climate change are not high and airlines are mostly interested in growth. It is therefore not considered in this sale opportunity analysis as a possible costumer[12]. With regards to the Australian market. Qantas is being helped by the government during COVID-19. They currently have a fleet of 108 medium ranged aircraft. Furthermore Qantas have set goals for sustainability with the most important one to cut emission by 50 % in 2050[13]. This is not as strict as the deadline of 2030 set by the European airlines. Furthermore Qantas is trying to accomplish this by cleaner fuel however this is a debated method. Therefore Qantas could definitely be a potential costumer. In the United States American Airlines, United Airlines and Delta Airlines have set a similar goal as Qantas. American Airlines has a medium range fleet of 760, United airline 586, and Delta Airlines 605 aircraft, which is bigger than the European market. In this analysis it was estimated that all these airlines will try to reduce the emission by 25 % in 2030. in order to work to their goal of 50 % in 2050. Using the same calculation as in Europe but instead with 25 % of the market in the USA and Australia for emission free aircraft will be another 176 aircraft.

[7] https://www.parool.nl/nederland/vraagtekens-rond-nederlands-steunpakket-voor-klm~b435f44e/?referer=https%3A%2F%2Fwww.google.com%2F [accessed on 18 June 2020]

[8] https://www.flightglobal.com/airlines/lufthansa-secures-600-million-state-aid-package-for-austrian/138737.article [accessed on 18 June 2020]

[9] https://www.leadersleague.com/en/news/italian-government-to-take-full-control-of-alitalia-in-june [accessed on 18 June 2020]

[10] https://www.cleansky.eu/free-radical-innovative-configurations-and-propulsive-concepts-for-the-2030s [accessed on 22 June 2020]

[11] https://www.trouw.nl/economie/schipholbaas-pas-in-2023-weer-maximaal-aantal-vluchten~b5ed111b/?referer=https%3A%2F%2Fwww.google.com%2F [accessed on 18 June 2020]

[12] https://www.latimes.com/business/story/2019-07-22/column-flight-shaming-wont-work-in-asia-to-cut-carbon-emissions [accessed on 19 June 2020]

[13] https://www.qantas.com/infodetail/about/environment/our-commitment-to-environmental-sustainability.pdf [accessed on 19 June 2020]

12.3.5. Hydrojet Market Share within Sustainable Aviation

To reduce the emissions that airlines and aircraft are creating, one can choose between four solutions. Firstly, you can increase the operational efficiency aspect of aviation. This includes a greener manufacturing, optimised air traffic management and more efficient ground operations. Secondly, reduced fuel burning by designing more efficient engines. Thirdly, innovative aircraft and engine designs. Lastly, alternative fuels that are eliminating particular emissions.[128]

Research and development is continuously performed by multiple companies in these different areas to find the best and optimal solution. Therefore they can all be identified as possible competitors for the Hydrojet. As the previous section already assumed an additional increase of 10 - 30 % for the first and second solution in the coming years, these competitors can be neglected. In other words the Hydrojet market share will depend on the dominance of competitors designing innovative aircraft using alternative fuels.

Creating a forecast market share diagram with all different fuels used in aviation is quite complex as it is influenced by several parameters. The amount of fuel that can be used depends on the production rate, international supply chain, total price per kg of fuel and feasibility. An first forecast estimation for 2025 is provided in Table 12.7.[14] Biofuel in aviation is already used nowadays and tends to grow over the years. Enough initiatives are taken the last year to enlarge the production and supply chain. Electrical power is a good alternative with a high potential but current technology is not yet ready to dominate the market. Hydrogen and hybrid models are also very promising solutions. There shares are estimated to be 14 % and 60 % respectively. The share of hydrogen is further divided over fuel cells and combustion. This former performs the best on small range aircraft, the latter best on medium and long range aircraft. Follows the GMF of Airbus the market will consist out of 60% medium range aircraft and 40% small range aircraft when neglecting the long range. Adopted these fractions over the market share results in the given values.

Table 12.7: Market share of alternative fuels within sustainable aviation

Alternative Aviation Fuels:	
Fuel	**Percentage**
Biofuel	25 %
Battery electric	1 %
Hybrid Electric	14 %
Hydrogen Combustion	36 %
Hydrogen Fuel Cell	24 %

From this table follows that within the sustainable aviation, a market share of **36%** can be obtained.[128] The last element that needs to be analysed now, is the competitors withing this branch. Hydrojet is not the only company creating such an aircraft and thus competition within this branch will cause the market share to be distributed once more.

12.3.6. Exploring Other Markets

Once the Hydrojet has been developed and it is in operational use, a lot of knowledge in and experience within hydrogen technology will be available. Specifically knowledge in hydrogen based transport vehicles, hydrogen production and hydrogen storage can be adopted to a variety of different markets and even be used for mass production. Namely, the introduction of such revolutionary technologies is only possible for low volume production lines, like for the Hydrojet. However, when these technologies have been developed, many opportunities arise for market expansion, which will be discussed in this subsection. Apart from hydrogen, the nose wheel motor technology can be sold to different aircraft manufacturers or airlines.

First of all, Hydrojet is planning to expand to the low budget aviation sector once the price of green hydrogen is below the price of kerosene. Since more and more green hydrogen is expected to be produced in the near future, partly by Hydrojet themselves, the price is expected to go down. At the same time, the price of kerosene or fossil fuels in general, will go up due to the finite nature of these fuels. To add to that, it is likely that governing bodies will raise the taxes on fossil based fuels in order to meet with the 2015 Paris climate accord. CNBC[15] even claims that "increasing the price of carbon is the most efficient and powerful method of combating global warming and reducing air pollution" as presented by the International Monetary Fund. As a result, the budget airlines will have an economic incentive to purchase the Hydrojet too.

Secondly, the ground transportation sector is also steadily adopting hydrogen powered vehicles. However, the automotive

---

[14]`https://www.easa.europa.eu/eaer/topics/sustainable-aviation-fuels/sustainable-aviation-fuel-overview` [accessed on 19 June 2020]

[15]`https://www.cnbc.com/2019/10/10/carbon-tax-most-powerful-way-to-combat-climate-change-imf.html` [accessed on 19 June 2020]

industry has not committed to hydrogen yet since the infrastructure is not present. The company Nikola[16] is convinced that "hydrogen power makes a ton more sense in a commercial application" and is thus rolling out a plan to build up the infrastructure, starting with hydrogen trucks. This is a clever strategy because "many commercial trucking routes run point to point" and hydrogen stations can be placed accordingly. Hydrojet would be able to support the buildup of these hydrogen stations and the development of the hydrogen tanks that are needed onboard of the vehicles. The company Nikola is worth $26.4 billion[17] at this moment. Thus, the future of hydrogen powered automobiles looks bright.

Hydrojet could potentially enter the commodity sector too. Hydrogen is widely used within industries already, since hydrogen is required for many different production processes. But 95 % of this hydrogen is unfortunately grey[18]. Besides that, sectors exist that are difficult to decarbonise, such as the production of steel, cement and chemicals or just heating in general, and heavy-duty trucking. This is the case since, for instance for steel production, really high temperatures are required that cannot be achieved with electricity[18] . Hydrogen is able to provide these high temperatures due to its high flame temperature. This means that these sectors can be decarbonised if the price of green hydrogen goes below that of fossil fuels and grey hydrogen. Wood Mackenzie's recent analysis[19] suggests that "green hydrogen could reach parity in Australia, Germany and Japan by 2030", meaning that green hydrogen will be as inexpensive as grey hydrogen. Additionally, it was stated that hydrogen can be used to tackle the intermittency of renewable energy forms: solar power peaks during the day and wind power when it is windy, but peak power is required in the evenings. By producing hydrogen with the excess of green electricity and by consuming it during peak hours, the available renewable energy is flattened out over time. Wood Mackenzie estimates that US$365 million has already been invested in the green hydrogen sector globally. Therefore, it is clear that Hydrojet without a doubt, has many financially interesting sectors to expand to when it comes down to the production and bulk storage of green hydrogen.

Lastly, the nosewheel motor technology will be interesting to many aircraft manufacturers and airlines once it has been developed and its benefits have been shown. Namely, the nosewheel motor will decrease the turnaround time by eliminating pushback and will reduce the fuel consumption and emissions during taxi. Also, airlines will be less dependent on airport facilities by removing the risk of a delay in the flight schedule, due to a pushback tractor being unavailable or late. In Section 12.4 will be explained that this system will be developed together with a partner, which means that both Hydrojet and the partner will have a share in the profit.

To conclude, after the Hydrojet has been developed and has become operational, the number of markets that Hydrojet can expand to, are endless. This is the direct result of the knowledge, experience and technologies gained from the project. Hydrogen will be part of the future and investors are interested in this sustainable energy form. As a result, the development cost of the Hydrojet can be spread over different markets, lowering the risk for investors. However, to be able to properly estimate the revenue and profit that can be gained, further research is still necessary.

12.4. Return on Investment

Now that the costs associated with the Hydrojet have been estimated and the market has been analysed, the return on investment (ROI) can be assessed. First, the profitability can be estimated, which shows how much can be earned with the sale of the Hydrojet. Furthermore, ways to increase the profitability and decrease the risks associated with developing the Hydrojet are assessed with a business model and the discussion of potential development partners.

12.4.1. Break Even Point and Profitability

The development cost for the Hydrojet has been approximated as well as the production cost per aircraft. These are the two main costs associated with the sale of the Hydrojet. The next step is to calculate the ROI, which is the profit made after all the sold Hydrojets are delivered. From the market analysis an amount of 228 potential sales was estimated. Together with a development cost of 4214.68 M€ and production cost of 108.6 M€ per aircraft a spreadsheet has been constructed.

In Table 12.8 a summary is given of this spreadsheet. It shows the estimated financial state of the project at the end of each year until 2030. This estimation includes an overview of the investments needed and also the costs that come with the project. The bottom row shows if the project as a whole made a profit or not at the end of the that year. The bottom right cell shows the total profit of the project in million Euros. This factor will provide an answer to the question: Is the project profitable? There is one parameter that could affect the table at this point in the analysis. That will be the unit price of the

---

[16]https://www.pv-magazine.com/2019/11/15/green-hydrogen-to-reach-cost-parity-by-2030/ [accessed on 19 June 2020]

[17]https://www.quotenet.nl/zakelijk/a32856605/flikt-nikola-motor-company-hetzelfde-kunstje-als-tesla/ [accessed on 19 June 2020]

[18]https://www.rechargenews.com/transition/-world-first-as-hydrogen-used-to-power-commercial-steel-production/2-1-799308 [accessed on 19 June 2020]

[19]https://www.pv-magazine.com/2019/11/15/green-hydrogen-to-reach-cost-parity-by-2030/ [accessed on 19 June 2020]

aircraft. It will increase the profit at first, however it will also decrease the amount of aircraft sold. For every price there is a so-called Break-Even Point (BEP). This is the amount of aircraft that should at least be sold to make profit. In case of a selling price of 120 M€ the BEP is 417 aircraft. In case of a price of 130 M€ which is a bit higher than the current competitive price the BEP point is at 222 aircraft. Which means that with a total sale of 228 aircraft the profit of the project will be 131 M€. This seems quite low however the amount of sales is a very low estimate and it does not take into account any contributions from government funds for sustainable aviation which could be very feasible for the project. Furthermore, the option of reducing cost using partners will be addressed later.

Table 12.8: Return on Investment calculation

	2020	**2021**	**2022**	**2023**	**2024**	**2025**	**2026**	**2027**	**2028**	**2029**	**2030**
Aircraft Sales	0	0	0	0	0	80	46	46	46	10	0
Aircraft Produced	0	0	0	0	2	2	45	45	45	45	44
Production Cost [M€]	0	0	0	0	-217	-217	-4886	-4886	-4886	-4886	-4777
Development Cost[M€]	-500	-1000	-1000	-1514	-100	-100	0	0	0	0	0
Interest over Loans[M€]	0	-20	-60	-103	-168	187	0	0	0	0	0
Turnover[M€]	0	0	0	0	0	10400	5980	5980	5980	1300	0
Total Per Year[M€]	-500	-1020	-1060	-1617	-485	9895	1094	1094	1094	-3586	-4777
Accumulated Profit[M€]	-500	-1520	-2580	-4198	-4683	5212	6306	7400	8494	4908	**131**

12.4.2. Business Model
Due to the demand by both airlines and consumers for sustainable air travel, the Hydrojet can be marketed to high-end airlines with a higher price than its conventional kerosene powered competitors. Airlines will be willing to pay more for the Hydrojet to reach their emission goals and consumers will pay a higher ticket price to lower their contribution to climate change. Later on, when the development costs have been covered by the sales and more direct competitors to the Hydrojet come on the market the unit price can be decreased, which expands the market to budget airlines and smaller airlines.

For airlines an alternative to buying an aircraft is leasing one. This is an option for small airlines that cannot afford to buy an aircraft outright or for airlines that want to expand their fleet for a short time. With aircraft leasing, a distinction is made between dry and wet leasing. With dry leasing the aircraft is delivered without providing fuel, flight crew and maintenance, while wet leasing means that the aircraft is provided with fuel, flight crew and maintenance. Leasing Hydrojets to small airlines could expand the market beyond airlines like KLM or Lufthansa. Wet leasing may be more profitable because the fuel can already be delivered from the hydrogen production facilities. Airlines that need time to train their pilots, due to the unconventional nature of the Hydrojet, can also profit from such an arrangement.

12.4.3. Partners
Subsection 12.3.6 explained that the development costs can be spread over different markets, lowering the investment risk for the long term. In order to reduce the costs of the aircraft for the short term, Hydrojet can partner up with other companies for the development and manufacturing of several subsystems, spreading the investment risks. Partnering up could increase the profits in the long term as it would reduce both the development cost and the manufacturing cost.

One subsystem that could be developed in collaboration with another company is the propulsion system. Aircraft manufacturers usually do not design their engines by themselves but order them from companies that specialise in aircraft engines. Some of these companies are: Rolls-Royce, Pratt & Whitney and General Electric. Existing turbofans made by one of these manufacturers could be modified for the use of hydrogen fuel.

Several systems like the motorised nosewheel have already been developed by other companies. One of these systems is the EGTS by Safran and Honeywell, which incorporates electric motors in the main landing gear. These motors are powered by the APU and enable the aircraft to taxi and pushback without the use of the main engines[20]. Another system which is more closely related to the one used in the Hydrojet is the WheelTug. This system consists of electric motors in the nose landing gear, which are also powered by the APU[21]. Both these systems could be incorporated into the Hydrojet.

The Hydrojet's APU, which powers these electric motors, is a hydrogen fuel cell. This fuel cell is an important part of the design and its development and manufacturing could be done in collaboration with the company Intelligent Energy. This company develops hydrogen fuel cells that are used in the automotive industry and to power Unmanned Aerial Vehicles (UAVs)[22].

---
[20]https://www.safran-landing-systems.com/sites/nmbd/files/egts_flyer.pdf [accessed on 19 June 2020]
[21]https://airportsinternational.keypublishing.com/2010/06/21/wheeltug/5420/ [accessed on 19 June 2020]
[22]https://www.intelligent-energy.com/our-products/product-information/ [accessed on 20 June 2020]

13
Compliance Matrix

In this chapter, an overview is given of the requirements that have been met or not. Therefore, this chapter is essential in order to determine the feasibility of the Hydrojet final design. It shows how the subsystem designs, which are the direct result of the subsystem requirements, are integrated together to comply with the top level requirements. This overview is presented in the compliance matrix, see Table 13.1, and incorporates the most important requirements on a system level. A (✓) indicates that the requirement is met by the final design, a (~) means that (further) research is necessary in order to proof compliance and a (X) means that the requirement cannot be met with the current design.

13.1. Compliance with Technical Requirements
To see if the technical requirements are met, a compliance matrix 13.1 is constructed.

Table 13.1: Requirement Compliance Matrix

Requirement ID	Requirement	Compliance	Relevant section(s) and notes
HPRA-STK-SUS-1	The aircraft shall emit zero emissions, except for water during operation.	✓	Chapter 11
HPRA-STK-SUS-2	The aircraft shall be 90% (weight fraction) recyclable.	✓	Chapter 11
HPRA-STK-PERF-1	The range of the aircraft shall be sufficient to fly between any two airports in the European Common Aviation Area.	✓	Subsection 4.2.5
HPRA-STK-PERF-2	Flight times of the aircraft shall be comparable with existing commercial aviation.	✓	Subsection 4.2.2
HPRA-STK-ENBU-1	The aircraft shall be able to carry 236 passengers and their luggage.	✓	Section 5.2
HPRA-STK-ENBU-2	The aircraft shall have a minimum lifetime of 25 years.	~	
HPRA-STK-ENBU-3	The ground hydrogen storage facility shall be suitable to service a fleet of 10 aircraft.	✓	Chapter 8
HPRA-STK-SR-1	The aircraft shall have a 50% availability including turnaround time and maintenance.	✓	Subsection 10.3.2
HPRA-STK-SR-2	The aircraft shall meet all European aviation standards.	~	Compliance with the most important CS-25 requirements has been shown.
HPRA-STK-SR-3	The aircraft shall have emergency procedures implemented for emergency hydrogen loss.	✓	Subsection 10.3.4
HPRA-STK-COS-2	The operational costs shall not exceed those of existing comparable commercial aviation.	✓	Chapter 9
PRA-STK-PAS-2	The propulsion system shall not be substantially louder than conventional propulsion systems.	✓	Subsection 7.3.7

HPRA-STK-RES-1	The noise produced by the aircraft shall not be of more harm than current aircraft to the residents in the vicinity of the airport.	✓	Subsection 7.3.7
HPRA-STK-APOR-1	The ground system required shall be implementable in the existing airport infrastructure.	✓	Chapter 8
HPRA-STK-APOR-2	The aircraft size shall not exceed the limits of the airport.	✓	Chapter 5
HPRA-STK-CREW-1	The work pressure during operation shall not be too straining on cabin personnel.	✓	Chapter 3: One crew member per thirty passengers
HPRA-STK-CREW-2	The aircraft shall be controllable by the pilots.	✓	Section 5.4
HPRA-STK-CREW-3	The cockpit shall have an engine information display.	✓	Section 9.3
HPRA-REQ-S&C-1	The aircraft shall be stable within all operational limits.	✓	Section 5.4

From the compliance matrix it is apparent that, at this stage, there are no top level requirements that cannot be met by the design. However, further research is still necessary for the HPRA-STK-ENBU-2 requirement: "the minimum lifetime of 25 years". This is because before anything sensible can be said about the lifetime of the actual aircraft, the Hydrojet must at least be in a later design phase, and preferably even have undergone some tests. It is expected, nonetheless, that since only the blended wing shape itself is relatively new, the lifetime of this aircraft will not vary substantially from that of a competitor - which indeed is around 25 years. Furthermore, the HPRA-STK-SR-2 requirement: "compliance with all European aviation standards" also needs further research in order to call the design fully feasible. This is because there are a lot of requirements coming from the European aviation standards that require actual testing, or for some other reason cannot be proven feasible at this stage of the design. It should be noted that those that could already be proven are indeed met. Concluding, apart from these two requirements, all major requirements on a system level are met and thereby the feasibility of this design is validated.

13.2. Compliance with Financial Requirements

It has already been proven that the Hydrojet is technically feasible, but the financial feasibility is just as important. For this reason, requirements for the operational and unit cost had been set from the beginning, alongside some other major requirements considering the aircraft manufacturing, which are all shown in Table 13.2.

Table 13.2: Requirement Compliance Matrix

Requirement ID	Requirement	Compliance	Relevant section(s) and notes
HPRA-REQ-COS-3	The maximum cost per available seat mile (CASM) shall not exceed €0.13.	✓	Subsection 12.3.1
HPRA-STK-COS-1	The aircraft shall have a maximum cost of €100 million.	X	Subsection 12.4.1

First of all, the Hydrojet CASM amounts 7.8 euro cents which is significantly below the requirement. The unit cost amounts 130 M€ and does therefore not meet with the requirement. However, further market analysis has shown that the competitive price for conventional aircraft lies around 119.6 M€ and due to the added value and in particular the high degree of sustainability of the Hydrojet, an even higher price can be expected to be competitive. Thus, it can be concluded that the Hydrojet is financially feasible in addition to being technically feasible. The aircraft has the potential to become a serious competitor on the aviation market. Hence, further research into the Hydrojet concept is recommended.

Now that everything is done for the detailed conceptual design phase and the compliance with the requirements has been checked, the next step would be to look at the future activities for the Hydrojet. First, future considerations on specific aspects of the project will be reflected upon in Section 14.1. After this, the project design and development logic will be elaborated in Section 14.2. Finally, a gantt chart is presented in for the post-DSE activities in Section 14.3.

14.1. Future Considerations

The current design detail of the Hydrojet is not yet at its deepest level. It is thus still possible to make changes and improvements on a relatively high level to make sure the design is optimal and all calculations are sufficiently accurate. Some considerations for further development are described below.

14.1.1. Aerodynamics

In Section 5.3.4, it was stated that the wing was slightly over-designed: the design lift coefficient for cruise was slightly lower than the lift coefficient yielding max. L/D, meaning the surface area was too large. The consequence: 1.3 % extra drag at cruise. Over the lifetime of a Hydrojet, it will carry out approximately 31,000 flights, hence this 1.3 % extra fuel used will amount to significant costs that could be prevented. Therefore, the wing area needs to be iterated further. This can be done by tweaking the wing geometry such as span, taper ratio and chord lengths. When the target surface area is achieved, the whole design is iterated, and the aerodynamic analysis is done to find the new drag polar. Now the new lift coefficient yielding max. L/D is compared to the corrected design lift coefficient. And if the surface area is still over or under by too much, the iteration is performed again. Eventually the unnecessary drag drops below a certain threshold, finalising the wing design.

To have a bigger margin for fitting the cabin, cargo hold and fuel tanks, a different airfoil for the inner wing could be chosen. The second-best option from Table 5.1 is the LA 2573 A, which has a larger thickness that could come in handy, as well as a positive moment coefficient, removing the need of negative wing sweep. The only drawback is a lower $C_{L_{max}}$ which has implications for take-off and landing.

14.1.2. Fuel Tanks

The current tanks (seen in Figure 7.12) are shaped to follow the airfoil and the sweep while featuring a cross-section being as elliptical as possible. This leads to a more difficult thermal analysis which only yields results on a preliminary level. This was not desired. A much more detailed mechanical and thermal analysis has already been done before in [70], for general cylindrical tanks with ellipsoid end caps. As explained in Section 7.5, it is still considered possible to shape the tanks to make use of this research by altering the planform, yet the implications of this change are too extensive to handle in time. Therefore, this is a perfect iteration to perform in the future. Then the design of the tank is more detailed and reliable. If a more drastic design change for the tank is desired, integrated tanks can be considered. These have the advantage of saving lots of weight, and thus fuel volume, yielding a higher degree of freedom to fit the required amount of fuel inside the structure. Therefore, it might be worth considering this in the future. It should be noted that the challenges that result from this is the integration of the insulation for the tanks, and the corresponding high thermal gradient on the tanks, that are now part of the primary structure. For this reason, non-integrated tanks were used and are still considered the most feasible. Finally, safety precautions during refuelling with liquid hydrogen should be considered as it could be harmful to the maintenance crew.

14.1.3. Propulsion

The placement of the engines has not been exactly defined yet. It was qualitatively chosen to place them on top and at the back, to generate boundary layer ingestion (BLI) and thus increase the aerodynamics. In addition, the engines are compactly placed close to the fuselage, to minimise yaw and pitch moments in the case of one engine inoperative. However, to quantify these effects, the placement of these engines and the effects of BLI should be further investigated. The design of the pylons is also yet to happen, but was not considered to be crucial or in need of innovative design solutions.

14.1.4. Materials and Structures

The project has featured an extensive material selection based on numerous criteria such as specific strength, recyclability rate and fatigue resistance. The latter however has not been investigated specifically on the structure level. Now that it is known that in the design life of 25 years, about 31,000 flights will be made, meaning 31,000 loading-unloading cycles of the cabin. The

structural aspects such as a margin for cabin wall thickness due to fatigue over those cycles has to be analysed in more detail. In addition, a crack analysis is in order, as this poses another danger due to the cyclic loading. According to the crack analysis, a better view is obtained on the necessary frequency of maintenance for each Hydrojet. In addition, the current Hydrojet does not contain windows. Yet from a passenger comfort perspective, the presence of windows, or at least the ability to look outside, is quite important. If a more thorough structural analysis is performed and/or some alterations made, the inclusion of windows might become feasible, which will be beneficial for the acceptance of the Hydrojet by the general public.

14.2. Project Design & Development Logic

For the project design and development logic, the activities that will occur post-DSE are presented with a prospective timeline using a block diagram. These activities will aid to achieve the requirements to a greater extend. In Section 14.2.1, the three design phases of the Hydrojet post-DSE are presented. Then, in Section 14.2.2, the post design phases are explained.

14.2.1. Design Phases

There are three design phases for aircraft: the conceptual, preliminary and the detailed design. This DSE project will only complete the conceptual and preliminary design phase of the Hydrojet up to a certain degree, hence the preliminary and detailed design will be continued post-DSE.

Conceptual Design Phase: The conceptual design phase is the subject of this DSE project which has a duration of eleven weeks, however it usually takes around 9-12 months.[66] For the post-DSE continuation of the project, the conceptual design will continue until the end of the year. This is to ensure that the main components of the Hydrojet, can be correctly designed. Furthermore, a decision on the inclusion of new technology must be made. Whether to design the propulsion system in-house, or wait for the technology to become available to market. There does not exist a propulsion system with a high technological readiness level (TRL) for the Hydrojet that can be ready by 2021, due to the added complexities that arise when cryogenic hydrogen is used. Hence, a conceptual propulsion system will be designed in the conceptual design phase. For hydrogen storage systems, some systems have a high TRL [1,2], however, more research must be done on the recyclability of these systems. Once the conceptual design phase is finished, the preliminary design phase is started.[1]

Preliminary Design Phase: The preliminary design phase focuses on specifying the design concept at the system level, including some subsystem trade-off and typically takes around 12 to 16 months.[66] For a novel aircraft such as the Hydrojet, 2 years of preliminary design is taken. Most of the time is taken to finish the design and analyse the hydrogen propulsion and storage systems. In Figure 14.1, the main activities of the preliminary design are shown, followed by a logical order of the rest of the activities. For the preliminary design, the ground hydrogen facility, and some subsystems should be decided on. Based on the preliminary design, a go-ahead moment will be taken by management to decide whether to stop the project design or continue with full scale development. If the go ahead is given, the project continues with the Detailed design phase. This is also when the sales effort would start to begin selling the Hydrojet.[1]
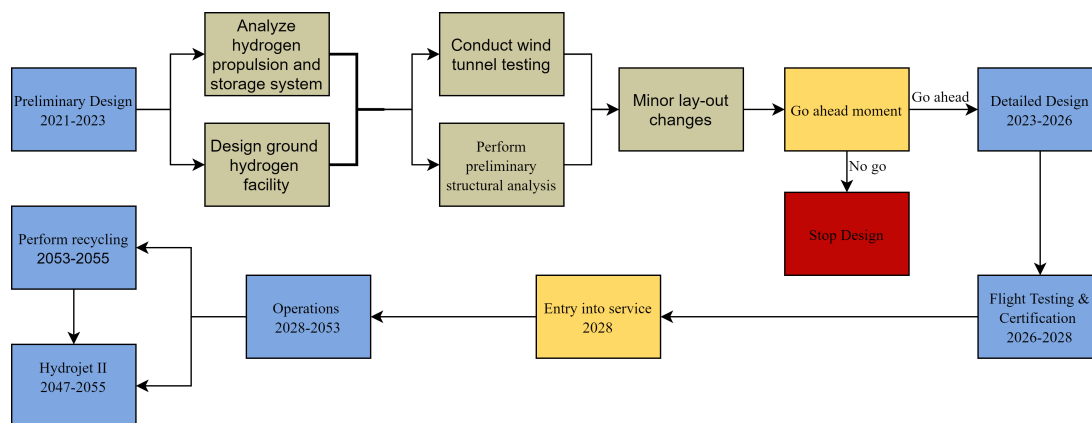

Figure 14.1: Preliminary design phase including other post-DSE phases, from [2]

Detailed Design Phase: In the detailed design phase, detailed part designs are completed. Parts will start to be fabricated and tests completed. This leads to the assembly of the aircraft with the first flight and certification.[129] In Figure 14.2, the activities for the detailed design phase are shown. The recycling tools are designed for use during manufacturing and end of life of the Hydrojet. The recyclable parts will be used for future sustainable aviation. For the Hydrojet, a minimum of 3 years

---

[1] https://www.hydrogen.energy.gov/pdfs/progress12/iv_e_5_ronnebro_2012.pdf[accessed on 19 May 2020]
[2] https://www.pnnl.gov/main/publications/external/technical_reports/PNNL-21473.pdf[accessed on 19 May 2020]

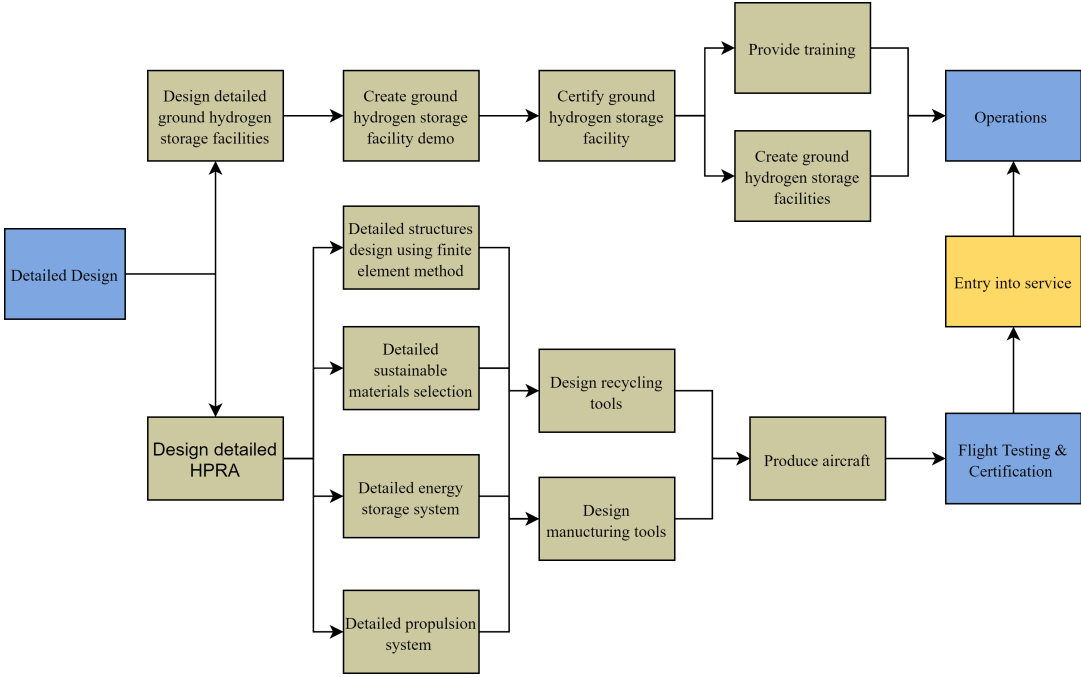of detailed design is taken, since the detailed design phase typically lasts between two and three years.[66]

Figure 14.2: Post-DSE detailed design phase of Hydrojet, from [2]

14.2.2. Post Design phases

As can be seen in Figure 14.3, after the detailed design, the flight test and certification phase is entered and this phase typically lasts one year. For the Hydrojet, two years are estimated for certification given that the novel propulsion system and hydrogen storage system is used and more flight tests and certification requirements will be required. Once the aircraft is assembled, ground testing of systems and structural strength testing is conducted in preparation for flight testing.[129] After this, the operations of the aircraft is started.[1]

Before reaching the end of the lifetime of the Hydrojet, a newer more sustainable version is designed, Hydrojet V2, which will make a point to use the parts and materials recycled from the original Hydrojet. As the Hydrojet reaches its end of life, it is returned to the manufacturer and recycled into the newer version, thus closing the loop.[1]

14.3. Project Gantt Chart

The project Gantt chart presents the post-DSE activities with their corresponding start and end date following from Figure 14.1.

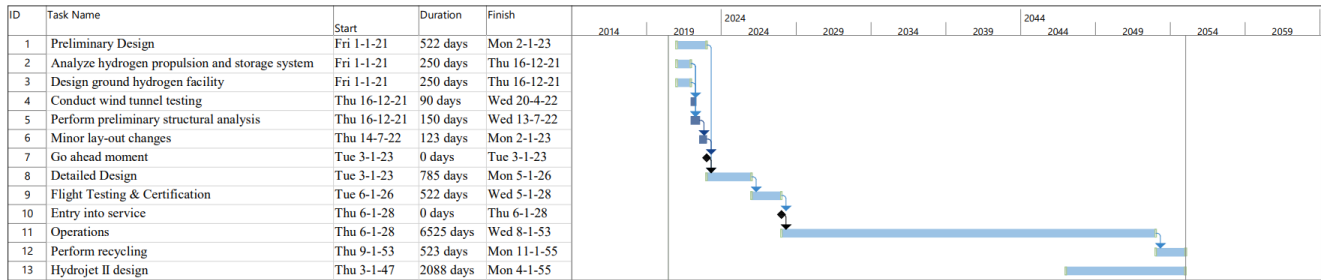| ID	Task Name	Start	Duration	Finish
1	Preliminary Design	Fri 1-1-21	522 days	Mon 2-1-23
2	Analyze hydrogen propulsion and storage system	Fri 1-1-21	250 days	Thu 16-12-21
3	Design ground hydrogen facility	Fri 1-1-21	250 days	Thu 16-12-21
4	Conduct wind tunnel testing	Thu 16-12-21	90 days	Wed 20-4-22
5	Perform preliminary structural analysis	Thu 16-12-21	150 days	Wed 13-7-22
6	Minor lay-out changes	Thu 14-7-22	123 days	Mon 2-1-23
7	Go ahead moment	Tue 3-1-23	0 days	Tue 3-1-23
8	Detailed Design	Tue 3-1-23	785 days	Mon 5-1-26
9	Flight Testing & Certification	Tue 6-1-26	522 days	Wed 5-1-28
10	Entry into service	Thu 6-1-28	0 days	Thu 6-1-28
11	Operations	Thu 6-1-28	6525 days	Wed 8-1-53
12	Perform recycling	Thu 9-1-53	523 days	Mon 11-1-55
13	Hydrojet II design	Thu 3-1-47	2088 days	Mon 4-1-55

Figure 14.3: Project Gantt Chart[2]

Conclusion

In this report, the feasibility of a hydrogen-fuelled, turbofan-powered, blended wing body aircraft has been investigated. This is done from an engineering perspective, but also from a sustainable and financial one. From the engineering standpoint, the Hydrojet has an overall feasible size and mass, with a span of 45 m, a length of 27 m and a MTOM of just over 92 metric tonnes. The main engineering challenges that had to be overcome are:

- Accommodating and insulating the 138.4 m^3 of liquid hydrogen at -252 °C, which was achieved by optimally using the space available in the blended wing planform and by placing two non-integral tanks with external insulation;

- Fitting 236 passengers, which was achieved by making the cabin shorter with 17 rows, yet wider with a maximum of 4 aisles yielding rows of 6x3 seats abreast, or 18 seats per row;

- Adapting a conventional turbofan to run on hydrogen without compromising for available power/thrust and efficiency, which was achieved by designing the combustion chamber accordingly, as well as using a heat exchanger that converts the liquid hydrogen to gaseous hydrogen at 150 K for the turbofan and 350 K for the fuel cell (both at a pressure of 3 bars);

- Designing an elliptical pressurised structure able to cope with the loads whilst fitting into the aerodynamic shape and accommodating the 236 passenger cabin, which was done by using 2 rather circular shells connected by a surrounding elliptical shell.

From the sustainable standpoint, the Hydrojet is very much feasible since that was the main purpose of its creation. It is 91.3 % recyclable (weight-wise), has no CO_2 emissions and lowers NO_x emissions by almost 97 % based on conventional passenger air travel. The hydrogen needed in order to power the Hydrojet, is produced in a sustainable way, using wind and solar power. It is required, however, that the necessary water is recycled from either seawater or other sources not acting as potable water. This latter has to be investigated further.

From the financial standpoint, the unit cost of one Hydrojet is €130 Million. This is 8 % more than the competitive price amongst conventional passenger aircraft with the same application, where the Hydrojet has additional value due to:

- 99.9 % total emission reduction (not including water vapour) compared to competitors;

- Security of fuel provision in a sustainable way;

- Competitive operational costs at a CASM of 7.8 euro cents;

- Increased fuel economy of at least 3.6 %, which can be increased even further by tailoring the payload-range combination of specific missions according to data obtained by the different airlines.

To conclude, the overall design of the Hydrojet and its accompanying ground facilities provide a small step for passenger air travel, but a giant leap towards long-term sustainable aviation.

Bibliography

[1] DSE Group 02. Midterm report hydrogen powered regional aircraft. Technical report, TU Delft, 2020.

[2] DSE Group 02. Baseline report hydrogen powered regional aircraft. Technical report, TU Delft, 2020.

[3] J.A. Melkert, R. Vos, and B.T.C. Zandbergen. Aerospace design & system engineering, 2020.

[4] D. Howe. Blended wing body airframe mass prediction. *Proceedings of the Institution of Mechanical Engineers, Part G: Journal of Aerospace Engineering*, 215(6):319–331, 2001.

[5] M. Brown. Conceptual design of blended wing body airliners within a semi-automated design framework. Master's thesis, Delft University of Technology, 2017.

[6] P. Okonkwo. *Conceptual design methodology for blended wing body aircraft*. PhD thesis, Cranfield University, 2016.

[7] Dr. F. Oliviero. Aerospace design & system engineering elements II: Aircraft aerodynamic analysis - lift & drag, 2019.

[8] B.V.S. Jyoti E. Gill, F. Oliviero and A. Cervone. System engineering & aerospace design, 2020.

[9] M. Brown and R. Vos. Conceptual design and evaluation of blended-wing-body aircraft. Technical report, TU Delft, 2018.

[10] D. Scholz. A student project of a blended wing body aircraft – from conceptual design to flight testing. Technical report, Hamburg University of Applied Sciences, 2007.

[11] D. P. Raymer. *Aircraft design: a conceptual approach*. American Institute of Aeronautics and Astronautics, 2006.

[12] W.A. Timmer, D. van Helvoort, and C. Kassapoglou. AE2111-I Systems Design: Reader – Aircraft Work Packages 4 & 5, 2018.

[13] M.T.H. Brown. Conceptual design of blended wing body airliners within a semi-automated design framework. Technical report, Delft University of Technology, 2017.

[14] Z. Berdowski. Survey on standard weights of passengers and baggage. Technical report, EASA, 2009.

[15] International Civil Aviation Organization. Tenth session of the statistics division: Available capacity and average passenger mass, 2009.

[16] D. Verstraete. The potential of liquid hydrogen for long range aircraft propulsion. Master's thesis, School of Engineering Cranfield University, 2009.

[17] R. Brar. Design of a blended wing body aircraft. Technical report, The Faculty of the Department of Aerospace Engineering San Jose State University, 2014.

[18] A. Baig, T. Cheema, Z. Aslam, Y. Khan, and H. Dar. A new methodology for aerodynamic design and analysis of a small scale blended wing body. *Journal of Aeronautics & Aerospace Engineering*, 07, 2018.

[19] S. Paudel, S. Rana, S. Ghimire, K. Subedi, and S. Bhattrai. Aerodynamic and stability analysis of blended wing body aircraft. *International Journal of Mechanical Engineering and Applications.*, 4(4):143 – 152, 2016.

[20] J. D. Anderson. *Introduction to Flight Eighth Edition*. McGraw-Hill Education, 2016.

[21] Dr. F. Oliviero. Aerospace Design & System Engineering Elements II: Aircraft Aerodynamic Analysis - Mobile Surfaces on the Wing, 2019.

[22] J. D. Anderson. *Fundamentals of Aerodynamics*. McGraw-Hill Education, 2011.

[23] Dr. F. Oliviero. Aerospace Design & System Engineering Elements II: Aircraft Aerodynamic Analysis - Software and Tools, 2019.

[24] P. Kumar and A. Khalid. Blended wing body propulsion system design. Technical report, Embry-Riddle Aeronautical University, 2017.

[25] D. Scholz and M. Nita. Estimating the oswald efficiency factor from basic aircraft geometrical parameters. Technical report, Hamburg University of Applied Sciences, 2012.

[26] J.A. Mulder, W.H.J.J. van Staveren, J.C. van der Vaart, E. de Weerdt, C.C. de Visser, A.C. in 't Veld, and E. Mooij. *Flight Dynamics Lecture Notes*. Delft University of Technology, 2020.

[27] M. H. Sadraey. *Aircraft Design: A Systems Engineering Approach*. John Wiley & Sons, 2013.

[28] J. van Dommelen and R. Vos. Conceptual design and analysis of blended-wing-body aircraft. *Proceedings of the Institution of Mechanical Engineers, Part G: Journal of Aerospace Engineering*, 228:2452–2474, 10 2014.

[29] M. Sargeant, T. Hynes, W. Graham, J. Hileman, M. Drela, and Z. Spakovszky. Stability of hybrid-wing–body-type aircraft with centerbody leading-edge carving. *Journal of Aircraft*, 47:970–974, 05 2010.

[30] L. V. Schmidt. *Introduction to Aircraft Flight Dynamics*. American Institute of Aeronautics and Astronautics, 2012.

[31] J. Roskam. *Airplane Design Part V: Component Weight Estimation*. DARcorporation, 2004.

[32] T. H. G. Megson. *Aircraft Structures for Engineering Students*. Elsevier Science & Technology, 2016.

[33] R. Kaur and Ambri. Spars and stringers- function and designing. *International Journal of Aerospace and Mechanical Engineering*, 1:59–60, 10 2014.

[34] R. Vos, F.J.J.M.M. Geuskens, and M.F.M. Hoogreef. A New Structural Design Concept for Blended Wing Body Cabins. In *53rd AIAA/ASME/ASCE/AHS/ASC Structures, Structural Dynamics and Materials Conference*, 2012.

[35] Y. Pan, Z. Hu, Y. Xiong, and J. He. Optimization Design of Keel Beam for CJ828 Structure.

[36] Z. Mikulik and P. Haase. CODAMEIN Composite Damage Metrics and Inspection. Technical report, Bishop GmbH - Aeronautical Engineers, 2012.

[37] S. Chintapalli, M.S.A. Elsayed, R. Sedaghati, and M. Abdo. The development of a preliminary structural design optimization method of an aircraft wing-box skin-stringer panels. *Aerospace Science and Technology*, 2010.

[38] J. Roskam. *Aircraft Landing Gear Design:Principles and Practices*. DARcorporation, 1989.

[39] N. S. Currey. *Airplane design Part IV: Layout Design of Landing Gear and Systems*. American Institute of Aeronautics and Astronautics, Inc., 1988.

[40] N.C. Heerens. Landing gear design in an automated design environment. Master's thesis, Delft University of Technology, 2014.

[41] T. Ikeda. Aerodynamic analysis of a blended-wing-body aircraft configuration. Master's thesis, RMIT University, 2006.

[42] A. Isikveren. *More-electric aircraft*. Emerald Group Publishing Limited, 2005.

[43] S. Chien Tan. Electrically assisted propulsion and power systems for short-range missions. Master's thesis, Delft University of Technology, 2018.

[44] ICAO. Aerodrome standards, operations and design. Technical report, 1999.

[45] M. Zhang. Multi-objective optimization of aircraft taxiing on the airport surface with consideration to taxiing conflicts and the airport environment. *Sustainability*, 2019.

[46] N. E. Daidzic. Determination of taxiing resistances for transport category airplane tractive propulsion. Technical report, AAR Aerospace Consulting, 2017.

[47] M. Pourbagian. *Aero-thermal optimization of in-flight electro-thermal ice protection systems in transient de-icing mode.* 2015.

[48] S. Xue and W. Ng. Turbine blade tip external cooling technologies. *MDPI Aerospace*, 2018.

[49] J.C. Han. Turbine blade film cooling using psp technique. Technical report, 2010.

[50] L. Wright J. Chin Han. Enhanced internal cooling of turbine blades and vanes. Technical report, 2005.

[51] L.M. Das. Exhaust Emission Characterization of Hydrogen-operated Engine System: Nature of Pollutants and Their Control Techniques. *International Journal Hydrogen Energy*, 16, 1991.

[52] I. Martinez. Aircraft environmental control. Technical report, 2007.

[53] F. M. Mirpuri. Turbofan engine optimization for low NOx emissions. Master's thesis, Técnico Lisboa, 2016.

[54] A. Gangoli Rao. Performance analysis of an aero engine with interstage turbine burner. Technical report, Delft University of Technology.

[55] A. Gangoli Rao. A hybrid engine concept for multi-fuel blended wing body. Technical report, Delft University of Technology, 2017.

[56] A. Gangoli Rao. Appu: Gas turbines and combustion tutorial, 2016.

[57] G. Huang, X. Xiang, C. Xia, W. Lu, and L. Li. Feasible Concept of an Air-Driven Fan with a Tip Turbine for a High-Bypass Propulsion System. *Energies*, 2018.

[58] B.G. Mckay and A. Barlow. The UltraFan Engine and Aircraft Based Thrust Reversing. 2012.

[59] J.A. Melkert. AE2230-II Propulsion and Power: Lecture 5: Real Cycles, 2020.

[60] C. John Marek. Low emission hydrogen combustors for gas turbines using ldi. Technical report, NASA Glenn research center, 2005.

[61] E.M. Greitzer, D.K. Hall, J.A. Pertuze, J.S. Hollman, and D. Kordonowy. N+3 Aircraft Concept Designs and Trade Studies, Final Report. Technical report, National Aeronautics and Space Administration, 2010.

[62] M.A. York. Turbofan Engine Sizing and Tradeoff Analysis via Signomial Programming. *Journal of Aircraft*, 2017.

[63] U. Schumann. The impact of nitrogen oxides emissions from aircraft upon the atmosphere at flight altitudes–results from the aeronox project. *Atmospheric Environment*, 31, 1997.

[64] A. Hasselrot F. Haglind and R. Singh. Potential of reducing the environmental impact of aviation by using liquid hydrogen. 2006.

[65] M. Gorji-Bandpy and M. Azimi. Technologies for jet noise reduction in turbofan engines. *Aviation*, 2013.

[66] E. Torenbeek. *Advanced aircraft design: conceptual design, technology and optimization of subsonic civil airplanes.* John Wiley & Sons, 2013.

[67] N.H. Saiyed, Mikkelsen, and J.E. K.L., Bridges. Acoustics and Thrust of Separate-Flow Exhaust Nozzles With Mixing Devices for High-Bypass-Ratio Engines. In *6th Aeroacoustics Conference and Exhibit*, 2000.

[68] S. C. Tan. Electrically assisted propulsion & power systems for short-range missions. Master's thesis, TU Delft; NLR, 2014.

[69] A. L. Dicks and D. A. J. Rand. Fuel cell systems explained (3rd edition), 2018.

[70] C. Winnefeld, T. Kadyk, B. Bensmann, U. Krewer, and R. Hanke-Rauschenbach. Modelling and designing cryogenic hydrogen tanks for future aircraft applications. *Energies - MDPI*, 2018.

[71] K. R. Robinson and C. P. Whitener. Cryogenic tank and aircraft structural interface. Technical report, United States Patents, 1975.

[72] A. Colozza and L. Kohout. Hydrogen storage for aircraft applications overview. Technical report, National Aeronautics and Space Administration, 10 2002.

[73] F. M. Anthony, J. Z Colt, and R. G. Helenbrook. Development and validation of cryogenic foam insulation for LH2 subsonic transports. Technical report, National Aeronautics and Space Administration, 1981.

[74] A. Zielinski. Hydrogen-assisted degradation of some non-ferrous metals and alloys. *Journal of Materials Processing Technology*, 109(1):206 − 214, 2001.

[75] G. D. Brewer. *Hydrogen aircraft technology*. CRC Press, 1991.

[76] D. R. Askeland and W. J. Wright. *The science and engineering of materials*. Cengage Learning, 2016.

[77] *BPVC 2010 - Section VIII, Division 1: Rules for Construction of Pressure Vessels*. ASME, 2020.

[78] S. M. Aceves, F. Espinosa-Loza, E. Ledesma-Orozco, T. O. Ross, A. H. Weisberg, T. C. Brunner, and O. Kircher. High-density automotive hydrogen storage with cryogenic capable pressure vessels. *International Journal of Hydrogen Energy*, 35(3):1219 − 1226, 2010.

[79] PowerCell MS-100 Datasheet, 2020.

[80] H. Barthelemy, M. Weber, and F. Barbier. Hydrogen storage: Recent improvements and industrial perspectives. *International Journal of Hydrogen Energy*, 42(11):7254 − 7262, 2017. Special issue on The 6th International Conference on Hydrogen Safety (ICHS 2015), 19-21 October 2015, Yokohama, Japan.

[81] J. Larminie and A. Dicks. *Fuel Cell Systems Explained*, chapter 8.9-8.10. John Wiley and Sons, Ltd, 2003.

[82] N. Parker. Using natural gas transmission pipeline costs to estimate hydrogen pipeline costs. *UC Davis: Institute of Transportation Studies*, 2004.

[83] K. Stolzenburg, D. Berstad, L. Decker, A. Elliott, C. Haberstroh, C. Hatto, M. Klause, N.D. Mortimer, R. Mubbala, O. Mwabonje, P. Nekså, H. Quack, J.H.R. Rix, I. Seemann, and H.T. Walnum. Efficient liquefaction of hydrogen: Results of the IDEALHY project, 2013.

[84] StartupBoeing. 747-400/-400ER, 2010.

[85] J. Wilkerson, M. Jacobson, A. Malwitz, S. Balasubramanian, R. Wayson, G. Fleming, A Naiman, and S. Lele. Analysis of emission data from global commercial aviation: 2004 and 2006. *Atmospheric Chemistry and Physics*, 2010:2945–2983, 02 2010.

[86] R. Stevens, B. Hobbs, A. Ramos, and C. Meneveau. Combining economic and fluid dynamic models to determine the optimal spacing in very large wind farms. *Wind Energy*, 08 2016.

[87] M. Perz-Osowska, K. Butlewski, R. Marchwicki, H. Szkudlarz, W. Puchalski, and R. Kolano. The flying laboratory – system of data registration and transmission from the airplane to the ground platform. 04 2011.

[88] L. Decker. Liquid hydrogen distribution technology. Linde, 12 2019.

[89] H. Li, X. Yuan, and H. Wang. *PEM fuel cell failure mode analysis*. Taylor & Francis Group, 2011.

[90] IATA. Aircraft operational availability. 2018.

[91] V. Manda, V. Kampurath, and M. Chaitanya. Aircraft servicing, maintenance, repair & overhaul-the changed scenarios through outsourcing. 05 2017.

[92] B. Khandelwal, A. Karakurt, P. Sekaran, V. Sethi, and R. Singh. Hydrogen powered aircraft : The future of air transport. *Progress in Aerospace Sciences*, 60:45–59, 07 2013.

[93] Dr. R. Faaß. Cryoplane flugzeuge mit wasserstoffantrieb. 12 2001.

[94] A. A. Mammoli Y. Villacampa Esteve, C. A. Brebbia. *Energy and Sustainability III*. WIT Press, 2011.

[95] European Aviation Safety Agency. Certification specifications for large aeroplanes cs-25. 03 2007.

[96] J. Sinke. AE3211-II Production of Aerospace Systems reader, 2020.

[97] Granta. CES EduPack, 2019.

[98] P. Teehan and M. Kandlikar. Comparing embodied greenhouse gas emissions of modern computing and electronics products. *Environmental Science & Technology*, 47(9):3997–4003, 2013.

[99] Office of Energy Efficiency and Renewable Energy. Hydrogen production: Electrolysis, 2020.

[100] Peeters P.M.and Middel J. and Hoolhorst A. Fuel efficiency of commercial aircraft fuel efficiency of commercial aircraft - an overview of historical and future trends. Technical report, Nationaal Lucht- en Ruimtevaartlaboratorium, 2005.

[101] Leeham Co. Embraer continues and refines its strategy at the low-end of 100-149 seat sector. *Leeham News*, 2014.

[102] V. Bhaskara. Analysis: A320neo vs. 737 max: Airbus is leading (slightly) – part II. *Airways News*, 2016.

[103] Leeham Co. CS300 first flight wednesday, direct challenge to 737-7 and A319neo. *Leeham News*, 2015.

[104] DNF. Analysing the options for 757 replacement. *Aircraft Commerce*, 2012.

[105] Kollmuss A. and Lane J. Carbon offsetting and air travel. Technical report, Stockholm Environment Institute, 2008.

[106] B. Fehrm. Redefining the 757 replacement: Requirement for the 225/5000 sector. *Leeham News*, 2015.

[107] DNF. Boeing: 777 way much better than A330. *Aspire Aviation*, 2010.

[108] S. McCartney. A prius with wings vs. a guzzler in the clouds. *Wall Street Journal*, 2012.

[109] Boeing. 737-600 performance summary, 2006.

[110] DNF. Boeing 737 max: performance with reported engine sfc shortfall. *Leeham News*, 2015.

[111] Fehrm B. and Hamilton S. 737 max 8 could be enabler for some LCC Long Haul. *Leeham News*, 2014.

[112] Boeing. 757-200/300 performance summary, 2007.

[113] Boeing. 767-200ER performance summary. *The Boeing Company*, 2006.

[114] J.A. Melkert. AE2230-II Propulsion and Power: Lecture 7: Combustion, 2020.

[115] G.A. Schmidt, R.A. Ruedy, R.L. Miller, and A.A. Lacis. Attribution of the present-day total greenhouse effect. *Journal of Geophysical Research*, 115, 2010.

[116] US Environmental Protection Agency. Nitrogen oxides (NOx), why and how they are controlled. Technical report, 1999.

[117] E. J. Penner, J. D. Griggs, H. D. Lister, J. D. Dokken, and MckFarland M. Aviation and the global atmosphere. Technical report, IPCC, 1999.

[118] S. R. Kawa and D. E. Anderson. Assessing the impact of aircraft emissions on the stratosphere. Technical report, National Aeronautics and Space Administration, 1999.

[119] J. Rybicka, A. Tiwari, and G. A. Leeke. Technology readiness level assessment of composites recycling technologies. *Journal of Cleaner Production*, 112:1001 – 1012, 2016.

[120] A. Protsenko, E.D. Pimenova, and V. Petrov. Recycling of glass fibers sheets from thermoset reinforced plastic using thermolysis method. *IOP Conference Series: Materials Science and Engineering*, 734:012185, 01 2020.

[121] X. Kuang, Y. Zhou, Q. Shi, T. Wang, and H. J. Qi. Recycling of epoxy thermoset and composites via good solvent assisted and small molecules participated exchange reactions. *ACS Sustainable Chemistry & Engineering*, 6(7):9189–9197, 2018.

[122] L. V. Golsteijn and E. V. Martinez. The Circular Economy of E-Waste in the Netherlands: Optimizing Material Recycling and Energy Recovery. *Journal of Engineering*, 2017.

[123] M. Leuenberger, N. Jungbluth, and S. Büsser. Environmental impact of canteen meals: comparison of vegetarian and meat based recipes.

[124] Wingas. Natural gas is the most climate-friendly fossil fuel in electricity production.

[125] R.Groves. AE4ASM504 Aircraft Structural Integrity & Maintenance Developments in NDT/SHM, 2020.

[126] J. Markish. Valuation techniques for commercial aircraft program design. Technical report, Aeronautics and Astronautics MIT, 2002.

[127] R. P. Henderson, J. R. R. A. Martinsy, and R. E. Perezz. Aircraft conceptual design for optimal environmental performance. *Aeronautical Journal -New Series*, 2012.

[128] P. Novelli. Sustainable alternative fuels for aviation. ICAO Air Transport Bureau, 2015.

[129] A. K. Kundu. *Aircraft Design*. Cambridge Aerospace Series. Cambridge University Press, 2010.